The role of oxygen in the oxidative dehydrogenation of propane

by

Derek Claude Creaser

A thesis
presented to the University of Waterloo
in fulfilment of the
thesis requirement for the degree of
Doctor of Philosophy
in
Chemical Engineering

Waterloo, Ontario, Canada, 1997

The University of Waterloo requires the signatures of all persons using or photocopying this thesis. Please sign below, and give address and date.

Abstract

The oxidative dehydrogenation of propane over Mg-V-O was investigated both under steady-state and transient reaction conditions. Nonlinear regression analysis was used to compare the applicability of various mechanistic models to the steady-state data. The oxygen surface concentration appeared not to be in equilibrium with the gas phase; models in which oxygen reoxidized the catalyst improved the fit of the data. Thus, Mars-Van Krevelen type kinetics were supported in which propane reacts with oxygen on the catalyst surface to produce propene and carbon oxides. Additional steady-state data were also collected over a wider range of oxygen partial pressures at constant propane partial pressure. Large improvements in propene selectivity were observed by operation at steady-state with low oxygen partial pressure. These selectivity improvements could not be attributed to the consecutive reaction mechanism. The increased propene selectivity at lower oxygen partial pressure suggested the reaction mechanism included reaction pathways in which carbon oxides were produced either by separate surface oxygen sites whose concentration were dependent on the gas-phase oxygen partial pressure or by the direct reaction of gas phase oxygen with adsorbed propene.

Transient responses of the reactants and products, during start-up and interruption of the reaction, supported Mars-Van Krevelen type kinetics. Oxygen mass balances confirmed that the catalyst was partially reduced during start-up of the reaction. Also, the catalyst was active in the absence of gas phase oxygen, at least while the catalyst contained sufficient oxygen. During operation of the reaction under transient conditions without gas phase oxygen, the propene selectivity was higher than at steady-state conditions. This was true even at comparable levels of conversion of the propane. Carbon mass balances indicated little to no carbon species accumulated on the catalyst during start-up with gas phase oxygen. However, temperature-programmed oxidation and desorption experiments revealed that significant, strongly bound carbon-containing species must be slowly deposited on the catalyst during steady-state reaction. During nonsteady-state reaction, without gas phase oxygen, weakly bound carbon species were deposited on the catalyst immediately after start-up which could be quickly oxidized from the catalyst surface upon subsequent exposure of the catalyst to oxygen.

It was found that by periodic operation of the reaction by alternate feeding of oxygen and propane at a 1:1 cycle split, a higher propene yield could be obtained compared to comparable steady-state conditions at cycle periods from about 50 to 150 s. Propene selectivity for periodic operation was always well above that at steady-state, due to the high selectivity observed without gas phase oxygen. However, it was unclear whether periodic

operation was superior to steady-state operation at all conditions. At low propane concentrations, it was found that the propene yield at steady-state conditions could also be improved simply by reducing the partial pressure of oxygen. Periodic operation was also performed without re-oxidation of the catalyst, by alternately feeding propane and pure helium. Under these conditions, comparison of the propene selectivity at about the same conversion of propane, at different degrees of catalyst reduction, indicated that the propene yield of the catalyst was proportional to the degree of reduction.

On the whole, the concentration of oxygen both in the gas phase and on the surface of the catalyst is crucial for determining the selectivity of the reaction for producing propene.

Acknowledgements

This research would not have been possible without the financial support of the Natural Science and Engineering Research Council of Canada and the Swedish Board for Industrial and Technical Development.

I have enjoyed lots of great supervision. Peter Silveston, Bob Hudgins and Bengt Andersson have contributed valuable advice, inspiration, criticism and ideas to my work.

I have had the tremendous privilege of carrying out a great deal of this research at the Department of Chemical Reaction Engineering, Chalmers University of Technology. I thank everyone there for their friendship and for making it such a great place to work.

I thank my parents, Kenneth and Joan, for all their support through the years and for always being there at the airport.

I would be a wretchedly depressed person if it weren't for some clowns who I met in this business and who always keep me smiling; Gary Podrebarac, Rob Rintjema and Chris Rourke.

She is at the bottom of this list, but tops in my heart, my wife, Helena.

Derek Creaser
March, 1997

Table of Contents

List of Tables

List of Figures

1. Introduction

Alkenes are an important feedstock for the petrochemical industry. The oldest industrial processes for their production are the steam cracking of higher molecular weight hydrocarbons such as naphtha and catalytic cracking in oil refining. Alkanes are the feedstocks for the newer commercial processes. They use $Pt(Sn)/Al_2O_3$ or Cr_2O_3/Al_2O_3 catalysts for direct dehydrogenation from the alkane, which in the case of propane is

$$C_3H_8 \rightarrow C_3H_6 + H_2 \qquad (1.1)$$

for which $\Delta H = +124$ kJ mol^{-1} and $\Delta G = +86$ kJ mol^{-1} at 25°C. At 700°C, $\Delta H = +130$ kJ mol^{-1} and $\Delta G = -6.5$ kJ mol^{-1} [1,2]. This reaction is endothermic and its conversion is limited by thermodynamic equilibrium. Reaction temperatures in excess of 600°C are needed to obtain 50% equilibrium conversion of propane and for the corresponding reaction with ethane a temperature of 700°C is needed [3]. At these high temperatures, cracking of the hydrocarbon can also occur, reducing the selectivity of the reaction. But more importantly, coke deposition causes a decrease in catalyst activity and frequent regeneration of the catalyst is needed. An additional problem is the need to provide heat to the reaction at high temperatures, which makes the process energy and capital demanding.

Many of the obstacles with direct dehydrogenation could be overcome if it were possible to oxidize the evolved hydrogen 'in situ' to produce water. At 25°C:

$$C_3H_8 \rightarrow C_3H_6 + H_2 \qquad \Delta H = +124 \text{ kJ mol}^{-1},\ \Delta G = +86 \text{ kJ mol}^{-1} \qquad (1.1)$$

$$H_2 + 0.5O_2 \rightarrow H_2O \qquad \Delta H = -242 \text{ kJ mol}^{-1},\ \Delta G = -229 \text{ kJ mol}^{-1} \qquad (1.2)$$

$$C_3H_8 + 0.5O_2 \rightarrow C_3H_6 + H_2O \qquad \Delta H = -118 \text{ kJ mol}^{-1},\ \Delta G = -143 \text{ kJ mol}^{-1} \qquad (1.3)$$

The net reaction (1.3), shown above for the case of propane, is oxidative dehydrogenation. By the addition of oxygen, the free energy of formation of water is sufficiently large to shift the reaction's equilibrium in favour of products and the heat of formation of water is large enough to convert an otherwise endothermic reaction into an exothermic one. If the reaction is performed catalytically, reactions (1.1) and (1.2), would likely not be the elementary reaction steps. However, the oxidative dehydrogenation route seemingly offers the advantages of potentially higher conversion achievable at a lower reaction temperature. Savings in heating costs can be made if the dehydrogenation reaction is made exothermic by the introduction of oxygen. Also, for a catalytic oxidative dehydrogenation process, deactivation would be reduced since coke formed on the catalyst should be removed by oxygen.

Unfortunately, there are selectivity problems with the oxidative dehydrogenation reaction. In the presence of oxygen, other oxidation reactions including partial oxidation of

the alkane to aldehydes or acids and combustion to carbon oxides can occur, reducing selectivity. The total oxidation of the alkane or alkene to carbon oxides is highly undesirable. Also, despite the favourable thermodynamic data at room temperature, reaction temperatures above 400°C are required to achieve acceptable reaction rates. Higher reaction temperatures may also improve the selectivity of the reaction. No commercial plants for the oxidative dehydrogenation of alkanes are known to be currently operational, but pilot and demonstration units have been built and operated [4].

1.1 Objective and scope of thesis

The objective of this study of the catalytic oxidative dehydrogenation reaction is to further our understanding of its kinetics and mechanisms. It is believed that these objectives could serve to overcome the principal obstacle preventing the commercialization of the reaction, which is controlling its selectivity for production of undesirable products, mainly carbon oxides.

The scope of the work is limited to an investigation of how reaction conditions affect kinetics, mechanism and consequently selectivity. However, the effects of the properties and composition of the catalyst on kinetics and mechanism are excluded. In order to proceed with this objective, it was decided at the outset to select one promising catalyst and catalyst composition from the literature and use it throughout the work. A search of the literature indicated that some of the highest yields for the reaction were obtained with Mg-V-O catalysts, so these catalysts were chosen for this study.

In the experimental work, the reaction is studied under both steady-state and transient conditions. The use of transient conditions not only provides information about the reaction kinetics and mechanism but also examines the possibility that operating the reaction under cyclical reaction conditions might result in an overall higher yield than under comparable steady-state conditions. Considerable modelling of the kinetics is carried out by examining the fit of models to experimental data. It is hoped that an improved understanding of the reaction kinetics and mechanism would aid in the development of either improved catalysts or knowledge of the reaction environments needed for optimal selectivity.

2. Oxidative dehydrogenation - a literature review

2.1 The catalytic reaction

There has been much interest within the last decade in developing suitable catalysts for the oxidative dehydrogenation of C_2-C_4 alkanes to alkenes. Ideally, such catalysts should be active at low temperature, should activate only the C-H bond of the alkane, and should not promote further oxidation of the alkenes produced. For the oxidative dehydrogenation of n-butane and propane, a great variety of primarily metal oxides have been tested. Dahl et al. [5] examined lithium hydroxide/lithium iodide melts, Ushkov et al. [6] investigated metal sulphates, Takita et al. [7] studied metal phosphates as catalysts, Mazzocchia et al. [8] used nickel molybdates and Yoon et al. [9] magnesium molybdates. Smits et al. [10-13] used various metals supported on niobium pentoxide, Romero and co-workers [14-16] reported on simple nickel and iron oxides, Rao and co-workers [17-19] worked with various supported bismuth molybdates, and Fujimoto et al. [20] worked with ZSM-5 based catalysts.

Catalysts active for the oxidative dehydrogenation of ethane have also been examined in the literature. It has been observed that good catalysts for propane and butane oxidative dehydrogenation are often not optimal for ethane and vice versa. This point is illustrated by Michalakos et al. [21] who compared the oxidative dehydrogenation of C_2-C_4 alkanes over magnesium vanadates and a vanadium phosphate. Many of the catalysts tested for ethane oxidative dehydrogenation are known to be active for the oxidative coupling of methane such as lithium-doped magnesium oxide (Li/MgO) [22,23] and Li/MgO promoted with other metals [24] and halides [25]. Many of the studies on these catalysts began with the aim of discovering factors promoting what was believed to be a secondary reaction in the oxidative coupling of methane, namely, the oxidative dehydrogenation of ethane.

By far the most intense research has concentrated on vanadium-bearing catalysts. Vanadium is a well-established element in commercial catalysts used in the partial oxidation of hydrocarbons, the best known commercial process probably being the selective oxidation of n-butane to maleic anhydride which uses a V-P-O based catalyst. Albonetti et al. [26] compared the performance of catalysts reported in the literature and claimed that vanadium, and to a lesser extent molybdenum, are present in all the best catalysts for selective oxidation of alkanes which maximize productivity and yield at minimum temperatures. Vanadium oxide based catalysts appear to have a specificity for C-H bond activation in alkanes and in some cases for oxygen insertion into the activated molecule.

Mamedov and Corberán [27] have written an extensive review of the many formulations of vanadium-containing catalysts tested for the oxidative dehydrogenation of light alkanes.

Vanadium oxide (V_2O_5) itself is active but its selectivity is low. The catalytic properties of vanadia can be improved by depositing it on supports such as silica, alumina and titania. For alumina and silica supported catalysts, it was found that a low coverage of vanadium oxide was more selective for alkene production [28], suggesting that the vanadia sites ideally ought to be isolated from one another. Perhaps as a result, there has also been some investigation of the use of microporous supports such as zeolites [29], aluminophosphates [30] and heteropolyoxometalates [31-33]. In most cases, these materials contained at least one transition metal such as vanadium. It was expected that the ordered structures of the microporous materials could offer a suitable matrix for isolating the metal molecules [26].

According to Mamedov and Corberán's survey, several binary metal oxide systems have been studied, such as vanadium phosphates, vanadium antimonates, vandium tin-oxides and transition metal vanadates. Some multi-component vanadium oxide based catalysts have been examined, containing metals such as bismuth, cobalt, anitmony, nickel, niobium, molybdenum, chromium and tin. Various alkaline vanadates have been studied, including lithium, potassium and barium vanadates. Magnesium vanadates have received the most attention of all the alkaline vanadates. Kung and co-workers [34,35], Sam et al. [36], Bhattacharyya et al. [37], Burch and Crabb [38], Corma et al. [39-41], Delmon and co-workers [42-44], and Gao et al. [45] have all studied magnesium vanadates (Mg-V-O). Kung and co-workers were the first to demonstrate the impressive alkene selectivities of Mg-V-O catalysts for n-butane [34] and propane [35] oxidative dehydrogenation. For n-butane, they reported a selectivity for butenes of 55% at a conversion of 30%. Few other catalysts rival the performance of the Mg-V-O catalyst and it was probably this observation that sparked the interest of other researchers in this catalyst.

For all of the catalysts, it is generally found that the selectivity for the alkene product(s) is inversely related to conversion, while selectivity for combustion products is directly related to conversion. This conversion-selectivity relation is normal for partial oxidation reactions. It suggests that a series type reaction mechanism prevails, in which the alkene is the main reaction product at the start of reaction, while carbon oxides are produced largely from the further oxidation of the alkene. For most catalysts, the products generated are the alkene(s), carbon oxides and cracking products. In some cases, oxygenated hydrocarbons, such as aldehydes and acids, are produced. Few catalysts have been found to deactivate to any significant degree due to coke deposition. This can be attributed to the likelihood that excess oxygen is present to prevent any carbonaceous build-up on the catalysts. Corma et al. [39] observed deactivation presumably due to some coke formation on catalysts under reaction conditions in which the total conversion of oxygen occurred. Burch et al. [38] also observed some significant deactivation, but again under oxygen-lean conditions.

2.2 Evidence for homogeneous reactions in the gas phase

At a sufficiently high reaction temperature, homogeneous gas phase reactions can play an important role in catalytic oxidation reactions. Gas phase reactions have been found to be dominant in the oxidative coupling of methane at temperatures in excess of 675°C [22]. These reactions may be initiated in the gas phase or they may involve only the further reaction of desorbed radical species from the catalyst. In this latter case, the catalyst serves as an initiator.

Burch and Crabb [23] found that the non-catalyzed oxidative pyrolysis of ethane occurred with 45% conversion and 74% selectivity to ethene at 600°C in an empty reactor with a large void volume of about 4 cm^3. In the homogeneous gas phase reaction, it was proposed that the role of molecular oxygen is to initiate the reaction, after which a free radical chain propagation mechanism continues. By packing the reactor's void volume with inert material such as quartz wool or chips, the contribution of the gas phase reactions could be minimized [22,23].

Kung and co-workers investigated the extent of gas phase reactions in the oxidative dehydrogenation of propane over V-Mg-O [46-48]. They considered only gas phase reactions initiated by the desorption of reactive intermediates from the catalyst surface such as propyl radicals. They observed gas phase oxidative pyrolysis reactions in the void volume of a reactor at temperatures greater that 556°C. They could be effectively quenched by filling the reactor completely with quartz chips. The oxidative pyrolysis reactions in a void volume of 5.6 cm^3 caused nearly the same conversion (14.6%) of propane as 21 mg of V-Mg-O (15.2%) at a reaction temperature of 570°C. The selectivities of the oxidative pyrolysis reaction tended to produce more cracking products such as ethene and methane. When the same void volume was positioned downstream of the catalyst, the overall conversion was much higher (46%) compared to the upstream positioning of the void volume (33%). Also, when the catalyst and downstream volume were separated by quartz chips, the propane conversion was lower (34%) than when they immediately followed one another. These results indicate that the enhancement of propane conversion when the catalyst is followed immediately by a void volume is probably due to gas phase reactions induced by the desorption of reaction intermediates from the catalyst. The enhanced propane conversion was observed at temperatures of 556 and 570°C but not at 540°C.

By modelling the reactions in the void volume located downstream from the catalyst, with literature kinetic models for the oxidative pyrolysis of propane, Kung and co-workers [46,47] studied the nature of the desorbing reaction intermediates. Comparison of the calculated and experimental results indicated propyl radicals were the most likely species to desorb from the catalyst; even so, the desorption of OH radicals could not be ruled out. The rate of propyl radical desorption was estimated to be 23% of the propane reaction at 570°C and 5% at 556°C.

Burch and Crabb [38] also studied the relative importance of surface and gas phase reactions in the oxidative dehydrogenation of propane over the V-Mg-O catalyst. In a reactor with a void volume of about 4 cm^3, a propane/air ratio of 1:3, and at 600°C, the propane conversion was about 32% with a propene selectivity of 52%. By reducing the reactor void volume to about 0.1 cm^3, at the same conditions, the propane conversion could be reduced to 0.2%. When the reactor void volume was doubled and the temperature reduced to 550°C, the propane conversion was 2%. Thus, it is possible to operate with exclusively the catalyzed reaction providing the reactor void volume is minimized and the reaction temperature is moderate. Burch and Crabb compared the performance of the oxidative pyrolysis and catalyzed oxidative dehydrogenation reaction. Over a range of conversions, the homogeneous contribution to propene selectivity rivaled that of the catalyzed contribution, prompting the emphatic declaration that, "even the best catalysts are only as good as no catalyst at all!" Despite these results, it is clear that the catalyzed reaction at least offers the advantage of a smaller reactor volume and/or lower reaction temperature to generate the same reaction rate as the non-catalyzed reaction. Kung and co-workers [48] estimated that under their reaction conditions a void volume of 5.6 cm^3 was required to produce an equal conversion of propane compared to a V-Mg-O catalyst occupying only about 0.01 cm^3.

2.3 The Mg-V-O catalyst preparation and structure

Both MgO and V_2O_5 have been tested as oxidative dehydrogenation catalysts. At comparable reaction conditions with propane, Chaar et al. [35] found that V_2O_5 was active with a conversion of 22% but its selectivity for propene was only 18%. On the other hand, MgO was less active with a conversion of 8% but with a higher selectivity of 33%.

It is possible to obtain magnesium vanadates (Mg-V-O) by calcining a physical mixture of MgO and V_2O_5, but long calcination times and high temperatures are required [40]. The Mg-V-O phase(s) formed have a unique crystal structure that is dependent on the proportions of the starting materials. The Mg-V-O phases in order of increasing vanadium content are magnesium orthovanadate $Mg_3V_2O_8$, magnesium pyrovanadate $Mg_2V_2O_7$ and magnesium metavanadate MgV_2O_6.

The structure of the magnesium orthovanadate phase is illustrated in Figure 2.1(a) as described by Krishnamachari and Calvo [49]. It consists of layers of magnesium ions octahedrally bonded to oxygen and vanadium ions tetrahedrally bonded to oxygen. These octahedral and tetrahedral structures are arranged in a nearly cubic closest packing. The structure of magnesium pyrovanadate (see Figure 2.1(b)), given by Gopal and Calvo [50], is that of rows of V_2O_7 groups with long V-O-V bridges between pairs of these groups. Each

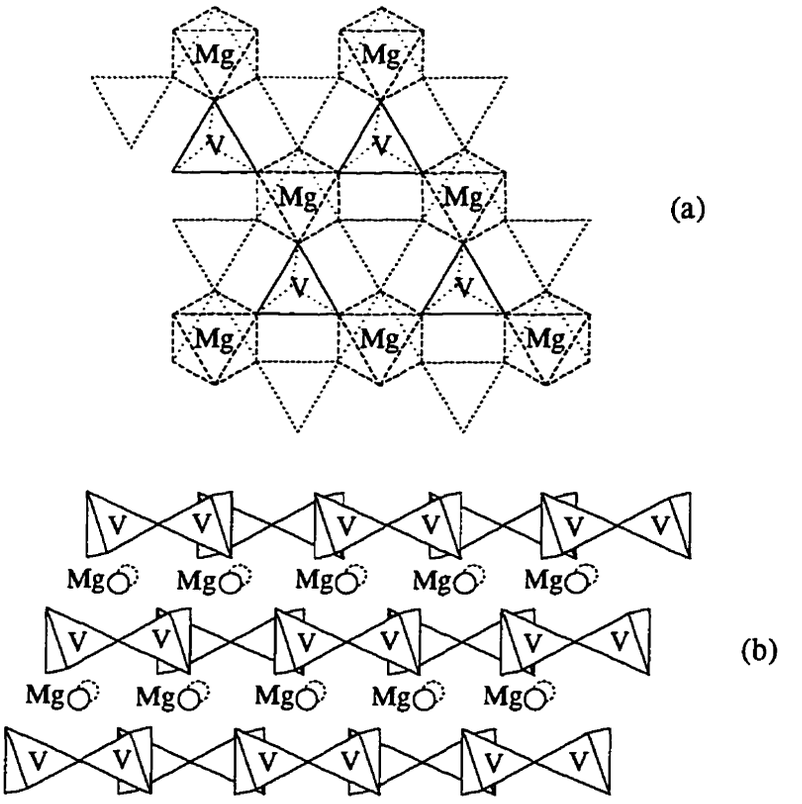

Figure 2.1 Magnesium Orthovandate (a) and Magnesium Pyrovanadate (b) structures. Adapted from [49] and [50].

of the terminal oxygen atoms of the V_2O_7 groups are shared with two magnesium ions. Ng and Calvo [51] have determined the structure of magnesium metavanadate to be that of VO_6 octahedra joined by edges and connected together through MgO_6 octahedra. A principal difference in the local environment of oxygen atoms between the different phases is that with magnesium orthovanadate, oxygen atoms are linked to both magnesium and vanadium atoms while in the pyrovanadate phase V-O-V linkages are present.

Compared to the calcination method, the magnesium vanadates are more efficiently produced by impregnating a magnesium-containing compound in solution with a vanadium-containing compound. The magnesium precursors often used are magnesium oxide [52], magnesium nitrate [42] and magnesium oxalate [40]. Some common vanadium precursors include ammonium metavanadate [52], and vandyl oxalate [40]. The chosen compounds are mixed in a solution with a controlled pH. Water is slowly evaporated and the resulting paste is dried. The main advantage of the impregnation method of preparing magnesium vanadates is that lower calcination temperatures (about 550°C) and shorter calcination times (3-6 h) are needed. The magnesium vanadate phases present in the final catalyst depend mostly on the starting ratio of magnesium and vanadium used. However, contaminants in the starting solutions [53], calcination temperature [42] and perhaps other factors in the

preparation procedure may all affect what phases are present in the final catalyst. Corma et al. [40] have found that the surface concentrations of magnesium and vanadium can vary from the bulk concentration depending on the magnesium and vanadium precursors used in the impregnation procedure and their relative concentrations.

2.4 The Mg-V-O catalyst structure and catalytic behaviour

2.4.1 Mg-V-O phases

There has been some evidence in the literature that the structure of certain Mg-V-O phases may be more favourable for selective oxidative dehydrogenation. This issue has been marked with some controversy with different research groups presenting conflicting results.

In Kung and co-workers' [34] initial study of the Mg-V-O catalyst for the oxidative dehydrogenation of n-butane, they prepared Mg-V-O catalysts which contained from 3 to 54 wt% V_2O_5. At such compositions MgO is present in such excess that the expected phases on a stoichiometric basis, if the maximum quantity of Mg is incorporated into the Mg vanadate phase, would be magnesium orthovanadate $Mg_3V_2O_8$ and excess MgO. X-ray diffraction analysis confirmed the presence of only these two phases. The increase in total selectivity for dehydrogenation products was greatest for catalysts containing from 3.5 wt% V_2O_5 to 19 wt% V_2O_5 and then remained nearly constant for up to 54 wt% V_2O_5. Kung and co-workers proposed that the most active and selective phase of the Mg-V-O catalyst for the oxidative dehydrogenation of alkanes was Mg orthovanadate. This hypothesis was based on the fact that structurally the orthovanadate phase contains only V-O-Mg linkages and no V-O-V or V=O bonds as are present in magnesium pyrovanadate, magnesium metavanadate and V_2O_5. Since magnesium is less easily reduced than vanadium, the presence of Mg-O-V bonds causes lattice oxygen to be less reactive, while the presence of V-O-V or V=O bonds causes lattice oxygen to be more reactive, allowing it to attack indiscriminately either C-H or C-C bonds, thus promoting the complete combustion of the alkane.

Sam et al. [36] thoroughly examined the importance of the Mg-V-O phases by preparing reference Mg orthovanadate, pyrovanadate and metavanadate catalysts. The appropriate stoichiometric ratios of MgO and V_2O_5 were used in their preparation. In contrast to Kung's hypothesis, the Mg pyrovanadate phase was found to be the most selective for the oxidative dehydrogenation of propane. The pyrovanadate phase selectivity for propene was 53% compared to 6 and 15% for the orthovanadate and metavanadate phases, respectively. The selectivity of each phase was measured at a propane conversion of about 7%. Later Gao et al. [42] also compared the catalytic behaviour of pure Mg-V-O phases and found that at iso-conversion conditions (1-3%) the propene selectivity followed the order pyrovanadate > orthovanadate > metavanadate.

Kung and co-workers [53] carried out a more detailed study to examine the validity of their original hypothesis. They pointed out that Sam et al. used a method to prepare MgO which resulted in traces of potassium (about 0.02 wt%) being present in the final catalyst. Kung's hypothesis was confirmed by the results for oxidative dehydrogenation of n-butane. The selectivity of the Mg orthovanadate phase was 43% for alkenes at 17% conversion, but for the pyrovanadate phase it was only 15%. However, the results for the oxidative dehydrogenation of propane indicated that both the Mg orthovanadate and pyrovanadate phases' selectivities for propene were about 62% at 7% conversion of propane. It was suggested that the difference in behaviour for butane and propane on Mg pyrovanadate could be explained by the phase structure and the sizes of the alkane molecules [21]. With Mg orthovanadate, the isolated VO_4 tetrahedra allow an adsorbed molecule to react with only one VO_4 unit. However, with Mg pyrovanadate a molecule can react simultaneously with two VO_4 units that are bridged by an oxygen atom, provided that the size of the molecule is sufficiently large. Propane may be too small to react with bridged VO_4 units, but the two end carbons of n-butane could react with two VO_4 units. Such an interaction may lead to the formation of a π-allyl complex and complete combustion of the molecule. Kung and co-workers [53] also examined the effect of traces of potassium in the V-Mg-O catalyst. Reference Mg orthovanadate and Mg pyrovanadate catalysts were prepared by the method of Sam et al. and their activities and selectivities were compared with those of potassium free catalysts. The orthovanadate with potassium was less selective than the corresponding catalyst free of potassium for both the propane and butane reactions. It was suggested, based on X-ray diffraction analysis, that the presence of potassium inhibited the formation of the orthovanadate phase. For the oxidative dehydrogenation of butane, the orthovanadate phase both with and free of potassium was more selective than the pyrovanadate phase.

Potassium contamination may explain the contradictory results of Kung's group and Sam et al. concerning the selectivity of Mg-V-O phases. However, Gao et al. [42] used a different method for preparation of the pure Mg-V-O phases, which they called the 'citrate' method. By this method, high purity Mg-V-O phases could be produced at a relatively low calcination temperature (550°C). Both Kung et al. and Sam et al. needed to use elevated calcination temperatures (in excess of 650°C) to produce sufficiently pure phases. On the other hand, their mixed phase catalysts were produced at lower calcination temperatures. Gao et al. found that the size and morphology of the pure phase Mg-V-O crystals was a function of calcination temperature.

It should be added that generally results of studies of V_2O_5 supported catalysts tend to support the Kung hypothesis that isolated VO_4 tetrahedra are more favourable for the oxidative dehydrogenation reaction. Mamedov and Corberán [27] have reviewed studies of V_2O_5 supported on silica, alumina and titania. They concluded that the dehydrogenation selectivity is best for these catalysts at low vanadium loadings, below monolayer coverage.

The supported vanadium species at low loadings are presumably isolated with two-dimensional arrays of tetrahedral VO_4. At higher vanadium loadings, dehydrogenation selectivity diminishes and crystalline V_2O_5 forms on the surface.

2.4.2 Mg-V-O phase mixtures

Gao et al. [43] later carried out an extensive study of the catalytic behaviour of mixed phase Mg-V-O catalysts. The selectivities of multi-phase Mg-V-O catalysts were found to be quite different from that of the pure phases. The selectivity of the orthovandate could be improved when it co-existed with a pyrovanadate phase or MgO, suggesting synergistic effects between the phases. This result may explain why Kung's group originally found that some of the best selectivities for butane oxidation were with catalysts containing magnesium orthovanadate and excess MgO.

2.4.3 Mg-V-O bulk/surface properties

Corma et al. [40] investigated the effect of preparation procedures on the surface as well as the bulk concentrations of vanadium and magnesium in Mg-V-O catalysts. They prepared catalysts with varying V/Mg ratios using different precursor compounds for vanadium and magnesium. For vanadium, the preparation compounds compared were ammonium vanadate and vanadyl oxalate. While for magnesium, the use of magnesium oxide and magnesium oxalate were compared. The bulk formation of magnesium vanadates was found to depend only on the V/Mg ratio of the preparation compounds. Magnesium orthovanadate and MgO phase mixtures were formed at low vanadium content and magnesium orthovandate and magnesium pyrovandate mixtures at higher vanadium contents. The BET surface areas of the catalysts increased with vanadium content, but also depended on the choice of preparation compounds. The surface concentration of vanadium and magnesium, determined by X-ray photoelectron spectroscopy (XPS) analysis did not in all cases coincide with the bulk concentrations. The differences depended on the precursor compounds used in catalyst preparation and the V/Mg ratio of the catalyst. In particular the use of ammonium vanadate as the starting precursor for vanadium tended to produce a catalyst with an enriched surface concentration of magnesium. Ammonium vanadate is a common starting material for Mg-V-O catalyst preparation and had been used previously by Kung's group and Sam et al. [36]. Also, catalysts with high concentrations of vanadium tended to have an enriched surface concentration of vanadium.

The effect of varying surface concentrations of vanadium and magnesium on catalytic properties was also determined [41]. It was found that the highest activity (based on BET surface area) and selectivity for the oxidative dehydrogenation of propane was obtained on catalysts with a magnesium enriched surface. Corma et al. [40] sided with the views of Kung regarding the selectivity effects of VO_4 species and findings with supported V_2O_5

catalysts, discussed above. They proposed that the superior performance of catalysts with magnesium enriched surfaces was due to the presence of only isolated VO_4 species on the surfaces. However, at high vanadium content, in which vanadium enrichment of the catalyst surface is obtained, the presence of associated vanadium complexes should be expected and should result in lower dehydrogenation selectivity. The work of Corma et al. shows that the *bulk* oxide lattice may not always represent the *surface* properties. If surface concentrations can vary from that of the bulk, it is reasonable that the coordination of vanadium species to oxygen may also vary from that in the bulk of the catalyst.

2.4.4 Acid-base properties

Various research groups, using a range of catalysts, have investigated the effect on activity and selectivity of manipulating the catalysts' acidity with alkaline promoters. It is believed that superior catalysts for oxidative dehydrogenation should have a basic character. Alkenes are basic and a basic catalyst ought therefore to facilitate the desorption of the alkene, preventing its further oxidation to carbon oxides. Alkaline promoters increase the basicity of the catalyst.

Grabowski et al. [54] found that the alkaline promoters lithium, potassium and rubidium reduced the activity of V_2O_5/TiO_2 and MoO_3/TiO_2 catalysts for the oxidative dehydrogenation of propane. However, at the same levels of conversion, the promoted catalysts had a higher selectivity for propene. Martin-Aranda et al. [55] and Vrieland et al. [56,57] investigated the effect of promoters such as lithium, sodium, potassium and cesium on the oxidative dehydrogenation of butane over Ni-Mo-O and Mg-Mo-O catalysts respectively. In both studies, the promoters again reduced the activity of the catalyst, although they improved the yield and selectivity for butenes and butadiene. Vrieland et al. found that additions of small amounts of potassium up to 0.4 wt% caused the production of carbon oxides to decrease while that of C_4-olefins increased. The potassium promoter seemed to selectively poison the production of carbon oxides while the production of olefins was unaffected.

The effect of alkali promoters on selectivity may not be the same for all alkanes. Galli et al. [58] compared the effect of potassium on the oxidative dehydrogenation of butane and ethane over V_2O_5/Al_2O_3 catalysts. Addition of potassium reduced the reducibility of the catalyst, measured by temperature-programmed-reduction with hydrogen, and the activity of the catalyst for reaction with both butane and ethane. However, potassium increased the selectivity for the formation of C_4-olefins from butane but decreased the selectivity for ethene from ethane.

Blasco et al. [59] compared the basicity of V/Al_2O_3, V/sepiolite, V/hydrotalcite and V/MgO catalysts. The basicity was measured by adsorption of pyridine measured by FTIR.

The selectivities of the catalysts for C_4-olefins from butane increased with increasing basicity of the catalyst.

Little is known about the effect of promoters in modifying the catalytic properties of Mg-V-O catalysts specifically. It has been reported that the addition of Cr_2O_3 and MoO_3 improved the activity of the catalyst, while TiO_2 increased the selectivity in the oxidative dehydrogenation of butane [37].

2.5 Catalyst redox properties and catalytic behaviour

2.5.1 A Redox Model

Kung and co-workers postulated a model relating the redox behaviour of a catalyst to its catalytic behaviour [61]. This model is based on the assumption that the activity and selectivity of an oxide catalyst in selective oxidation reactions should be related to the ease or rate of reduction of the oxide. An oxide that is difficult to reduce will be inactive, but probably selective. However, one which is easily reduced is very active but nonselective, because it would promote the combustion of the reactants. An ideally active and selective catalytic rate of reduction would be within an optimal range, as shown graphically in Figure 2.2 (a).

However, the rate of reduction of an oxide should depend not only on its structure and composition, but also on its existing extent of reduction. The more reduced is an oxide, the slower is its rate of reduction. In a steady-state process, the oxide catalyst is undergoing simultaneous reduction and reoxidation. The extent of reduction of the oxide depends on the rates of these opposing processes, which in turn depends on the present extent of reduction of the oxide. The state of the catalyst is determined by the intersection of its reduction and reoxidation curves, as shown in Figure 2.2(b). The ideally active and selective catalytic steady-state rates of reduction and reoxidation would lie within an optimal region as indicated by the curves marked A. Another catalyst B, for structural or composition reasons might have an overall higher rate of reoxidation despite a similar rate of reduction to that of catalyst A. The higher rate of reoxidation of B causes it to be in a more oxidized state which in turn increases its rate of reduction. This increased rate of reduction promotes the nonselective combustion of reactants, causing it to be more active than is optimal. Thus, catalyst B might be useful as a combustion catalyst but of no interest for partial oxidation.

2.5.2 Manifestations of redox model

The significance of the reduction potential of Mg in the V-Mg-O catalyst was examined by replacing Mg with other cations such as Nd, Sm, Zn, Cr, Eu, Ni, Cu and Fe [60]. The aqueous reduction potential of these cations increase in the order

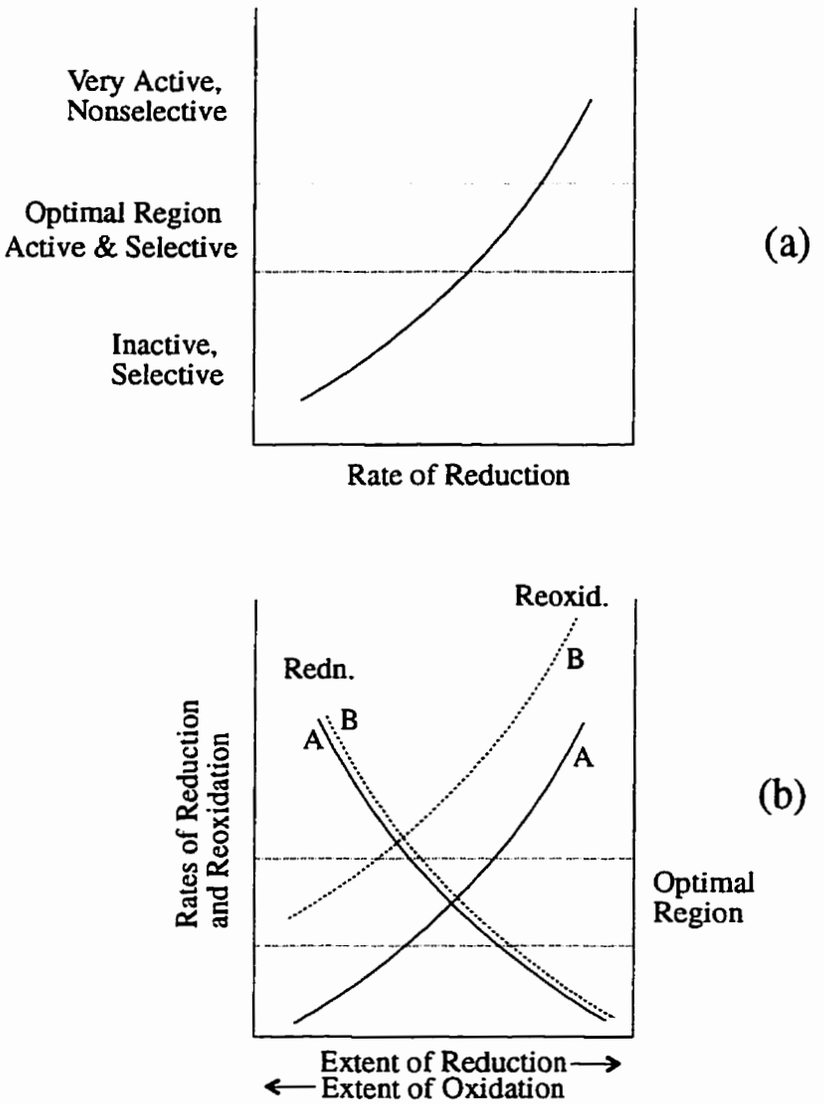

Figure 2.2 Relation between catalyst redox properties and catalytic behaviour

Mg<Nd<Sm<Zn<Cr<Eu<Ni<Cu<Fe. The selectivity for alkenes in the oxidative dehydrogenation of n-butane from vanadates made from these cations decreased in an almost similar order: Mg>Nd>Sm>Zn>Eu>Ni>Cr>Fe>Cu. The selectivities for alkenes ranged from 59 to 2% and were each measured at an n-butane conversion of between 11 to 16%. This result supports Kung and co-workers' hypothesis that the higher degree of selectivity of the V-Mg-O catalyst can be attributed to the relative non-reducibility of Mg ions that lower the reactivity of lattice oxygen.

Temperature-Programmed Reduction/Oxidation (TPR/TPO) experiments were also performed with Mg orthovanadate and other orthovanadates in which the Mg was replaced with Eu and Nd [61]. The TPR/TPO equipment consisted of a closed recirculation system with a heat-flow type scanning calorimeter. The catalysts were first oxidized with oxygen,

reduced with CO and then re-oxidized with oxygen. The amount of oxygen consumed during re-oxidation was determined from the pressure drop in the system. From the TPR curves, there was no clear indication that the orthovanadate with a more easily reducible ion tended to begin to reduce at a lower temperature. In general, reduction of the orthovanadates began at above 500°C and was completed at about 800°C. From the quantity of oxygen consumed during the reoxidation cycle, the oxidation state of the vanadium ions could be determined. The oxidation state of vanadium in the reduced Mg, Nd and Eu orthovanadates was 3.51, 3.40 and 3.50, respectively. Again, what was expected to be the most easily reducible orthovanadate (Eu) was not any more reduced than the other orthovanadates. It was suggested that the orthovanadate structure may only sustain a limited degree of reduction, any further reduction requiring more severe conditions.

The effect of the catalyst oxidation state on oxidative dehydrogenation selectivity has been investigated for vanadium oxide on alumina catalysts (V_2O_5/Al_2O_3) [62]. The V_2O_5/Al_2O_3 catalyst was reduced with successive pulses of butane. The extent of reduction of the catalyst and its selectivity for dehydrogenation products was determined by analysis of each product pulse. It was found that the selectivity of the catalyst increased with its extent of reduction. However, simultaneously the conversion of butane decreased as the catalyst was reduced and since the oxidation of dehydrogenation products to carbon oxides is a secondary reaction, the improvement of selectivity with lower conversion was no surprise. But when reaction conditions were manipulated to lower the conversion of butane on the more oxidized catalyst to a level comparable to that obtained when the catalyst was in a more reduced state, the selectivity for the more oxidized catalyst was still significantly lower. A similar relationship was found for propane oxidative dehydrogenation over a Mg-Mo-O catalyst [9]. Also, in this case the alkane, propane, was fed without oxygen to the catalyst. The selectivity for propene increased as the degree of reduction of the catalyst increased. These results support the notion that selectivity is affected by the binding energy of lattice oxygen. When the catalyst is in a more oxidized state and lattice oxygen is loosely bound, it is more likely to promote the deep oxidation of hydrocarbons to carbon oxides.

Gao et al. [42] and Soenen et al. [63] have compared the reducibility of different pure Mg-V-O phases. Gao et al. measured the weight loss upon exposure to hydrogen at 460°C and Soenen et al. electrical conductivity changes upon exposure to propane at 520°C. Both techniques indicated that magnesium pyrovanadate was the most easily reducible magnesium vanadate. From a structural point of view, the easy reducibility of the pyrovanadate phase is expected because of the ease of removal of oxygen in V-O-V linkages. However Gao et al. also found the pyrovanadate was the most selective pure phase for oxidative dehydrogenation of propane. Their finding that the more easily reducible catalyst is the most selective does not agree with Kung's theory regarding the redox properties and catalytic behaviour of catalysts discussed above. If the pyrovanadate is truly the more selective for propane

oxidative dehydrogenation, it may possess other favourable structural characteristics that compensate for its easy reducibility.

The reducibility of V/Al_2O_3, V/sepiolite, V/hydrotalcite and V/MgO catalysts have been compared by the onset temperature of hydrogen consumption during temperature-programmed-reduction [59]. The reducibility of the catalysts paralleled their catalytic activity for the oxidative dehydrogenation of butane, whereby the most easily reducible catalyst was most active. The selectivity of a typical catalyst for dehydrogenation products was not notably related to its reducibility but correlated well with its basicity.

2.6 Aspects of the catalytic reaction mechanism

2.6.1 C-H bond activation

Kung and co-workers [64] have compared the relative rates of reaction of different alkanes over a V-Mg-O catalyst. The alkanes included 2-methylpropane, n-butane, propane and ethane. The rate of reaction at 500°C was found to decrease in the order 2-methylpropane > n-butane > propane > ethane. C-H bond energies are known to vary according to the position of the carbon atom in the hydrocarbon. They decrease in the order primary > secondary > tertiary. The alkane reaction rates paralleled the strength of their C-H bonds. 2-methylpropane which has one tertiary carbon reacted fastest, while ethane which has only primary carbons reacted slowest. Mamedov and Corberán [27] have compared rate data from different authors and similarly found that the reaction rates of alkanes increased with the number of carbon atoms in the hydrocarbon chain. These results are consistent with their claim that the rate limiting step of the reaction is the breaking of the first C-H bond. Breakage of the C-H bond may occur either heterolytically, with the formation of a hydride ion and a carbocation, or homolytically with the formation of an alkyl radical. The ease of breakage of the C-H bond probably only controls the rate of conversion of the alkane, and the nature of the subsequent reaction steps influences the product distribution among dehydrogenation, oxygenation and combustion products.

2.6.2 The redox mechanism

It has been found that the electrical conductivity of pure Mg-V-O phases is independent of the gas phase oxygen partial pressures to which they are exposed [56]. Since these catalysts are active for oxidative dehydrogenation, their reaction mechanism must involve O^{2-} anions from the lattice. Exposure of the pure phases to propane increases the conductivity, indicating the phases become reduced while re-exposure to oxygen decreases the conductivity. Results from pulse experiments with butane, discussed earlier, indicate that lattice oxygen can be involved in the reaction [62]. The reaction of the alkane has been

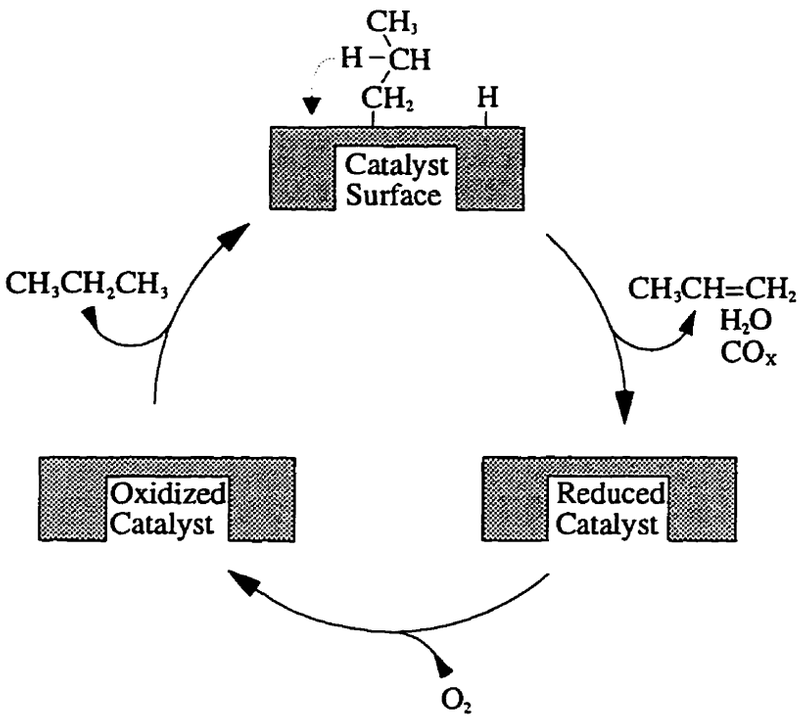

Figure 2.3 Catalytic cycle

shown to occur for propane [9] and butane [56,57] in the absence of gas phase oxygen. These findings, in addition to those discussed earlier concerning redox properties of the catalyst, all support the proposal that the oxidative dehydrogenation of lower alkanes occurs via a Mars-Van Krevelen redox type mechanism [65,66]. As illustrated by the schematic of the catalytic cycle in Figure 2.3, in this type of mechanism, reaction of the alkane to either alkenes or carbon oxides reduces the catalyst and in a separate reaction, oxygen from the gas phase re-oxidizes the catalyst.

2.6.3 Subsequent reaction steps

The reaction of the alkane with the catalyst could result in an adsorbed alkyl and/or alkene on the catalyst surface. Kung's group [21,65,66] has proposed that two competing processes, involving the adsorbed alkyl or alkene, comprise the 'selectivity-determining step'. In the case of an adsorbed alkyl species, the competing processes are the breakage of a C-H bond to form a dehydrogenation product or the formation of a C-O bond to form oxygen-containing products such as oxygenates or carbon oxides (see Scheme 1 in Figure 2.4). If the adsorbed species is an alkene the competing processes are its desorption or it can react further to form a C-O bond and subsequently oxygen containing products (see Scheme 2 in Figure 2.4). It has been argued that the ease of removal of oxygen species from the catalyst to form C-O bonds and oxygenated products determines the outcome of the selectivity-determining step. This concept explains fairly well the increase in

Scheme 1:

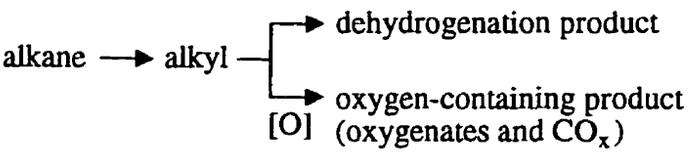

Scheme 2:

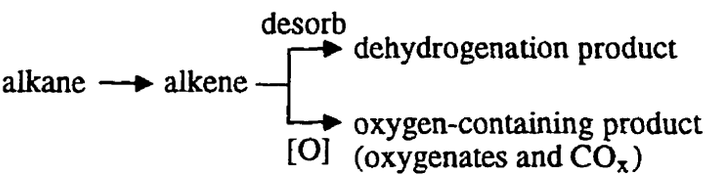

Figure 2.4 Selectivity-determining steps

dehydrogenation selectivity when the reducibility of the M cation in the orthovanadate structure decreases [60] or the degree of reduction of the catalyst is increased [62,9], but it fails to explain the contrary relationship between these characteristics established for the three Mg-V-O pure phases [42].

There is one report in the literature in which the addition of carbon dioxide into the feed for oxidative dehydrogenation increased the propene selectivity on a $PrVO_4$ catalyst [67]. The enhanced propene selectivity was observed at isoconversion conditions. The authors suggested that carbon dioxide adsorption on the catalyst blocks sites responsible for total oxidation.

2.6.4 Kinetic studies

Andersson [68] gathered kinetic data for the oxidative dehydrogenation of propane over $V/AlPO_4$ at a range of temperatures, vanadium loadings, and propane and oxygen partial pressures. From this data, a kinetic model for the production of propene was proposed. In the model, propane in the gas phase was purported to react with adsorbed oxygen species on the catalyst surface by an Eley-Rideal type mechanism. Here, the reaction mechanism was not of a redox type because gas phase oxygen was considered to be in equilibrium with the adsorbed oxygen. None of the products, propene, carbon monoxide or carbon dioxide was considered to adsorb to the catalyst surface. Carbon oxides were assumed to be produced either directly from the reaction of propane or from the further oxidation of propene. Le Bars et al. [69] used a simple Mars-Van Krevelen redox type model to describe the oxidative dehydrogenation of ethane over a V_2O_5/SiO_2 catalyst. This model only described the production of ethene. Rate equations for production of carbon oxides from either ethane or ethene were not included. The limiting step of ethane oxidative dehydrogenation was found

to be the reduction of oxidized sites by ethane. Thus, the catalyst was considered to work in a highly oxidized state.

Sloczynski [70] modelled the individual reduction and reoxidation reactions from cyclical experiments for the oxidative dehydrogenation of propane over V_2O_5/TiO_2. In general, it was found that the initial rates of reoxidation were 1-2 orders of magnitude higher than the rates of reduction. These results also suggest that during the steady-state reaction the catalyst is highly oxidized and that the rates of reduction of the catalyst by propane and intermediates are overall rate-determining.

Pantazidis and Mirodatos [71] have recently published results of non-steady-state and isotope exchange experiments aimed at proposing a qualitative mechanism for oxidative dehydrogenation of propane over a Mg-V-O catalyst. They propose that propane reacts with lattice oxygen species, probably O^{2-}, to form an intermediate species on the catalyst surface, probably a propyl group. Desorption of the intermediate species forms propene. They further find a weak dependence of carbon oxide formation on the oxygen partial pressure. They suggest that oxidation of the adsorbed intermediate species involves an oxygen adspecies, such as O^-, arising from gaseous oxygen activation. Selectivity thus depends on the fate of the intermediate species through competition between desorption and reaction with an oxygen adspecies. However, neither diffuse reflectance infra-red fourier transform (DRIFT) spectroscopy nor isotope exchange experiments indicated the presence of such an adsorbed hydrocarbon intermediate species.

2.7 Summary and foreshadowing

Much of the literature supports a Mars-Van Krevelen or redox type mechanism for the oxidative dehydrogenation reaction. In such a mechanism, the alkane reacts with surface or lattice oxygen causing reduction of the catalyst and simultaneously oxygen reacts to oxidize the catalyst. This is supported by observations that the reaction of propane [9,70] and butane [56,57,62] occur in the absence of gas phase oxygen. In addition, the electrical conductivity of a catalyst has been shown to vary upon exposure to propane and subsequently oxygen [56]. In one study the kinetics of the oxidative dehydrogenation of ethane was successfully modelled by a simple redox type model [69], but another model for the oxidative dehydrogenation of propane, involved an equilibrium between gas phase and surface adsorbed oxygen [68].

It is widely believed that the properties of the catalyst and/or surface oxygen influence the selectivity of the reaction. Catalysts with a basic character are thought to be superior oxidative dehydrogenation catalysts because they facilitate the desorption of the alkene, thus preventing its further oxidation to carbon oxides. Supporting this claim, alkaline promoters have been shown in some cases to improve the selectivity of catalysts for the production of dehydrogenation products [54-59].

In keeping with the general redox mechanism, the binding strength of lattice oxygen is thought to govern the selectivity of the reaction. Highly reactive, loosely bound oxygen might indiscriminately break C-C and C-H bonds leading to deep oxidation while less reactive, strongly bound oxygen, is less likely to attack the hydrocarbon structure, thus preferentially producing partial oxidation products. This was supported by the finding that the selectivity of various metal vanadates varied with the reduction potential of the metals [60]. Also, the selectivity for the oxidative dehydrogenation of butane [62] and propane [9] was found to increase for dehydrogenation products as the degree of reduction of the catalyst increased, when the reactions were carried out without gas phase oxygen. These claims are based on the fact that as the catalyst is increasingly reduced the binding strength of the catalyst's remaining lattice oxygen increases. Findings that the nature of coordination of oxygen on the catalyst surface [27,34,41], due to the surface concentration of supported metal oxides such as V_2O_5, affects the selectivity of the catalyst, further support the belief that the binding strength of oxygen influences selectivity. However, contrary to a relation between oxygen binding strength and selectivity, the reducibility of different vanadium-bearing catalysts [59] and Mg-V-O pure phases [63] have not been found to correlate well with their selectivities for dehydrogenation products.

It is evident that much of the research concerning oxidative dehydrogenation has involved finding correlations between properties of the catalysts and catalytic behaviour, and from these attempting to infer the reaction mechanism. Few extensive kinetic studies have been carried out on the reaction. This is one of the objectives of this thesis. Kinetic data for the reaction are collected under both steady-state and transient conditions. The transient responses of the reaction are used as an additional tool for diagnosing the reaction mechanism, the degree of reduction of the catalyst, and whether hydrocarbon species are adsorbed to the surface of the catalyst. Since much of the literature in the area suggests that the state of the catalyst and/or surface oxygen influences selectivity, of particular interest is the role of oxygen in the reaction and whether it can change depending on the reaction conditions, thus affecting the selectivity of the reaction.

3. Experimental methods

3.1 Preparation and characterization of Mg-V-O catalyst

Because of its high yields reported in the literature, the Mg-V-O catalyst was chosen for this study of the catalytic oxidative dehydrogenation reaction. Kung and co-workers [35] examined Mg-V-O catalysts containing between 20 and 60 wt% V_2O_5. An optimum propene selectivity of about 42% at about 33% propane conversion was obtained for catalysts with between 20 and 40 wt% V_2O_5. Consequently, an Mg-V-O catalyst with 40 wt% V_2O_5 was used in this study. The high V_2O_5 content was chosen so that the magnesium vanadate phase(s) present in the catalyst could be identified unambiguously by X-ray diffraction analysis.

The catalyst was prepared according to the method described by Kung and co-workers [52]. A 1 L aqueous solution containing 0.5 wt% NH_4VO_3 and 1 wt% NH_4OH was heated to 70°C while being stirred. Then 5.84 g of MgO was slowly added to this stirred solution of NH_4VO_3. The solution was continuously stirred for about 1 h, during which the solution evaporated to a thick paste. The paste was further evaporated in an oven at 80°C overnight, after which it became a white powder. The catalyst was then calcined at 550°C for 6 h in a flow of air of about 20 ml min^{-1} STP. The resulting catalyst composition was 60 wt% MgO and 40 wt% V_2O_5 or 36.2 wt% Mg and 22.4 wt% V as verified by atomic absorption. After calcination, the colour of the catalyst was a pale yellow. Once used, the catalyst became grey to green-gray in colour.

For experimental runs, anywhere between 15 and 40 mg of Mg-V-O catalyst was used at a time. Before reaction, the catalyst sample was placed in the reactor and exposed to 10% oxygen in helium with a total flow rate of 50 ml min^{-1} STP at 550°C for 3 h.

X-ray diffraction was performed on a Siemens D5000 diffractometer, equipped with Cu radiation. JCPDS-ICDD (1988-1994) standard spectral software was used to determine the phases. The diffractogram of the unused catalyst is shown in Figure 3.1. The symbols in the figure indicate the peaks in the diffractogram of the catalyst that match peaks in the diffractograms of the pure phases. The peaks were generally broad, probably because the crystal sizes were small. The two phases clearly identified were magnesium oxide and magnesium orthovanadate ($Mg_3(VO_4)_2$). In addition, a trace of vanadium oxide (V_3O_5) was identified.

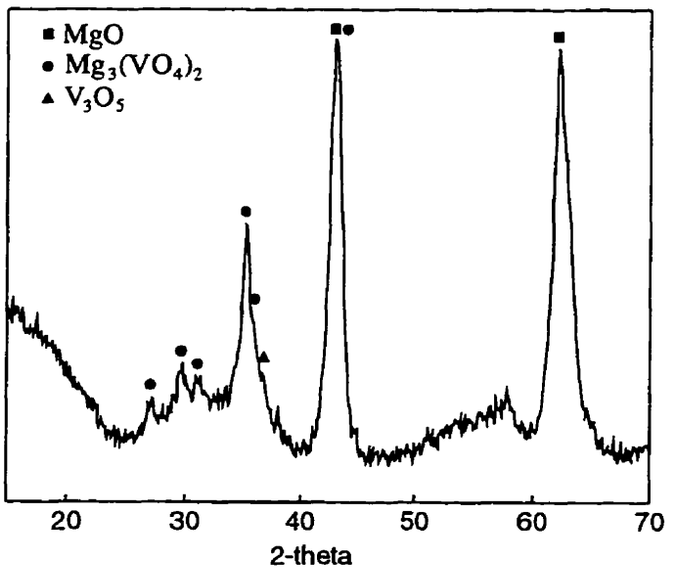

Figure 3.1 X-ray diffractogram of fresh Mg-V-O catalyst

3.2 Equipment for studying catalytic reaction

3.2.1 Quartz glass reactor

The quartz glass U-tube reactor used is illustrated in Figure 3.2. The outside diameter of the quartz tube was 6 mm. The catalyst was located in a bulb in one arm of the U-tube. Reactants were fed first through the left arm of the U-tube in Figure 3.2, and then up through the catalyst bed. The inside diameter of the arm, upstream from the catalyst was 1 mm. The inside diameter of the bulb was 8 mm and the tube downstream from the catalyst had an inside diameter of 4 mm. At the bottom, inside the bulb was located a quartz glass frit on which the catalyst bed was supported. First, a layer of granular quartz glass (crushed to < 1 mm) with a depth of a few millimetres was placed on top of the frit. On top of this was placed the catalyst with a depth of 5 to 10 mm, depending on the quantity of catalyst. An additional layer of granular quartz glass was placed on top of the catalyst, to fill the bulb. Some quartz wool was placed in the tube, downstream from the bulb. A quartz glass thermowell, in the downstream arm, penetrated the upper layer of granular quartz glass and was arranged so as to be just in contact with the top of the catalyst bed. In experiments operated at steady-state the design of the reactor was as in Figure 3.2, except that the bulb was omitted and replaced by a length of quartz tube with an inside diameter of 4 mm. The catalyst was placed inside this tube. Upstream of the catalyst, any empty length of 4 mm ID tube was packed with quartz wool. With the catalyst inside a bulb, the catalyst bed created just a small pressure drop, allowing at least 40 mg of catalyst to be used.

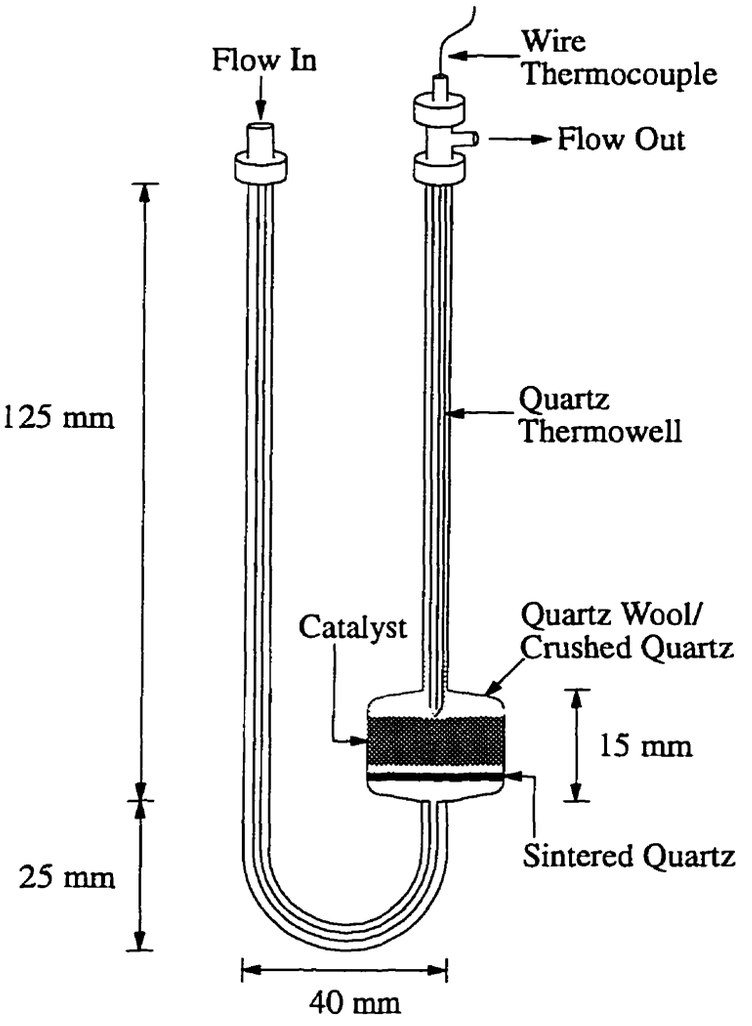

Figure 3.2 The quartz U-tube reactor

One of the primary requirements of the design of the reactor was that the void volume should be minimized so that gas phase-initiated reactions could be avoided. This is why the arm of the reactor, upstream from the catalyst, was designed with a reduced inside diameter. Any remaining volume in the reactor not occupied by the catalyst bed was filled with granular quartz glass or quartz wool. The presence of the quartz thermowell, downstream from the catalyst bed, also reduced void volume in the reactor. Blank experiments in which the reactor contained no catalyst were performed at reaction temperatures ranging from 510 to 550°C with both reactor designs by replacing the catalyst with a similar quantity of granular quartz and/or quartz wool. The reactant concentrations were 4.5% propane and 9% oxygen. Helium diluted the reaction gas mixture and the total flowrate was 50 ml min^{-1} STP. No conversion of propane or formation of products was detected in the blank experiments; thus, the absence of gas-phase-initiated reactions under reaction conditions was assured.

Inside the quartz thermowell was placed an uninsulated wire thermocouple with an outside diameter of 0.5 mm. The quartz reactor was connected with the rest of the reactor system by 0.25-inch stainless steel Swagelok® couplings with Teflon® ferrules. A thermowell was positioned at the reactor outlet, while product gas exited through a sidearm (Figure 3.2). Teflon ferrules made the connection between the thermowell and Swagelok fitting gas-tight.

The quartz reactor was placed inside a cylindrical shaped furnace. The furnace consisted of two semi-circular insulating shells with heating elements inside. The shells were hinged together and could be closed around the reactor. The Swagelok couplings were located outside of the furnace, while both arms of the reactor extended through the 40 mm thick insulating wall of the furnace. A separate thermocouple was placed inside the furnace and positioned at about equal distance between the arms of the quartz reactor, with its tip positioned at the height of the catalyst bed. The temperature measurements of the thermocouple outside of the reactor were used to regulate the operation of the furnace. The thin wire thermocouple inside the reactor measured the actual catalyst bed temperature.

3.2.2 Reactor system and operation

Reactant gas mixtures

Figure 3.3 is a schematic drawing of the reactor system. Unless otherwise stated, all tubing in the reactor system was 0.125-inch (outside diameter) stainless steel and it was connected to the various parts of the system by appropriately sized Swagelok couplings. Feed gases were supplied to the reactor system from gas cylinders and their flowrates were regulated by individual mass-flow controllers (MFC). The MFCs were arranged into two sets A and B. Each set of MFCs produced a different reactant gas mixture that could be fed to the reactor. The numbers of MFCs and types of gases in each set of MFCs were not always as shown in Figure 3.3. These were varied depending on the requirements of each experiment. However, helium was always a component in each MFC set and MFC set A always contained supplies of at least both propane and oxygen in addition to helium. MFC set A produced a reactant gas mixture with a dual purpose. It could be fed to the reactor or directly to the analytic instruments for calibration purposes.

Another MFC, located downstream from MFC set A, regulated the flow of the reactant gas mixture from MFC set A to the reactor. A fraction of the MFC set A reactant gas mixture always bypassed the reactor. A pressure relief valve, on the bypass line, was set to open at about 1.5 bar and thus maintained back pressure to allow the flow controller for the

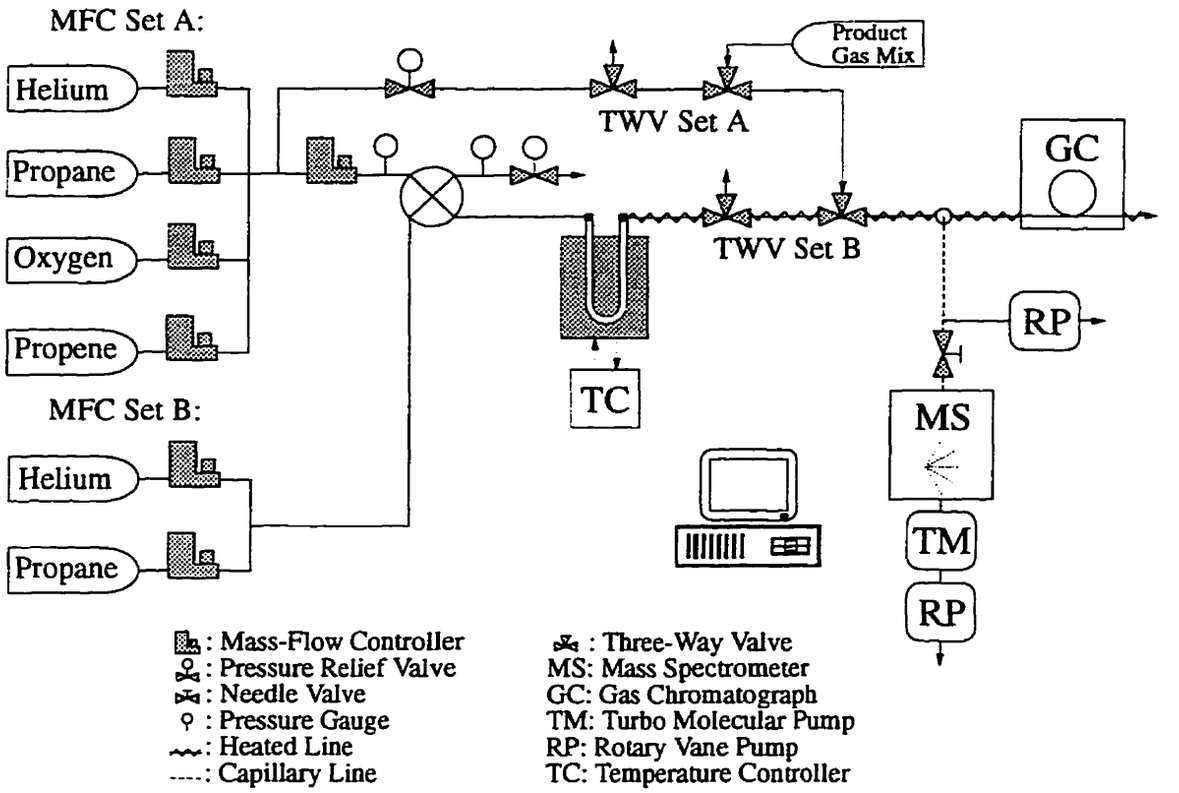

Figure 3.3 Reactor system

MFC set A reactant gas mixture to operate. All of the reactant gas mixture produced by MFC set B was available as feed to the reactor.

Selection of feed to reactor

An air-actuated 4-way valve controlled which of the reactant gas mixtures was fed to the reactor. The gas mixture not fed to the reactor was vented. One pressure gauge was located upstream from the 4-way valve on the MFC set A reactant feed line. A second was positioned downstream from the 4-way valve on the vent line. With the MFC set A reactant mixture fed to the reactor and MFC set B reactant mixture vented, a pressure relief valve was adjusted to equalize the pressure measurements upstream and downstream from the 4-way valve. This was done to equalize the back pressure on the two reactant mixture lines and avoid downstream pressure fluctuations when step-changes were made between reactant mixtures. With the method employed it was assumed of course that the pressure drop across the 4-way valve was negligible. This was necessary because placing a pressure gauge between the 4-way valve and reactor would add undesirable void volume to the reactor system.

Valve arrangement for analytical instrument calibration

Two pairs of magnetically actuated 3-way valves (TWV) select which of three gas streams is sent to the analytical instruments. The three gas streams include the product stream from the reactor, a reactant gas mixture (from MFC set A) and a product gas mixture. The valve arrangement allowed for convenient on-line calibration of the analytical instruments with the reactant and product gas mixtures. The product gas mixture (AGA specialty gas) was supplied from a gas cylinder at about 0.25 bar gauge. TWV set B was located downstream from the reactor and upstream from the analytical instruments. It allowed either the reactor product gas stream or the one of the calibration gas streams (reactant or product gas mixtures) to be sent to the analytical instruments. TWV set A allowed either the reactant or product gas mixtures to be sent to TWV set B. The reactant and reactor product gas streams were vented if not sent to the analytical instruments.

Analytical instruments

The gas stream selected by the sets of TWVs is sent to the gas chromatograph (GC). Inside the GC oven was an electrically driven 6-way valve (Carle Model 2018). The gas stream flowed through a sample loop on the 6-way valve and then was vented from the reactor system. During sampling of the gas stream, for GC analysis, the GC carrier gas flushed out the contents of the sample loop.

A tee was located upstream from the GC in which was located the mass spectrometer (MS) sample capillary. The sample capillary line was made of deactivated fused silica, had an inside diameter of 320 μm and a length of about 1.5 m. It was under vacuum and thus extracted a portion of the gas stream and sent it to the MS system. A rotary vane pump (Edwards Model E2M2) maintained the vacuum in the MS sample capillary. A fine needle valve located between the sample capillary and the MS regulated the flow of sample to the MS and thus the internal pressure of the MS. The vacuum within the MS was maintained by a turbo-molecular pump (Balzer Model TPH/TPU 170) with a backing rotary vane pump (Edwards Model EDM2).

Temperature measurement and control

The uninsulated wire thermocouple inside the quartz reactor measured the actual catalyst temperature. Another insulated thermocouple was placed inside the furnace between the arms of the reactor with its tip positioned at the height of the catalyst. Transient experimental conditions could cause fluctuations in the catalyst temperature. Thus for stable temperature control, the thermocouple outside of the reactor was connected to the temperature control unit (Eurotherm Series 560) that regulated the operation of the furnace.

Reactor system control

A personal computer (386 processor, 4 MB RAM) with the Styrman® control program operated the reactor system. Styrman is a Visual Basic® program that operated the mass flow controllers, the 3-way magnetic valves, the air-actuated 4-way valve and the electrically driven 6-way valve. The computer sent temperature set points via serial communication to the temperature-control unit. The signal from the wire thermocouple inside the reactor was monitored by the computer. Serial communication was maintained between the computer and the MS via an interface instrument (Balzer QDP 101). The computer could command the MS to perform scans at specific intervals, the results of which were acquired by the computer and recorded in log files. In addition, all flowrate and temperature measurements could be recorded in log files. The Styrman program could also carry out an experimental run automatically by operating from a command file.

3.3 Analytical methods

3.3.1 Gas chromatography

The GC (Varian Model 3300) was equipped with a capillary column (Chrompack Poraplot Q), methanizer catalyst and flame ionization detector (FID). The capillary column had a length of 25 m and an inside diameter of 0.32 mm. Helium was used as the carrier gas and it was supplied at a pressure of about 1.7 bar gauge to the injector. The volume of the sample collected in the six-way valve sample loop was approximately 0.1 ml. The quantity of sample injected into the GC column could be adjusted with a split ratio valve at the injector. The split ratio was adjusted to maximize the detection sensitivity while maintaining an effective separation of components. During an analysis, the GC oven was first operated isothermally at 50°C for 6 min. The temperature was then ramped at a rate of 10°C min^{-1} to 120°C and finally maintained at 120°C for 2 min. Thus, the total analysis time was 15 min. The cool-down time for the GC was about 7 min.

The separated components from the column were fed into the methanizer reactor which consisted of a U-shaped 0.125 inch diameter stainless steel tube, packed with about 0.5 g of the methanizer catalyst. Hydrogen was also fed to the inlet of the methanizer reactor at a flowrate of about 30 ml min^{-1} STP. The methanizer reactor was maintained at 350°C in a separate heated zone within the GC. The methanizer catalyst consisted of a 2 wt% coating of nickel on Chromosorb G support. It was prepared by adding the Chromosorb G to a quantity of nickel nitrate solution just sufficient to wet the support without excess. The slurry was dried on a hot plate at about 80°C with constant stirring. Once dry, the catalyst was calcined in air at 400°C for 2 h.

The function of the methanizer catalyst was to reduce carbon monoxide and carbon dioxide to methane for detection by the FID. The quantity of hydrogen supplied to the

methanizer reactor was sufficient to both completely reduce the carbon oxides and fuel the FID. The FID was supplied directly with only air at a flow rate of about 300 ml min^{-1}. The GC was calibrated for detection of propane by analysis of the reactant gas mixture which typically contained between 3 to 6% propane. Analysis of the product gas mixture calibrated the GC for detection of propene, carbon monoxide and carbon dioxide. The product gas mixture contained 2.01% propene, 0.99% carbon monoxide and 1.03% carbon dioxide in helium. The GC could not detect oxygen or water and thus only a carbon mass balance could be determined. Concentrations of oxygen and water could only be determined indirectly, based on the analysis of the carbon containing components. The total quantity of carbon determined by GC analysis at the reactor outlet was typically between 90 and 110% of the total carbon fed to the reactor. The GC was tested with varying concentrations of the components to ensure a linear response and that the methanizer catalyst completely converted the carbon oxides. In Appendix A, sample GC analysis data are shown and the method of calculation of component concentrations is demonstrated.

3.3.2 Mass spectrometry

Mass spectrometry (MS) analyses can be performed at high frequency. The time required for a mass scan is usually on the order of a tenth of a second or less. It is thus a valuable gas phase chemical analysis tool for non-steady-state operation of chemical reactions. This section presents the principles of quantitative analysis by mass spectrometry as well as some of the practical problems. The system of chemical species considered here is rather complex with many species producing ions with the same mass. Considerable time and effort in this project has been spent on finding reliable methods of collecting and analyzing MS data. A brief description of the data analysis and calibration techniques used to overcome the practical problems is given.

In the simplest method of qualitative analysis by mass spectrometry the sensitivity coefficients, S_{ij}, must be known for each component, j, at each of the mass values, i. The number of mass peaks, n, must equal the number of components in the mixture. If the concentrations of the components of the mixture are partial pressures, p_j, the sensitivity coefficients express the mass peak intensity per unit pressure. Then a set of n simultaneous linear equations must be solved to determine the partial pressure of each component.

$$
\begin{aligned}
S_{11}p_1 + S_{12}p_2 + \dots + S_{1n}p_n &= I_1 \\
S_{21}p_1 + S_{22}p_2 + \dots + S_{2n}p_n &= I_2 \qquad (3.1) \\
\dots\dots\dots\dots\dots\dots\dots\dots & \\
S_{n1}p_1 + S_{n2}p_2 + \dots + S_{nn}p_n &= I_n
\end{aligned}
$$

Thus the sum of ion contributions from each component equals the total ion current intensity, I_i, at each mass peak, i, in the spectrum. The above system of equations can be

expressed in matrix notation as:

$$\boldsymbol{Sp} = \boldsymbol{I} \tag{3.2}$$

The sensitivity coefficients must be determined by analysis of calibration mixtures in which the concentration of each component is known.

The MS system used consisted of an analyzer (Balzer QMA 140), control unit (Balzer QMS 311) and a computer interface unit (Balzer QDP 101). Figure 3.4 is a simple schematic of the internal parts of the MS analyzer unit and its gas sampling system. The sample gas mixture flowed through a tube near the outlet of the reactor system. Through the heated capillary, placed inside the tube, a portion of the sample mixture flowed to the MS. The capillary was about 1.5 m long. The quantity of the sample mixture entering the MS was dependent on the pressure difference between that of the sample mixture, P_x, and the pressure inside the MS chamber, P_{MS}. The sample molecules were ionized in an axial beam ion source. This was an electron impact type ion source with the electron beam and ion extraction in an axial direction. A rhenium cathode filament was used and the emission current was 0.9 mA. The ionizing electron energy was 95 eV. The quadrupole mass filter allowed only ions of a selected mass to reach the faraday cup ion detector where the ion current was measured. The pressure of the sample mixture was slightly above atmospheric and the internal pressure of the MS was about 10^{-8} bar. The sample mixture concentration may be unknown or it may be the calibration mixture of known concentration. One practical problem was the difficulty to ensure that the total pressure of the calibration mixture was identical to that of the unknown mixture. Very small pressure differences in the sample mixtures could cause large changes in the quantity of the sample entering the MS.

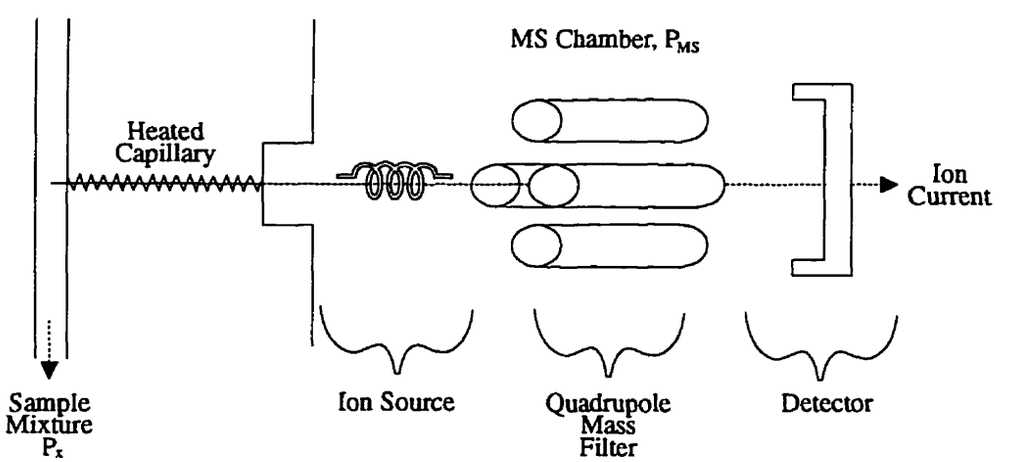

Figure 3.4 Schematic of MS and sampling system

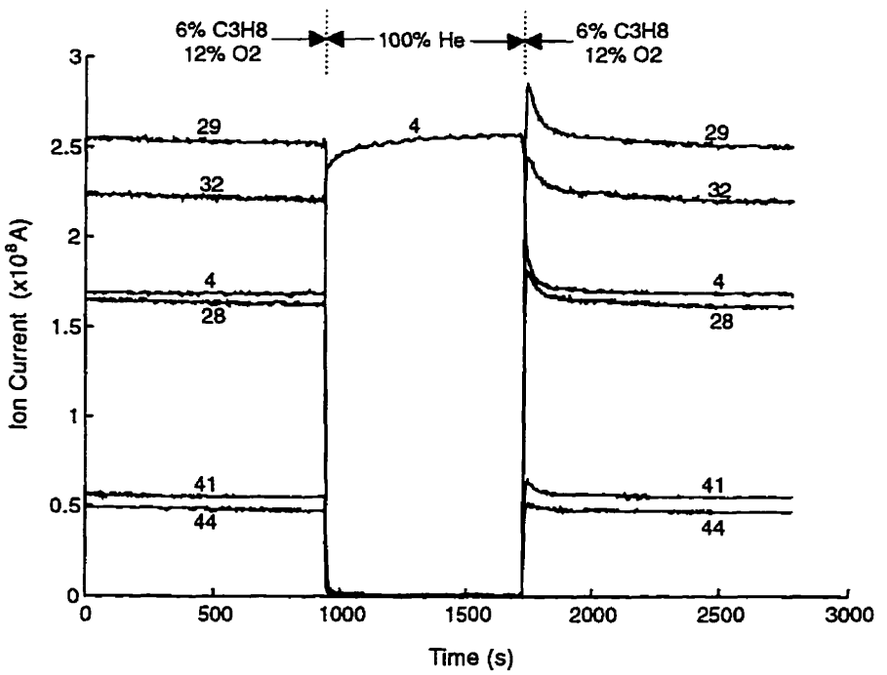

Figure 3.5 MS signal response to step-changes in sample concentration

An even more serious problem with the application of quantitative mass spectrometry, is that the pressure inside the MS, is a function of the sample composition. The quantity of the sample entering the MS through the capillary depends on its composition. Figure 3.5 shows some raw MS data. The intensity of the mass peaks at 4, 28, 29, 32, 41 and 44 m/e were measured while the sample mixture contained 6% propane and 12% oxygen in helium. The mass peaks at 4 and 32 m/e were from helium and oxygen, respectively, while those at 28, 29, 41 and 44 m/e were from propane. At 940 s, with a switch of the 4-way valve, the sample mixture was changed to 100% helium and then at 1730 s it was changed back to the original propane, oxygen and helium mixture. After the first switch to pure helium, the mass signals from both propane and oxygen dropped quickly to zero, while that of helium, 4 m/e, increased slowly until the switch back to propane and oxygen was made. At this point, the mass signals from propane and oxygen increased quickly but then decreased along with the helium mass signal. It was apparent from Figure 3.5 that two simultaneous transients were occurring. There were, of course, changes in the sample mixture causing transients depending on the gas-holdup and dispersion in the reactor system. These transient responses should occur probably over some seconds. But also, there was a much slower transient caused by the internal pressure of the MS, P_{MS}, lasting over some minutes. After the switch to pure helium, the internal pressure of the MS slowly increased and after the switch back to propane and oxygen, it decreased. If the compositions of the calibration mixture and unknown mixture differ greatly or even if the composition of the unknown

mixture itself vary greatly, pressure differences inside the MS are clearly important. In short, the application of qualitative mass spectrometry is severely limited by the direct application of equation 3.2, unless accurate measurements of the pressure inside the mass spectrometer and the pressure of each sample mixture are available.

In this work we used a method of treatment of the mass spectrometry data, that avoids the problems described above. The main features of the method are that the sample (unknown and calibration) mixtures were allowed to be at different and unknown pressures. In addition a normalizing procedure was used that allows the pressure inside the MS to vary without affecting the accuracy of the analysis. The method is presented in detail in Appendix B. It was adapted from a more general method first described by Ruth [72]. The limitations of the method are that the identity of every component in the mixture to be analyzed must be known and included in the analysis. Also, if more than one calibration mixture is used, at least one of the components must be present in all of the mixtures.

The components included in the analysis were helium, water, carbon monoxide, propane, oxygen, propene and carbon dioxide. Table 3.1 shows the primary mass peaks, which are the tallest mass peaks in the spectrum of each component. Some of the components produce secondary mass peaks which have the same mass as the primary mass peak of other components. The ratio of the primary and secondary mass peaks is

$$r_{ij} = \frac{I_{ij}}{I_{Pj}} \tag{3.3}$$

and its value, measured at an ionizing electron energy of 95 eV, is also shown in Table 3.1.

Table 3.1: Primary and Secondary Mass Peaks of Components

Component	Primary m/e (I_{Pj})	Secondary m/e (I_{ij})	Ratio (r_{ij})
helium	4	-	-
water	18	-	-
carbon monoxide	28	-	-
propane	29	28	0.67
		41	0.23
		44	0.22
oxygen	32	-	-
propene	41	28	0.03
carbon dioxide	44	28	0.16

Three different calibration gas mixtures were used. The first was the feed gas which typically contained 3 to 6% propane and 6 to 12% oxygen in helium. The second was a product gas mixture containing 2.01% propene, 0.99% carbon monoxide and 1.03% carbon

dioxide in helium. Finally, to calibrate the MS for analysis of water, water was produced by reacting propane and oxygen over a platinum mesh catalyst. The feed concentrations of propane and oxygen were 3 and 6% respectively, the reaction temperature was 550°C and about 0.4 g of platinum mesh was used. At these conditions, the limiting reactant was oxygen, and the products almost entirely consisted of carbon dioxide, water and unreacted propane. But traces of carbon monoxide and propene were also present. The product water concentration was approximately 5% as determined by GC analysis.

Appendix B describes in detail the method of treatment of the calibration data. Recalibration of the MS was carried out daily during periods when experiments involving MS analysis were carried out. Figure 3.6 shows the calculated concentrations for the raw data in Figure 3.5, after application of the method of data treatment in Appendix B. The pressure transient, evident in the MS signal data, is removed from the concentration data. At steady-state operation, typically the total concentrations of carbon and oxygen in the product gas, determined by MS analysis, were between 90 and 110% of their concentrations in the reactor feed.

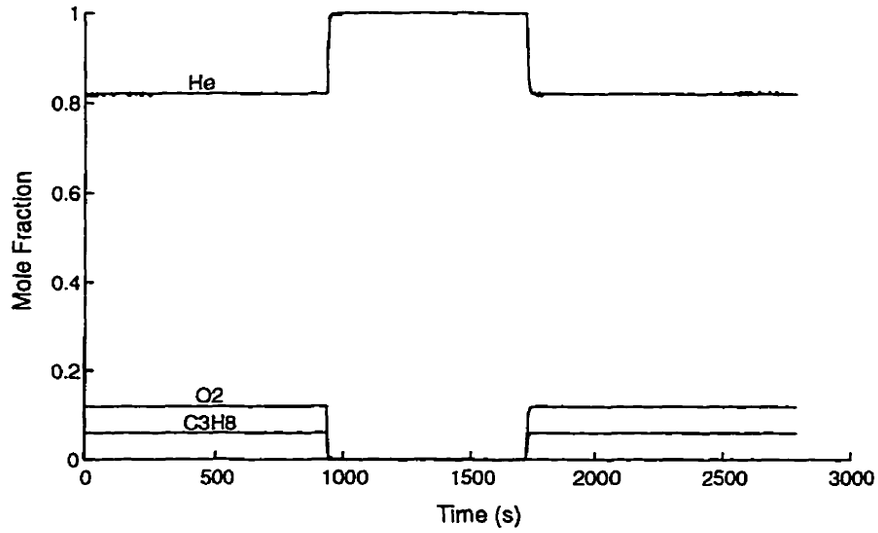

Figure 3.6 Calculated concentrations from step-changes in sample concentration

4. Steady-state kinetics

This chapter presents the results of a study of the steady-state reaction kinetics of the oxidative dehydrogenation of propane over Mg-V-O by nonlinear regression analysis. Both simple power law and mechanistic models were tested on kinetic data collected over a range of reaction conditions. The results of this study have been previously published [73].

4.1 Experimental plan and modelling methods

The reaction kinetics were studied by performing a full two-level factorial design of experiments around a set of standard reaction conditions. Such a design of experiments not only efficiently covered the experimental volume, but also minimized correlations between the factors of interest, so that the influence of each factor was maximized [74]. The factors chosen were the reactant concentrations (propane, oxygen and propene) and the reaction temperature. Propene was included as a reactant because its rate of combustion to carbon oxides was also of interest. Table 4.1 lists the levels of the factors used. In all experiments, the mass of Mg-V-O catalyst used was 15 mg and the total flow rate of reactants including the diluting helium was 50 ml min^{-1} (STP). At the reaction conditions used, the only carbon-containing products were propene, carbon monoxide and carbon dioxide. The standard set of reaction conditions were levels of the factors midway between the high and low levels in the factorial design, except the propene concentration.

Table 4.1
High and low levels of factors

Factor	Low level	High level
Propane Conc. (%)	3	6
Oxygen Conc. (%)	6	12
Propene Conc. (%)	0	2
Temperature (°C)	510	550

Table 4.2 contains the measured outlet concentrations and calculated reactant conversions for the factorial design conditions. Some difficulties were encountered in collecting the data. The selectivity of the catalyst seemed to be dependent on previous conditions to which it had been exposed. Details of the methods used to collect the data are dicussed in Chapter 5. Replicate experiments at three sets of factorial design conditions were performed. In addition, eight replicates at the standard reaction conditions were included in the analysis.

Table 4.2
Product concentrations and reactant conversions at experimental conditions

Inlet Conc. (%)			Temp.	Outlet Concentration (%)[a]					C_3H_8	O_2	Carbon
C_3H_8	O_2	C_3H_6	(°C)	CO	CO_2	C_3H_6	C_3H_8	O_2[b]	conv. (%)	conv. (%)[b]	balance[c]
6	6	0	510	0.083	0.126	0.101	5.83	5.64	2.85	5.96	100.5
3	12	0	510	0.087	0.286	0.040	2.84	11.40	5.47	4.98	98.7
6	12	0	510	0.086	0.328	0.082	5.78	11.31	3.66	5.74	99.5
3	6	0	510	0.038	0.188	0.035	2.89	5.63	3.67	6.24	98.8
6	6	0	550	0.183	0.261	0.268	5.58	5.22	6.94	13.05	99.5
3	12	0	550	0.162	0.452	0.125	2.67	11.00	10.98	8.37	97.7
6	12	0	550	0.212	0.464	0.234	5.54	10.86	7.66	9.48	101.4
3	6	0	550	0.107	0.191	0.139	2.76	5.49	7.93	8.53	96.1
6	6	2	510	0.185	0.320	1.908	5.92	5.30	1.28	11.72	100.0
3	12	2	510	0.272	0.411	1.880	2.89	11.06	3.58	7.84	97.6
6	12	2	510	0.236	0.432	1.876	5.90	11.07	1.64	7.78	100.5
3	6	2	510	0.171	0.299	1.944	2.90	5.33	3.37	11.18	100.1
6	6	2	550	0.631	0.976	1.891	5.57	3.69	7.10	38.46	98.9
3	12	2	550	0.509	0.831	1.794	2.76	10.12	8.01	15.63	98.1
6	12	2	550	0.652	1.045	1.896	5.54	9.55	7.69	20.42	100.2
3	6	2	550	0.421	0.716	1.837	2.81	4.49	6.26	25.09	97
4.5	9	0	530	0.097	0.256	0.122	4.26	8.40	5.31	6.66	98.4[d]
4.5	9	0	530	0.104	0.266	0.109	4.27	8.38	5.16	6.88	99.4[d]
4.5	9	0	530	0.108	0.289	0.113	4.25	8.34	5.45	7.39	99.5[d]
4.5	9	0	530	0.071	0.246	0.102	4.29	8.46	4.60	6.04	101.1[d]
4.5	9	0	530	0.075	0.279	0.100	4.28	8.40	4.85	6.70	98.1[d]
4.5	9	0	530	0.104	0.266	0.118	4.26	8.38	5.36	6.93	98.4[d]
4.5	9	0	530	0.098	0.232	0.117	4.27	8.44	5.06	6. 23	98.2[d]
4.5	9	0	530	0.106	0.273	0.119	4.25	8.36	5.45	7.09	99.0[d]
3	12	0	510	0.087	0.298	0.025	2.85	11.39	5.13	5.10	97.5[e]
6	6	0	550	0.173	0.260	0.263	5.59	5.23	6.79	12.77	99.4[e]
6	6	2	550	0.548	0.831	1.882	5.66	4.03	5.70	32.76	98.2[e]

[a]Normalized carbon distribution.
[b]Calculated from normalized carbon distribution in products and assuming the only additional product is water.
[c]Ratio of carbon in products to carbon in reactants.
[d]Standard condition experiments.
[e]Replicate experiments.

Nonlinear regression analysis was used to examine the fit of different kinetic models to the data. Calculations were performed by a Fortran program using NAG sub-routines. For a given model, reaction rates were integrated over the mass of catalyst at each of the experimental conditions to calculate the outlet reactant and product concentrations predicted by the model. A derivative-free algorithm, supplied with initial parameter values, searched for the values of the model parameters that minimized the sum of the squared residuals. In some cases it was found the resulting parameter values the apparently minimized the sum of the squared residuals were dependent on the initial parameter values supplied to the program. As a result, the search algorithm was restarted with a range of initial parameter values to try to ensure that the final sum of the squared residuals was truly a global minimum as opposed

to only a localized minimum. The linear correlation of parameters was calculated and used as an estimate of the correlation between parameters in the non-linear models.

Since only GC analysis was performed on the reaction products independent measurements of only propane, propene, carbon dioxide and carbon monoxide concentrations were made. Only these components were included in the regression analysis. In some cases, factors were centered about their mean values. For example, when the partial pressure of a species is raised to a power in a rate expression the following form was assumed:

$$r_i = k_i\left(\frac{P}{P^m}\right)^a \tag{4.1}$$

where the partial pressure (P) was divided by an approximated mean value (P^m). Such a centering procedure eases the parameter search by minimizing correlations between the order (a) and the pre-exponential factor. The distribution of the factors about their mean is emphasized instead of their absolute values [75]. Similarly, rate constants were expressed in the following Arrhenius form:

$$k_i = k_{i0}\exp\left[-\frac{E_{ai}}{R}\left(\frac{1}{T}-\frac{1}{T^m}\right)\right] \tag{4.2}$$

where the inverse temperature is centred about the inverse mean temperature, such that the fitted pre-exponential factors are determined at the mean temperature (530°C).

In order to reduce the number of parameters to be fitted in the regression analysis, constant estimated values of the entropy change of adsorption (ΔS°_{ads}) at standard conditions (1 atm and 25°C) were used. The translational contribution to the gas phase entropy was calculated from quantum mechanical theory, while the vibrational contribution can be considered negligibly small for low molecular weight molecules [76]. With literature values for the total gas phase entropy for each component [77], the rotational contribution was calculated. Mixture effects on the gas phase entropy were considered negligible. It was assumed that upon adsorption, a molecule loses all of its translational entropy and two thirds of its rotational entropy. Such an estimate of ΔS°_{ads} must be considered a maximum since it is possible for a molecule to have some limited mobility on the catalyst surface and thus retain part of its translational entropy. The estimated values of ΔS°_{ads} for oxygen, propene and carbon monoxide were -178, -230 and -174 J mol^{-1} K^{-1}, respectively. The adsorption equilibrium constant of a species may be expressed as

$$K_{ads} = \exp\left(\frac{\Delta S^\circ_{ads}}{R}-\frac{\Delta H^\circ_{ads}}{RT}\right) \tag{4.3}$$

and thus only the enthalpy change upon adsorption (ΔH°_{ads}) is left as an adjustable parameter. The development of equation 4.3 and the calculation of the ΔS°_{ads} values is shown in greater detail in Appendix C.

The variance of results from the replicated conditions was used to estimate the error resulting from uncontrollable variations during the experiments. For a model to be considered adequate, the variance of the model from the data ought to be no greater than the estimated uncontrollable experimental variance. The two variances were compared with an F-test at a 95% significance level. In the case of nonlinear regression, the F-distribution is not strictly applicable, but without knowledge of the true distribution it still provides some measure of the lack of fit of the model [78].

4.2 Power law models

Power law models examined the effect that gas phase concentrations of the reactants had on the reaction rates. However, before power law rate models could be constructed, reaction schemes had to be selected. In the following series type reaction scheme, all propene is produced from the oxidation of propane and all carbon oxides are produced from the further oxidation of propene:

$$C_3H_8 + 0.5O_2 \rightarrow C_3H_6 + H_2O \quad (4.4)$$

$$C_3H_6 + 3O_2 \rightarrow 3CO + 3H_2O \quad (4.5)$$

$$C_3H_6 + 4.5O_2 \rightarrow 3CO_2 + 3H_2O \quad (4.6)$$

The corresponding rate equations are

$$r_1 = k_1\left(\frac{P_{C_3H_8}}{P^m_{C_3H_8}}\right)^a\left(\frac{P_{O_2}}{P^m_{O_2}}\right)^b \quad (4.7)$$

$$r_2 = k_2\left(\frac{P_{C_3H_6}}{P^m_{C_3H_6}}\right)^c\left(\frac{P_{O_2}}{P^m_{O_2}}\right)^d \quad (4.8)$$

$$r_3 = k_3\left(\frac{P_{C_3H_6}}{P^m_{C_3H_6}}\right)^e\left(\frac{P_{O_2}}{P^m_{O_2}}\right)^f \quad (4.9)$$

Expressions for the rate constants in the form of Equation 4.2, were used. This model will be called PL1. An alternative to the above scheme, is to produce all carbon dioxide from the further oxidation of carbon monoxide. In such a scheme reaction 4.6 is replaced by

$$CO + 0.5O_2 \rightarrow CO_2 \quad (4.10)$$

and Equation 4.9 becomes

$$r_3 = k_3\left(\frac{P_{CO}}{P_{CO}^m}\right)^e\left(\frac{P_{O_2}}{P_{O_2}^m}\right)^f \qquad (4.11)$$

This alternative model will be called PL2. Table 4.3 shows the values of the fitted parameters for PL1 and PL2 and their approximate 95% confidence intervals. In Table 4.4, the sum of the squared residuals (SS) for PL1 and PL2 are compared. The two resulting power law models had an equal number of parameters (12). Both models fit the data rather well with no significant lack of fit indicated for either. Also, the linearly estimated correlations between parameters was very low, being in all cases less than 0.6.

Table 4.3
Parameters of PL1 and PL2 by least-squares regression

Model	Parameter	Value	Confidence Interval (95%)	Units
PL1	k_{10}	7.45	$\pm 4.97\times10^{-1}$	ml STP min^{-1} $(g\ cat)^{-1}$ $bar^{-(a+b)}$
	k_{20}	2.74	$\pm 2.77\times10^{-1}$	ml STP min^{-1} $(g\ cat)^{-1}$ $bar^{-(c+d)}$
	k_{30}	5.34	$\pm 2.64\times10^{-1}$	ml STP min^{-1} $(g\ cat)^{-1}$ $bar^{-(e+f)}$
	E_{a1}	1.24×10^{5}	$\pm 2.11\times10^{4}$	J mol^{-1}
	E_{a2}	1.23×10^{5}	$\pm 2.62\times10^{4}$	J mol^{-1}
	E_{a3}	1.02×10^{5}	$\pm 1.41\times10^{4}$	J mol^{-1}
	a	5.30×10^{-1}	$\pm 1.87\times10^{-1}$	
	b	2.89×10^{-1}	$\pm 1.60\times10^{-1}$	
	c	3.80×10^{-1}	$\pm 6.50\times10^{-2}$	
	d	1.65×10^{-1}	$\pm 1.78\times10^{-1}$	
	e	2.56×10^{-1}	$\pm 2.93\times10^{-2}$	
	f	2.82×10^{-1}	$\pm 1.06\times10^{-1}$	
PL2	k_{10}	7.45	$\pm 5.03\times10^{-1}$	ml STP min^{-1} $(g\ cat)^{-1}$ $bar^{-(a+b)}$
	k_{20}	8.15	$\pm 3.78\times10^{-1}$	ml STP min^{-1} $(g\ cat)^{-1}$ $bar^{-(c+d)}$
	k_{30}	1.23×10^{1}	± 1.44	ml STP min^{-1} $(g\ cat)^{-1}$ $bar^{-(e+f)}$
	E_{a1}	1.24×10^{5}	$\pm 2.11\times10^{4}$	J mol^{-1}
	E_{a2}	1.08×10^{5}	$\pm 1.27\times10^{4}$	J mol^{-1}
	E_{a3}	3.11×10^{4}	$\pm 2.27\times10^{4}$	J mol^{-1}
	a	5.31×10^{-1}	$\pm 1.86\times10^{-1}$	
	b	2.89×10^{-1}	$\pm 1.60\times10^{-1}$	
	c	2.96×10^{-1}	$\pm 2.95\times10^{-2}$	
	d	2.43×10^{-1}	$\pm 9.11\times10^{-2}$	
	e	6.22×10^{-1}	$\pm 1.06\times10^{-1}$	
	f	1.51×10^{-1}	$\pm 1.24\times10^{-1}$	

Table 4.4
Sum of squared residuals (SS) for PL1 and PL2

Model	Number of Parameters	SS
PL1	12	7.47×10^{-2}
PL2	12	7.53×10^{-2}

Power law models based on other reaction schemes were examined. One was a completely competitive reaction scheme, whereby propene, carbon monoxide and carbon dioxide are all produced from the oxidation of propane. The SS for this model was very high (6.2×10^{-1}) and it was rejected due to lack of fit. The residuals were particularly high for experiments in which propene was a feed reactant, indicating of course that such a reaction scheme could not adequately describe the quantities of carbon oxides produced only from propane. Reaction schemes that combined the series and competitive schemes were also examined. These models have an increased number of parameters because they allow for alternative routes for producing carbon oxide: either directly from propane or from the intermediate propene. There were high correlations between parameters in these models and only a small decrease in the SS was achieved compared to the series models. The simple series type models adequately described the data and produced well-defined parameters.

In both the series-type power law models the power on propane pressure was about 0.5 and on propene about 0.3. The power on oxygen pressure tended to be less, ranging from 0.15 to 0.3. Moreover, the confidence intervals were larger for the power of oxygen pressure, showing they were less significant. The general conclusion could be drawn that the hydrocarbon gas phase partial pressures tended to have a greater effect on the reaction rates than did oxygen. From a mechanistic viewpoint, it suggested that the catalyst at these reaction conditions was nearly saturated with oxygen or completely oxidized.

4.3 Mechanistic Models

To construct mechanistic models, plausible reaction mechanisms must be formulated based on physical and chemical grounds. Four different mechanistic models are formulated and compared here. Other models were tested; however those presented here show interesting characteristics of the data and, more or less, successfully describe the data.

The first step may be the adsorption of propane or the reaction of propane with the catalyst surface. Since the alkane lacks π–bonding electrons, it is reasonable to assume that propane, if it adsorbs on the surface, is immediately dehydrogenated to propene, upon reaction with surface oxygen

$$C_3H_8 + \bullet \rightarrow \bullet C_3H_8 \text{ (slow)} \qquad (4.12a)$$

$$\bullet C_3H_8 + \bullet O \rightarrow \bullet C_3H_6 + H_2O + \bullet \text{ (fast)} \qquad (4.12b)$$

where • represents a free surface site. An alternative to the above is that gas phase propane reacts directly with surface oxygen and is dehydrogenated, producing propene

$$C_3H_8 + \bullet O \rightarrow \bullet C_3H_6 + H_2O \qquad (4.13)$$

In either case, it is assumed that an equilibrium is established between adsorbed and gas phase propene:

$$\bullet C_3H_6 \leftrightarrow \bullet + C_3H_6 \qquad (4.14)$$

Finally, the adsorbed propene may further react with surface oxygen to produce carbon oxides

$$\bullet C_3H_6 + 3(n+1)\ \bullet O \rightarrow 3\ CO_n + 3\ H_2O + 3n + 4\bullet \qquad (4.15)$$

where n equals 1 or 2. Oxygen may be adsorbed from the gas phase onto the catalyst surface

$$O_2 \leftrightarrow 2\ \bullet O \qquad (4.16)$$

Reaction products may also be adsorbed. An alternative to oxygen being supplied to the surface by adsorption from the gas phase, is to consider reactions 4.12b or 4.13 and 4.15 to reduce the catalyst surface. Gas phase oxygen, then in a separate reaction with its own kinetics, re-oxidizes the catalyst surface

$$O_2 \rightarrow 2\ \bullet O \qquad (4.17)$$

The relative rates of the reducing and oxidizing reactions govern the oxidation state of the catalyst. This redox type of reaction scheme represents Mars-Van Krevelen type kinetics.

For all of the mechanistic models, it was not possible to account for the oxidation of carbon monoxide to carbon dioxide or express their production with separate equations without introducing significant correlations among parameters. This is due to the small variation in the ratio of the carbon oxide products in the data collected. Thus all of the mechanistic models developed only estimate the total quantities of carbon oxides produced. For purposes of accurately estimating the consumption of oxygen, all of the mechanistic models contained a power law model that determined the ratio of carbon dioxide to carbon monoxide, which was normally close to 1.5.

The reactions for the first model are 4.12 and 4.15 above. Oxygen, propene and carbon monoxide compete for the same adsorption sites. This kinetic model will be called LH1. The appropriate rate equations are:

$$r_1 = k_1 P_{C_3H_6} \theta^a \qquad (4.18)$$

$$r_2 = k_2 \theta_{C_3H_6} \theta_O^b \qquad (4.19)$$

where θ represents the fraction of free sites on the catalyst surface. Equation 4.19 expresses the total production of carbon oxides. The expressions for the fractional coverage of oxygen

(θ_O) and propene (θ_{C3H6}), based on Langmuir adsorption isotherms, are

$$\theta_O = \frac{\sqrt{K_{O_2} P_{O_2}}}{1 + K_{C_3H_6} P_{C_3H_6} + \sqrt{K_{O_2} P_{O_2}} + K_{CO} P_{CO}} \tag{4.20}$$

$$\theta_{C_3H_6} = \frac{K_{C_3H_6} P_{C_3H_6}}{1 + K_{C_3H_6} P_{C_3H_6} + \sqrt{K_{O_2} P_{O_2}} + K_{CO} P_{CO}} \tag{4.21}$$

Including carbon monoxide adsorption improved the fit of the model. In all models tested in which oxygen competed with other species for adsorption sites, the least squares solution for the parameters tended towards a small coverage of oxygen. The result was that ΔH°_{O2} became highly correlated with k_{20} such that the least squared solution could not be found. To prevent this correlation, a lumped parameter expressing $k_{20} K_{O2}^{0.5b}$ was estimated. This approach tested the suitability of the model and avoided excessive correlation of parameters.

In the next model, oxygen adsorbs on separate sites. In addition, it will be assumed that gas phase propane reacts directly with oxygen on the catalyst surface. This model will be called LH2 and its reactions are 4.13 and 4.15. The LH2 rate equations are

$$r_1 = k_1 P_{C_3H_6} \theta_O \tag{4.22}$$

$$r_2 = k_2 \theta_{C_3H_6} \theta_O \tag{4.23}$$

Oxygen and propene adsorbed on separate sites and including carbon monoxide adsorption did not improve the fit of the model. The expressions for the fractional coverage of oxygen (θ_O) and propene (θ_{C3H6}) are

$$\theta_O = \frac{\sqrt{K_{O_2} P_{O_2}}}{1 + \sqrt{K_{O_2} P_{O_2}}} \tag{4.24}$$

$$\theta_{C_3H_6} = \frac{K_{C_3H_6} P_{C_3H_6}}{1 + K_{C_3H_6} P_{C_3H_6}} \tag{4.25}$$

For the LH2 model, the entropy of adsorption of oxygen was not estimated, thus one additional parameter was used to describe the adsorption of oxygen. The expression used for the adsorption equilibrium constant for oxygen, in this case, was:

$$K_{O_2} = K^{\circ}_{O_2} \exp\left[\frac{-\Delta H^{\circ}_{O_2}}{R}\left(\frac{1}{T} - \frac{1}{T^m}\right)\right] \tag{4.26}$$

Upon fitting the LH2 model it was found that the parameter K°_{O2}, was highly correlated with k_{10}, k_{20}, E_{a1} and E_{a2}. Attempts at reducing the correlation by estimating lumped parameters failed. But despite the correlation problems, a least-squares solution was found.

Table 4.5 shows the values of the fitted parameters for LH1 and LH2 and their confidence intervals. No significant lack of fit was indicated for either model.

The rate equations for the first Mars-Van Krevelen type kinetic model, which will be called MV1, are

$$r_1 = k_1 P_{C_3H_8} \theta^{\alpha} \tag{4.27}$$

$$r_2 = k_2 \theta_{C_3H_6} (1-\beta) \tag{4.28}$$

$$r_3 = k_3 P_{O_2} \beta \tag{4.29}$$

where β represents the degree of reduction of the catalyst. Equations 4.27 and 4.28 above represent the rate at which the catalyst is reduced, while equation 4.29 is the rate at which it is re-oxidized. At steady-state, the total rate of oxygen consumption from the catalyst surface, must equal the rate at which it is replaced from the gas phase. Thus, it is possible to

Table 4.5
Parameters of LH1 and LH2 by least-squares regression

Model	Parameter	Value	Confidence Interval (95%)	Units
LH1	k_{10}	1.48×10^{2}	$\pm1.70\times10^{1}$	ml STP min^{-1} $(g\ cat)^{-1}$ bar^{-1}
	$k_{20}K_{O2}^{0.5b}$	3.03×10^{1}	$\pm1.78\times10^{1}$	ml STP min^{-1} $(g\ cat)^{-1}$
	E_{a1}	1.04×10^{5}	$\pm2.16\times10^{4}$	J mol^{-1}
	E_{a2}	1.05×10^{5}	$\pm3.04\times10^{4}$	J mol^{-1}
	ΔH°_{C3H6}	-2.20×10^{5}	$\pm4.69\times10^{3}$	J mol^{-1}
	ΔH°_{CO}	-1.85×10^{5}	$\pm6.84\times10^{3}$	J mol^{-1}
	a	1.84×10^{-1}	$\pm9.83\times10^{-2}$	
	b	5.68×10^{-1}	$\pm3.43\times10^{-1}$	
LH2	k_{10}	3.36×10^{2}	$\pm1.91\times10^{2}$	ml STP min^{-1} $(g\ cat)^{-1}$ bar^{-1}
	k_{20}	3.16×10^{1}	$\pm1.84\times10^{1}$	ml STP min^{-1} $(g\ cat)^{-1}$
	E_{a1}	1.23×10^{4}	$\pm1.25\times10^{5}$	J mol^{-1}
	E_{a2}	2.34×10^{4}	$\pm1.31\times10^{5}$	J mol^{-1}
	ΔH°_{C3H6}	-2.29×10^{5}	$\pm1.53\times10^{3}$	J mol^{-1}
	ΔH°_{O2}	3.56×10^{5}	$\pm3.59\times10^{5}$	J mol^{-1}
	K°_{O2}	3.58	±7.18	bar^{-1}

solve for β as

$$\beta = \frac{0.5k_1 P_{C_3H_8}\theta^a + \frac{3(3x+2)}{2(x+1)}k_2\theta_{C_3H_6}}{k_3 P_{O_2} + \frac{3(3x+2)}{2(x+1)}k_2\theta_{C_3H_6}} \tag{4.30}$$

where x is the ratio of carbon dioxide to carbon monoxide. Propene was assumed to be the only species that adsorbs to the catalyst surface, and its fractional coverage was represented by

$$\theta_{C_3H_6} = \frac{K_{C_3H_6}P_{C_3H_6}}{1 + K_{C_3H_6}P_{C_3H_6}} \tag{4.31}$$

In MV1 the rate of reaction of propane is assumed to depend on the fraction of free sites (equation 4.27). An alternative is to have it depend on the quantity of oxygen on the catalyst or the degree of oxidation of the catalyst. Such a kinetic model will be called MV2. Its rate equations are the same as those for MV1 except equation 4.27 is replaced by

$$r_1 = k_1 P_{C_3H_8}(1-\beta) \tag{4.32}$$

and the corresponding expression for β becomes

$$\beta = \frac{0.5k_1 P_{C_3H_8} + \frac{3(3x+2)}{2(x+1)}k_2\theta_{C_3H_6}}{k_3 P_{O_2} + 0.5k_1 P_{C_3H_8} + \frac{3(3x+2)}{2(x+1)}k_2\theta_{C_3H_6}} \tag{4.33}$$

Table 4.6 shows the values of the fitted parameters and their confidence intervals for both MV1 and MV2. No significant lack of fit was indicated for either model and correlations between parameters were moderate at less than 0.8 in all cases. In Table 4.7, the SS is compared for each of the mechanistic models. The SS values for the mechanistic models do not vary greatly, but the MV2 model does have the lowest SS.

In the LH1 mechanistic model, all of the parameters included in the regression analysis were significant. However, the value of parameter a was small at 0.18, indicating the reaction rate of propane has little dependence on the fraction of free sites. The value of parameter b is also small at 0.57. This power on the fraction of oxygen coverage was included because it was thought that the rate of reaction 4.15 may have a higher order dependence on the oxygen coverage. Parameter b was moderately correlated with ΔH°_{C3H6}, which accounts for its large confidence interval. If parameter b is removed from the model

Table 4.6
Parameters of MV1 and MV2 by least-squares regression

Model	Parameter	Value	Confidence Interval (95%)	Units
MV1	k_{10}	1.43×10^{2}	$\pm1.28\times10^{1}$	ml STP min^{-1} $(g\ cat)^{-1}$ bar^{-1}
	k_{20}	1.63×10^{1}	±3.45	ml STP min^{-1} $(g\ cat)^{-1}$
	k_{30}	2.12×10^{2}	$\pm1.05\times10^{2}$	ml STP min^{-1} $(g\ cat)^{-1}$ bar^{-1}
	E_{a1}	1.08×10^{5}	$\pm2.17\times10^{4}$	J mol^{-1}
	E_{a2}	7.06×10^{4}	$\pm4.60\times10^{4}$	J mol^{-1}
	E_{a3}	3.26×10^{5}	$\pm1.11\times10^{5}$	J mol^{-1}
	ΔH°_{C3H6}	-2.27×10^{5}	$\pm1.74\times10^{3}$	J mol^{-1}
	a	1.42×10^{-1}	$\pm6.69\times10^{-2}$	
MV2	k_{10}	1.63×10^{2}	$\pm1.69\times10^{1}$	ml STP min^{-1} $(g\ cat)^{-1}$ bar^{-1}
	k_{20}	1.88×10^{1}	±3.44	ml STP min^{-1} $(g\ cat)^{-1}$
	k_{30}	1.58×10^{2}	$\pm4.18\times10^{1}$	ml STP min^{-1} $(g\ cat)^{-1}$ bar^{-1}
	E_{a1}	7.55×10^{4}	$\pm2.77\times10^{4}$	J mol^{-1}
	E_{a2}	6.40×10^{4}	$\pm3.63\times10^{4}$	J mol^{-1}
	E_{a3}	2.90×10^{5}	$\pm6.32\times10^{4}$	J mol^{-1}
	ΔH°_{C3H6}	-2.26×10^{5}	$\pm1.79\times10^{3}$	J mol^{-1}

Table 4.7
Sum of squared residuals (SS) for mechanistic models

Model	Number of Parameters	SS
LH1	8	7.68×10^{-2}
LH2	7	7.71×10^{-2}
MV1	8	7.86×10^{-2}
MV2	7	7.29×10^{-2}

and the dependence on oxygen coverage is set to an order of one, the SS became inflated such that significant lack of fit resulted. The total power on the gas phase oxygen pressure (P_{O2}) in LH1 is 0.28 (0.5xb), which is close to the power on oxygen in the power law models for the production of carbon oxides. The results of the LH1 and power law models concerning the oxygen coverage appear to be contradictory. The low dependence on oxygen pressure in the power law models suggest the catalyst surface is nearly saturated with oxygen, yet the LH1 model demands a low oxygen surface coverage. However, crucial to the LH1 model's satisfactorily fitting the data is the low value of parameter b that forces the dependence on oxygen partial pressure to be nearly that in the power law models.

In the LH2 model an order of one on the oxygen coverage for the reaction of propane was sufficient. The most striking result of the model was the positive value for the heat of

adsorption of oxygen (ΔH°_{O2}). The model apparently required a higher concentration of oxygen on the catalyst surface at higher temperatures.

Both of the Mars-Van Krevelen type kinetic models, MV1 and MV2 fit the data satisfactorily without large correlations between the parameters. In MV1, the value of parameter a is low, indicating, as with the LH1 model, only a small dependence of the propane reaction rate on the fraction of empty sites. Thus, the reaction rate of propane is better described as being dependent on the degree of oxidation of the catalyst as in MV2, or similarly LH2. This is further supported by the lower SS for the MV2 model than the MV1 model in Table 4.7. For both Mars-van Krevelen type models, the activation energy for the oxidation reaction (E_{a3}) is greater than that for either of the reducing reactions (E_{a1} and E_{a2}). This indicates that the catalyst tends to be more oxidized at higher temperatures which corresponds to the higher oxygen surface concentration at higher temperatures predicted by the LH2 model.

4.4 Conclusions and critical analysis

The fact that no reactions occurred in the blank experiments indicated that gas-phase-initiated reactions do not occur at the reaction conditions considered. In addition, reactions in the gas phase involving desorbed radical species were not considered to play a role because of the moderate reaction temperatures and because of precautions taken to minimize the void gas volume in the reactor.

Figure 4.1 depicts the reaction mechanism, at the reaction conditions examined, suggested by the kinetic modelling. The low dependence of the propane reaction rate on free sites on the catalyst in the LH1 and MV1 models and the absence of gas phase initiating reactions indicated that gas phase propane reacts with oxygen on the catalyst surface by an Eley-Rideal type mechanism. It is possible that propane is initially only dehydrogenated to form an adsorbed propyl species ($\bullet C_3H_7$). In the models examined, it is assumed that this species is easily further dehydrogenated to adsorbed propene, which is in equilibrium with gas phase propene. The adsorbed propene can be further oxidized by surface oxygen species to carbon oxides. The difficulty in describing the surface oxygen concentration by the LH1 and LH2 models suggest that kinetic models of the Mars-van Krevelen type are more suitable. Apparently, the oxygen surface concentration cannot be described as in equilibrium with the gas phase; instead, oxygen reacts with the catalyst with its own kinetics. Of course this model is probably simplistic and there could be multiple steps involved in the transformation of gas phase oxygen into active lattice or surface oxygen.

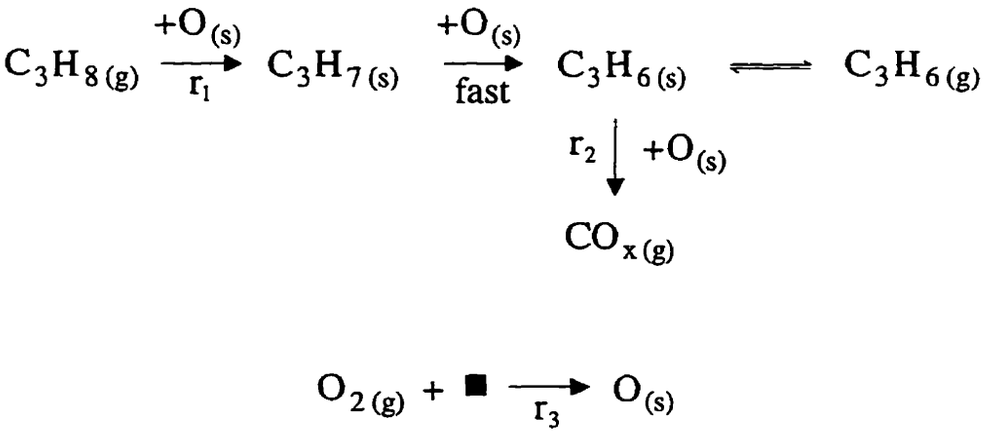

Figure 4.1 Proposed reaction mechanism; (■) oxygen vacancy

The proposed reaction mechanism is entirely consecutive. Propene is the initial product and carbon oxides are formed from the further oxidation of propene. It is conceivable that some carbon oxides could be produced directly from the oxidation of propane. Huff and Schmidt have found that at very short residence times from 6 to 10 ms, the selectivity for the oxidative dehydrogenation of isobutane is nearly constant and independent of the conversion [79]. But when residence times were increased beyond this range and conversion further increased, selectivity for dehydrogenation products decreased sharply. Presumably at the very short residence times, carbon oxides were formed almost exclusively from isobutane; however, at higher residence times, a consecutive mechanism began to dominate and carbon oxides were increasingly produced from the dehydrogenation products. For the set of data examined here, including a competitive route for production of carbon oxides from propane did not improve the fit of the models, as discussed for the power law models. In addition the parameters for the competitive route were highly correlated with those for the consecutive route. For the set of data examined, the consecutive reaction route probably dominated.

Based on the proposed reaction mechanism, the key to obtaining a high selectivity for propene, is preventing its further oxidation. In particular, the strength of adsorption of propene to the catalyst largely influences the selectivity. Recent work investigating the effect of the catalyst basicity, which presumably influences the adsorption of the alkene, largely supports this finding [54-59].

It should be emphasized that no effort was made to examine the reaction kinetics that determine the selectivity between carbon monoxide and carbon dioxide. Kinetic data were inadequate for such an investigation and it was considered secondary to the overall kinetics governing propene and carbon oxide selectivity.

5. Reaction-condition-induced changes in catalyst

During collection of the data for the factorial design of experimental conditions discussed in chapter 4, it was found that the selectivity of the catalyst may have been affected by previous conditions to which the catalyst had been exposed. In the experimental procedure, special precautions were taken to ensure that data were collected with the catalyst in about the same condition. This chapter describes the procedures followed to collect the factorial design data and the observed changes in the catalyst selectivity. In addition, the results of some further experiments, that seem to indicate the type of reaction conditions having the largest influence on selectivity are discussed.

5.1 Collection of factorial design experimental data

In a typical experimental run to collect the factorial design data, the catalyst was first exposed to a standard set of reaction conditions. The standard reaction conditions were propane, oxygen and propene feed concentrations of 4.5%, 9% and 0%, respectively, and a reaction temperature of 530°C. After 3 h at the standard reaction conditions, the conditions were changed successively to three sets of randomly chosen conditions from the factorial design. Each set of the factorial design conditions was maintained for 3 h. Afterwards, the reaction conditions were again returned to the standard reaction conditions after which another three sets of factorial design conditions were run. This process was repeated for each set of the factorial design conditions.

Figures 5.1a and 5.1b show the product selectivities and reactant conversions respectively at the standard reaction conditions for a typical experimental run. The initial selectivity for propene was just over 60% and decreased during the first 3 h of reaction while at the same time the selectivity for carbon dioxide increased from about 23% to about 50% and the selectivity for carbon monoxide appeared to be about constant. This trend continued after the first batch of three factorial design conditions were run. In this period, the conversion of propane was constant at about 5.5%. Reflecting the change in selectivity from propene to carbon dioxide, the conversion of oxygen increased. Before the second batch of factorial design conditions was run, the selectivities for propene and carbon dioxide reached about constant levels at 45% and 40% respectively. The selectivities remained constant until the fourth batch of factorial design conditions were run; thereafter, the selectivity for propene decreased dramatically to about 33% while that for carbon dioxide increased to 50%. This large change in selectivities was accompanied by an increase in the conversion of oxygen to about 9.5%, but again the conversion of propane remained constant. Further batches of

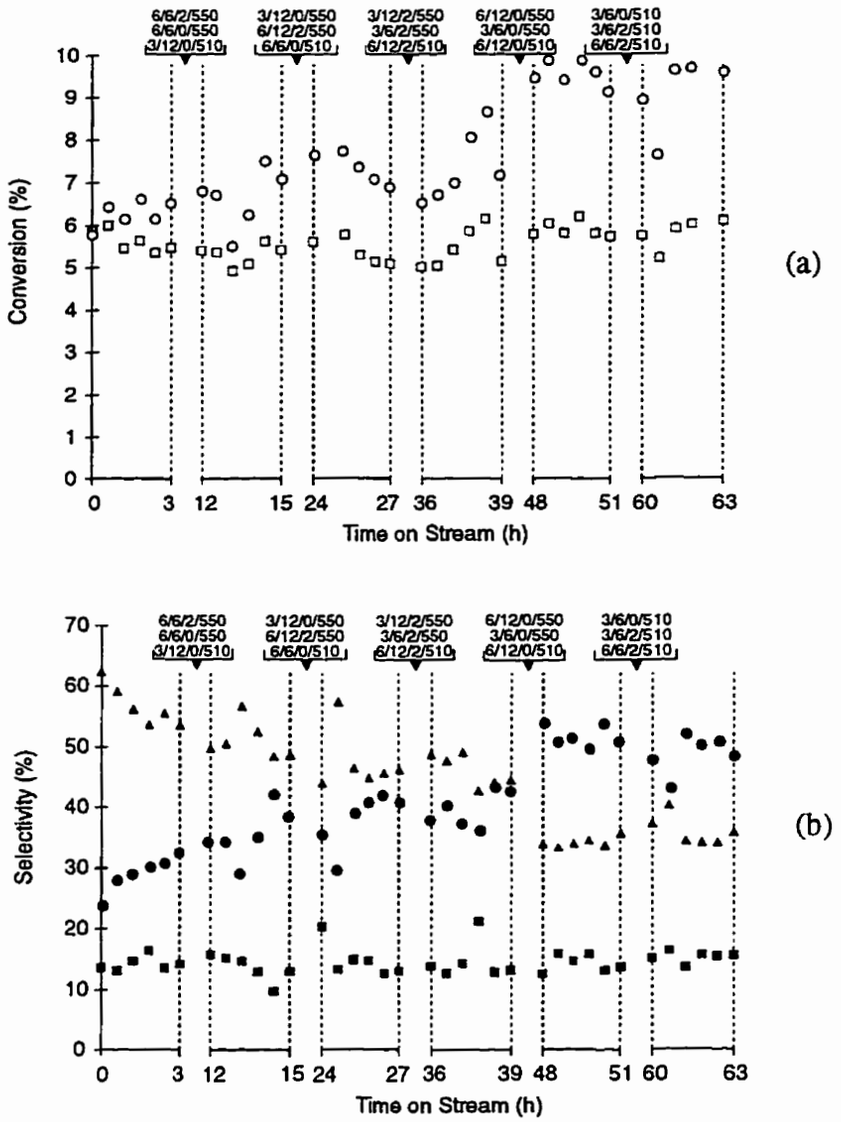

Figure 5.1 Typical activity and selectivity measurements at standard conditions 4/9/0/530 (this notation meaning 4% propane, 9% oxygen 0% propene and 530°C) during an experimental run: (□) propane, (○) oxygen, (●) carbon dioxide, (■) carbon monoxide, (▲) propene.

factorial design conditions were run but the selectivity of the catalyst for propene remained at this low level; thus, the change in selectivity seemed irreversible.

The tendency for the selectivity of carbon dioxide to increase at the expense of propene initially and then reach about a constant level for a period of varying length was reproducible for each experimental run with fresh samples of catalyst. In addition during this period, the conversion of propane was about constant. The further large decrease in selectivity for propene occurred after three to five batches of factorial design conditions were run. It seems that the activity and selectivity characteristics of the catalyst at a given set of reaction

conditions were dependent on previous conditions to which the catalyst had been exposed. Because the factorial design conditions were run in random batches of three, it was difficult to clearly determine if any particular type of conditions caused the shift in selectivity from propene to carbon dioxide. However, it should be noted that in all of the factorial design conditions in the fourth batch, in Figure 5.1, the ratio of oxygen to propane was two to one, suggesting reaction conditions with an excess of oxygen may have a particularly strong influence on the behaviour of the catalyst.

For the intended study of the reaction kinetics, only data for factorial design conditions were included if the standard reaction conditions, run before and after, produced about the same selectivities and conversion of reactants. Thus, the standard reaction conditions were used to decide if significant changes in the catalyst had occurred. A set of kinetic data for the reaction, with the catalyst in presumably the same condition, was collected. Thus, the kinetic models in chapter 4, do not account for any of these observed changes in selectivity.

5.2 Effect of different previous reaction conditions on selectivity

Further experiments were performed to examine the effect of the initial reaction conditions on the selectivity at standard reaction conditions. Two different initial reaction conditions were compared: one in which the reactant concentrations were 12% oxygen and 3% propane, which from this point on will be called the "oxidizing conditions". For the other conditions, the reactant concentrations were 6% oxygen and 6% propane, which will be called the "reducing conditions". The reaction temperature was 530°C. The names of the reaction conditions are not chosen to suggest that the catalyst is necessarily reduced or oxidized at either of them, but are used only to express the differences in the ratios of the reactants between the conditions.

Figures 5.2a and 5.2b show the results when the fresh catalyst is exposed to the reducing conditions. In contrast to the results for the standard reaction conditions, there is no initial decrease in the selectivity for propene. As Figures 5.3a and 5.3b indicate, when the fresh catalyst is exposed to the oxidizing conditions, the selectivity for propene decreased and became nearly constant after 9 h on stream, while the conversion of propane was about constant. After exposure of the catalyst to the oxidizing and reducing conditions, the activity and selectivity at the standard conditions were measured. When the fresh catalyst was first exposed to the oxidizing or reducing conditions, the activity and selectivity at the standard conditions were constant.

In Table 5.1, the activity and selectivity of the two sets of reaction conditions after 9 h of reaction on the fresh catalyst are compared to those predicted by the series-type power law model in which all carbon oxides are produced from the further oxidation of propene. The activity and selectivity predicted by the model can be regarded as the results expected if the fresh catalyst were first exposed to the standard conditions. The propane conversion differs

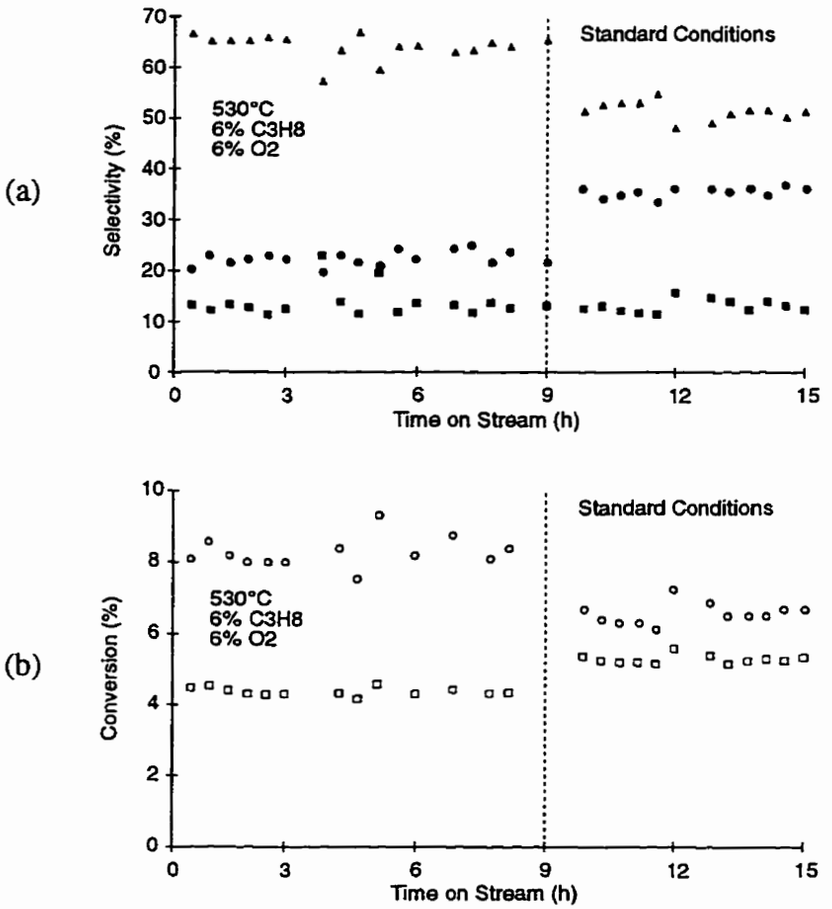

Figure 5.2 Activity and selectivity of fresh catalyst exposed to reducing conditions, symbols as in Fig. 5.1

Table 5.1
Comparison of catalyst performance under oxidizing and reducing conditions

	Oxidizing conditions (3% C_3H_8, 12% O_2)		Reducing conditions (6% C_3H_8, 6% O_2)	
	Fresh Catalyst[a]	Model[b]	Fresh Catalyst[a]	Model[b]
C_3H_8 conv. (%)	6.1	6.6	4.4	3.8
C_3H_6 selec. (%)	30	51	64	61

[a] After 9 h on stream.
[b] Predicted by power law model.

little between either the reducing and oxidizing conditions or the model predicted conversions. However, the measured selectivity for propene, of about 30% under oxidizing conditions is considerably lower than that predicted by the model. For the reducing conditions, the selectivity for propene is only slightly higher than that for the model and may be no greater than a difference due to experimental error.

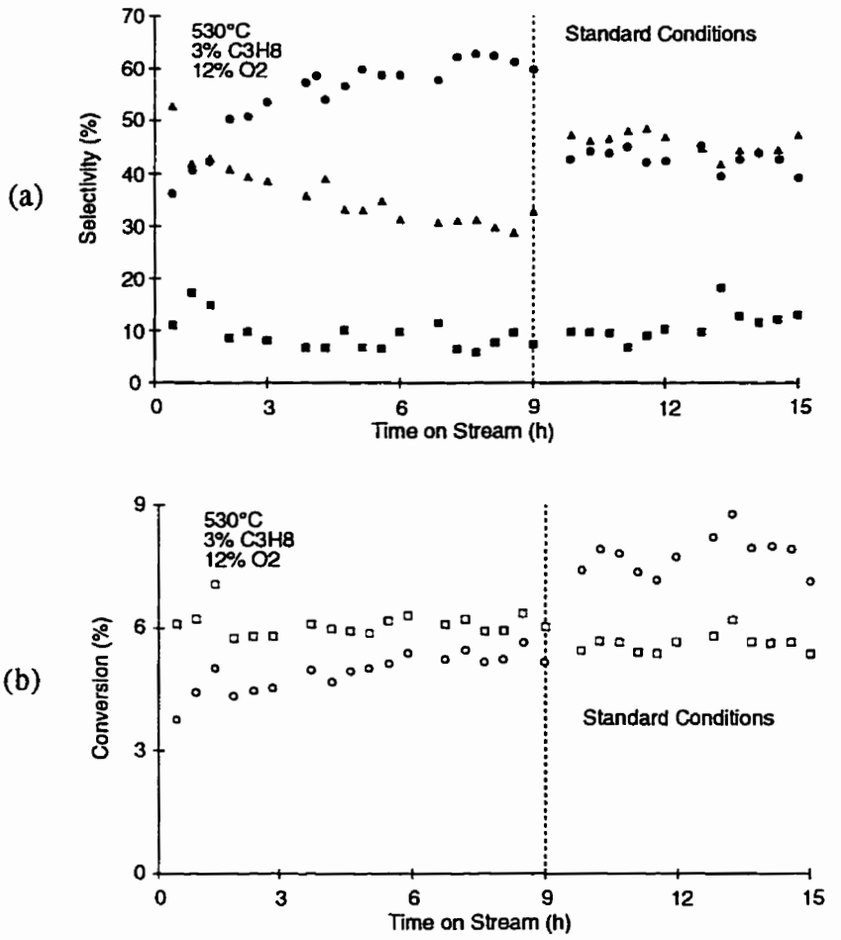

Figure 5.3 Activity and selectivity of fresh catalyst exposed to oxidizing conditions, symbols as in Fig. 5.1.

In Table 5.2, the activity and selectivity are compared for the standard conditions, after the fresh catalyst was exposed to the two sets of initial conditions tested. The mean activity and selectivity of the standard conditions, can be regarded as those expected after the fresh catalyst was exposed to the standard conditions. The conversion of propane is about the same at all of the conditions in Table 5.2. However, the selectivity for propene at the oxidizing conditions is 3% lower than that expected if the initial conditions were the standard conditions. For the reducing conditions, the opposite is true, the selectivity for propene is 2% higher. Since the range of propene selectivities at the standard conditions was from 46% to 51%, these differences are probably attributable only to experimental error.

Table 5.2
Comparison of performance at standard conditions after varying initial conditions

	Initial conditions[a]		
	Standard conditions[b]	Oxidizing conditions	Reducing conditions
C_3H_8 conv. (%)	5.2	5.6	5.3
C_3H_6 selec. (%)	49	46	51

[a] Conditions to which fresh catalyst was exposed.
[b] Obtained from average of standard conditions.

In Figure 5.4, diffractograms are shown of catalyst samples run for 12 h at the oxidizing and reducing conditions. The only phases identified in either catalyst sample were magnesium oxide and magnesium orthovanadate. There are no significant differences between the diffractograms of the catalyst run at the two reaction conditions. There are, however, differences between the diffractograms of the fresh catalyst (Figure 3.1) and the used catalysts. In Figure 5.4, the peaks associated with the magnesium oxide phase are smaller and slightly broader. Exposing the catalyst to reaction conditions appears to degrade the crystals of the magnesium oxide phase, while those of the magnesium orthovanadate phase are unaffected.

Overall, the trend in Table 5.2 and the results for the oxidizing conditions in Table 5.1 indicate that initially exposing the catalyst to conditions with an excess of oxygen reduces the selectivity for propene. This adverse effect of reaction conditions with excess oxygen on the catalyst's selectivity has not previously been reported in the literature for the Mg-V-O catalyst or to my knowledge any other oxidative dehydrogenation catalyst. However, the importance of the influence of the reaction environment on the selectivity of partial oxidation catalysts at future reaction conditions has been recognized and reviewed [80]. Various physical changes to the catalyst surface have been suggested as causes for this type of phenomenon. The XRD analysis results indicate there are no detectable differences in the bulk structure of the catalyst exposed to either the oxidizing or reducing conditions, and so the changes to the catalyst may be limited to the surface. One could speculate that the oxidizing conditions may increase the concentration or promote the creation of more weakly bound, less selectively reacting surface oxygen, which persists even after the reaction conditions are changed to those that are less oxidizing.

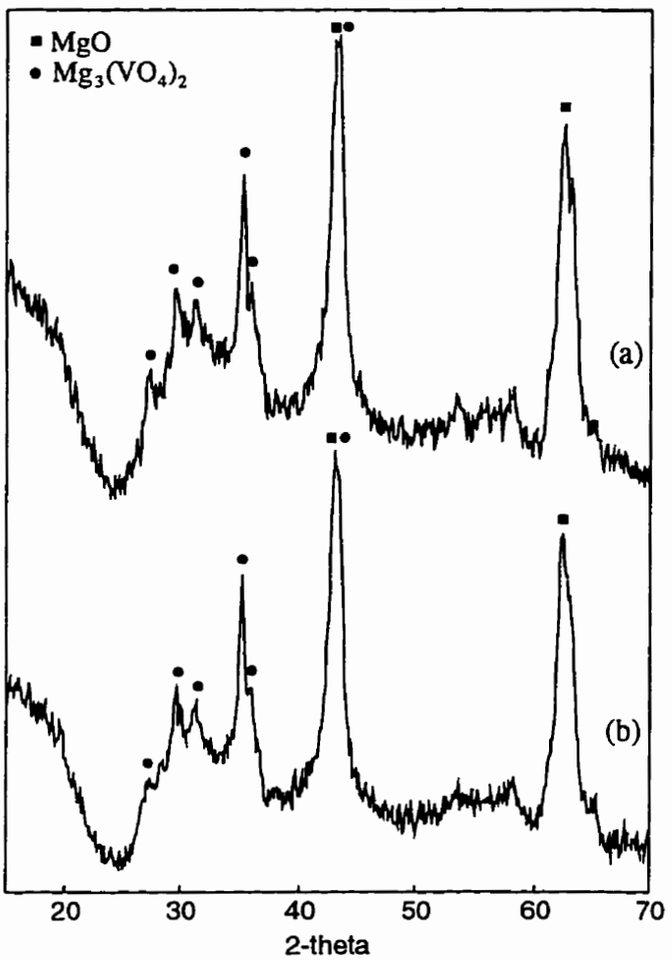

Figure 5.4 X-ray diffractograms of Mg-V-O catalyst exposed to (a) oxidizing and (b) reducing conditions.

6. Step-change transient kinetic analysis

6.1 Transient response techniques

The simplest method for studying a reaction mechanism is the fitting of steady-state data to various kinetic models, which is the approach used in Chapter 4. The steady-state data are gathered over a range of reaction conditions. A problem with this method is that often many kinetic models fit equally well to the same set of data. As with all experimental work, a portion of the variation of the data results from uncontrollable experimental error. The remaining variation of the data, which is assumed to result from variations in reaction conditions, can be too small to distinguish among different kinetic models. Also, for a complex reaction it is often necessary to collect kinetic data over a wide range of conditions at many concentration levels of reactants and products in order to infer a complete reaction mechanism. Steady-state data can often provide useful empirical models even though such models may have no mechanistic interpretation.

A catalytic reaction, either homogeneous in the gas phase or heterogeneous, consists of a series of elementary steps. Their sequential structure means that at steady-state, the rate of the overall reaction is only as fast as the slowest or rate-determining step. When a reaction is disturbed from its steady-state, other steps in the reaction mechanism can temporarily become rate-determining during the transient period as the new steady-state is approached. The result is that the transient response curves of the products will display characteristic time constants according to the kinetic structure of the reaction.

Transient response techniques for investigations of reaction mechanisms have been reviewed [81,82]. Kobayashi [83] used a series of model reaction mechanisms to simulate product transient response curves resulting from a step-change in the reactant feed concentration. The simulated reactions were heterogeneous and occurred over a catalyst with one or more types of active sites, unconstrained by the rate of mass transfer. The reactor was operated differentially, i.e. conversion was low and concentration gradients along the reactor axis could be neglected. Figure 6.1 shows four basic types of transient product responses resulting from a step-change increase in the reactant concentration at time zero. For the Type I response, the product concentration increases immediately. This means there are negligible quantities of adsorbed surface intermediates and the surface reaction itself or the adsorption of the reactant is the rate-determining step. The Type II response is a monotonic increase in product concentration. Here, the desorption of the product alone or product desorption in combination with surface reaction or reactant adsorption are the rate-determining steps. Next is the Type III, overshoot response. This response indicates that regeneration of either active

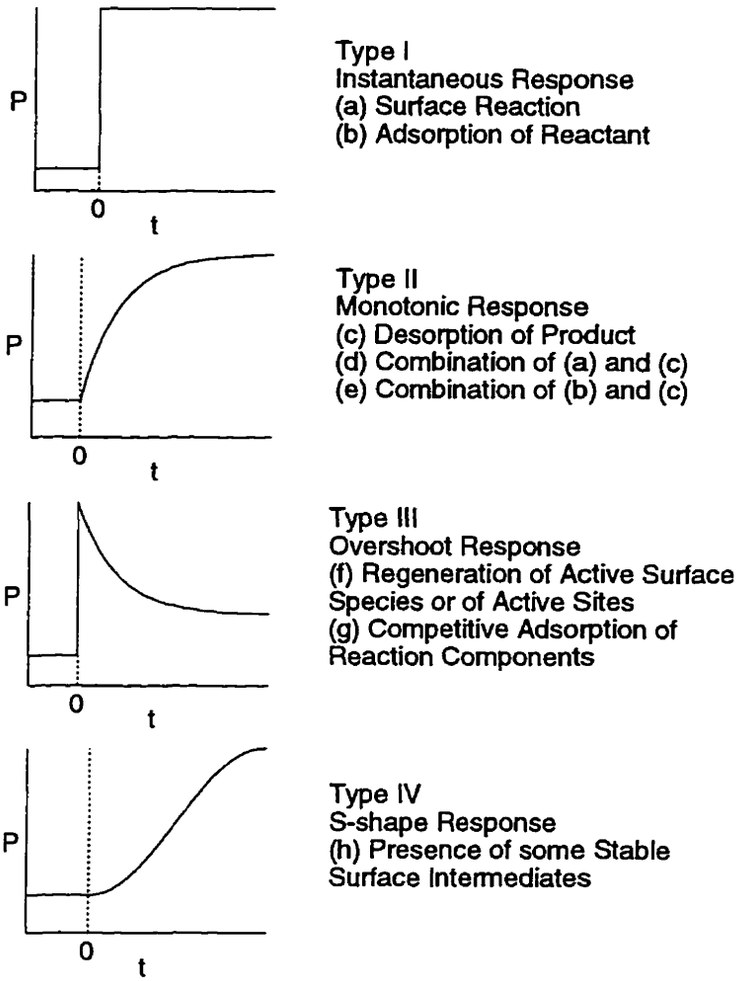

Figure 6.1 Product transient responses and rate-determining steps

surface species or sites is rate controlling. The overshoot response results when fresh catalyst, initially with a maximum number of active sites, is first exposed to the reactant. The reaction may be very fast, and begins to deplete the active sites. In a separate, slower reaction, the active sites are regenerated. The result is a rapid initial reaction rate, followed by a reduced rate as steady-state is approached. The S-shape response is Type IV. For this response, an induction period occurs, indicating the development of a significant concentration of stable intermediate species on the catalyst surface. The appearance of the product is delayed until enough of the intermediate species accumulate. The types of responses discussed here are only the very simplest. In a real reaction, one could expect combinations of these simple responses occurring. For example, the Type II and III responses could occur simultaneously. The increase in product concentration may be slow at first, occurring monotonically, due to readsorption of the product. However, it could reach a maximum later and then decrease as the regeneration of active sites becomes rate limiting.

Thus, for complex reaction mechanisms with several products, combinations of responses may occur, each being different for each product.

The variable most often used to force a transient response on a reaction system is one or all of the reactant feed concentrations, because they can be changed so abruptly. Forcing repeated and regular changes in reactant concentration (often in the form of square-wave inputs) on a reaction system is referred to as periodic operation. In such a case, the reaction may be in a constant state of transient response. An exception occurs when the changes are made at such a low frequency that the system has time to reach a steady-state between the changes. There are many examples in the literature of the use of transient response techniques and/or periodic operation for the study of reaction mechanisms [84,85].

Transient response methods do suffer from some weaknesses. In particular, it may be possible that the reaction mechanism inferred from the transient response is different from that inferred from steady-state behaviour. This is particularly true if large disturbances to the reaction are imposed such as during start-up. Large changes in the reaction environment can cause structural changes in the catalyst, a point that must be borne in mind in the design and interpretation of transient experiments. Otherwise, transient results can be misunderstood.

To ensure the observation of steady-state kinetics, ideally only very small step-changes in reactant concentration should be imposed. However, from a practical viewpoint, it can be very difficult to measure the resulting transients, especially if the reactor is operated differentially and the product concentrations are already very low. As a result, experiments involving start-up and interruption of a reaction are most often used in transient kinetic studies. With transient response techniques, another important consideration is that, if possible, the reactor be designed to eliminate mass transfer interferences so that only the effect of the reaction kinetics is observed. However, particularly in small-scale reactors, mass transfer effects in the catalyst bulk can often be convoluted with the transient responses. Also, if the reaction occurs at high temperature or, more importantly, is very fast, measuring transients requires high-speed analytical equipment.

6.2 Transient response techniques applied to oxidative dehydrogenation

Various step-change experiments were carried out on oxidative dehydrogenation of propane over Mg-V-O, both on starting-up and on interrupting the reaction from steady-state. The objective of this non-steady-state kinetic investigation was to extensively investigate the reaction mechanism.

The reaction conditions used were close to those used in the steady-state investigation of the reaction kinetics, discussed in Chapter 4. In all experiments, reaction was carried out at 510°C with 15 to 30 mg of catalyst. The reactor was operated at or near differential conversions of the reactants: steady-state propane and oxygen conversion were always less than 6 and 14% respectively. The total feed flowrate was held constant at 50 ml (STP) min^{-1}.

To provide insight into the state of the catalyst during reaction, the masses of carbon or oxygen either accumulated or removed from the catalyst during step-changes were estimated. Due to unavoidable dispersion and mixing effects, true step-changes in the feed concentration could not be generated. Instead, mass balance calculations were based on measurements of the 'real step-changes' in feed concentrations obtained. These were measured by carrying out the step-changes at the same conditions except that the catalyst was replaced by a similar quantity of granular quartz chips.

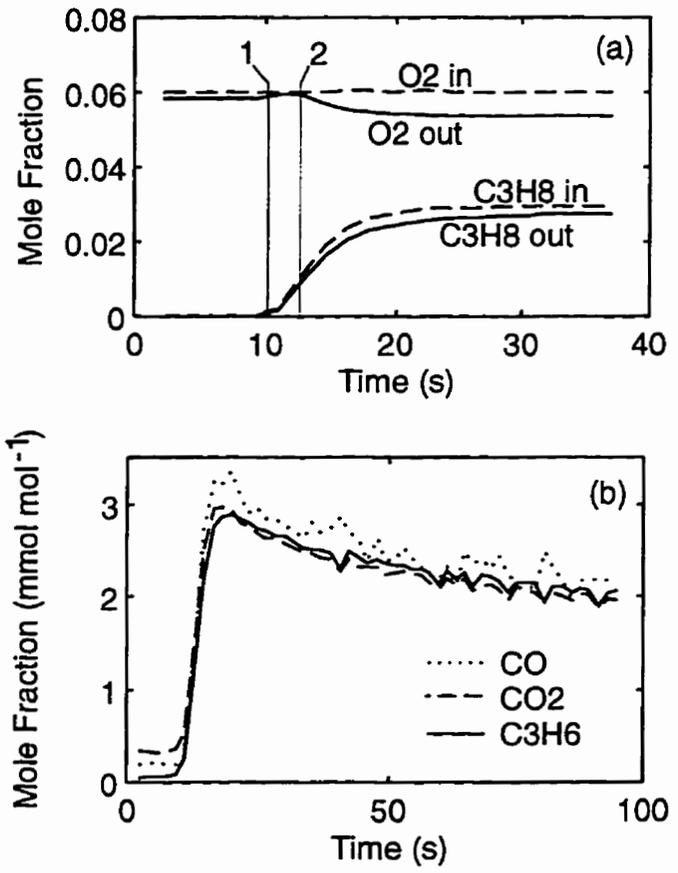

Figure 6.2 Reactant and product responses after reaction start-up

6.3 Reaction start-up with fresh catalyst

Figure 6.2 shows the results of a step-change from an initial feed containing 6% oxygen to a reaction mixture of 6% oxygen and 3% propane over 21 mg of fresh catalyst. The step-change is shown at time zero. From the delayed response of propane, it can be seen that the lag due to the gas hold-up for the reactor system was about 9 s. The broken curves in Figure 6.2a show the inlet concentrations of the reactants estimated by performing the step-change at the same conditions except with the catalyst replaced by quartz chips. The transient

responses support a redox type of reaction mechanism in which propane reacts with oxygen on the catalyst and gas phase oxygen re-oxidizes the catalyst. Figure 6.2a shows that with the fully oxidized fresh catalyst, propane began to react immediately (line 1), while the reaction of oxygen was delayed about 4 s (line 2) until the catalyst was partially reduced. All of the products followed an overshoot type of response. Initially with an excess of oxygen on the catalyst, the reaction rate was high, causing first a peak in the product concentrations, but then as the catalyst was reduced, the reaction rate decreased and steady-state was approached. From Figure 6.2b, responses of the three carbon-containing products are nearly identical.

The transient response of water is not shown in Figure 6.2b. Its form was the same as the other products; however, it was delayed by as much as 100 s. It was believed that water adsorbed to the reactor walls and internals of the MS sampling system, causing a chromatographic effect. Thus the water response does not unambiguously suggest a mechanism for the reaction, but neither does it preclude the possibility that water or water precursors (such as OH species) adsorb to the catalyst surface. Figure 6.3 shows the instantaneous accumulation of carbon and oxygen on the catalyst for the data in Figure 6.2. Water is excluded from these mass balance calculations. It is assumed the moles of water leaving the reactor always corresponded to the quantity of the other products, adjusted for the stoichiometry. One must bear in mind that the chemical analysis was always subject to some bias, and even at steady-state a perfect carbon and oxygen mass balance was rarely achieved, although, the steady-state mass balances always closed to within about 10%. Even though it

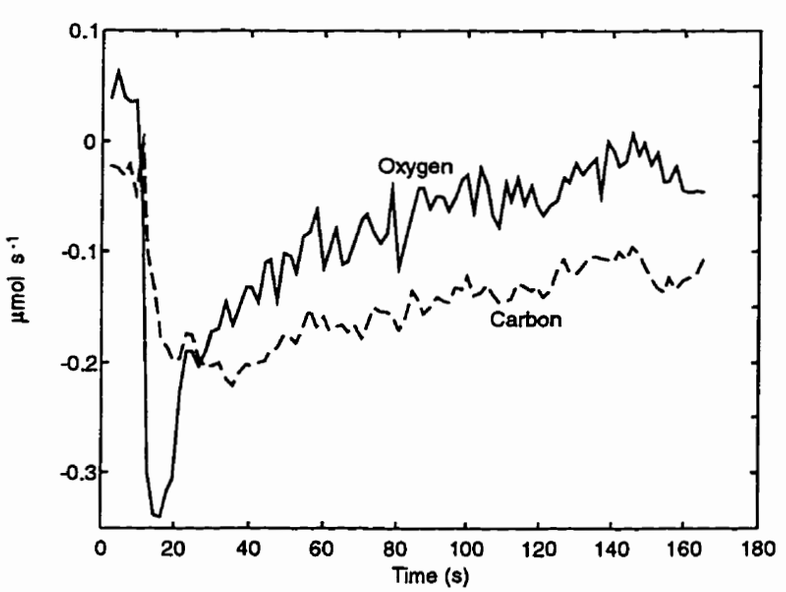

Figure 6.3 Instantaneous accumulation of carbon and oxygen on catalyst.

might appear that carbon was removed from the catalyst, this was not possible since the fresh catalyst did not contain carbon. After about 150 s, the carbon and oxygen balances became almost constant. At this point, the reaction is at steady state and the differences between the mass balances and zero indicate the analysis bias. It is evident that the chemical analysis bias for carbon is greater than that for oxygen. Thus, the mass balance results were confounded with biases in the chemical analysis. Also, small abrupt pressure disturbances may have affected the results, although, measures were taken to control such disturbances (see section 3.2.2). The oxygen response for the feed to the reactor in Figure 6.2 appears stable, suggesting pressure disturbances were negligible. The oxygen mass balance in Figure 6.3 indicates that a relatively large quantity of oxygen was removed from the catalyst and then the mass balance nearly agreed at steady-state. However, the carbon mass balance also decreased immediately after the step-change, but only recovered slightly as steady-state was approached. The loss of oxygen from the catalyst during the transient would appear to be a real effect, while the apparent loss of carbon is probably only a symptom of analytical bias. It can at least be concluded that little to no carbon species adsorb to the surface of the catalyst. An attempt was made to estimate roughly the amount of oxygen removed by integrating with respect to a linear baseline between 10 to 150 s. In this case, the total quantity of oxygen removed was estimated as 15 μmol. If it is assumed that only oxygen can be removed from the magnesium orthovanadate phase, and the catalyst consists of only the orthovanadate and magnesium oxide phases, then 4.1% of the maximum oxygen available was removed. Similar results were obtained for start-up of the reaction with a step-change from pure helium to both reactants, propane and oxygen.

6.4 Reaction Interruption

Figure 6.4 shows the product transient responses for step-changes causing the interruption of the reaction from its steady-state. In Figure 6.4a the step-change was made from propane and oxygen to pure helium while for Figure 6.4b the step-change was made from propane and oxygen to oxygen and helium. The quantities of propane and catalyst also differed; for Figure 6.4a, 6% propane and 30 mg of catalyst were used while for Figure 6.4b, the quantities were 3% propane and 21 mg of catalyst. For the step-change to pure helium, the decrease in the carbon monoxide concentration appeared to lag that of propene and carbon dioxide. However, for the step-change to oxygen and helium, the concentrations of all carbon containing products decreased at the same rate. The carbon monoxide lag suggests that a small quantity of carbon species may in fact be present on the catalyst. When a step-change was made to helium and oxygen, these species may have been quickly oxidized, but with a step-change to only helium, only oxidation by surface oxygen occurred, which was perhaps a slower process. An alternative explanation is that carbon monoxide

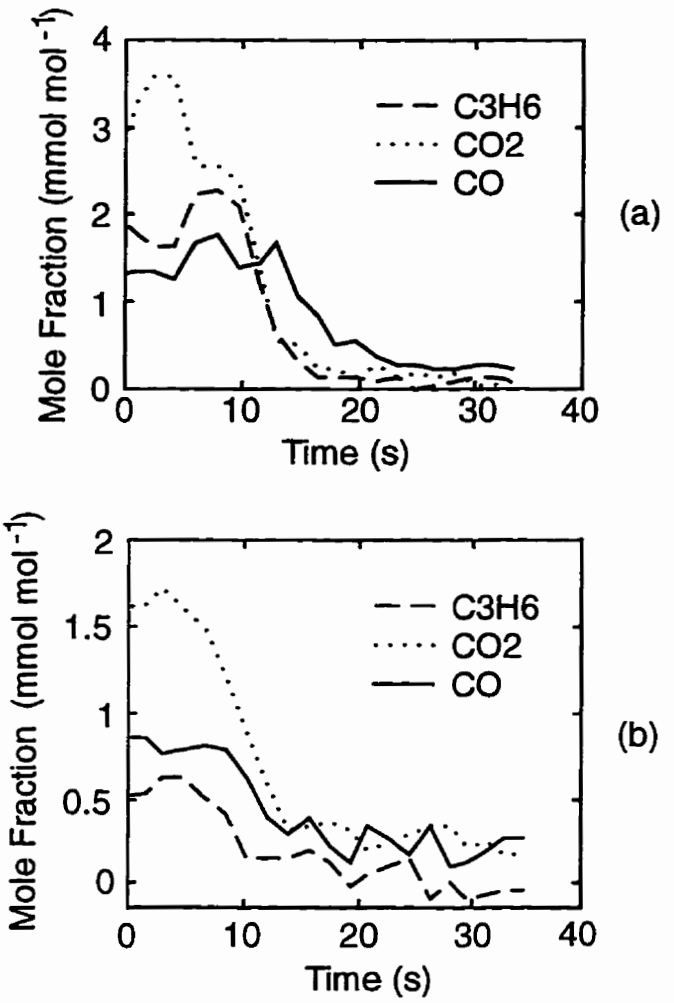

Figure 6.4 Product transient responses after interruption of reaction; (a) 30 mg cat., 6% propane, 6% oxygen before and helium after interruption, (b) 21 mg cat., 3% propane, 6% oxygen before and 6% oxygen after interruption.

itself is adsorbed on the catalyst; however, it must desorb more quickly after a step-change to oxygen than after a step-change to pure helium.

The quantity of carbon on the catalyst was estimated by integrating the area below the carbon monoxide signal and above the carbon dioxide and propene signals. It was assumed that carbon monoxide would decrease at the same rate as carbon dioxide and propene if no carbon was present on the catalyst. The excess carbon monoxide indicated by the delayed signal was small, amounting to 0.23 μmol. For comparison, the catalyst contained 132 μmol of vanadium.

For the step-change to oxygen and helium, the mass balances clearly indicated that oxygen was adsorbed or that the catalyst was re-oxidized. The quantity of oxygen accumulated on the catalyst was estimated as 6.7 μmol. When the reaction was started with fresh catalyst, the oxygen removed was estimated as 15 μmol. Thus, perhaps less than half

of the oxygen removed was replaced by re-oxidation. The catalyst, for which the reaction was interrupted with a step-change to pure helium, was also re-oxidized by exposure to 6% oxygen at the same reaction temperature, 510°C. Again, the mass balance calculations indicated that only a fraction of the original oxygen estimated to be removed was replaced.

6.5 Reaction start-up with only propane

If the oxidative dehydrogenation reaction occurs by a redox mechanism, it should also occur to some degree with only propane in the gas phase until the catalyst is fully reduced. This section deals with experiments performed to determine to what extent the catalyst alone can provide oxygen to drive the reaction and to examine differences in the activity and selectivity of the catalyst without gas phase oxygen. Cyclical experiments were carried out in which the catalyst was repeatedly reduced by reaction with only propane and then re-oxidized with oxygen. Between the reduction and oxidation steps the catalyst was sometimes flushed with pure helium. Beforehand the catalyst had been exposed to steady-state reaction conditions with propane and oxygen for at least 3 h. Two types of cyclic experiments were performed, one with a 4-part cycle and the other with a 2-part cycle. For the 4-part cycle experiment, the catalyst was first exposed to 6% oxygen for 10 min, followed by pure helium for 5 min. Next, 6% propane was fed for 10 min, again followed by 5 min of pure helium. This process was repeated five times and throughout, the reaction temperature was maintained at 510°C. The process for the 2-part cycle experiment was the same, except that the helium flush steps between the oxidation and reduction steps were omitted.

Figure 6.5a shows the product concentrations, during the first exposure to propane for a 4-part cycle experiment with 17 mg of catalyst. Within about the first 100 s, the product concentrations, decreased quickly, after which they decreased more slowly as the catalyst's supply of oxygen was depleted. The water concentration, although not shown here, was sufficient to account for all of the carbon containing products. Thus, there was no evidence that hydrogen was a product. For comparison purposes, Figure 6.5b shows the product concentrations, during the same period, when the same quantity of catalyst was exposed to both 6% propane and 6% oxygen. The catalyst for Figure 6.5b was first exposed to steady-state reaction conditions for 3 h, then only to oxygen for 30 min, followed by pure helium for 30 min. Thus the catalysts for Figures 6.5a and 6.5b before the step-change were in about the same condition. The propene concentration in Figures 6.5a and 6.5b are very close, particularly immediately after the step-change. However, the carbon oxide concentrations are considerably lower when oxygen was not present in the gas phase. The reaction without oxygen in the gas phase had much higher selectivity for propene (over 75%) compared to that with gas phase oxygen (about 60%), but at a lower conversion of propane. However, the lower propane conversion was mainly due to lower yields of carbon oxides, since the

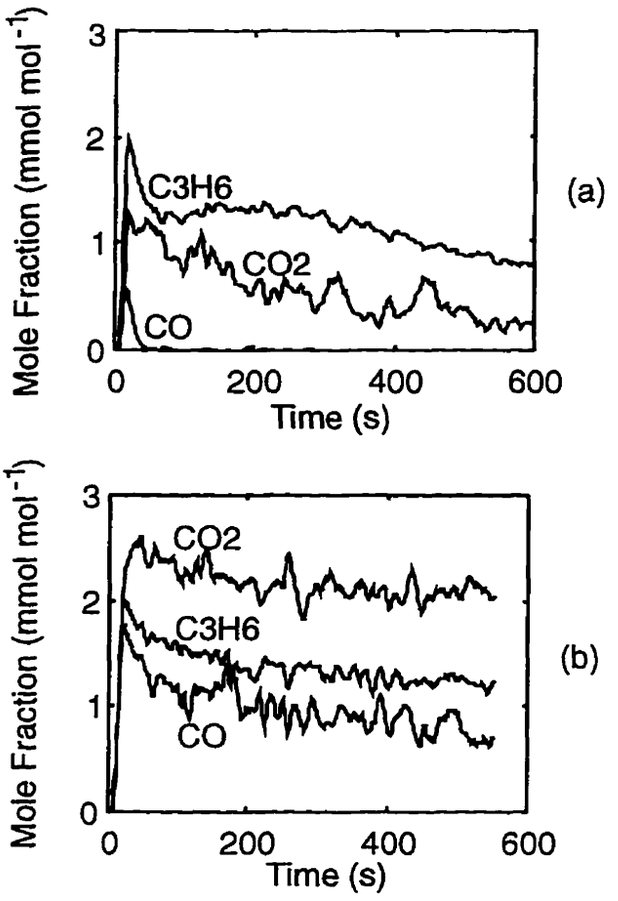

Figure 6.5 Product response at reaction start-up; (a) 6% propane, (b) 6% propane and 6% oxygen

propene concentrations were so close. When the cyclic experiment was performed with 30 mg of catalyst it was similarly observed that the same quantity of propene, could be initially produced without gas phase oxygen as with gas phase oxygen, but with lower concentrations of carbon oxides.

The catalyst was found to be rather robust during the cyclic experiments. Each cycle of propane exposure produced the same quantities of products, thus no deactivation was observed. Figure 6.6 compares the product concentrations during propane exposures, for a 2-part and 4-part cyclic experiment each with 30 mg of catalyst. In both cases the propene selectivity was high (over 70%). The product concentrations were somewhat higher for the 4-part cycle experiment, but these differences were considered to result only from uncontrollable experimental deviation. Overall, the product transient responses are identical between the 2-part and 4-part cyclic experiments. It was thought that the propene selectivity may be superior with the 4-part cycle, due to its helium flush between exposures to propane and oxygen. During re-oxidation, it was considered possible that some weakly bound and

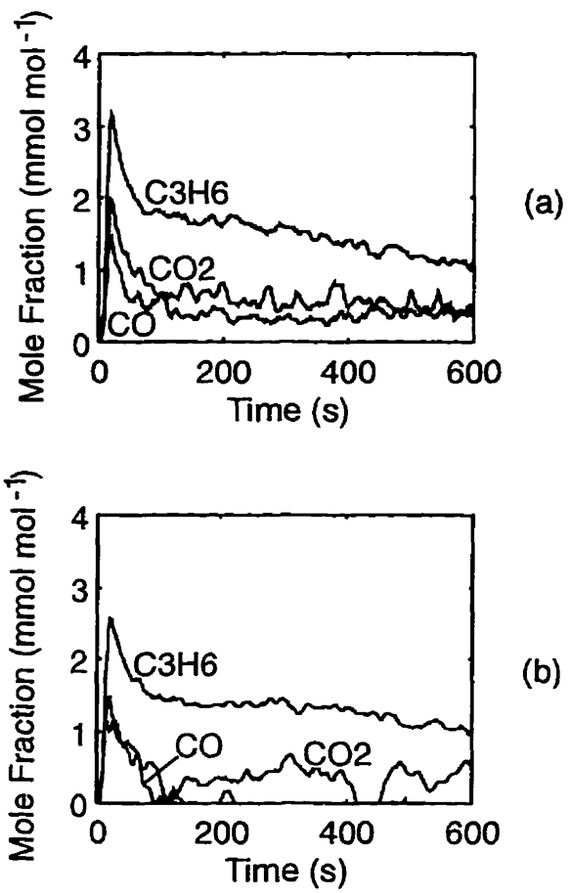

Figure 6.6 Product transient responses after reaction start-up without gas-phase oxygen; (a) 4-part cycle, (b) 2-part cycle.

non-selective oxygen could be left on the catalyst surface, and the helium flush might remove these species. This was apparently not the case.

Carbon balance calculations for the cyclic experiments indicated that carbon in some form was present on the catalyst surface. In contrast, the transient reaction start-up experiments with gas phase oxygen indicated that no carbon was present on the catalyst surface. Figure 6.7 shows the instantaneous accumulation of carbon and oxygen during the first 3 min of exposure to propane for the 4-part cycle experiment with 30 mg of catalyst. The carbon adsorbed on the catalyst very early during the first 30 s after the step-change to propane. The quantity of carbon was estimated for each cycle and is shown in Table 6.1. After this large initial adsorption of carbon on the catalyst, there was no evidence that large quantities of carbon continued to accumulate on the catalyst, because the carbon balance was within the normal ±10% experimental error. Still, it is possible that some small quantities of carbon continued to adsorb on the catalyst surface, contributing to some deactivation of the catalyst. Table 6.1 also shows the estimated quantities of oxygen removed from the catalyst during each of the 10 min cycles of propane exposure.

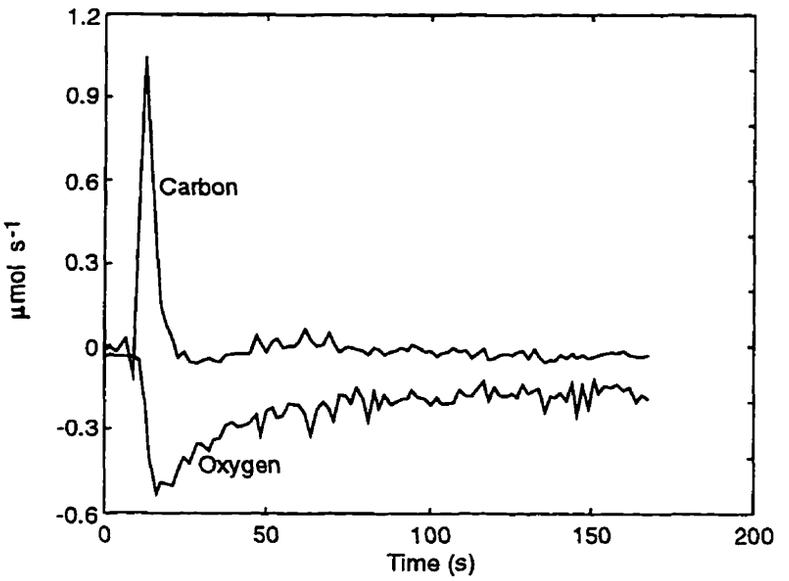

Figure 6.7 Instantaneous accumulation of carbon and oxygen on catalyst after reaction start-up without gas-phase oxygen.

Table 6.1
Oxygen removal and carbon adsorption during exposures to propane

Cycle No.	Quantity of oxygen removed (µmol)	Percentage of total oxygen	Quantity of carbon adsorbed (µmol)
1	74	14.1	4.9
2	86	16.2	5.6
3	97	18.3	5.2
4	95	17.9	4.6
5	100	19	5.4

During the oxygen-adsorption parts of the cycles, oxygen was adsorbed by the catalyst for about 150 s. The total quantity of oxygen adsorbed was estimated for two of the cycles to be 44 µmol and 47 µmol which corresponded to 8.2% and 8.8%, respectively, of the total quantity of removable oxygen. The total quantity of oxygen adsorbed by the catalyst between the propane exposures was less than half of the oxygen estimated to be removed by reaction with propane. Considering the absence of deactivation of the catalyst during successive cycles, it is likely that this discrepancy was due mainly to inaccuracies of the mass balance calculations. Immediately after the step-change to oxygen during the cyclic experiments, small quantities of carbon oxides were produced. The quantity of this carbon, estimated by integration of the carbon oxide signals was 1.4 µmol.

Figure 6.8 compares the propane conversion and propene selectivity for two quantities of catalyst at the same reaction conditions with and without gas phase oxygen. For the results without gas phase oxygen, the results of one cycle of a 4-part cyclic experiment are

shown with 17 and 30 mg of catalyst. The ranges of conversions and selectivities are plotted for the duration of the 10 min period of exposure to 6% propane. The propene selectivity tended to increase somewhat as the propane conversion decreases. For comparison, the results obtained with the same quantities of catalyst, operated at steady-state with 6% gas phase oxygen, are plotted. It is clear that even at the same conversion of propane, much higher propene selectivity was obtained without gas phase oxygen.

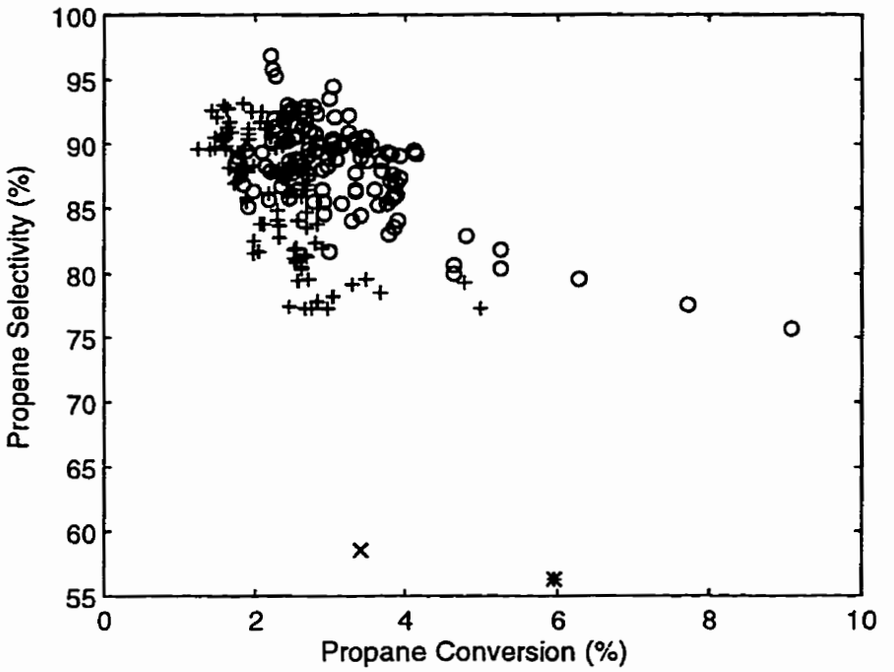

Figure 6.8 Selectivity and Conversion; (×) 17 mg cat., 6% propane, 6% oxygen at steady-state, (✱) 30 mg cat., 6% propane, 6% oxygen at steady state, (+) 17 mg cat., 6% propane during 10 min exposure, (o) 30 mg cat., 6% propane during 10 min exposure.

6.6 Conclusions

The transient response experiments provided considerable qualitative information regarding the oxidative dehydrogenation reaction mechanism. A number of the findings support the redox reaction mechanism whereby reaction of propane and intermediate products reduce the catalyst and gas phase oxygen re-oxidizes it. These include:

- During start-up of the reaction with fresh catalyst, propane began to react immediately while the reaction of oxygen was delayed by a few seconds.
- The transient response of the products consisted of an overshoot type response, during start-up of the reaction, suggesting the reaction rate was initially high because of excess

oxygen on the catalyst surface but then the reaction rate slowed as the catalyst was reduced and steady-state was approached.

- Mass balance calculations indicated the catalyst was partially reduced at the reaction conditions, perhaps losing 4% of the oxygen contained in the magnesium orthovanadate phase.
- The catalyst was active without the presence of gas phase oxygen for at least 10 min at the reaction conditions examined.

During start-up of the reaction with gas phase oxygen there was no indication that any carbon species were present on the catalyst surface. This finding agrees with DRIFT spectroscopy and isotope exchange results in the literature with a Mg-V-O catalyst, which also found no evidence of adsorbed hydrocarbon species on the catalyst [71]. However, during interruption of the reaction with a step-change that stopped the feed of both propane and oxygen, a lag in the carbon monoxide signal was observed. This suggested that perhaps a small quantity of carbon species was present on the catalyst and by a slow reaction the catalyst oxygen oxidized these species. When the same step-change was performed and only the propane feed was stopped, while oxygen feed was maintained, no lag in the responses of any of the products was observed. During start-up of the reaction without gas phase oxygen, the mass balance calculations clearly indicated that some carbon species were deposited on the catalyst, immediately after the step-change.

When the reaction was operated without gas phase oxygen, and only the catalyst supplied oxygen for the reaction, the propene selectivity was superior compared to the steady-state operation of the reaction with gas phase oxygen. This was the case even at the same level of conversion of propane.

7. Transient kinetic modelling

Often it is not sufficient to analyze transient responses only qualitatively, particularly if they are complex in nature. It is taken as axiomatic that a reaction mechanism can best be understood by mathematical modelling of the kinetics. Yet modelling of dynamic kinetics is a much more complex task than the modelling of steady-state kinetics because it requires considerably more information than steady-state runs provide. Often the kinetic parameters determined under steady-state conditions are in a lumped form. For example, for a species that is adsorbed on the catalyst surface, its steady-state surface and gas phase concentrations are in equilibrium and the rates of adsorption and desorption are equal. Only an equilibrium constant is needed. During a transient response, the system may no longer be at equilibrium, and knowledge of the individual rates of adsorption and desorption are required and even the total number of adsorption sites.

In this chapter, one of the steady-state kinetic models developed in chapter 4 is used as a starting point for modelling the transient kinetic responses presented in chapter 6. The transient data further test the applicability of the kinetic models and suggest some new and interesting insights into the reaction dynamics.

7.1 The transient kinetic model

7.1.1 Rate models

The kinetic modelling, discussed in chapter 4, revealed that a Mars-Van Krevelen type kinetic model, based on the reaction scheme in Figure 4.1, best described the steady-state data. The transient response data, discussed in chapter 6, also supported such a redox type of reaction mechanism. The Mars-Van Krevelen type kinetic model referred to as MV2 was used to model the transient data. The values of the model parameters are shown in Table 4.3. The rate equations for this kinetic model were

$$r_1 = k_1 P_{C_3H_8}(1-\beta) \tag{7.1}$$

$$r_2 = k_2 \theta_{C_3H_6}(1-\beta) \tag{7.2}$$

$$r_3 = k_3 P_{O_2} \beta \tag{7.3}$$

where β represents the degree of reduction of the catalyst and θ_{C3H6} the fractional coverage of propene on the catalyst surface. Equation 7.1 is the rate of reaction of propane to form propene on the catalyst surface. Equation 7.2 expresses the rate at which propene on the catalyst surface reacts to form carbon oxides. The kinetic model does not describe the selectivity between carbon monoxide and carbon dioxide. It is assumed that they are

produced only at some fixed ratio. The rate Equation 7.3 expresses the rate at which gas phase oxygen re-oxidizes the catalyst.

The following differential equations express the transients in the gas phase concentration of each component:

$$\frac{dP_{C_3H_8}}{dt} = \frac{u}{L\varepsilon}(P_{C_3H_8in} - P_{C_3H_8}) - \frac{WRT}{V_b\varepsilon}r_1 \tag{7.4}$$

$$\frac{dP_{O_2}}{dt} = \frac{u}{L\varepsilon}(P_{O_2in} - P_{O_2}) - \frac{WRT}{V_b\varepsilon}r_3 \tag{7.5}$$

$$\frac{dP_{C_3H_6}}{dt} = \frac{u}{L\varepsilon}(P_{C_3H_6in} - P_{C_3H_6}) - \frac{WRT}{V_b\varepsilon}(k_{ads}P_{C_3H_6}(1-\theta_{C_3H_6}) - k_{des}\theta_{C_3H_6}) \tag{7.6}$$

$$\frac{dP_{CO}}{dt} = \frac{u}{L\varepsilon}(P_{COin} - P_{CO}) + \frac{WRT}{V_b\varepsilon}\left(\frac{3}{x+1}\right)r_2 \tag{7.7}$$

$$\frac{dP_{CO_2}}{dt} = \frac{u}{L\varepsilon}(P_{CO_2in} - P_{CO_2}) + \frac{WRT}{V_b\varepsilon}\left(\frac{3x}{x+1}\right)r_2 \tag{7.8}$$

$$\frac{dP_{H_2O}}{dt} = \frac{u}{L\varepsilon}(P_{H_2Oin} - P_{H_2O}) + \frac{WRT}{V_b\varepsilon}(r_1 + 3r_2) \tag{7.9}$$

Since the reaction rates are dependent on the surface concentrations of propene ($\theta_{C_3H_6}$) and oxygen (1-β), expressions for their rates of change are needed:

$$\frac{d\theta_{C_3H_6}}{dt} = \frac{\left(r_1 - r_2 + k_{ads}P_{C_3H_6}\left(1-\theta_{C_3H_6}\right) - k_{des}\theta_{C_3H_6}\right)W}{Q_{C_3H_6}} \tag{7.10}$$

$$\frac{d\beta}{dt} = \frac{\left(r_1 + \left(\frac{3(3x+2)}{x+1}\right)r_2 - 2r_3\right)W}{Q_O} \tag{7.11}$$

The rate equations derived from the steady-state data did not provide all of the information required by the transient kinetic models. A few parameters had to be estimated and/or adjusted to fit the measured transient responses. From the steady-state kinetics only the adsorption equilibrium constant for propene was estimated ($K_{C_3H_6}$); however, the transient kinetic model required values for the individual rate constants for adsorption (k_{ads}) and desorption of propene (k_{des}). It was assumed that they were related by:

$$K_{C_3H_6} = \frac{k_{ads}}{k_{des}} \tag{7.12}$$

To fit the transient responses, values of k_{des} were chosen and the corresponding value of k_{ads} was calculated from Equation 7.12.

Two parameters which had a large influence on the character of the transient responses are the number of adsorption sites for oxygen (Q_O) and propene ($Q_{C_3H_6}$). The number of oxygen sites should be some fraction of the quantity of oxygen that the catalyst contains, representing the quantity of oxygen available for reaction at the surface. X-ray diffraction analysis of the catalyst revealed that it consists predominantly of magnesium oxide (MgO) and magnesium orthovanadate ($Mg_3V_2O_8$) phases. The magnesium orthovanadate phase is considerably more reducible and is probably heavily involved in the redox reaction. Thus the quantity of oxygen in the catalyst involved in the reaction is thought to consist mainly of that contained in the magnesium orthovanadate phase; however, probably only a fraction of that oxygen is available on the surface. In modelling the transient response data, Q_O was estimated by an adjustable fraction of the oxygen contained in the maximum quantity of the magnesium orthovanadate phase (X_O).

The quantity of sites for propene adsorption is more difficult to base on some character of the catalyst. However, it is possible that the vanadium metal may serve as adsorption sites for propene. Again, only a fraction of the vanadium is accessible on the surface. For modelling the data, $Q_{C_3H_6}$ was estimated by an adjustable fraction of the vanadium contained in the catalyst ($X_{C_3H_6}$).

The void fraction of the catalyst bed (ε) is also unknown. However, for small spherical particles packed in a relatively large diameter tube it is known to approach 0.4 [86].

7.1.2 Diffusion process

It is generally assumed that transport of oxygen from the bulk of the catalyst to the reduced surface plays an important role in the transient responses. A simple model for the rate of diffusion of bulk oxygen is used, based on the film theory of mass transport. The rate of change of the bulk oxygen concentration (C_{O_b}) is expressed as:

$$\frac{dC_{O_b}}{dt} = \frac{\rho}{W} k_D A \frac{1}{\delta} (C_{O_b} - C_{O_s}) \tag{7.13}$$

The driving force for the diffusion process is the difference between the oxygen concentration in the bulk and at the surface (C_{O_s}). The instantaneous surface oxygen concentration is estimated as a function of the initial bulk concentration of oxygen ($C_{O_{bi}}$) and the degree of reduction of the catalyst surface by:

$$C_{O_s} = C_{O_{bi}} (1 - \beta) \tag{7.14}$$

The initial bulk concentration of oxygen was estimated as 3519 mol m^{-3}. It is difficult to estimate independently the diffusivity of oxygen (k_D), the area for transport (A), and the penetration depth (δ). Therefore, these parameters were lumped together and estimated by

one adjustable parameter:

$$\omega = \frac{k_D A}{\delta} \tag{7.15}$$

When bulk oxygen transport is included in the transient kinetic modelling, it is assumed to occur in parallel with the normal kinetic process defined by equations 7.4 to 7.11. Equation 7.13 is added to the problem and equation 7.11 altered to account for the contribution of oxygen transport to the surface from the catalyst bulk. It is noteworthy that, as modelled above, the oxygen transport process will not affect the steady-state of the system. At steady-state the driving force for oxygen transport becomes zero.

7.1.3 Reactor model

The reactor is modelled as a series of volume elements each representing a well-stirred tank reactor. Each volume element contained an equal quantity of catalyst. A sufficient number of volume elements is included such that the complete reactor approaches that of a fixed bed with plug flow. This approach simplifies the computational demands of the problem by allowing it to be modelled with only ordinary differential equations.

During start-up of the reaction, the temperature rise due to reaction was about 3°C. Since the catalyst temperature was measured near the end of the bed, it indicates the temperature gradient over the catalyst bed. A 3°C increase in the reaction temperature above 510°C, causes only small increases of 4% in the reaction rates r_1 and r_2. This estimate is based on the predicted activation energies for the MV2 model, r_1 and r_2 rates. The rate of re-oxidation of the catalyst (r_3) is more temperature-sensitive because of its higher activation energy. The corresponding increase in its rate is higher at 18%. Still, these temperature effects are relatively small and do not significantly affect the transient responses. This justifies the use of an isothermal model.

The pressure drop across the reactor was less than about 10 kPa, thus it is assumed isobaric. The increase in the superficial gas velocity, due to expansion of the gas by reaction, is neglected, because of the low conversions (below 10% for both oxygen and propane) and the low partial pressures of the reactants. The catalyst was a fine powder. It is estimated the catalyst particles were less than 50 μm in diameter. Activation energies for the steady-state kinetic models developed in chapter 4, were usually greater than 70 kJ mol^{-1}, in the range expected for kinetically controlled reaction rates. Thus, intra particle mass transfer can be safely assumed insignificant.

The simulations were performed with MATLAB (version 4.2). The numerical integration was performed with a subroutine that uses a semi-implicit Runge-Kutta technique that is capable of solving even stiff systems of ordinary differential equations.

7.2 Modelling results

7.2.1 Reaction start-up

Figure 7.1 compares experimental and simulated results for the transient responses of reactants and products from a step-change in the propane concentration from 0 to 3%. The step-change is made at time zero. In the experiment, the oxygen feed concentration is held constant at 6%, the mass of catalyst is 21 mg and the reaction temperature is 510°C. The catalyst was pre-treated at the reaction conditions for 3 h, and then exposed to oxygen for 0.5 h before the step-change.

Table 7.1 shows the values of the adjustable parameters chosen for the dynamic model. The values of the parameters were chosen by a simple visual fit of the predicted transients to the experimental transients. Transport of bulk oxygen was not included in the model used for Figure 7.1. Ten discrete volume elements were used to simulate the reactor. In fitting the

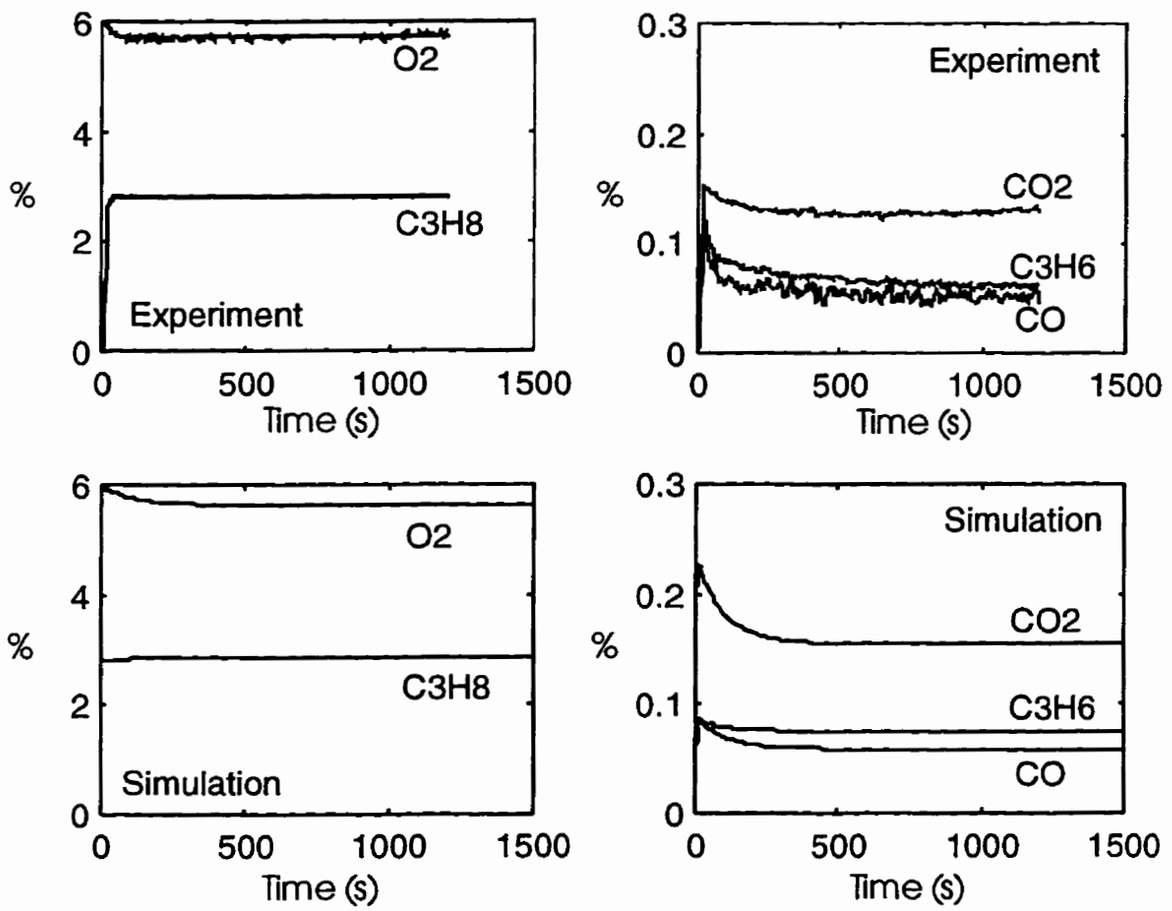

Figure 7.1 Experimental and simulated results for reaction start-up with 6% oxygen and 3% propane.

Table 7.1: Dynamic model parameter values used in Figure 7.1

Parameter	Value
X_O	0.38
$X_{C_3H_6}$	0.01
k_{des}	1 mol min^{-1} (g cat.)$^{-1}$
ε	0.4

transient data, the value for the propene adsorption equilibrium constant ($K_{C_3H_6}$) from the MV2 model was not directly used. From the MV2 model, the value of $K_{C_3H_6}$ at 510°C was 1156 bar^{-1}. The value used in the transient model was 231 bar^{-1} because this lower value better predicts the observed steady-state propene selectivity. The propene adsorption equilibrium constant determines the selectivity among propene and the carbon oxides. The propene selectivity predicted by the model is considerably lower than that of the transient data, even once steady-state is achieved. As discussed in chapter 5, the propene selectivity of the catalyst deteriorates with age at reaction conditions with an excess of oxygen. The MV2 model is derived from data collected after considerable aging of the catalyst (at least 6 h) under such conditions. On the other hand, the transient data were collected after a much shorter catalyst time-on-stream. Thus, there is justification for adjusting the value of the propene adsorption equilibrium constant.

Agreement of the simulated and experimental results is reasonably good, considering almost all of the kinetic parameters used, except the adsorption equilibrium constant for propene, $X_{C_3H_6}$ and X_O, are estimated from data collected at steady-state conditions.

The overshoot type response observed experimentally is reproduced by the model. During the transient the catalyst was reduced, so it is the rate of re-oxidation of the catalyst that becomes rate controlling. Figure 7.2 shows the change with time of the reduction of the catalyst and the surface coverage of propene axially along the reactor. Both increase rapidly after the step-change and approach steady-state at about the same time as the gas phase concentrations in Figure 7.1. The surface propene concentration reaches a peak, as does the gas phase concentration before decreasing and approaching steady-state. It is somewhat surprising to find that the degree of reduction increases along the length of the reactor. One might expect that the reduction might be greatest at the front of the reactor where the propane concentration is highest. Although not shown here, the propene concentration increases almost monotonically along the reactor, whereas the carbon oxide concentrations increase more rapidly almost exponentially. This is due to the consecutive nature of the kinetic sequence assumed. At higher conversion along the reactor, the selectivity to propene decreases and formation of carbon oxides extracts considerably more oxygen from the catalyst, accelerating reduction of the catalyst bed at the end of the reactor.

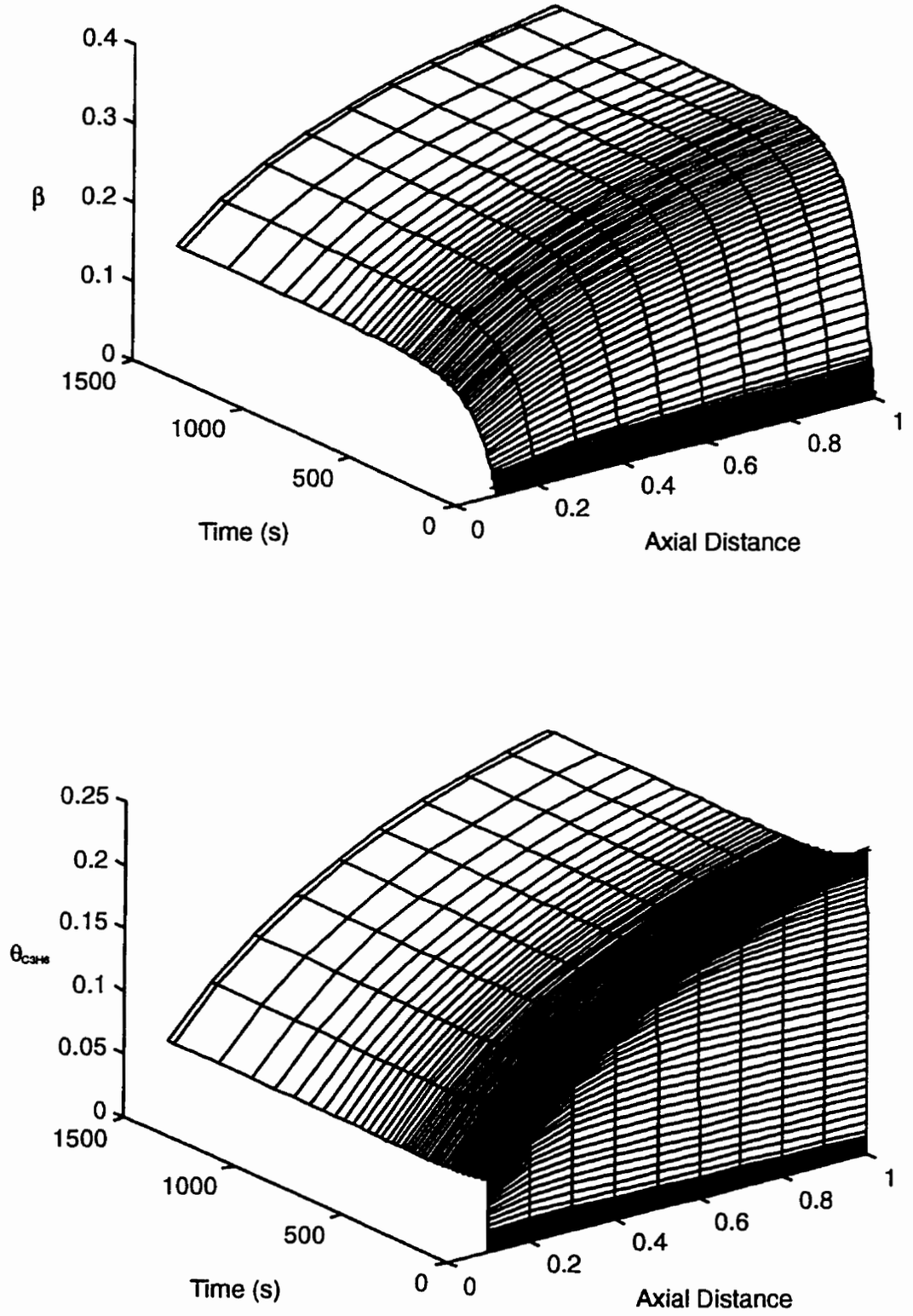

Figure 7.2 Predicted degree of reduction and surface coverage of propene

7.2.2 Model testing and parameter sensitivity

A large number of well-mixed volume elements increases the accuracy of the reactor model. However, the computer simulation time also increases with the number of volume elements. Thus a compromise is necessary. The effects of the number of volume elements on conversion and selectivity are shown in Table 7.2.

Table 7.2: Effect of volume elements on steady-state model predictions

Number of Volume Elements	Propane Conversion (%)	Oxygen Conversion (%)	Propene Selectivity (%)
1	4.9	5.6	45.7
3	5.0	5.4	52.6
5	5.1	5.3	54.4
7	5.1	5.3	55.2
10	5.1	5.3	55.9
13	5.1	5.3	56.3
16	5.1	5.2	56.4

It can be seen that propane and oxygen conversion are constant after only about 5 volume elements are used. Propene selectivity is more sensitive to the number of volume elements. Higher conversions of the reactants should be observed as plug flow is approached and the number of volume elements increases. Yet, this was true for propane but not for oxygen. Oxygen conversion decreases because propene selectivity increases. Because conversion of propane and oxygen are low, the reactor is nearly gradientless with respect to their concentrations and only five volume elements were needed to adequately model plug flow. However, the selectivity to propene is about 55%, meaning that because of the consecutive steps in the reaction mechanism, the conversion of propene, produced from propane, is also on the order of 50%. The propene concentration changes greatly along the reactor and the secondary reaction, the conversion of propene to carbon oxides, is sensitive to its variation. A relatively large number of volume elements is needed to accurately model the propene concentration gradient. In all of the simulations presented in this chapter, the number of volume elements used is 10.

The void fraction of the catalyst bed has only a very weak influence on the simulation results. It was varied between 0.3 to 0.7 and the model predictions showed little sensitivity. At low values of the desorption rate constant for propene (k_{des}), about 0.1 mol min^{-1} (g cat.)$^{-1}$, the selectivity to propene is sensitive to this parameter. Increasing k_{des}, increases the selectivity to propene. However, beyond a certain value, it has little effect on the simulation results and the propene selectivity is unchanged, because k_{ads} according to equation 7.12 becomes sufficiently large. At this point, gas phase and surface concentrations are in equilibrium throughout the transient. The value of k_{des} used in the simulations, unity, is in the range where propene selectivity is independent of k_{des} and equilibrium is maintained.

The predicted propene selectivities, controlled by the value of the propene equilibrium constant, are close to those observed experimentally.

The dynamic model parameters with the largest effect on the simulation results are X_O and $X_{C_3H_6}$. X_O affects the height of the overshoot peak and the time to reach steady-state. By increasing the amount of oxygen available on the catalyst, the maximum reaction rate increases and it takes a longer time to reach steady-state. $X_{C_3H_6}$ influences the time at which the peak rate is reached. With a large number of sites for propene adsorption, the fraction of occupied surface adsorption sites increases slowly, causing the secondary reaction (which depended on $\theta_{C_3H_6}$) to increase slowly as well. In the experimental results the peak rate is reached very quickly, about 10 s after the step-change (not including gas holdup time). To obtain this very fast response, a low value for $X_{C_3H_6}$, 0.01, was used. Since $X_{C_3H_6}$ represents the fraction of the vanadium content of the catalyst that is propene adsorption sites, the low value of $X_{C_3H_6}$ perhaps suggests that the vanadium metal may not serve as adsorption sites for propene. It can be seen in Figure 7.2, that $\theta_{C_3H_6}$ increases rapidly after the step-change. At low values of $X_{C_3H_6}$, the height of the overshoot peak, normally controlled by X_O, becomes insensitive to the quantity of oxygen on the catalyst surface and the maximum rate depended on the number of sites for propene adsorption.

As pointed out earlier, the catalyst used for the results in Figure 7.1 was pre-treated at reaction conditions. Step-change measurements were also made with fresh catalyst and the transient responses appear in Figure 6.2. An overshoot response was observed. The main difference between responses was that for the fresh catalyst, a considerably higher peak reaction rate was observed. The peak carbon dioxide concentration was almost 0.4%. No combination of reasonable values for the adjustable parameters can reproduce such a large response. The inability of the model to fit step-changes for fresh catalyst samples is not surprising. The fresh catalyst may undergo structural changes when first exposed to reactants and the rate controlling step may change or there is some irreversible reduction of the catalyst.

Experimental mass balances, discussed in chapter 6, did not indicate carbon deposition on the catalyst surface during reaction start-up with both propane and oxygen. However, for step-changes that interrupted the reaction, the response of the carbon monoxide signal lagged propene and carbon dioxide, indicating the possible oxidation of carbon species adsorbed on the catalyst surface. For an experiment in which 30 mg of catalyst was used the estimated quantity of carbon oxidized from the catalyst surface was 0.23 μmol. For 21 mg of catalyst, this would correspond to about 0.16 μmol. The 21 mg of catalyst contained 92 μmol of vanadium. The small quantity of adsorbed carbon predicted by the simulation agrees with the experimental measurements. In addition, DRIFT spectroscopy and isotope exchange experiments reported in the literature [63] found no evidence of adsorbed hydrocarbon species on a Mg-V-O catalyst. This finding supports our results indicating that carbon on the

catalyst, if present at all, must be at low concentration. Figure 7.2 indicates the average coverage of propene is about 0.15, this corresponds to 0.42 μmol of carbon. The predicted quantity is greater than that measured experimentally, but the agreement is reasonable considering the error of the measurement.

Experimental mass balances clearly indicated that oxygen was removed from the catalyst during reaction start-up with both oxygen and propane. For the experimental results in Figure 7.1, it was estimated that 1.7% of the oxygen from the orthovanadate phase was removed during the step-change. Figure 7.2 indicates the average degree of reduction of the catalyst surface is about 0.25 as steady-state is approached. To satisfactorily model the transients, the catalyst surface is set to contain 38% (X_O) of the oxygen content of the orthovanadate phase. The simulation predicts that 9.5% of the oxygen is removed. In this case, the experimental and simulated results differed more.

7.2.3 Transport of bulk oxygen

Figure 7.3 shows the simulated transient responses with allowance for the transport of bulk oxygen. They can be compared to the corresponding experimental results in Figure 7.1. The value of the lumped parameter for oxygen transport (ω) is 17.5×10^{-9} m^3 min^{-1}. The inclusion of oxygen transport from the catalyst bulk smoothes the transient responses and delays the onset of steady-state, but does not affect the overshoot peak, probably because the transport does not occur until the catalyst surface has been partially reduced. Including oxygen transport in the dynamic model moderately improves the agreement between simulated and experimental results in Figure 7.1.

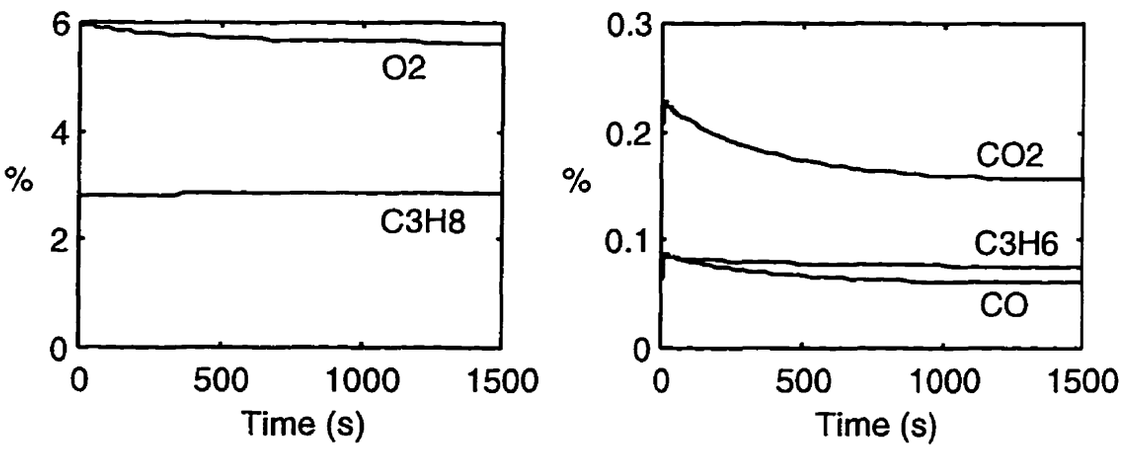

Figure 7.3 Simulated results with oxygen transport for reaction start-up with 6% oxygen and 3% propane (experimental results in Fig. 7.1).

X_O and ω seem to be inversely correlated; thus, it is difficult to assign values to them. A high value of X_O and a low value of ω slow the approach to steady-state. More information

regarding the physical properties of the catalyst may be needed to estimate values for these parameters.

7.2.4 Reaction without gas phase oxygen

The top two graphs in Figure 7.4, are repeated from Figure 6.5. They compare transient response results with and without gas phase oxygen. In both cases the catalyst had been exposed to reaction conditions for 3 h. Thereafter, the catalyst was treated by a stream containing 6% oxygen in helium for 0.5 h, followed by pure helium for 0.5 h. In both cases the catalyst mass was 17 mg and the reaction temperature 510°C. Step-changes were made at time zero. In both transients the response of propene is similar for about the first 300 s. The most striking difference between the two transients is the considerably reduced production of carbon oxides in the absence of gas phase oxygen. Selectivity for carbon oxides was reduced immediately after the step-change.

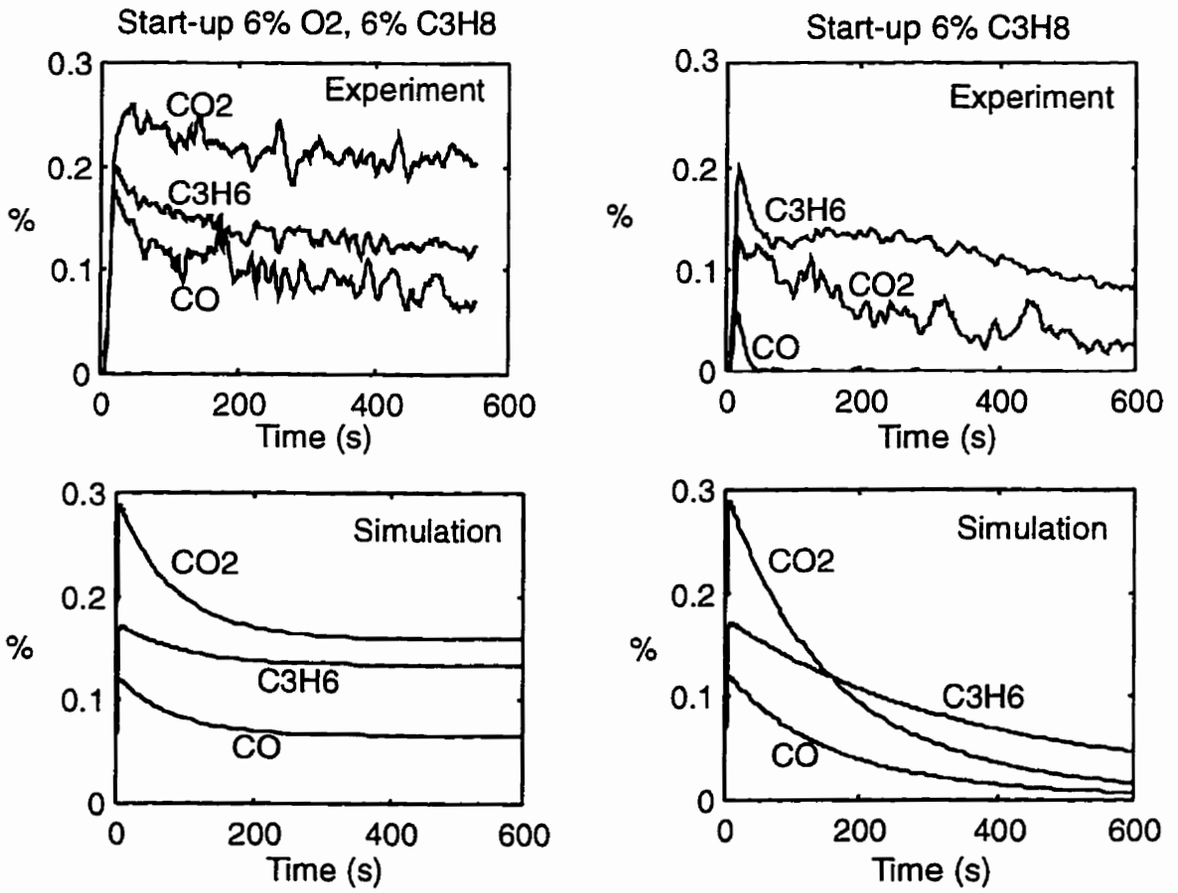

Figure 7.4 Experimental and simulated results for reaction start-up demonstrating effect of gas phase oxygen.

The bottom two graphs in Figure 7.4 show the corresponding simulated transients. For both simulations the values of the dynamic model parameters are those in Table 7.1. For the transient with gas phase oxygen, the simulated and experimental results match reasonably well. However, in the absence of gas phase oxygen, the dynamic model fails to predict the improved propene selectivity observed experimentally. The propene transient is correct, but the levels of carbon oxides are too high. The overshoot peak concentrations of carbon oxides for the transient without gas phase oxygen are the same as with gas phase oxygen. This result is not surprising, since it is not until after the catalyst is partially reduced that the re-oxidation of the catalyst with gas phase oxygen begins. Only after this point, should the absence of gas phase oxygen become noticeable. After partial reduction of the catalyst, the carbon oxide concentrations decline rapidly and improved propene selectivity is predicted. Thus, the mechanistic model used predicts improved propene selectivity when gas phase oxygen is absent. The model essentially consists of two consecutive reactions, both consuming oxygen. By the initial reaction, production of propene occurs, but without re-supplying the catalyst's oxygen reserve, the secondary reaction, oxidation of propene, is stifled. According to the kinetic model, propene selectivity should improve only after partial reduction of the catalyst.

7.3 Conclusions and discussion

A dynamic model based on a redox type kinetic model, with a simple consecutive reaction scheme successfully models the observed transients, during start-up of the reaction with catalyst previously exposed to reaction conditions. This confirms that the observed overshoot response is due to the partial reduction of the catalyst during the transient. The dynamic model cannot simulate the large overshoot response observed during start-up of the reaction with fresh catalyst. To obtain a good fit of the dynamic model a very small number of sites for surface propene adsorption, compared to the vanadium content of the catalyst, had to be assumed. This result agrees with experimental mass balances which indicated that little to no carbon is present on the catalyst surface.

Mass transport of oxygen from the catalyst bulk to the surface may be an important process during the transient responses. However, the rate of oxygen transport is correlated with the quantity of oxygen species on the surface available for reaction. Thus, it is not possible to unambiguously quantify the rate of oxygen transport and the oxygen initially on the catalyst surface.

When start-up of the reaction occurs in the absence of gas phase oxygen, a similar overshoot response is observed. However, the high propene selectivity observed immediately after the step-change is not correctly predicted by the dynamic model. This indicates that there are inadequacies with the kinetic model. Apparently, the presence of gas phase oxygen promotes the production of carbon oxides, even immediately after start-up of

the reaction when the catalyst is not partially reduced. A number of possible explanations can be proposed to explain the observed phenomenon. One possibility is that the gas phase oxygen reacts with propene or other carbon species adsorbed on the catalyst surface to produce carbon oxides. Also, it has often been suggested for partial oxidation reactions, including the oxidative dehydrogenation reaction [62], that the selectivity is dependent on the binding strength of the oxygen species. Loosely bound surface oxygen is considered more reactive, and thus, likely to cause carbon-carbon bond breakage and promote total oxidation. Whereas, strongly bound lattice oxygen is less reactive and favours partial oxidation. There may be different types of oxygen species on the catalyst surface, including some that are reactive enough to cause the direct and total oxidation of propane. This would add an additional route for the production of carbon oxides to the reaction mechanism. It seems reasonable that such non-selective surface oxygen species may be more prevalent when gas phase oxygen is present.

We speculate that the state of reduction of the catalyst may have to be included in the dynamic model and perhaps allowance must be made for the exposure history in order to achieve a model capable of describing all our transient observations. Building such an extensive dynamic model is well beyond the objectives of this thesis.

8. Periodic operation

The selectivity of partial oxidation reactions may be highly dependent on how the reactants - hydrocarbons and oxygen - are contacted with the catalyst. If so, non-conventional reactor designs or operation could be used to tailor reactant and catalyst contact to minimize deep oxidation. To this end, there have been some recent studies into the use of catalytic membrane reactors for the oxidative dehydrogenation of ethane [87,88] and propane [89,90]. It is thought that by controlled feeding through a membrane, the oxygen could be better distributed to regulate the extent of the side reactions, thus leading to higher yields and selectivities.

Both Pantazidis et al. [89] and Téllez et al. [90] have examined the use of different inert membrane materials to distribute oxygen to a fixed bed of Mg-V-O catalyst for propane oxidative dehydrogenation. Pantazidis et al. claimed that use of the membrane feeding of oxygen resulted in a marked increase in propene yields, compared with conventional gas phase co-feeding. Téllez et al., on the other hand, did not find any notable improvement in yields by such a reactor configuration. Instead they pointed out that one can extend the range of safe reactor operation by avoiding flammable mixtures of the reactants by distributing the oxygen feed. Also, the formation of hot spots could be decreased.

In another study, the electrocatalytic oxidation of propane on Mg-V-O catalysts was tested [91]. The Mg-V-O catalyst was deposited on a silver electrode to which oxygen ions could be electrochemically pumped. It was claimed that the electrochemically supplied oxygen was more selective for propene production than that supplied by the gas phase.

In this chapter, a non-conventional mode of reactor operation is examined for oxidative dehydrogenation: periodic operation. The reaction is carried out by cyclically feeding reactant mixtures of different compositions. Transient responses to this type of forcing can reveal additional information regarding the reaction mechanism and kinetics [84,85].

8.1 Potential benefits of periodic operation

Silveston [92] has reviewed the application of periodic operation to complex reactions for selectivity improvements. Many of these reactions consist of consecutive-competitive reaction schemes, like the following:

$$A + B \rightarrow C, \quad C + B \rightarrow D$$

$$A + B \rightarrow D$$

where A and B are reactants, C is the desired product and D is undesired. Partial oxidation reactions often follow this scheme where A is a hydrocarbon and B is oxygen. By applying periodic operation to these consecutive-competitive reaction schemes, selectivity

improvements can be achieved. The concept is simple: when A and B are fed, the first reaction in the consecutive path builds up the concentration of C; at the same time, the second reaction, forming D, begins to accelerate. By temporarily cutting off the feed of B and perhaps also A, the second reaction can be choked before the concentration of C is reduced to its steady-state level.

For the oxidative dehydrogenation of propane, the transient experimental results, discussed in chapter 6, demonstrate that even at the same conversion of propane, carrying out the reaction without gas phase oxygen results in improved propene selectivity. The modelling results, in chapter 7, suggest that this improved selectivity is not merely the result of exploiting the consecutive reaction scheme. The dynamic model consisting of a consecutive reaction scheme, could not account for the improved propene selectivity observed immediately after start-up of the reaction without gas phase oxygen. These findings indicate that the oxidative dehydrogenation reaction is a promising candidate for operation by some sort of composition modulation scheme. Apparently, improved selectivity can be achieved not only by exploiting the consecutive reaction scheme but also by preventing some total oxidation pathways involving the presence of gas phase oxygen.

Periodic operation of the oxidative dehydrogenation reaction has already been studied. Phillips Petroleum [93], Atlantic Richfield [94], and Dow Chemical [95] have obtained patents for oxidative dehydrogenation processes involving alternating feeds of air or oxygen and an alkane over different metal oxide catalysts. A Ukrainian research group seem to have been the first to publish results for the oxidative dehydrogenation of butane over Mg-Mo-O and Mg-V-Mo-O catalysts by alternating feeds of air and butane [96-98]. They reported butene selectivities of 65% at 70% butane conversion. More recently, researchers at Dow Chemical extended the Ukrainian research [56,57]. Their aim was to develop a practical transported bed catalyst. Commercialization of a cyclic process would require the use of a fluidized bed reactor where the catalyst would be transported to a separate reactor for re-oxidation. The Dow group call their process 'Anaerobic Oxidation of Butane'. Experimentally, they simulate the two vessel fluidized bed reactor system by performing the reaction in a fixed bed reactor operated with alternating pulses of butane and oxygen. They have reported butene selectivities of up to 80% at about 50% butane conversion.

The Dow Chemical researchers have pointed out that an additional advantage of their process is that the detonation hazards of mixtures of butane and oxygen are avoided. But, other than reporting attractive results, groups that have studied oxidative dehydrogenation under periodic operation have not explained why such a mode of operation results in superior selectivity.

8.2 Experimental Methods

In all periodic operation type experiments, 20-40 mg of catalyst was used and the reaction temperature was 510°C. Feed to the reactor alternated between two feed streams that were mixtures of propane and oxygen, both diluted in helium. Thus a 2-part feed cycle was used; cycle periods were between 10 to 400 s.

Typically periodic operation experiments were performed with the same sample of catalyst. After pre-treatment of the catalyst (as described in Section 3.1), steady-state reaction with 6% propane and 6% oxygen was carried out for 3 h. A series of periodic operation experiments were then consecutively performed in a random order. After each periodic operation experiment, steady-state conditions were re-introduced for at least 1 h and product analysis was performed to ensure that the catalyst retained the same activity and selectivity. Each periodic operation condition was run for at least 10 cycles. Typically after about five cycles, the response was reasonably constant. The product concentrations were integrated over the final five cycles to calculate time-average concentrations, conversion, and selectivity.

For each periodic operation condition, the corresponding time-average steady-state conditions were also run. Periodic operation results are compared to these steady-state results.

8.3 Modes of Cyclic Operation

8.3.1 Variation of cycle periods at 1:1 split

Since the selectivity of the reaction is improved by reacting propane without gas phase oxygen, an obvious strategy was to operate the reaction by alternately feeding propane and oxygen. In these initial experiments, 30 mg of catalyst was used. Feed to the reactor alternated between 6% propane and 6% oxygen, both diluted in helium. A feed cycle consisted of exposures to propane and oxygen of equal duration (1:1 cycle split), varying between 10 and 400 s.

Figure 8.1 shows the product responses during the final three cycles at four cycle periods. At the longest cycle period, 400 s, product responses are similar to those observed during the step-change experiments without gas phase oxygen. After the switch to propane feed there is an overshoot, then the product concentrations decline rapidly during about the first 50 s. They continue to decline, but much more slowly during the remainder of the propane feed half of the cycle. During the initial rapid decline in product concentrations, the decline in the carbon oxide concentrations is slightly steeper than that of propene, so that the selectivity increases for 20 to 30 s after the peak in product concentrations. For the remainder of the propane-feed half of the cycle, the selectivity is about constant. At shorter

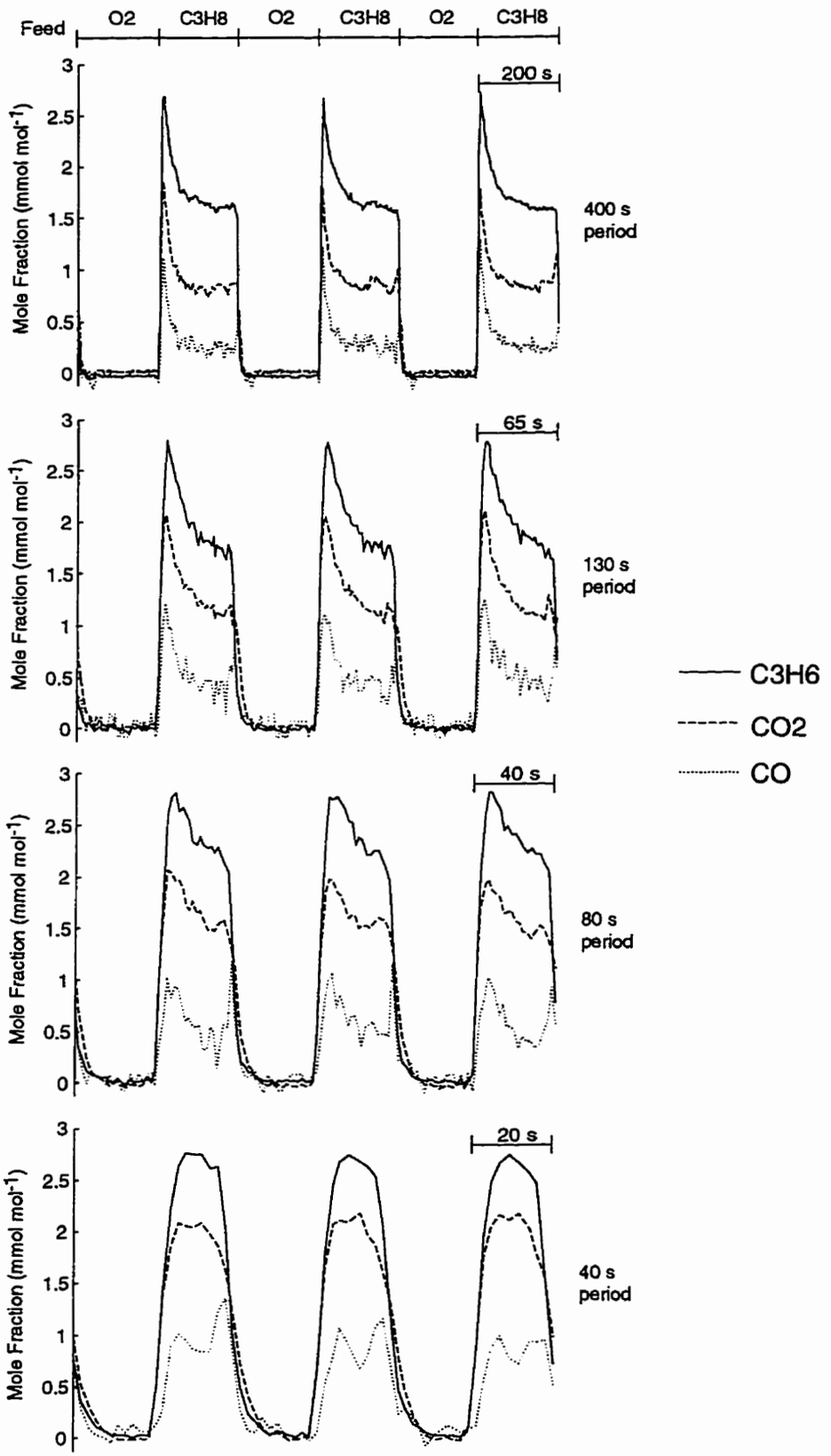

Figure 8.1 Product responses during periodic operation with 1:1 split

cycle periods the responses are similar, except the interval of decline is shortened, until at the 40 s cycle period, when only the peak in product concentrations remains.

During the oxygen-feed half of the cycle the product concentrations always decline to zero within about 10 s (Figure 8.1). Mass balances for step-change experiments indicated that a small amount of carbon was deposited on the catalyst during start-up of the reaction without gas phase oxygen (see Section 6.5). Thus, it would not be surprising if carbon oxides were produced during the oxygen-half of the cycle. Figure 8.1 shows that immediately after the switch to oxygen, the decline of the carbon dioxide concentration lags slightly behind the decline of propene and carbon monoxide. This is clearest at the shorter cycle periods. This lag in the carbon dioxide signal may be due to oxidation of carbon or carbon-containing species on the catalyst surface.

Although not shown here, the product responses at the very shortest cycle periods, 10 and 20 s, were somewhat different. At the 20 s period, the responses were similar to those at 40 s, except the product concentrations peaked at a lower level than for the 40 s period, before they declined after the switch to oxygen feed. During the oxygen-feed half of the cycle, not all of the product concentrations declined to zero; in particular, the carbon dioxide concentration remained relatively high. At the shortest period, 10 s, product responses neither peaked during the propane feed half-cycle nor declined to zero during the oxygen feed half-cycle. The selectivity was different; the carbon dioxide concentration was always greater than the propene concentration. The responses were erratic because the cycle frequency was close to the maximum scanning frequency of the mass spectrometer (about 1.8 s). Also, under this condition of rapid cycling, the catalyst is not exposed to pure feeds of oxygen and propane because of mixing in the reactor system.

Figure 8.2 shows the time-average propane conversion, propene selectivity and propene yield at each cycle period tested. Yield is simply the product of conversion and selectivity (conversion $\times$ selectivity). For all periodic operation conditions, the corresponding time-average steady-state conditions are a feed of 3% oxygen and 3% propane. Results at these steady-state conditions are indicated on the axis of the plots for comparison. Operating the reaction without gas phase oxygen increases propene selectivity. Not surprisingly, the propene selectivity during periodic operation with cycle periods greater than 10 s is always high, at least 70%, and well above the 51% selectivity at steady-state. At all cycle periods, the time-average propane conversion is lower than the comparable steady-state conversion. The propane conversion tends to increase as the cycle period is shortened, due to the overshoot responses. At long cycle periods, greater than 200 s, the increase in propane conversion is small, because the decline in the product concentrations is slower after long exposures to propane. The increased propane conversion at shorter cycle periods comes with a penalty in the propene selectivity. The propene selectivity is highest at the longest cycle period and slowly declines as the period is shortened. This occurs because immediately after

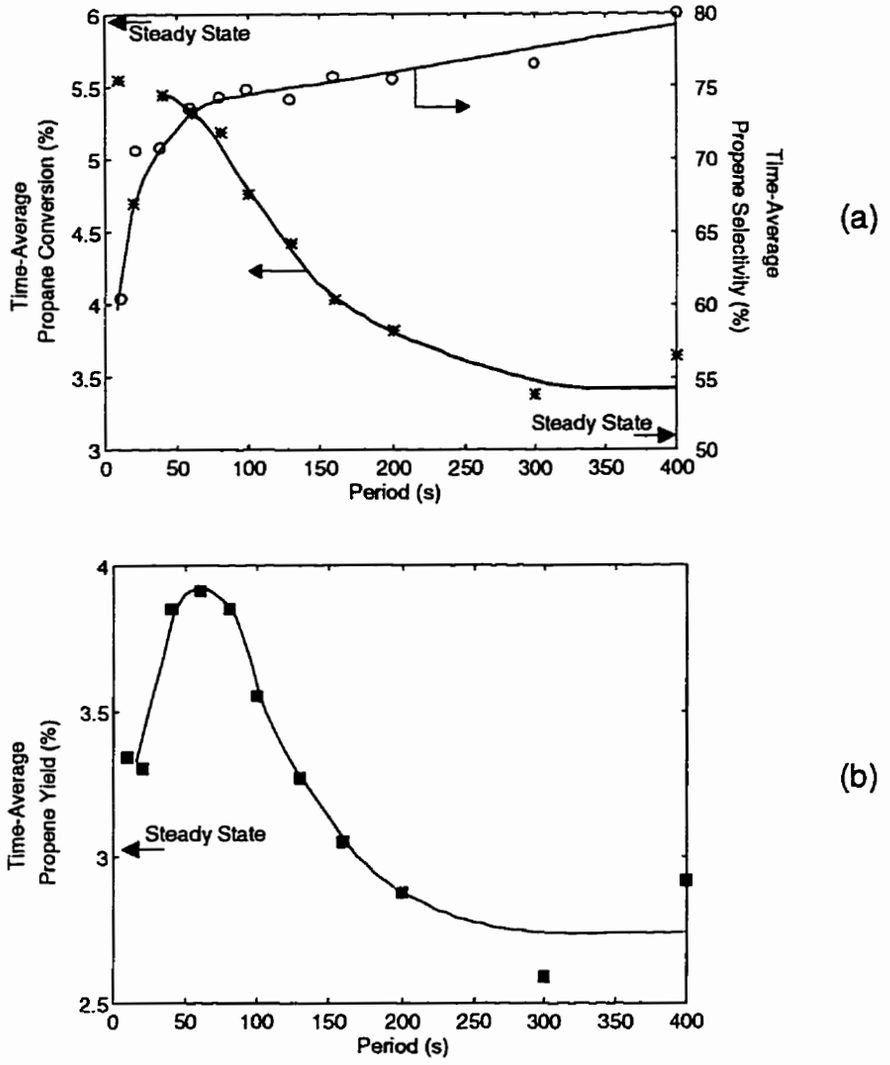

Figure 8.2 Time-average conversion, selectivity and yield; ○ selectivity, * conversion, ■ yield.

the catalyst is re-exposed to propane, following the peak in product concentrations, there is a short interval (20-30 s) of increasing selectivity. Also, after the switch to oxygen, as the product concentrations decline rapidly, the carbon dioxide concentration lags slightly and the propene selectivity is again low (see Figure 8.1). As the cycle period is shortened, these intervals of start-up and suppression of the reaction dominate the responses and contribute to a net reduction in the time-average propene selectivity.

From the 40 to 20 s cycle period, the time-average propane conversion abruptly dropped and was only 4.7% for the 20 s period. At the 20 s period the duration of the propane exposure was apparently not long enough for the peak in product concentrations to be reached before the switch to oxygen feed. The time-average propene selectivity was only slightly lower at the 20 s period than at the 40 s period. At the 10 s cycle period, the time-

average propene selectivity drops sharply to about 60%, close to the time-average steady-state result. The time-average propane conversion is high at about 5.5% and again close to the result at time-average steady-state. At the 10 s period, the process appears to be close to 'relaxed' steady-state operation which refers to conditions when cycling is performed rapidly enough such that the reaction behaves as though it is at steady-state conditions. This phenomena occurs because the rate of cycling exceeds the response time of the catalytic reaction. However, in this case this apparent relaxed steady-state behaviour may owe its cause not simply to the slower dynamics of the catalytic reaction compared to the feed switching, but also to gas mixing in the reactor that prevents the catalyst from being exposed to pure feeds of propane and oxygen under the most rapid cycling. Figure 6.2 indicates that the response time for a step-change in the propane feed concentration, measured without catalyst, is about 10 s (not including dead-time due to the gas hold-up on the reactor system).

From a process design viewpoint, what is most important is the propene yield as shown in Figure 8.2 b. At long cycle periods, although the propene selectivity is highest, the propane conversion is low and thus the yield is lower than at steady-state. It is only at cycle periods of less than about 160 s, that the propane conversion is sufficiently high for the periodic operation propene yield to compete with and even exceed that at steady-state. At cycle periods of less than about 80 s, there are smaller gains in propene yield, and even eventually a decline, as the time-average propene selectivity falls.

8.3.2 Comparison to other steady-state conditions

The superior performance of periodic operation compared to time-average steady-state conditions, shown in the previous section, is due to the better selectivity of the reaction without gas phase oxygen, as observed from step-change experiments in chapter 6. A more demanding test of periodic operation is to compare it to a broader range of steady-state conditions. Can we conclude that periodic operation of the reaction is globally superior to all steady-state conditions? Or is there, for any given periodic operation, some set of steady-state conditions that provide an equally good performance?

To answer these questions, it was necessary to determine whether superior steady-state performance can be achieved by lowering the feed partial pressure of oxygen. In all steady-state data collected thus far, the oxygen-to-propane feed ratio has been at least one. Table 8.1 shows some steady-state results with low feed concentrations of oxygen. Details about the methods used to collect this data and additional similar data are discussed in chapter 9.

Table 8.1 shows that at both feed concentrations of propane, as the oxygen-to-propane ratio is lowered from 1 to 0.2, the propene selectivity increases by 7 to 10%. At a feed concentration of 3% propane, the propane conversion is essentially constant, varying from 5.3 to 5.8%. But with a feed of 4% propane, the propane conversion decreases from 5 to 4.3%. The result is that the propene yield tends to increase at lower feed concentrations of

propane but remains about constant at 4% feed propane, as the oxygen feed concentration is lowered.

The selectivity of the reaction appears to be at least partially a function of the gas phase oxygen concentration, with higher selectivity favoured at low oxygen partial pressure. The literature suggests that higher propene selectivity occurs when the catalyst is more reduced. At the lower feed concentration of propane and the lowest concentration of oxygen, the re-oxidation reaction is sufficiently fast to maintain the same oxidation state of the catalyst and the same level of conversion of propane. This result agrees with the steady-state modelling results (see Section 4.2) that indicated that the reaction rate of propane had only a weak dependence on the partial pressure of oxygen. However, at higher feed concentrations of propane (4% propane and additional results at 6% propane to be shown in chapter 9), the same level of conversion of propane cannot be maintained as the oxygen feed concentration is lowered.

Table 8.1
Steady-state reaction with varying feed oxygen concentration*

Feed Concentration (%)		Ratio	Conversion (%)		Propene	Propene
Propane	Oxygen	O_2/C_3H_8	Propane	Oxygen	Selec. (%)	Yield (%)
3	3.6	1.2	5.3	11.0	53	2.8
3	3	1	5.4	12.3	57	3.1
3	2.4	0.8	5.6	16.3	57	3.2
3	1.8	0.6	5.3	18.3	62	3.3
3	1.2	0.4	5.8	29.8	63	3.7
3	0.6	0.2	5.4	52.5	64	3.5
4	4	1	5.0	10.8	60	3.0
4	3.2	0.8	5.2	13.9	61	3.1
4	2.4	0.6	4.9	16.5	63	3.1
4	1.6	0.4	4.6	21.3	68	3.1
4	0.8	0.2	4.3	36.8	70	3.0

Under reaction at low concentrations of oxygen, the propene selectivity is improved and, at least at a low concentration of propane, conversion can be maintained such that the yield is improved. Thus, at the right conditions, operating the reaction at steady-state with a low concentration of oxygen may increase propene yields to levels comparable to time-average yields obtained by periodic operation.

8.3.3 Variation of cycle splits

One factor that places periodic operation with a 1:1 split at a disadvantage relative to steady operation is that half of the time no products are produced while the catalyst is being

re-oxidized. This greatly limits the time-average conversion. In the next series of experiments, the propane-oxygen feed split is varied to determine if the oxygen-feed half of the cycle can be reduced and a desired propane conversion maintained. These experiments compare the relative rates of the oxidation and reduction processes that occur during the catalytic reaction.

Figure 8.3 shows the product responses during periodic operation at four different cycle splits. For all experiments in which the cycle split was varied, the propane exposure part of the cycle was maintained at 50 s. The oxygen exposure part of the cycle was varied between 5 and 60 s. The cycle split notation used corresponds to the propane:oxygen ratio. Thus a 1:0.4 split means the cycle period consisted of a 50 s feed of propane and a 20 s feed of oxygen.

The product responses during the propane exposure part of the cycle was essentially identical when the oxygen part of the cycle was varied between 20 and 60 s, even though Figure 8.3 shows only the results for oxygen exposures of 30 and 50 s. The product concentrations reached a peak after exposure to propane and then declined until the switch to oxygen feed. As with the 1:1 split results, the decline of the carbon dioxide concentration lagged slightly behind the other products during the oxygen feed part of the cycle. When the oxygen feed duration fell to 10 s or less, the peak in the product concentrations after exposure to propane was lower; however, the product concentrations at the end of the propane exposure were at about the same level as for splits with longer exposures to oxygen.

Figure 8.4 shows the propane conversion, oxygen conversion, propene selectivity and propene yield for periodic operation with varying cycle splits. The periodic operation results are compared to their corresponding results at the same time-average steady-state conditions. The oxygen/propane ratio refers to the ratio of the duration of oxygen to propane exposures for periodic operation or the ratio of oxygen to propane concentration in the feed for time-average steady-state conditions. Thus an oxygen/propane ratio of 0.4 refers to a periodic operation cycle split of 1:0.4 and the corresponding time-average steady-state conditions are a feed of 4.3% propane and 1.7% oxygen.

The propane conversion was constant for periodic operation when the oxygen exposure was greater than 20 s or the oxygen/propane ratio was greater than 0.4. At shorter oxygen exposures, the propane conversion decreased because of the lower peak product concentrations as indicated in Figure 8.3. For the time-average steady-state results, the propane conversion always decreased as the oxygen/propane ratio was decreased. The oxygen conversion for both periodic operation and steady-state conditions increased as the proportion of oxygen feed was decreased. Oxygen conversion was always higher for steady-state conditions reaching as much as 70% at low oxygen concentration. As with the propane conversion, the propene selectivity was constant for periodic operation when the oxygen exposure was greater than 20 s, because product responses were identical during the propane

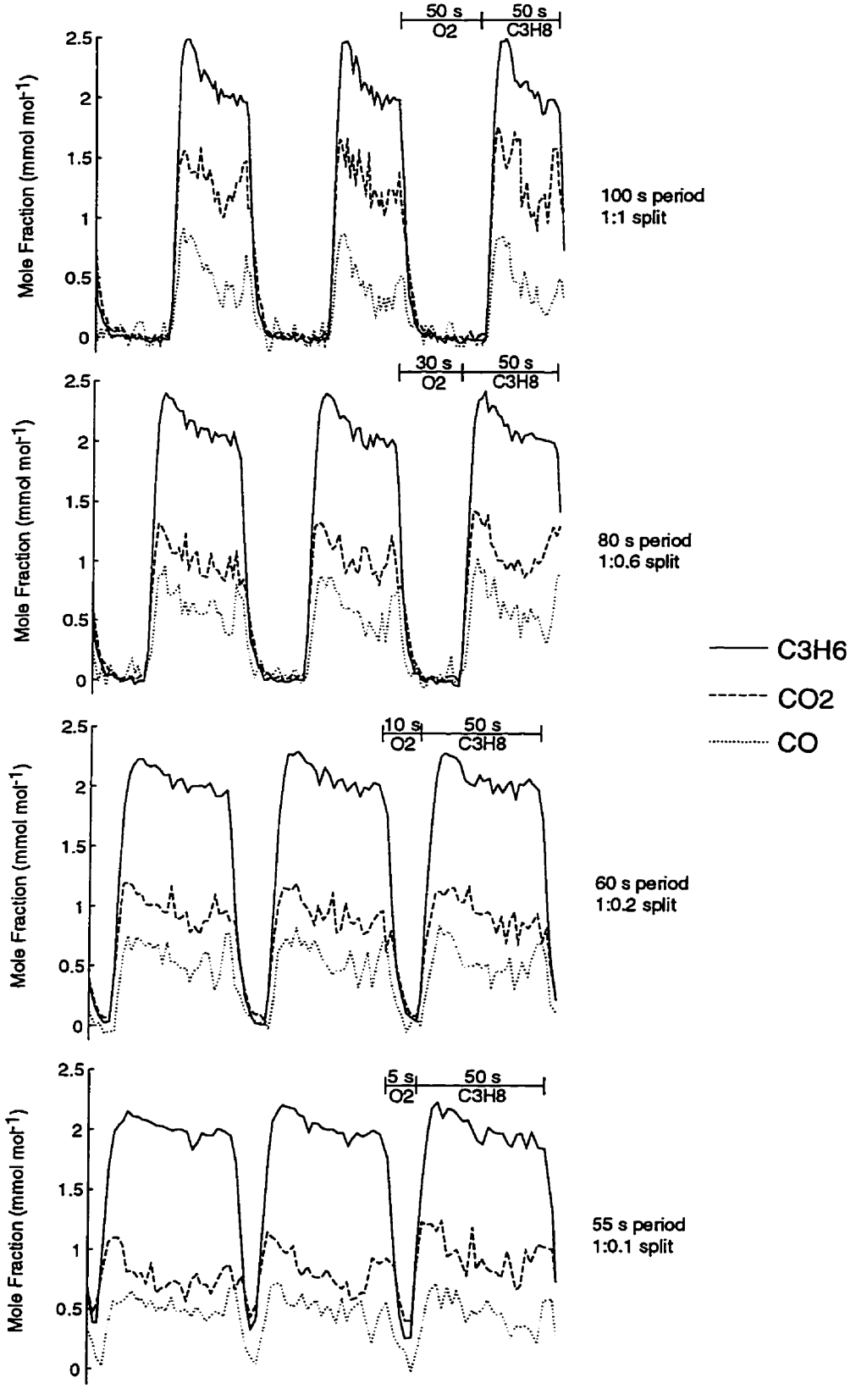

Figure 8.3 Product responses for periodic operation with varying cycle split

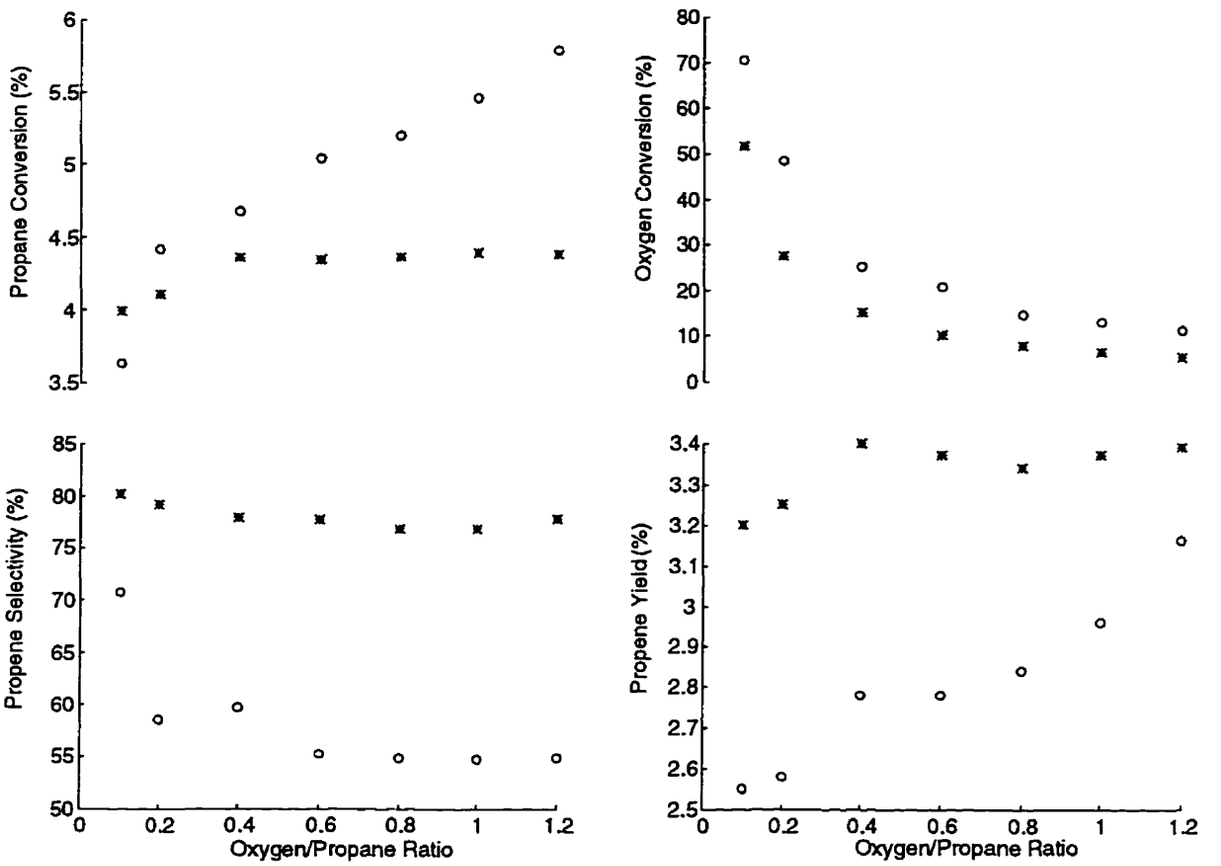

Figure 8.4 Time-average conversion, selectivity and yield for periodic operation and time-average steady-state conditions; * periodic operation, ○ steady-state

exposures over this range of splits. The propene selectivity increased slightly at the lowest oxygen exposures. The propene selectivity was always higher for periodic operation compared to steady-state. For steady-state, the propene selectivity was constant when the oxygen/propane ratio was greater than 0.6, but increased at lower oxygen concentrations. This follows the behaviour reported for improved propene selectivity at lower gas phase oxygen partial pressures from Table 8.1. The propene yield is higher at all of the periodic operation conditions compared to steady-state.

For periodic operation, the duration of the oxygen exposure could be shortened to as little as 20 seconds at the same propane conversion and propene selectivity. The results indicate that the rate of re-oxidation of the catalyst is rapid. For a cycle period consisting of a 50 s exposure to propane, the catalyst re-oxidizes almost completely during the first 10 s of exposure to oxygen. After about 20 s, further exposure to oxygen is unnecessary. By varying the split, so as to reduce the oxygen exposure time, the performance of periodic operation for propene yield remains constant as long as the oxygen exposure is not too short, but the productivity of the catalyst is improved. At shorter oxygen exposures of 10 and 20 s,

the catalyst is not re-oxidized to the same extent as at longer oxygen exposures. It was observed for the 1:1 split results that during the propane-feed half of the cycle the propene selectivity increased for a short interval after the peak in product concentrations. At the shorter oxygen exposures in Figure 8.3, this change in selectivity is not as apparent, which explains the slightly higher selectivity indicated in Figure 8.4 for these cycle splits. It is also possible that at the shortest oxygen exposures, preventing 'over-oxidation' or 'full-oxidation' of the catalyst may improve the initial selectivity after exposure to propane. Alternatively, the initially stable selectivity, immediately after exposure to propane, may simply be a consequence of the consecutive sequence of the reaction mechanism because the propane conversion changes relatively slowly during this interval.

8.3.4 Variation of the propane feed scheme with 1:1 splits

Thus far, in all of the periodic operation experiments feed to the reactor has been alternated only between propane and oxygen. This is often referred to as 'bang-bang' cycling. In the previous section, evidence indicated that preventing the complete oxidation of the catalyst may improve selectivity. Thus, it could be of some benefit to feed some propane during the oxidation part of the feed cycle to prevent complete oxidation. To investigate this possibility, experiments were undertaken in which the feed scheme of propane was varied.

Figure 8.5 illustrates how the feed scheme was varied. From bang-bang operation, in which feed is alternated between propane and oxygen, successively more propane is fed during the oxidation half of the feed cycle. Finally, the feed of propane is re-distributed to the point where propane is fed constantly at 3% and only oxygen is fed intermittently. Of course, in all of the experiments the time-average steady-state feed is the same: 3% propane and 3% oxygen. The experiments in Figure 8.5 were performed at cycle periods of 60 and 100 s.

Figure 8.6 shows the product responses for the final three cycles of periodic operation with the feed scheme as illustrated in Figure 8.5. The cycle period for the results in Figure 8.6 is 100 s, the corresponding results at a cycle period of 60 s are shown in Figure 8.7. There are few differences between the product responses at the two different cycle periods for identical feed schemes.

Considerable quantities of products were produced during the oxidation half of the feed cycles even when only 1% propane was fed. During these periods of simultaneous feed of propane and oxygen, the propane conversion was high but the propene selectivity was low with the dominant product being carbon dioxide. The selectivity differences of the two halves of the feed cycle were most clearly shown when propane was fed constantly at 3% and only oxygen was fed intermittently. In this case the concentration of propene and carbon

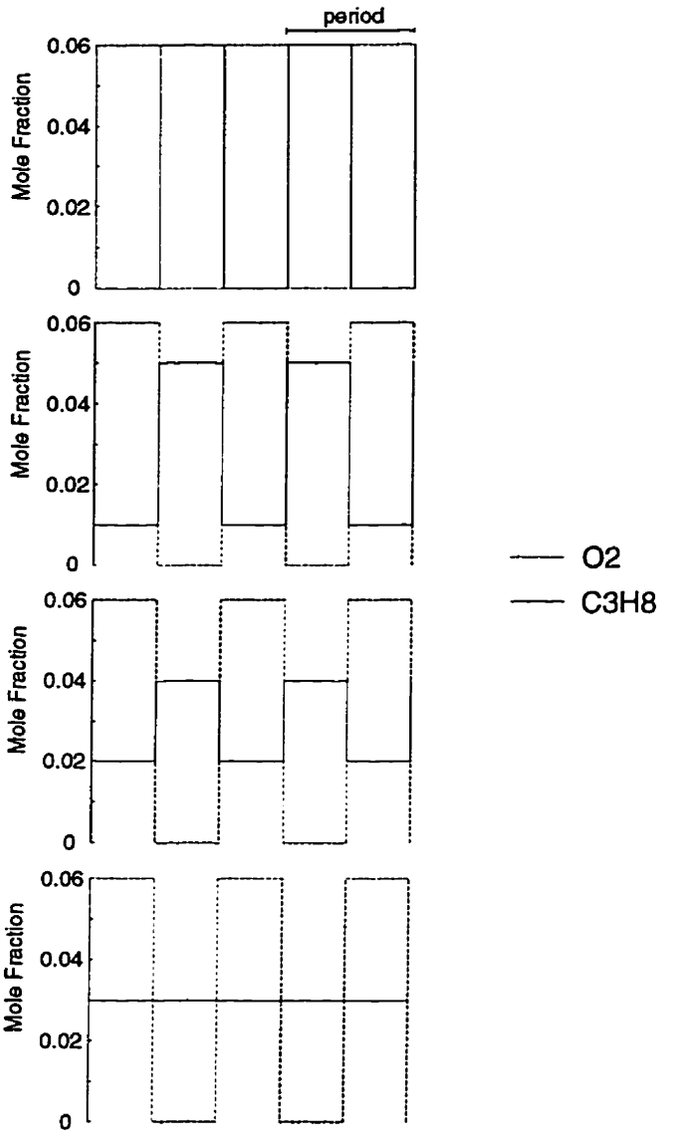

Figure 8.5 Variation of propane feed scheme

monoxide were almost constant while the concentration of carbon dioxide cycled between very high and low values, reflecting the feed of oxygen. During 'bang-bang' cycling a strong overshoot in the product responses was observed. As more of the propane was fed during the oxidation half of the cycle, it was expected that the catalyst would be less oxidized at the beginning of the propane feed half of the cycle. This appears to result in a progressive weakening in the overshoot response. However, even when propane was fed constantly at 3%, a small overshoot in the propene concentration occurred when oxygen was removed from the feed. Upon start-up of the reaction with propane and oxygen, during step-change response experiments, an overshoot response was observed (see section 6.3), presumably

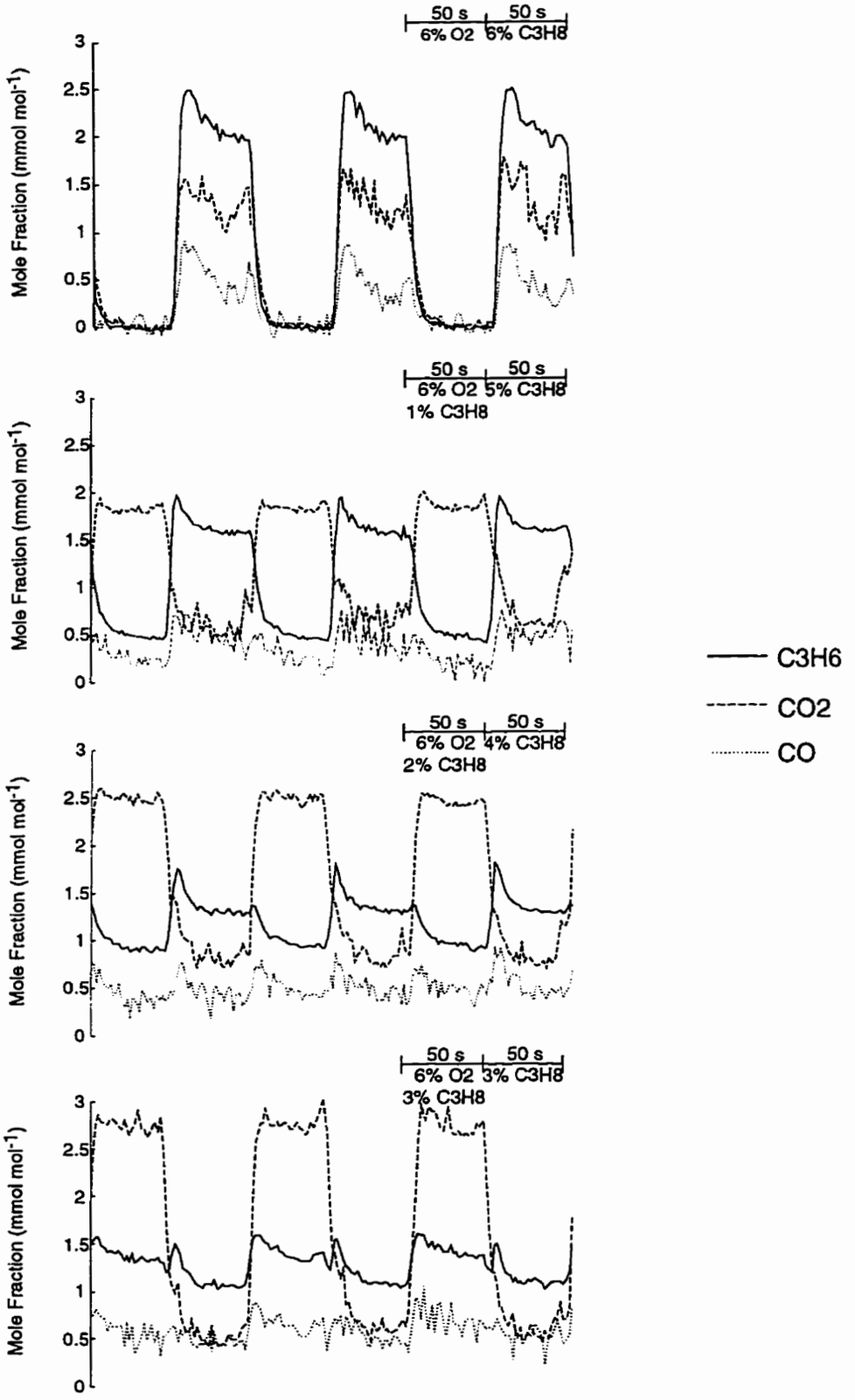

Figure 8.6 Product responses during periodic operation and variation of propane feed scheme; 100 s cycle split.

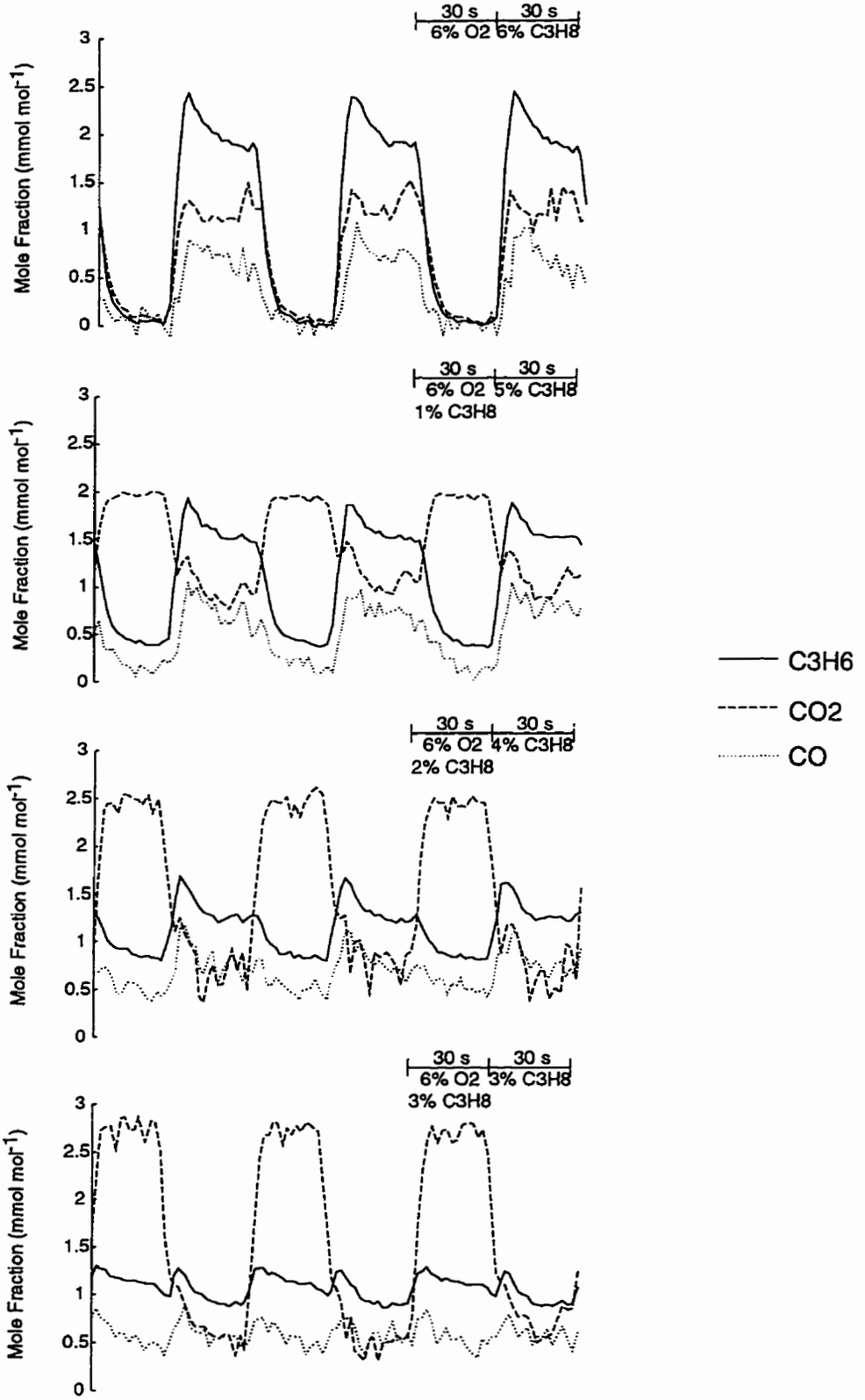

Figure 8.7 Product responses during periodic and variation of propane feed scheme; 60 s cycle period.

because the catalyst was reduced as steady-state was approached. In Figures 8.6 and 8.7, during the oxidation half of the feed cycle, when propane and oxygen were both fed, an overshoot response was not observed. In this case, the catalyst appeared to be in a reduced state before the propane and oxygen were fed and was probably re-oxidized during this half of the cycle, despite the introduction of some propane, as indicated by the overshoot response when the feed is switched to only propane.

Figure 8.8 shows the time-average conversion, selectivity and yield at the two cycle periods tested. The corresponding steady-state results are indicated on the axes of the plots. As more of the propane is fed during the oxidation half of the cycle, propane conversion tended to increase; however, at the same time, the propene selectivity tended to decrease. The propene selectivity is highest during bang-bang cycling because of the apparently high selectivity of the reaction when it occurs in the absence of gas phase oxygen. Selectivity is sacrificed for higher propane conversion as more propane is co-fed with oxygen. Even when propane is fed at a constant level throughout the cycle period, the propene selectivity is still higher than at the corresponding steady-state conditions. It is interesting that the propane

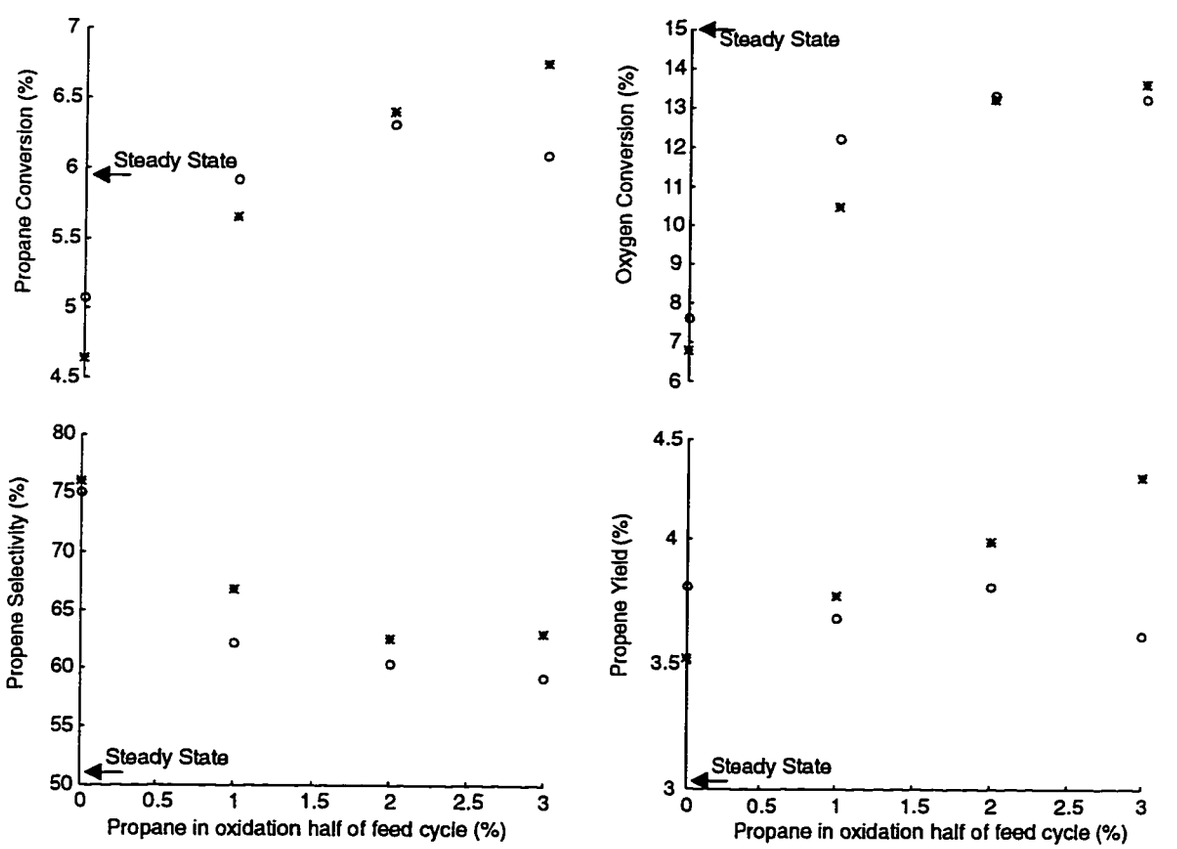

Figure 8.8 Time-average conversion, selectivity and yield for periodic operation with varying propane feed scheme; * 100 s period, ○ 60 s period.

conversion appears to exceed the steady conversion when 2 and 3% propane are fed during the oxidation half of the cycle. This may result because of the very different stoichiometry and oxygen demands of the reactions for producing carbon oxides versus propene. One can think of bang-bang cycling and steady-state operation as two extremes. With bang-bang cycling the selectivity is highest but conversion is low, while the opposite is true for steady-state operation. In accordance with Mars-Van Krevelen kinetics, the oxygen supply on the catalyst drives the reaction and governs conversion. When some of the propane is fed during the oxidation half of the cycle, conditions are between the two extremes of bang-bang operation and steady-state. Selectivity is still somewhat better than for steady-state operation. The key is that the production of propene consumes 7 to 10 times less oxygen than the production of carbon oxides. Thus, it seems possible, under conditions that favour a little higher selectivity to obtain a higher propane conversion because of a lower demand for oxygen. In effect, oxygen is used more efficiently.

As expected, the oxygen and propane conversion increased as more propane was fed during the oxidation half of the cycle. However, since the propene selectivity was always higher than for steady-state operation, the oxygen conversion never exceeded the steady-state conversion. For bang-bang cycling at cycle periods of 60 and 100 s, the propene yield was higher than at steady-state. Propene yield is a balance between conversion and selectivity. It appears that at a cycle period of 100 s, the gain in conversion was high enough and the loss in selectivity was low enough that yield increased as more propane is fed during the oxidation half of the cycle. On the other hand at a cycle period of 60 s, the propene yield was nearly steady. The unsteadiness in the propene yield is likely contributed by errors in both conversion and selectivity, leading to some uncertainty of interpretation. However, the differences in the trends for propene yield at the 60 and 100 s cycle periods may stem from the fact that for bang-bang cycling the propene yield at a 60 s cycle period is near optimum. Thus perhaps further improvements in the propene yield cannot be obtained at the 60 s cycle period by changing the feed scheme of propane.

8.4 Catalyst reduction by propane pulsing

Experiments were performed in which the catalyst was continuously reduced by pulsing or periodic feeding of propane alternated with helium, without any feed of oxygen. Changes in the product responses during the short propane-feed pulses after significant reduction of the catalyst are shown in Figure 8.9. A propane pulse consisted of 6% propane fed to the catalyst for 30 s; between pulses of propane, helium was fed for 20 s. Samples of catalyst with masses 20, 30 and 40 mg were exposed to 30 pulses of propane feed.

Previously experiments were performed in which catalyst was exposed continuously to propane for up to 10 min (see section 6.5). In the bang-bang cycling experiments, at the

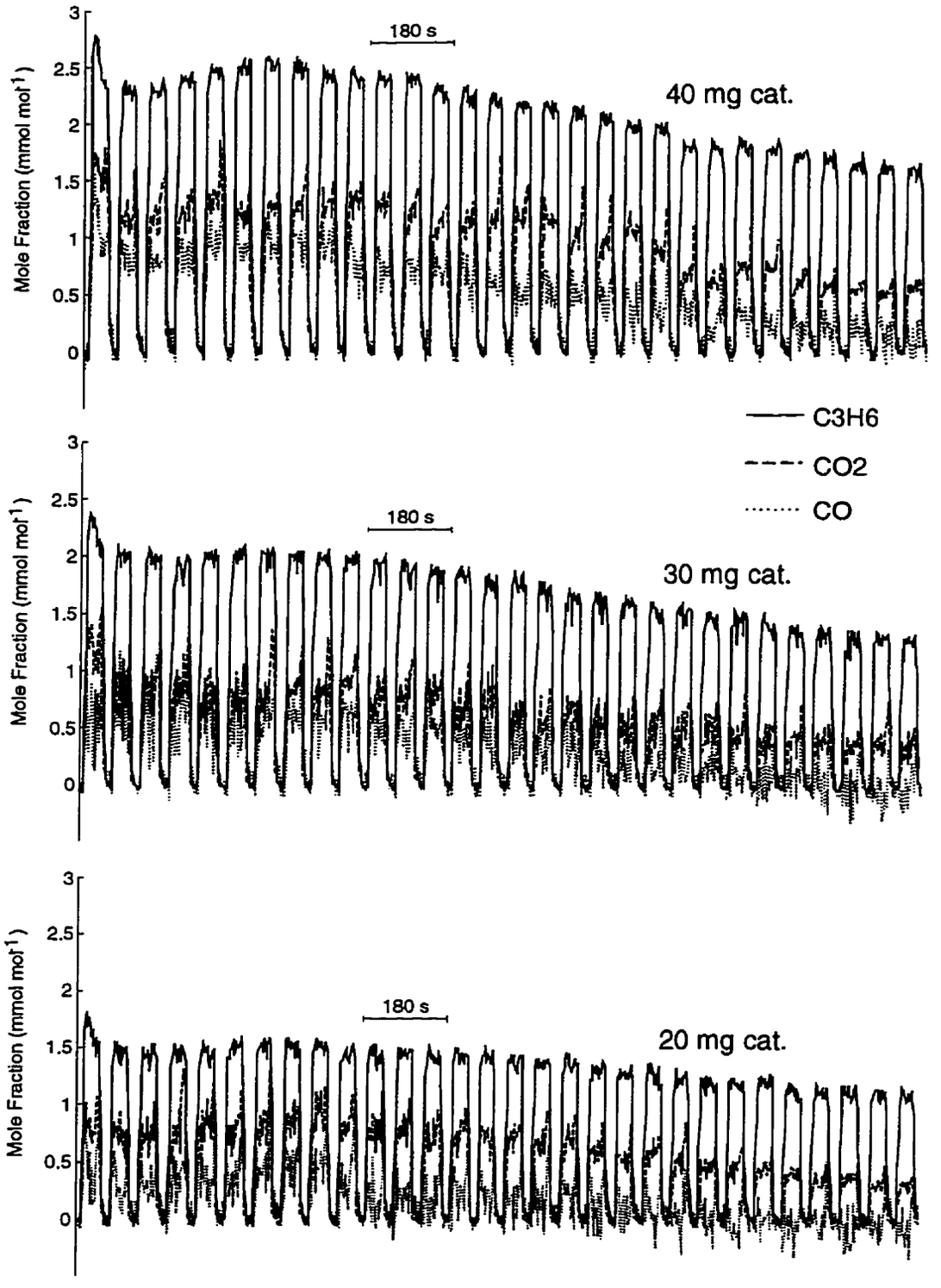

Figure 8.9 Product responses during pulsing of propane alternated with helium.

longest cycle period, the catalyst was exposed to propane for 200 s. In these previous experiments, an overshoot always occurred after the catalyst was exposed to propane. All products appeared immediately and for a short interval after the peak in product concentrations, the selectivity increased as product concentrations quickly decayed. Beyond this point, the selectivity remained stable as product concentrations declined more slowly as the catalyst was depleted of oxygen. Responses for periodic feeding of propane, shown in Figure 8.9 are different. For the first pulse of propane there is a fast decline in activity, as observed earlier. In subsequent pulses, no overshoot response is observed and the activity returns to about the level in the previous pulse because the catalyst is not re-oxidized between pulses, even though, over the entire 30 pulses a declining trend in activity is evident. The trend in activity during about the first 10 pulses is notable. The activity first declines then increases for about five more pulses and then declines thereafter. This temporary restoration in activity is never observed when the catalyst is continuously exposed to propane. Some sort of mass transport effect may lie behind the restoration in activity: perhaps after some critical degree of reduction of the catalyst surface is reached, transport of oxygen from the catalyst bulk begins, temporarily increasing the activity. Even so if transport of oxygen from the catalyst bulk were important, at least some overshoot might be expected during the propane pulses, since the surface should be re-oxidized during the helium-feed half of a cycle. Another suggestion for the restoration in activity is transport of oxygen along the length of the catalyst bed. A strong gradient in the degree of oxidation of the catalyst may develop along the length of catalyst bed. When reaction is interrupted, the oxygen in the catalyst bed may redistribute. A final possibility is that some restructuring of the catalyst surface occurs during the helium feed that increases the reactivity of the oxygen remaining on the catalyst surface.

Figure 8.10 provides a closer look at the product responses for a selection of pulses from the experiment with 40 mg of catalyst. As the catalyst is reduced, there appears to be a slight lag in carbon oxide production compared to propene, when the reaction re-starts. The propene selectivity increases as the catalyst is reduced; on the other hand, this may be simply a result of the decreasing conversion of propane. In the bang-bang cycling experiments, a lag in the response of the carbon dioxide concentration is observed upon switching to oxygen feed. This may result from the oxidation of carbon species on the catalyst. In propane pulsing results, no such lag in carbon dioxide is evident upon switching to helium. In this case, there may not be sufficient oxygen on the catalyst to oxidize any surface carbon species.

Figure 8.11 shows the average conversion, selectivity and cumulative oxygen removal from the catalyst for each pulse of propane. The trends in activity observed in Figure 8.9 are reflected in the average propane conversion in Figure 8.11. After the first pulse, there is a

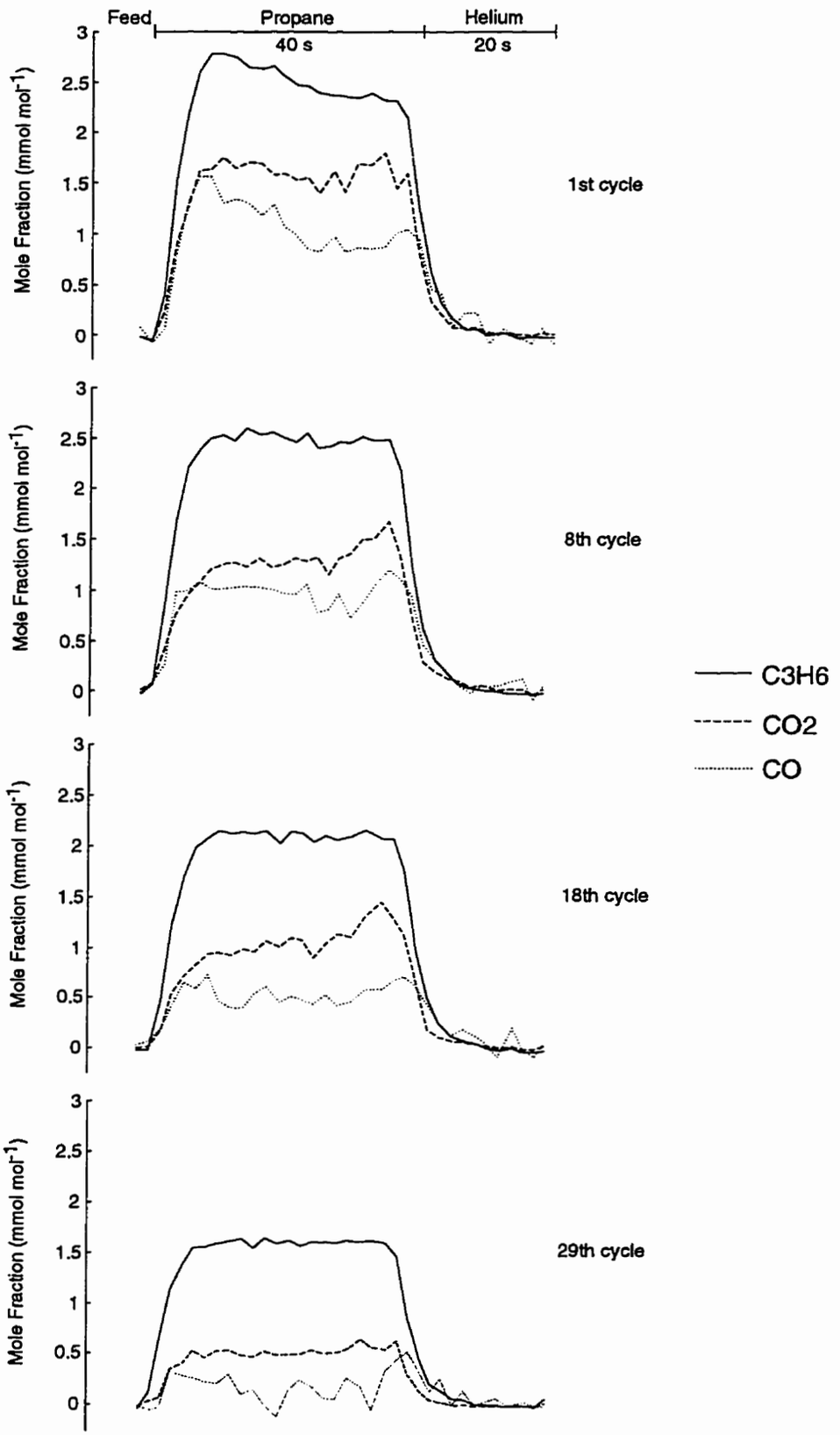

Figure 8.10 Product responses for a selection of pulses over 40 mg of catalyst.

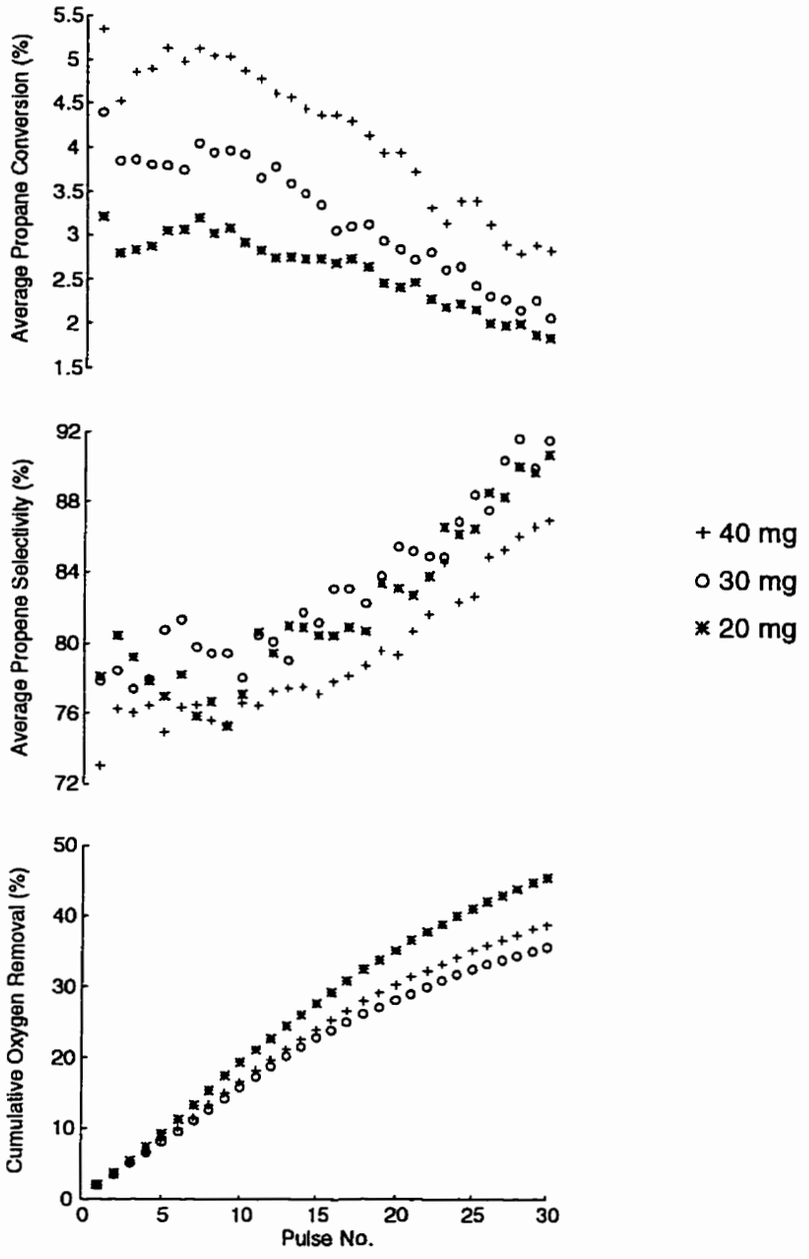

Figure 8.11 Average conversion, selectivity and cumulative oxygen removal for propane pulsing.

large decrease in propane conversion, but in the next 3 to 6 pulses the conversion increases again slightly, before continuing to decrease. Propene selectivity increases as more oxygen is removed from the catalyst and the propane conversion decreases. It is well-known that with such a partial oxidation reaction an inverse relation exists between conversion and selectivity to the intermediate product. However, in a comparison of the selectivity and conversion for individual pulses, this relation is not entirely followed. Although the conversion is higher with 30 mg of catalyst than with 20 mg, the selectivity differs little

between these two masses of catalyst. Only with 40 mg of catalyst does conversion seem high enough to cause a drop in selectivity. The conversion with 20 and 30 mg of catalyst may be too low for any significant consecutive reaction (oxidation of propene to carbon oxides) to occur, causing the selectivity to be independent of the propane conversion. For the final pulses of propane over 40 mg of catalyst, the conversion drops to between 2.5 to 3%. This is about the same conversion for the initial pulses over 20 mg of catalyst. For the final pulses over 40 mg of catalyst, the catalyst is considerably more reduced and the propene selectivity is about 86% compared to between 75 to 80% for the initial pulses over 20 mg of catalyst. It is apparent that part of the increase in propene selectivity is due to an improvement in the selectivity of the catalyst at higher degrees of reduction. The higher selectivity of a more reduced catalyst is also true at the same level of conversion of propane. Even so, it seems to require rather significant reduction of the catalyst before selectivity improvements are realized. It is only after about 10 pulses and 15 to 20% oxygen removal that the selectivity begins to increase. The literature suggests that this relation between selectivity and catalyst reduction is the result of the increasing bond strength and thus more favourable activity of the oxygen remaining on a more reduced catalyst [60,61]. These findings confirm experimental results of Kung and Andersen, for the oxidative dehydrogenation of butane over V_2O_5/Al_2O_3 [62].

The cumulative oxygen removal, shown in Figure 8.11, is based only on the oxygen in the magnesium orthovanadate ($Mg_3V_2O_8$) phase. It is further assumed that all vanadium is present in the orthovanadate phase. The oxygen in the MgO phase is not included in the oxygen removal calculation because magnesium is not as easily reduced as vanadium. Reducing the vanadium from V^{+5} to its lowest oxidation state V^{+2}, corresponds to the removal of 37.5% of the oxygen. After the 30 pulses of propane, vanadium would appear to be completely reduced in each catalyst sample. It is possible though that some oxygen in the MgO phase is active and there may be additional adsorbed oxygen at or near the catalyst surface, disregarded by these bulk calculations. However, it is clear that a relatively large quantity of oxygen is removed from the catalyst. During the propane pulsing experiment with 40 mg of catalyst, the mass spectrometer signal at mass 2 was monitored to check for the evolution of hydrogen via the direct thermal dehydrogenation reaction. There was no increase in the mass 2 signal beyond its background value throughout the experiment. However, the mass spectrometer was somewhat less sensitive to the detection of hydrogen than other products. The ratio of the linear sensitivity coefficients for carbon monoxide, propene and carbon dioxide to hydrogen were 1.45, 1.34 and 1.22 respectively. Thus, small undetectable quantities of hydrogen may have been produced. But water was a product throughout the reduction so oxidative dehydrogenation must have still been the dominant reaction for production of propene at these conditions.

8.4.1 Temperature-programmed oxidation/desorption

Temperature-programmed oxidation (TPO) experiments were undertaken to check whether any carbonaceous species were deposited on the catalyst during the propane pulsing experiments. Before the propane pulsing experiments, the catalyst was run at steady-state with 6% propane and 6% oxygen at 510°C for about 4 h. The catalyst was then exposed only to 6% oxygen for 5 min before the propane pulsing was carried out. Figure 8.12(a) shows the results of the TPO analysis performed on 40 mg of catalyst directly after propane pulsing. The results in Figure 8.12(b) are for the same quantity of catalyst, except in this case TPO was performed after a 4 h run at steady-state conditions. The catalyst was exposed to helium for 5 min before the TPO was performed.

During TPO experiments, the feed to the catalyst was switched from helium to 6% oxygen at time zero. Also temperature ramping was begun. The temperature was ramped from the reaction temperature 510°C at a rate of about 10°C min^{-1} to about 645°C. The final temperature was maintained constant for about 12 min. The catalyst bed temperature, throughout TPO, is shown in Figure 8.12.

In Figure 8.12(a), immediately after the switch to oxygen, a peak of carbon dioxide is produced and then disappears after about 100 s. As the temperature is ramped, more carbon dioxide is produced, peaking after about 800 s. In previous results (see section 6.5), after the catalyst had been exposed continuously to propane for 10 min, this same peak in carbon oxides was produced, immediately after exposure to oxygen; however, in that case the temperature was not ramped beyond the reaction temperature. Consequently, additional carbon species are on the catalyst which can only be oxidized at elevated temperatures. However, Figure 8.12(b) indicates that these carbon species are also present on a catalyst exposed only to steady-state conditions. The only additional carbon species on the catalyst exposed to propane pulsing seem to be mostly oxidized at or near the reaction temperature 510°C. No deactivation of the catalyst at steady-state conditions was observed. Thus, the carbon species oxidized at elevated temperatures present on both catalysts are probably rather inert and do not seem to block active sites.

There may also be some increase in the carbon monoxide signals in Figure 8.12, but there is considerable noise in these signals at the very low range of concentrations shown in the figure. The negative mole fractions of carbon monoxide result because of the method of treatment of the MS data, which accounts for cross-contributions of ion species in the mass spectrum, particularly at mass 28. However, as inferred from the carbon dioxide signal, the integrated quantity of carbon oxidized from the catalyst exposed to propane pulsing was 19.4 μmol. For the catalyst only exposed to steady-state conditions, 17.4 μmol of carbon was oxidized. The difference between these values, 2 μmol, is the additional carbon on the catalyst exposed to reaction conditions without gas phase oxygen. The catalyst surface bears

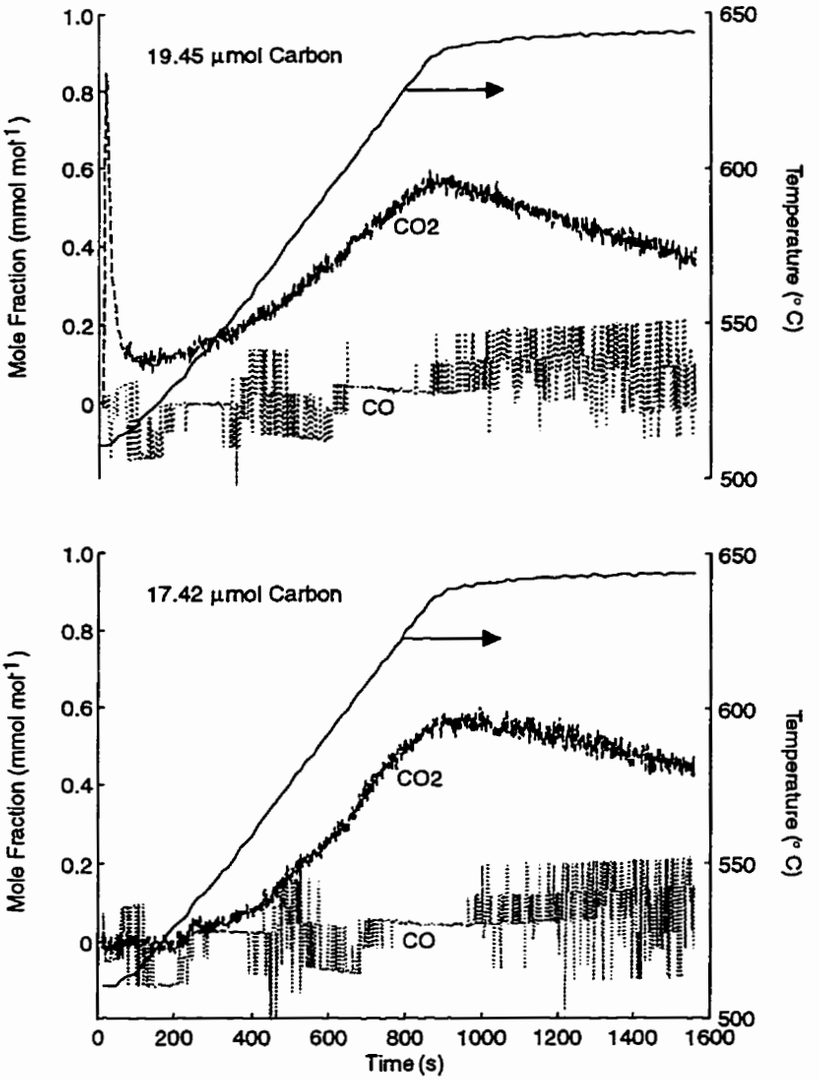

Figure 8.12 Temperature-programmed oxidation results; (a) after propane pulsing, (b) after only steady-state reaction.

more than 17.4 µmol of the apparently inert carbon, since if the oxidation had been carried out for a longer period of time, and/or the temperature had been ramped further, it is likely that more carbon dioxide would have been produced. For purposes of comparison, 40 mg of catalyst contains 176 µmol of vanadium.

Temperature-programmed desorption (TPD) was also performed with catalyst samples that had previously undergone propane pulsing and steady-state reaction. The TPD experimental method was the same as for the TPO except the catalyst was exposed only to pure helium at the same total flowrate during the temperature ramp rather than an oxygen and helium mixture. Figure 8.13 shows the results of these experiments which correspond to the TPO results shown in Figure 8.12.

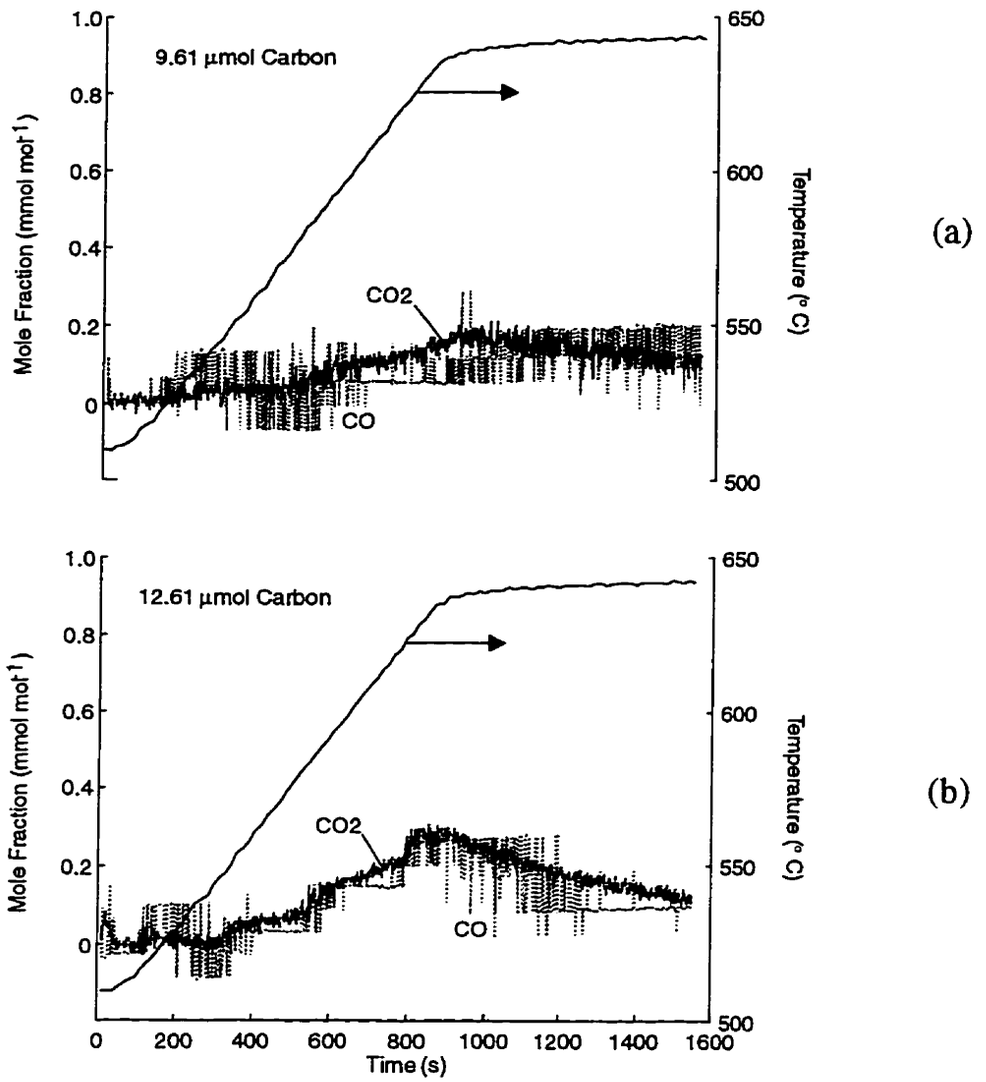

Figure 8.13 Temperature-programmed desorption results; (a) after propane pulsing, (b) after only steady-state reaction.

Without the gas phase oxygen, a considerably smaller quantity of carbon oxides is produced from the catalyst samples. Because of the oxygen-sparse conditions, some carbon monoxide in addition to carbon dioxide is produced, particularly from the catalyst exposed only to steady-state reaction. The results indicate that the carbon oxides formed result from carbonaceous species on the catalyst surface and not simply adsorbed carbon oxides. These carbonaceous species must be oxidized either by the gas phase oxygen or the lattice oxygen of the catalyst, since regardless of the previous reaction conditions, a smaller quantity of carbon oxides were formed without gas phase oxygen. Also without gas phase oxygen, carbon oxides are less plentiful from propane pulsing than from steady-state reaction. The catalyst subjected to propane pulsing is more reduced and thus lacks the oxygen to oxidize the carbonaceous species. Even so, this catalyst is likely covered by a greater quantity of

these carbonaceous species, as indicated by the larger quantity of total carbon formed from the propane pulsing catalyst during TPO.

Without gas phase oxygen, no low-temperature carbon oxides were produced from the propane pulsing catalyst. Some of the carbonaceous species that are oxidized only at high temperatures can be oxidized by lattice oxygen, though they do not seem to cause deactivation of the catalyst and block active sites. It is possible that at the higher reaction temperatures, the surface and/or lattice oxygen become mobile and can migrate to and oxidize these normally isolated carbonaceous species. Otherwise, these carbonaceous species block sites or are in the vicinity of sites (the 'sites' in this case may also be thought of as surface oxygen) that are not active at low reaction temperatures (510°C). These sites are activated as the temperature is elevated.

8.5 Further discussion and conclusions

8.5.1 General results

The results presented in this chapter contribute to a clearer picture of the effect of reaction conditions and condition of the catalyst on the selectivity of the reaction. When the reaction is operated at steady-state, higher selectivity for propene production is favoured at lower gas phase concentrations of oxygen (this is further supported by experimental results in chapter 9). The highest selectivity attainable would seem to be by the non-steady-state operation of the reaction with the complete absence of gas phase oxygen. When the reaction is operated periodically with alternating feeds of propane and oxygen, an overshoot is obtained in product concentrations during the propane-feed half of the cycle. During the initial sharp decline in activity, the selectivity further increases. This may be due to the initially high degree of oxidation of the catalyst or may simply result due to the consecutive nature of the reaction mechanism. During the later slower decline in activity, the selectivity is stable. The propane pulsing experiments indicate that an additional improvement in the selectivity of the catalyst occurs when the catalyst is further deeply reduced, beyond the removal of about 20% of the magnesium orthovanadate phase oxygen. Thus, there are two factors contributing to improved selectivity for production of propene. First, a low concentration of gas phase oxygen and secondly a low concentration of lattice oxygen. With the presence of gas phase oxygen some highly active and strongly oxidizing species may form on the catalyst surface. The concentration of these non-selective oxygen species may be proportional to the gas phase oxygen concentration. More strongly bound and less active oxygen species are less likely to cause deep oxidation. Thus, when the catalyst is almost completely reduced, it is most selective for production of propene.

The TPO and TPD experiments indicate that even under non-steady-state operation, the catalyst surface contains a significant quantity of carbonaceous material. This carbonaceous material can be oxidized at elevated reaction temperatures. When the reaction is operated without gas phase oxygen, an additional quantity of carbonaceous material exists on the catalyst surface. This is oxidized almost immediately upon exposure of the catalyst to oxygen at the reaction temperature.

8.5.2 Periodic operation and other forms of non-conventional operation

By operating the oxidative dehydrogenation reaction in a periodic manner with alternating feeds of propane and oxygen, high selectivity for the production of propene can be obtained. However, operation at steady-state with a low oxygen partial pressure, and particularly with a low propane partial pressure, may also result in as high yields for propene as with periodic operation. It is unclear whether periodic operation is a superior mode of operation compared to all steady-state conditions.

One must keep in mind though that the comparison between steady-state and periodic operation made in this chapter has been rather restrictive. The main factor that has limited the performance with periodic operation has been the time-average conversion. Only at the shortest cycle periods is the time-average conversion under periodic operation sufficient to exceed the yield at a comparable time-average steady-state condition. It is unlikely though that the reaction would be operated industrially with alternating feeds of propane and oxygen through a fixed bed of catalyst. It is more likely that the catalyst would be transported continuously as a fluidized bed between oxidation and reduction reactors as illustrated in Figure 8.14. Such reactor technologies are well-established, such as for catalytic cracking. Researchers at Dow Chemical who recently investigated the periodic operation of the oxidative dehydrogenation of butane did not consider the 'time-average' conversion of butane [56,57], i.e. the down-time of the reactor for re-oxidation of the catalyst. Their intention was that, beyond the lab-scale, the reaction would be operated with a fluidized bed as in Figure 8.14. From this perspective, the disadvantages of periodic operation over a fixed bed at steady-state are a more expensive and complex reactor system and loss of catalyst because of erosion. If one does not consider the 'time-average' propane conversion, the propene yields in Figure 8.2 would all be twice as high, since during half the

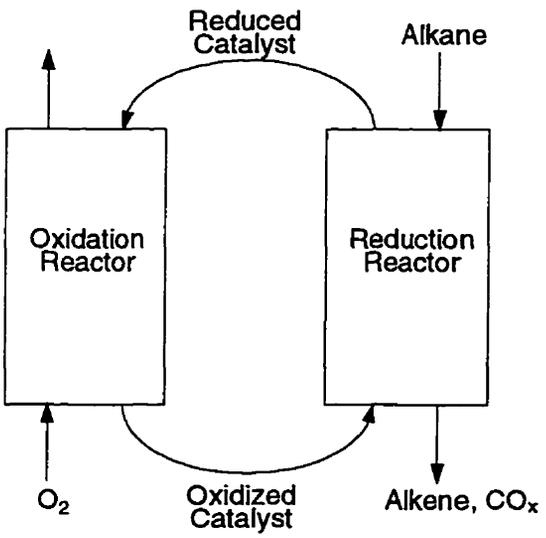

Figure 8.14 Redox fluidized bed reactor

cycle oxygen is fed and no products are produced. With such a less demanding comparison, one could conclude that the yield at periodic operation is superior than at all steady-state conditions, since it is clear that the highest possible propene selectivity is obtained without gas phase oxygen.

Periodic operation via a fluidized catalyst bed has additional advantages compared to steady-state operation. The best yields of propene at steady-state seem to be attainable at high propane to oxygen ratios, which can be close to spontaneously flammable mixtures of the reactants. By reducing and oxidizing the catalyst in separate reactors, contact between oxygen and hydrocarbons is minimized, resulting in a safer operation. Also, with a fluidized bed of catalyst, mixing results in a uniform temperature profile in the bed so that hot spots that can occur in fixed catalyst beds are avoided.

There are some potential problems with periodic operation using a fluidized bed redox reactor. Reaction rates tend to be low when the reaction occurs without gas phase oxygen. Also, as Figure 8.2 indicated, the best yields are obtained at short cycle periods because propane conversion is highest due to the overshoot response of the reactants. Thus the best performance of the redox reactor may require an exceedingly high rate of circulation of the catalyst. Recently, Ramos et al. [99] published results for testing of what they call an 'in situ' redox fluidized bed reactor which would seem to circumvent such problems. The basic design of such a reactor is illustrated in Figure 8.15. The oxygen is fed into the bottom of the reactor while the alkane would be fed through a distributor at some location near the top of the fluidized bed. Conditions should be such that the complete conversion of oxygen occurs. Oxidation of the catalyst would occur in an area near the bottom of the fluidized bed and the reduction of the catalyst and reaction would occur near the top. Ramos et al. concentrated on studying the operating conditions for a lab-scale reactor that would effectively separate the oxidation and reduction zones for the oxidative coupling of methane. This 'in situ' redox reactor offers the added advantage of flexibility of operation. It may not be optimal to completely separate the oxidation and reduction zones. It was demonstrated by the results in section 8.3.4, that by feeding mixtures of propane and oxygen, the time-average periodic operation propane

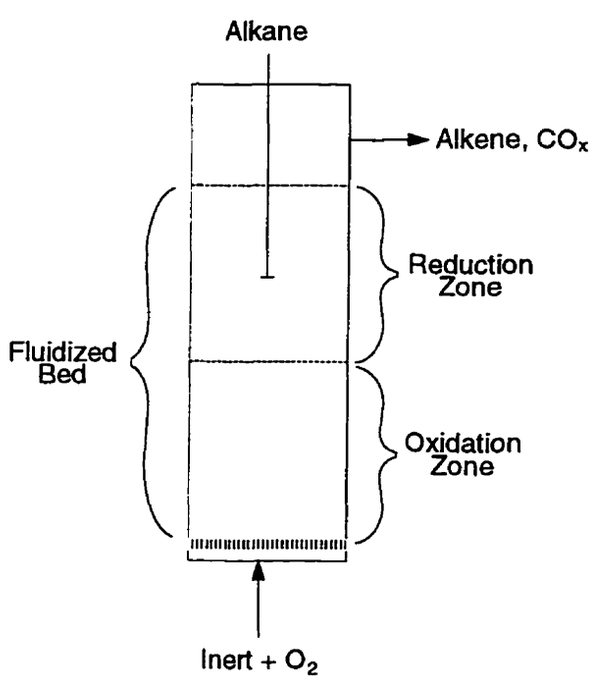

Figure 8.15 *In situ* redox fluidized bed reactor

conversion could be boosted without large loses in selectivity. This provides an increased propene yield.

Also, with some sort of fluidized bed redox reactor system it may be possible to operate a kind of 'hybrid' reaction. The researchers at Dow Chemical found that at sufficient levels of reduction of their catalyst, direct thermal dehydrogenation would occur to some degree producing alkenes and hydrogen [56,57]. With severely limited oxidation of the catalyst, it may be possible to thermally couple oxidative dehydrogenation and the direct thermal dehydrogenation reactions. The aim of such an operation would be to perform oxidative dehydrogenation just enough to maintain the catalyst clean of deactivating carbonaceous deposits, minimize production of carbon oxides and produce sufficient heat to be consumed by the direct thermal dehydrogenation. Indeed, a careful balancing act!

The results in this chapter indicate that operation of oxidative dehydrogenation with a membrane reactor should be attractive. In the research performed with membranes thus far, mostly inert membrane reactors have been used [87-90]. The basic configuration of these reactors is shown in Figure 8.16. The alkane is fed only through the central part of the reactor where the fixed bed of catalyst is located while oxygen is fed only in the outer annular space. It is important to note that the membrane is catalytically inert. Oxygen must diffuse through the membrane and its gas phase partial pressure is considerably lower in the inner region of the reactor. Pantazidis et al. [89] reported that the use of such a reactor for the oxidative dehydrogenation of propane with a Mg-V-O catalyst resulted in an increase in propene yields compared with co-feeding propane and oxygen through the inner region of the reactor. The results in this chapter suggest that the improvements in yield occurred because the membrane maintained a low oxygen concentration in the gas phase region of the catalyst bed. One might think that similar results could be obtained by co-feeding the propane and oxygen in the inner region, with just a lower concentration of oxygen. However, the principal advantage of the inert membrane is that the oxygen feed is distributed along the catalyst bed, so that all of the catalyst can be maintained at an optimal level of oxidation. If lower concentrations of oxygen were simply fed in the inner region, high conversion of oxygen would result in a steep gradient in the oxygen partial pressure along the catalyst bed.

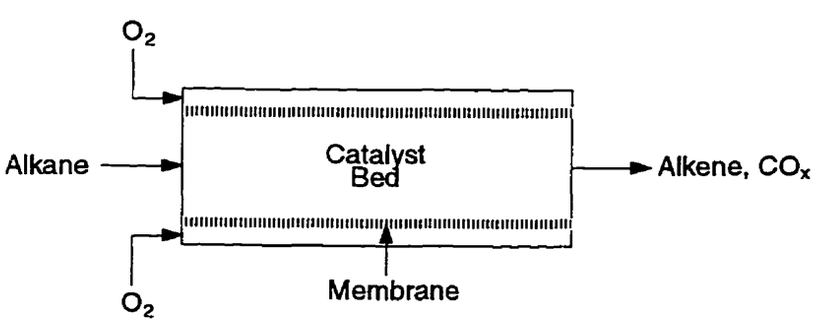

Figure 8.16 Inert-membrane reactor

A superior membrane reactor might be a truly catalytic-membrane reactor. In such a reactor, the catalyst bed would be absent and the catalyst would be deposited on the inner walls of the reactor. Oxygen would diffuse through the membrane to oxidize the catalyst and ideally there would be no gas phase oxygen in the inner region of the reactor. The principal disadvantage of a catalytic-membrane reactor is that the reaction rate would be limited by the rate of diffusion of oxygen through the membrane. Pantazidis et al. attempted to obtain such a reactor configuration by supporting Mg-V-O and nickel based catalysts on a commercial porous alumina membrane. However, the membrane material proved to be an ineffective barrier for the oxygen and the oxygen partial pressure in the inner region of the reactor was not much lower than in the annular region. The development of effective membrane materials for the high reaction temperatures of partial oxidation reactions seems to be a major challenge in membrane reactor technology.

9. Oxygen partial pressure effects

It was shown in chapter 6 that the selectivity of oxidative dehydrogenation was higher when performed without gas phase oxygen at the same levels of conversion of propane. Some steady-state results, in Section 8.3.2, suggested that higher selectivity may be obtained at steady-state conditions provided the oxygen concentration is kept low. In this chapter, the effect of oxygen partial pressure on the selectivity of the reaction is examined further. The purpose of this is to determine whether the higher yield of the reaction at non-steady-state/periodic operation conditions without gas phase oxygen is simply a continuation of improved performance of the reaction at steady-state conditions with low oxygen partial pressures. First, steady-state results with varying oxygen partial pressures will be presented which confirm that the selectivity of the reaction is improved at steady-state with low oxygen partial pressures at a constant conversion. Secondly, kinetic models, based on the redox models presented in chapter 4, are developed to explain the steady-state data. Finally, these kinetic models are applied to some periodic operation conditions to determine if they too can describe the selectivity and dynamics of the reaction.

9.1 Oxygen partial pressure effects at steady-state

9.1.1 Method of data collection

Steady-state data were collected by performing the reaction with a varying feed ratio of oxygen-to-propane from 0.1:1 to 1:1. The experiments were repeated with feed propane concentrations of 6 and 4% and catalyst masses of 20, 30 and 40 mg. The reaction temperature was always 510°C.

The steady-state data were collected in a manner similar to that described in chapter 5. For a given mass of catalyst, the reaction was started with a standard set of reaction conditions. The standard set of reaction conditions consisted of feed concentrations of 6% propane and 6% oxygen. With the fresh catalyst, the standard reaction conditions were run initially for at least 3 h. The catalyst was then exposed in turn to different sets of reaction conditions in a random order. The catalyst was exposed to each set of reaction conditions for 1.5 h. During this period, the product gases were analyzed by gas chromatography (GC) every 0.5 h. The first analysis was done 0.5 h after the catalyst was exposed to a chosen set of reaction conditions. The results presented are an average of three analyses collected over 1.5 h.

Between every set of reaction conditions, the catalyst was exposed to the standard conditions. Unlike the results in chapter 5, there was never any significant change in the

selectivity of the catalyst at these standard conditions, during collection of the data. Presumably this is because the oxygen concentration for all of the reaction conditions was low, with the oxygen concentration never exceeding that of the propane. The variations in selectivity observed for the data in chapter 5, seemed to result from reaction conditions with excess oxygen concentrations.

For all reaction conditions, no trends in the conversion or selectivity were discernible among the three analyses performed. For example, at conditions with very low oxygen partial pressures which tended to have high conversions of oxygen, it might be expected that some deactivation of the catalyst might occur. However, for the short periods of time that these conditions were run (1.5 h), no appreciable deactivation was observed.

9.1.2 The steady-state data

Figures 9.1 and 9.2 show conversions and selectivities for the steady-state data collected with varying oxygen-to-propane feed ratios. Generally, propane conversion decreases as the feed concentration of oxygen is lowered, but at the same time, the propene selectivity increases. If one compares the propene selectivity at different oxygen feed concentrations and about the same propane conversion, lower gas phase concentrations of oxygen favours higher propene selectivity. Table 9.1 lists results from Figure 9.1 at about 4% propane conversion. As the oxygen feed concentration is lowered from 6 to 0.6% and the catalyst mass is increased to maintain the propane conversion, the propene selectivity increases from 42 to 74%.

Table 9.1
Effect of oxygen feed concentration on selectivity at constant propane conversion*

Catalyst Mass (g)	Oxygen feed Conc. (%)	Propane Conversion (%)	Propene Selectivity (%)
20	6	4.1	42
30	2.4	3.9	65
40	0.6	4.4	74

* 6% propane feed, 510°C

For a consecutive reaction scheme, which at least partly describes partial oxidation, conversion and selectivity to the intermediate product, will be inversely related. Comparing propene selectivities, in Figures 9.1 and 9.2, at the same feed concentrations of both propane and oxygen, conversion and selectivity are not always inversely related, probably because the expected selectivity-conversion relation is convoluted with the effects of oxygen conversion on selectivity. For example, for a consecutive reaction, the selectivity for experiments with 40 mg of catalyst, which always exhibit the highest conversion, should be lower than selectivity with 30 and 20 mg of catalyst at the same reaction conditions.

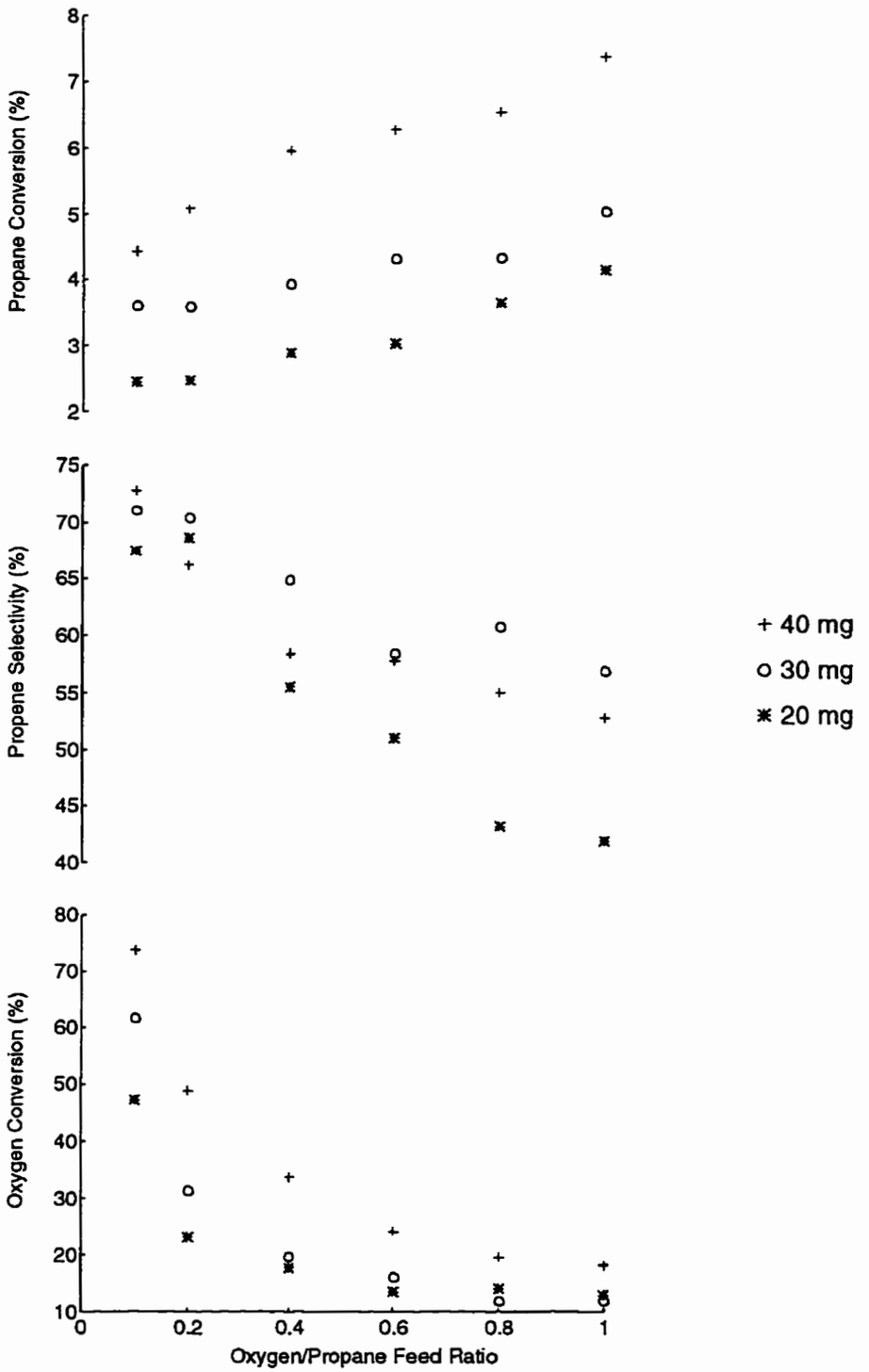

Figure 9.1 Conversion and selectivity for steady-state reaction with 6% propane

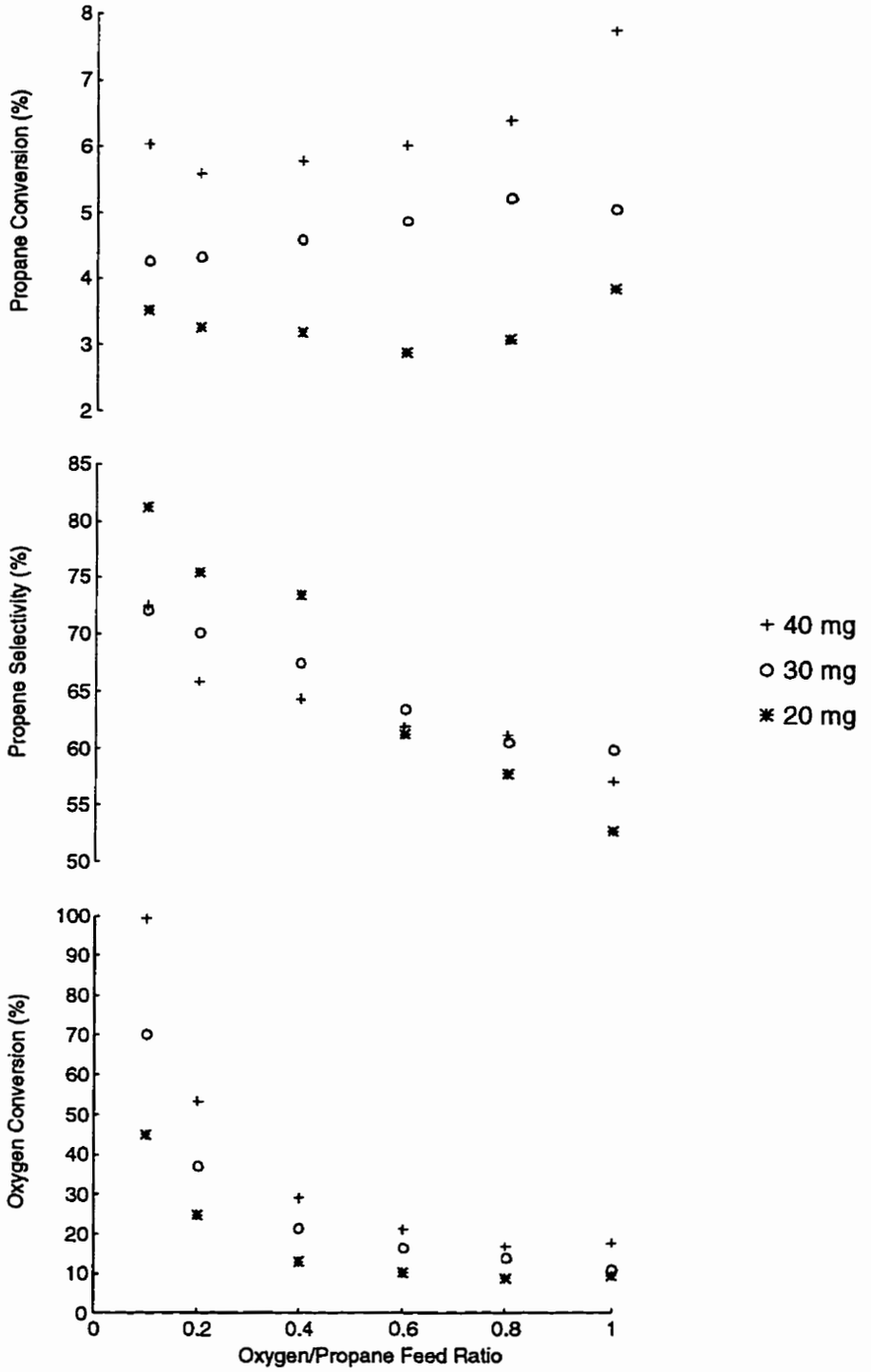

Figure 9.2 Conversion and selectivity for steady-state reaction with 4% propane

However, oxygen conversion is also always highest with 40 mg of catalyst. The lower gas phase concentration of oxygen, however improves the selectivity.

A simpler explanation for the weak selectivity-conversion relation observed is that at these reaction conditions little consecutive reaction occurs. The carbon oxides at these low conversions of propane are produced directly from propane. In the steady-state kinetic modelling exercise in chapter 4, a strictly consecutive reaction model best described the data. However, for about half of the results in chapter 4, 2% propene was fed to the reactor. At these relatively high gas phase concentrations of propene, the intermediate product, it is likely that the consecutive reaction - the production of carbon oxides from propene - predominated.

For reaction conditions with a low feed concentration of propane and/or low conversion due to a low catalyst mass, the propane conversion seemed to be less dependent on the oxygen feed concentration. This is indicated by the smaller change in propane conversion in Figure 9.2 with 4% propane than in Figure 9.1 with 6% propane. This was particularly the case with lowest mass of catalyst, 20 mg. Of course, at a lower propane concentration, the absolute change in oxygen concentration was lower since the feed ratio of oxygen and propane was varied. This also explains the rather small changes in propane conversion for the steady-state experiments with 3% propane shown in section 8.3.2. The propane conversion may also be less dependent on changes in the oxygen concentration at lower conversions (due to a lower mass of catalyst) because the catalyst may be more fully oxidized at these conditions and the rate of reduction of the catalyst more rate-determining. Thus, changes in the oxygen concentration and rate of reoxidation have just a small effect on the conversion of propane.

The selectivity among the carbon oxides also varied as the feed concentration of oxygen is lowered. In Figure 9.3, the ratio of carbon monoxide to carbon dioxide is compared for each of the steady-state experiments. As the conversion of propane decreases, the total production of carbon oxides decreases; however, carbon dioxide tends to decrease more sharply than carbon monoxide. This indicates that some of the carbon dioxide arises from further oxidation of carbon monoxide.

9.2 Steady-state kinetic modelling

The data in Figures 9.1 and 9.2 indicate a relation between the oxygen gas phase concentration and selectivity which cannot be explained simply by the conversion-selectivity relation for a consecutive reaction. The steady-state kinetic models developed in chapter 4 do not account for this effect. In the following sections, extensions are made to these redox models to allow for the apparent relation between selectivity and gas phase oxygen concentration.

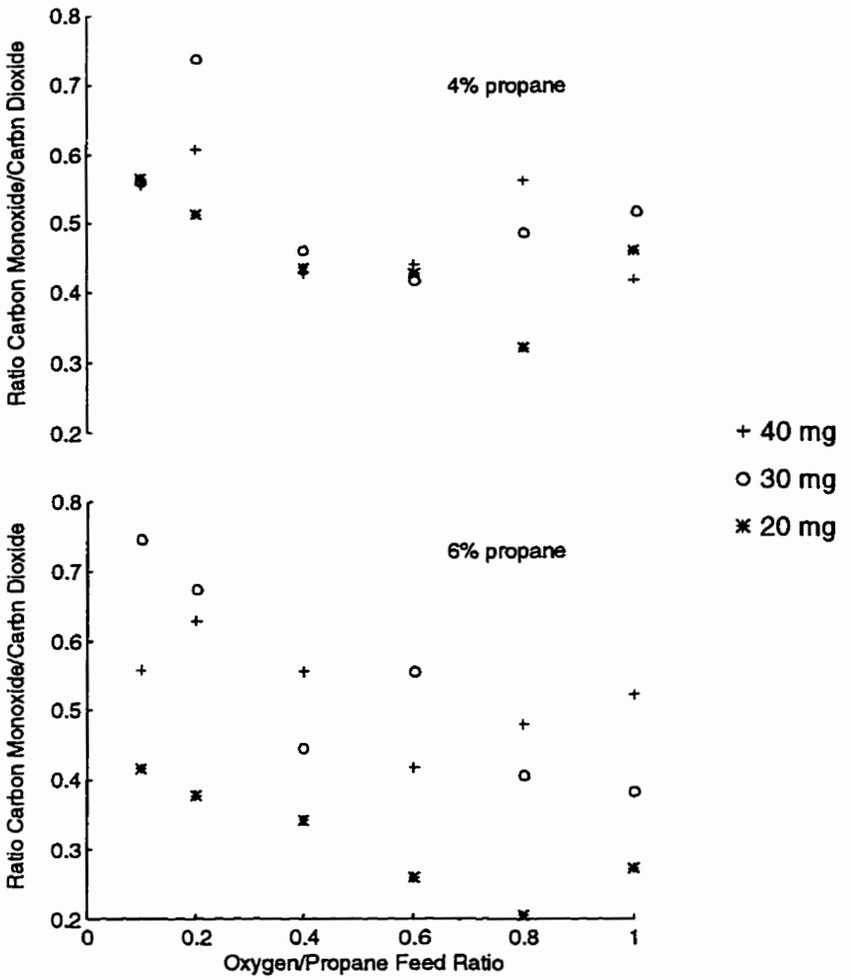

Figure 9.3 Variation of ratio of carbon oxides

9.2.1 Kinetic modelling methods

As with the data in chapter 4, nonlinear regression methods were used to fit kinetic models to the data in Figures 9.1 and 9.2. Reaction rates for each of several models were integrated over the mass of catalyst, at each of the experimental conditions, to calculate the predicted outlet reactant and product concentrations. A derivative-free algorithm searched for values of the model parameters that minimized the sum of the squares of the residuals. Only propane, propene and carbon oxide concentrations were included in the analysis because only their concentrations were independently measured by the GC analysis.

The selectivity between propene and total carbon oxide production was the focus of the modelling work. None of the kinetic models examined described the selectivity of the reaction between carbon monoxide and carbon dioxide. As a result, only the total production of carbon oxides is included in the regression analysis. However, it is evident from Figure 9.3 that the ratio of carbon monoxide to carbon dioxide production varied with reaction

conditions. This ratio affects the consumption of oxygen and, in turn, for most models, the degree of catalyst reduction. To account for this variance, an estimate for the ratio of production of carbon dioxide to carbon monoxide was included in each model. A power law rate model, with the same form as PL1 (see chapter 4, section 4.2) was fitted to the data and its estimates for the rates of production of carbon dioxide and carbon monoxide were used to calculate the needed ratio. The decreasing ratio of carbon dioxide to carbon monoxide with increasing oxygen feed was estimated by

$$x = \frac{17.08 P_{C_3H_6}{}^{0.1589} P_{O_2}{}^{0.4529}}{96.62 P_{C_3H_6}{}^{0.6223} P_{O_2}{}^{0.2540}} \tag{9.1}$$

This ratio was only used for calculations of the rate of oxygen consumption based on the rate of production of total carbon oxides.

9.2.2 Redox model with single carbon oxide production path

To demonstrate the inadequacies of the redox models developed in chapter 4, in describing the effect of oxygen partial pressure on selectivity, a redox model similar to the MV2 model (see section 4.3) was fitted to the data. The rate equations for this kinetic model were

$$r_1 = k_1 P_{C_3H_8} (1-\beta) \tag{9.2}$$

$$r_2 = k_2 P_{C_3H_6} (1-\beta) \tag{9.3}$$

$$r_3 = k_3 P_{O_2} \beta \tag{9.4}$$

The rate of production of propene and carbon oxides are represented by r_1 and r_2 respectively. These reactions consume oxygen from the catalyst. The rate of reoxidation of the catalyst is r_3. The degree of reduction of the catalyst (β) can be calculated because at steady-state, the total rates of reduction and oxidation of the catalyst are equal. In this case the appropriate equation is

$$\beta = \frac{0.5 k_1 P_{C_3H_8} + \frac{3(3x+2)}{2(x+1)} k_2 P_{C_3H_6}}{k_3 P_{O_2} + 0.5 k_1 P_{C_3H_8} + \frac{3(3x+2)}{2(x+1)} k_2 P_{C_3H_6}} \tag{9.5}$$

The only difference between this model and MV2 is that, equation 9.3, the rate of production of carbon oxides is based on the gas phase partial pressure of propene and not on a surface concentration of propene. When the MV2 model was fitted to the data k_2 and the adsorption equilibrium constant for propene were highly correlated. This model based simply on the propene partial pressure yielded a lower residual sum of squares (SS) than MV2. Adsorption of propene on to the catalyst surface was more important for the data in chapter 4, from

which the MV2 model was developed, probably because of the high propene partial pressures in that set of data.

Table 9.2 shows the values of the fitted rate constants. The residual sum of squares was 5.31×10^{-2} and there was little correlation among the parameters. Figure 9.4 compares the model predictions and experimental data for 4% propane feed. The data for 6% propane feed showed similar results. As the oxygen-to-propane feed ratio decreases, the degree of reduction of the catalyst increases, resulting in a decrease in the propane conversion as would be expected for a redox model. The propene selectivity simultaneously increases, although there is a large spread in the selectivities predicted with different quantities of catalyst. This is not reflected in the data. The model predicts that the lowest selectivity should be obtained with the largest quantity of catalyst. According to the data, lower selectivity is not obtained with the largest quantity of catalyst. The increasing propene selectivity predicted by the model is merely the result of the decreasing propane conversion which stems from the consecutive reaction mechanism. According to the data, the propene concentration remains almost constant as the oxygen-to-propane feed ratio decreases, but the model predicts a decrease in the propene concentration. The propene concentration must decrease because the degree of reduction of the catalyst is increasing and both the production rates of propene and carbon oxides depend on the degree of oxidation of the catalyst.

Table 9.2
Parameters of redox model based on MV2 by least-squares regression

Parameter	Value	Units
k_1	2.74×10^{-1}	ml STP min^{-1} (g cat)$^{-1}$ bar^{-1}
k_2	1.37×10^{-3}	ml STP min^{-1} (g cat)$^{-1}$ bar^{-1}
k_3	2.04	ml STP min^{-1} (g cat)$^{-1}$ bar^{-1}

9.2.3 Redox models with dual carbon oxide production paths

In order to describe the effects of the oxygen partial pressure on selectivity, it would seem that a kinetic model must include an additional pathway for the production of carbon oxides that depends on the gas phase partial pressure of oxygen. Periodic operation results, shown in chapter 8, indicated that at the switch between feeds of oxygen and propane, the selectivity of the reaction was immediately high; however, it increased for a brief period (20-30 s) and then was rather constant. Even without gas phase oxygen, carbon oxides were produced; thus, the production of carbon oxides must not depend only on the presence of gas phase oxygen.

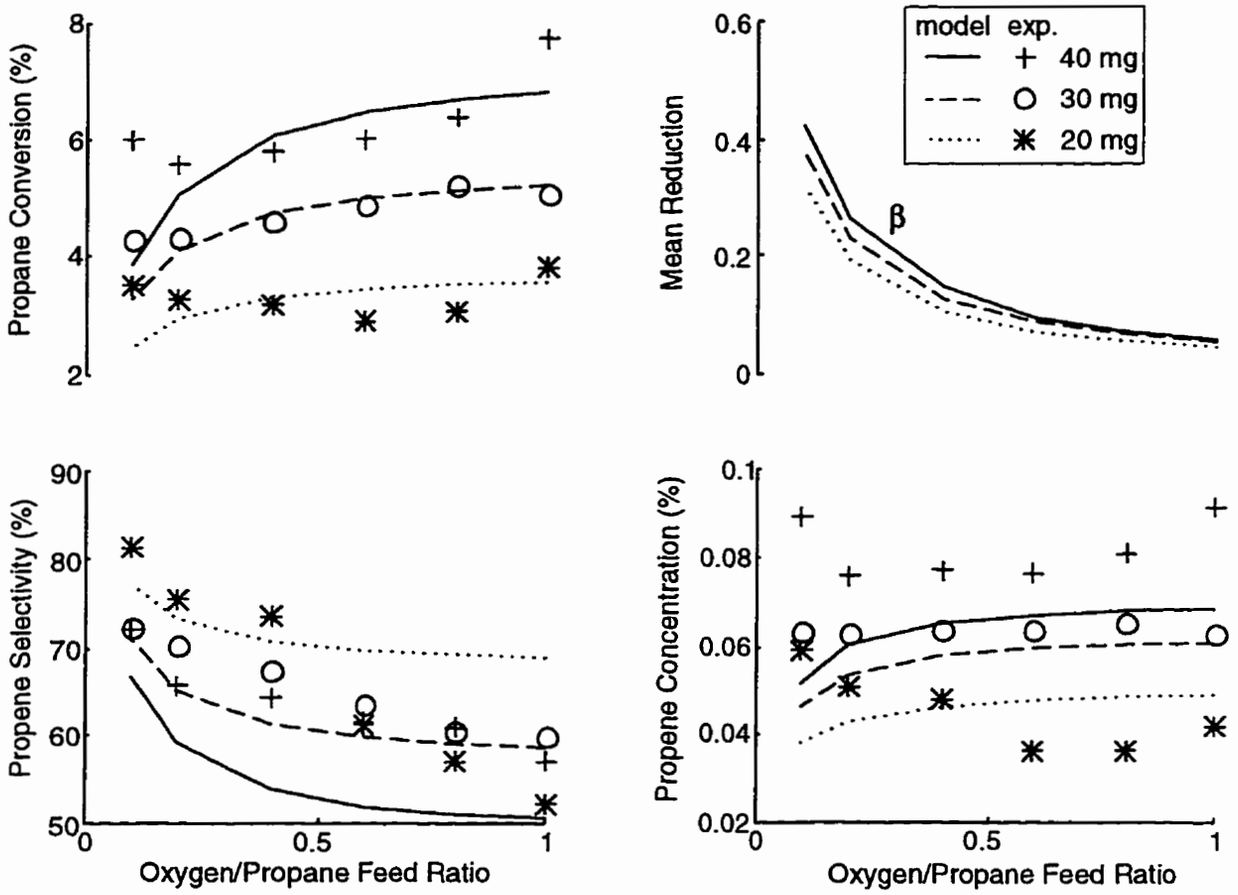

Figure 9.4 Comparison of experimental data at 4% propane and redox model predictions

Figure 9.5 illustrates the kinetic models containing alternative pathways for production of carbon oxides that were examined. All of these models are at least partially of a redox nature where the catalyst's surface oxygen reacts with hydrocarbons to produce the products. These models will be called DMV for dual Mars-Van Krevelen models. For the models DMV1, DMV2 and DMV3, two kinds of surface oxygen exists which will be referred to as α and β surface oxygen. In the kinetic models, the symbols α and β will be used to represent the degree of reduction of the α and β surface oxygens, respectively. It is well-known that partial oxidation catalysts may contain different types of surface oxygen species that promote different reactions. The α-oxygen only contributes to the production of carbon oxides, while the β-oxygen produces both propene and carbon oxides. The data in Figures 9.1 and 9.2 indicate that there is little relation between propane conversion and propene selectivity, suggesting that the reaction mechanism may not be entirely consecutive. For this reason, variations of the four main models were examined in which the carbon oxides were produced either from propane or propene. Propene was of course always produced from propane and

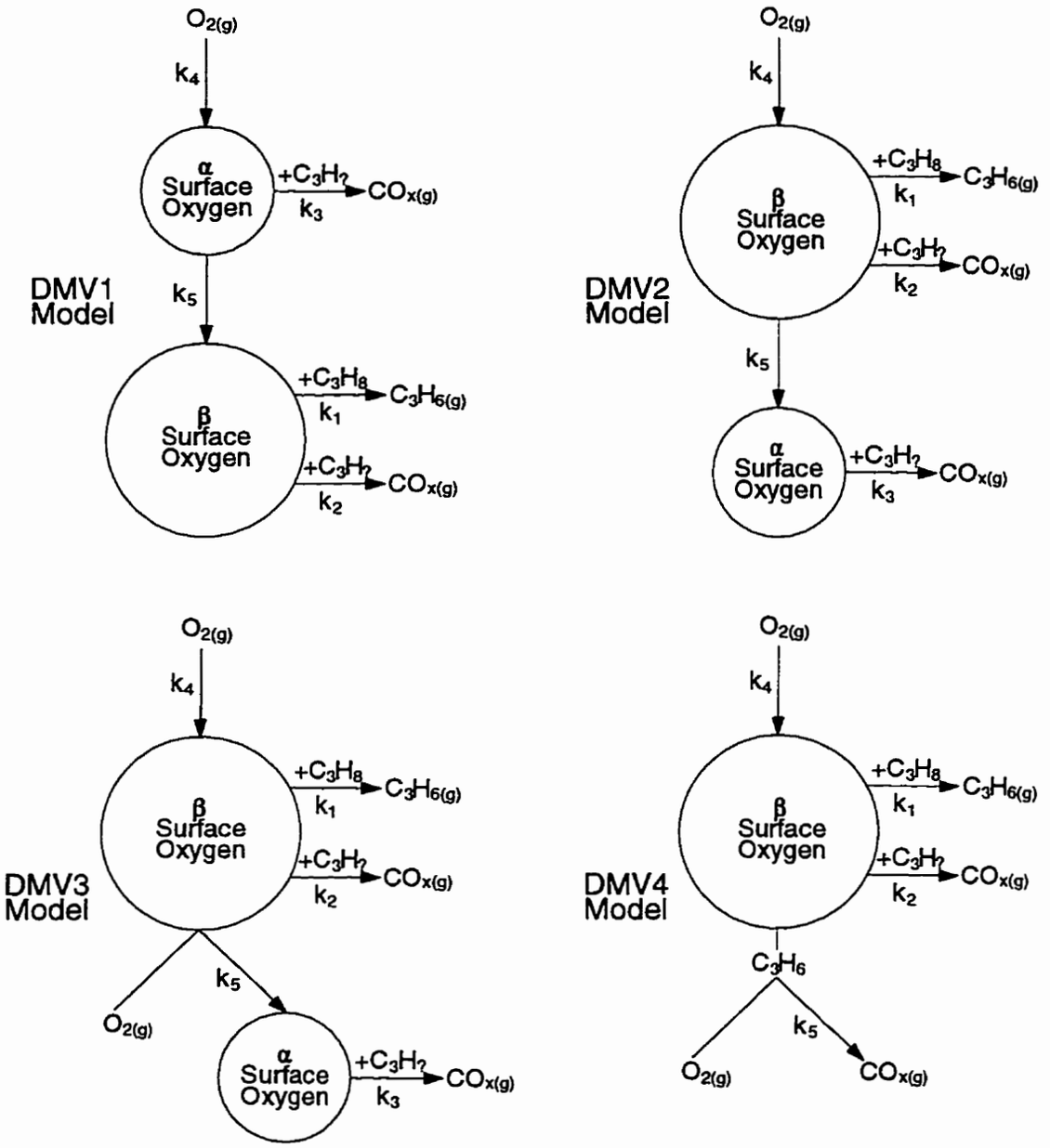

Figure 9.5 Kinetic models with dual carbon oxide production paths

from only the β-oxygen. For the models DMV1, DMV2 and DMV3 there are three variations. The carbon oxides from both α and β surface oxygen may be produced from propane:

α: $C_3H_8 \rightarrow CO_x$

β: $C_3H_8 \rightarrow CO_x$

which is a completely parallel mechanism and will be referred to as sub-model P, and for the DMV1 model it is denoted as DMV1-P. Since it always produces only carbon oxides the α-oxygen is perhaps a more reactive and non-selective oxygen that can completely oxidize

propane directly. Thus, by a mixed parallel and series reaction mechanism, the α-oxygen produces carbon oxides from propane and the β-oxygen produces carbon oxides from propene:

α: $C_3H_8 \rightarrow CO_x$

β: $C_3H_6 \rightarrow CO_x$

This sub-model will be referred to as S1, and for the DMV1 model it is denoted as DMV1-S1. By an alternative mixed reaction mechanism α-oxygen produces carbon oxides from propene and the β-oxygen produces carbon oxides from propane:

α: $C_3H_6 \rightarrow CO_x$

β: $C_3H_8 \rightarrow CO_x$

This sub-model will be referred to as S2, and for the DMV1 model it is denoted as DMV1-S2.

In the literature on catalytic oxidative dehydrogenation, it has often been proposed that the loosely bound oxygen promotes the production of carbon oxides [9,60-62]. The α-oxygen can be considered a loosely bound excess surface oxygen that is present only with gas phase oxygen. On the other hand, β-oxygen can be considered strongly bound lattice oxygen. There ought to be relatively much less α than β-oxygen, since according to the transient reaction data, without the presence of gas phase oxygen, the selectivity of the reaction is almost immediately higher, suggesting the α-oxygen is either quickly consumed or converts quickly into β-oxygen.

For the DMV1 model, the α-oxygen is a kind of intermediate oxygen species between the gas phase oxygen and the more strongly bound lattice β-oxygen. In the case of the DMV2 model, the α-oxygen can be considered an 'overflow' surface oxygen that tends to be produced when all the sites for β-oxygen are occupied. By the DMV3 model, α-oxygen is produced by the interaction of gas-phase oxygen and β-oxygen. This model is congruent with the suggestion [71] that total oxidation involves an oxygen adspecies, O^-, arising from gaseous oxygen activation with the lattice oxygen O^{2-}:

$$0.5\ O_2 + O^{2-} \rightarrow 2O^-$$

where the β-oxygen would be O^{2-} and α-oxygen would be the adspecies, O^-.

According to the DMV4 model, the additional pathway for production of carbon oxides simply involves the reaction of gas-phase oxygen with surface adsorbed propene. There are only two variations of this model. In the first, the β-oxygen produces carbon oxides from propane which will be denoted as DMV4-P. Alternatively, the β-oxygen produces carbon oxides from propene which will be denoted as DMV4-S.

9.2.4 Application of dual redox models to data

DMV1 and DMV2 models

The rate equations for the DMV1-S1 model are

$$r_1 = k_1 P_{C_3H_8}(1-\beta) \tag{9.6}$$

$$r_2 = k_2 P_{C_3H_6}(1-\beta) \tag{9.7}$$

$$r_3 = k_3 P_{C_3H_8}(1-\alpha) \tag{9.8}$$

$$r_4 = k_4 P_{O_2}\alpha \tag{9.9}$$

$$r_5 = k_5\beta(1-\alpha) \tag{9.10}$$

The rate equations for the other DMV1 sub-models are the same except r_2 and/or r_3 would depend on the appropriate reactant partial pressure, propane or propene, depending on the series or parallel nature of the model. For steady-state conditions, equations expressing the exchange of oxygen between the two pools of oxygen on the catalyst surface and the gas phase can be formulated. From these equations, it is possible to solve for the degrees of reduction of each type of oxygen. The resulting expressions for the DMV1-S1 model are

$$\alpha = \frac{f - \sqrt{f^2 - 4eg}}{2e} \tag{9.11}$$

$$\beta = \frac{c+d}{c+d+k_5(1-\alpha)} \tag{9.12}$$

where

$$e = k_5(a+b) \tag{9.13}$$

$$f = ac + ad + bc + bd + k_5(2a+b+c+d) \tag{9.14}$$

$$g = ac + ad + k_5(a+c+d) \tag{9.15}$$

and

$$a = \frac{10x+7}{2(x+1)} k_3 P_{C_3H_8} \tag{9.16}$$

$$b = k_4 P_{O_2} \tag{9.17}$$

$$c = 0.5 k_1 P_{C_3H_8} \tag{9.18}$$

$$d = \frac{3(3x+2)}{2(x+1)} k_2 P_{C_3H_6} \tag{9.19}$$

The above expressions for the other DMV1 sub-models are the same except that a and/or d depend on the appropriate reactant partial pressure, propane or propene, and stoichiometric coefficient.

When the DMV1 models were fitted to the data, it was found that k_2 was very small and nearly zero. This is the rate constant for the production of carbon oxides from the β-oxygen. If k_2 were zero, then all of the carbon oxides would be produced from the α-oxygen. The quantity of α-oxygen varies the greatest as the feed ratio of oxygen-to-propane is decreased, because it is produced directly from the gas-phase oxygen. Due to this variation, at transient reaction conditions without gas phase oxygen, there would be little to no α-oxygen remaining on the catalyst. Calculations indicated that the propene selectivity of the reaction, occurring only from the β-oxygen, would be near 100%, considerably more than was observed for the periodic operation experiments. In order that the DMV1 model not predict such a high propene selectivity under transient conditions, the value of k_2 was set as a fraction of the k_1 value, such that the selectivity of the reactions from the β-oxygen would be about 80%.

Table 9.3 shows the values of the least-squares parameters for each of the DMV1-type models. Correlations among parameters was low for all of the models. The residual sum of squares (SS) were 3.7×10^{-2}, 3.3×10^{-2} and 4.2×10^{-2} for the S1, P and S2 sub-models respectively. Based on the lower SS values, the DMV1-type models did seem to describe the data better than the redox model with just one type of surface oxygen.

Table 9.3
Parameters of DMV1 models by least-squares regression*

Parameter	DMV1-S1	DMV1-P	DMV1-S2	Units
k_1	1.72×10^{-1}	1.39×10^{-1}	2.18×10^{-1}	ml STP min^{-1} $(g\ cat)^{-1}$ bar^{-1}
k_3	9.08×10^{-2}	9.21×10^{-2}	9.39×10^{-4}	ml STP min^{-1} $(g\ cat)^{-1}$ bar^{-1}
k_4	9.02×10^{-1}	8.71×10^{-1}	1.04	ml STP min^{-1} $(g\ cat)^{-1}$ bar^{-1}
k_5	6.16×10^{7}	7.73×10^{5}	6.47×10^{1}	ml STP min^{-1} $(g\ cat)^{-1}$

* $k_2 = 0.25\ k_1$

Figures 9.6 and 9.7 compare model predictions and experimental data for the DMV1-S1 and DMV1-P models, respectively, for data with 4% propane feed. Both models describe the increase in selectivity as the oxygen-to-propane feed ratio decreases more successfully than the redox model with one type of oxygen (Figure 9.4). The spread in the selectivity between the different masses of catalyst is smaller. The models also predict an almost constant propene concentration as the oxygen-to-propane feed ratio is decreased. There is somewhat more spread in the selectivity between masses of catalyst for the S1 model compared to the P model because it retains a consecutive reaction characteristic. For both of these models, the degree of reduction of the α-oxygen showed a large variation over the range of oxygen-to-propane feed ratios while the β-oxygen remained almost completely oxidized. The improvement in selectivity results mainly from the decrease in the α-oxygen because it produces only carbon oxides.

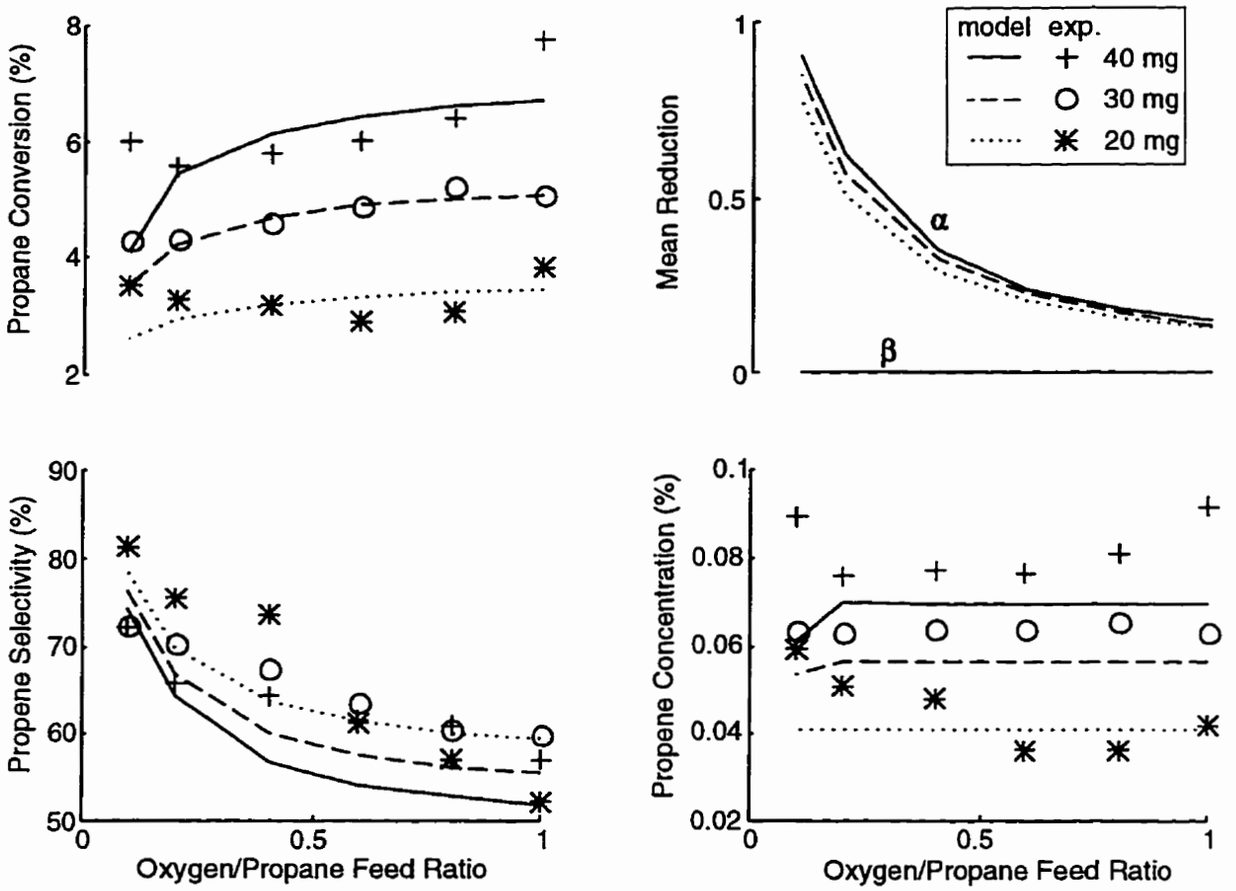

Figure 9.6 Comparison of experimental data at 4% propane to predictions of DMV1-S1 model

The constant complete oxidation of the β-oxygen created problems in determining k_5. The rate constant, k_5, expresses the rate of conversion of oxygen from α-oxygen to β-oxygen. To maintain the complete oxidation of the β-oxygen required a large value for k_5, as can be seen in Table 9.3. However, k_5 could be infinity, so no unique optimal value for k_5 existed. Consequently the confidence intervals for k_5 were very large; about an order of magnitude larger than the value for k_5 in Table 9.3. The precision of other parameters were much greater, since their confidence intervals were in the range of about an order of magnitude less than the predicted values. Clearly though, k_5 must be large for the DMV1-S1 and P models, but from steady-state data, no unique value could be determined.

For the DMV1-S2 model, predictions were similar to that for the DMV1-S1 model since both are mixed series/parallel models. However, there were less problems with determining k_5 for the DMV1-S2 model. Also, the reduction of the α-oxygen varied greatest to obtain the needed variation in selectivity. However, the β-oxygen was not completely oxidized for all oxygen-to-propane feed ratios.

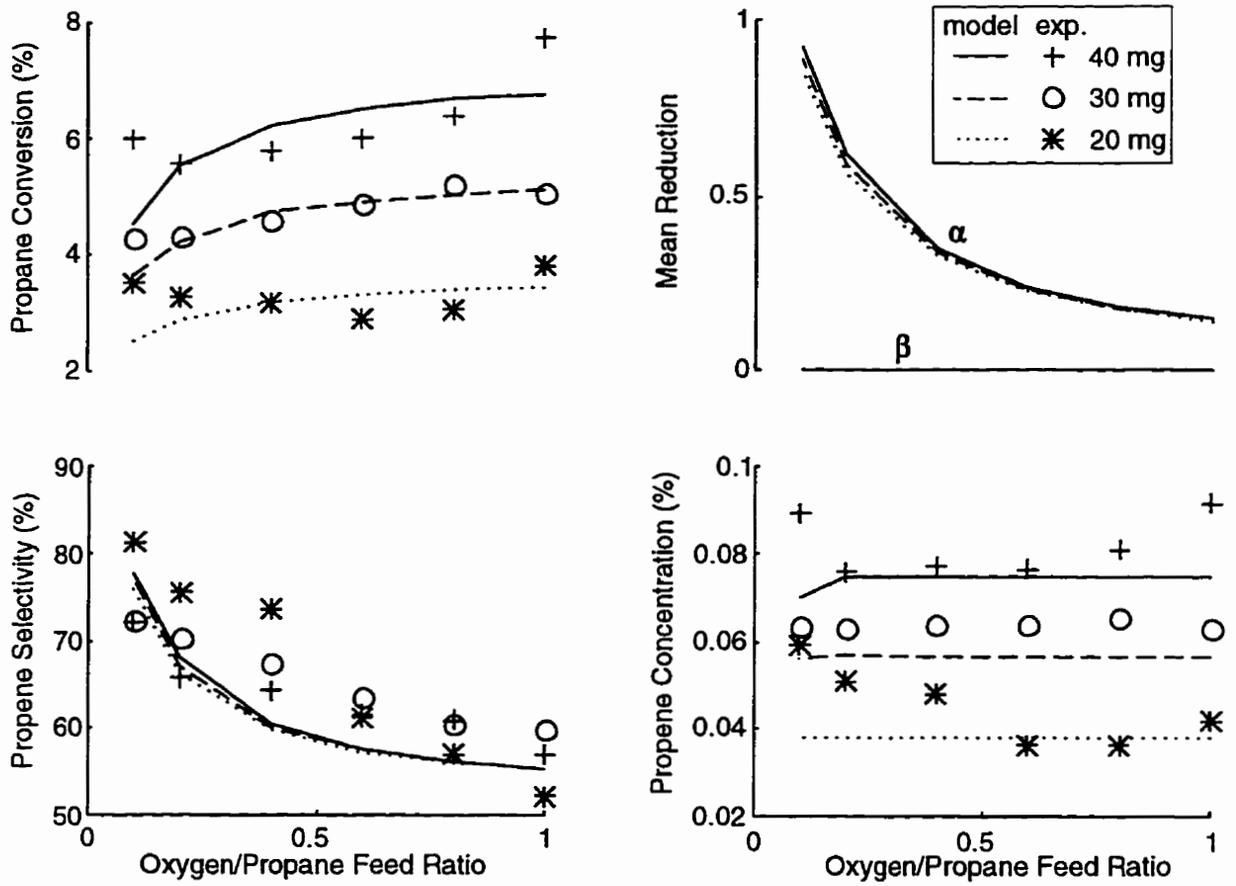

Figure 9.7 Comparison of experimental data at 4% propane to predictions of DMV1-P model

The DMV2 models were fitted to the data, but were not able to describe the experimental data better than the redox model with one type of oxygen. The SS for the DMV2-S1 model was 5.1×10^{-2}. For this model it was found that the coverage of β-oxygen decreased more than that of α-oxygen as the oxygen-to-propane ratio decreased. As with the DMV1 models, the α-oxygen produced only carbon oxides. Thus no improvement in selectivity was predicted beyond what a consecutive reaction mechanism allows. For the DMV2 models, in contrast to the DMV1 models, gas-phase oxygen forms β-oxygen first. Obviously, the α-oxygen, since it produces only carbon oxides, must have a direct connection to the changing gas-phase oxygen partial pressure in order that the propene selectivity will increase with lower oxygen partial pressure.

DMV3 model

The rate equations for the DMV3-S1 model are same as for the DMV1-S1 model shown above except equations 9.9 and 9.10 are replaced by

$$r_4 = k_4 P_{O_2} \beta \tag{9.20}$$

$$r_5 = k_5 P_{O_2} (1-\beta)\alpha \tag{9.21}$$

Rate equations for the other DMV3 sub-models are the same except r_2 and/or r_3 depend on the appropriate reactant partial pressure, propane or propene, depending on the series/parallel structure of the model. From an oxygen mass balance, the degrees of reduction of each type of oxygen could be solved. The expressions obtained are

$$\beta = \frac{c+d}{c+d+b} \tag{9.22}$$

$$\alpha = \frac{ak_4}{ak_4 + bk_5(1-\beta)} \tag{9.23}$$

where a, b, c and d are the same as defined in equations 9.16 to 9.19. The above expressions for the other DMV3 sub-models are the same except a and/or d would depend on the appropriate reactant partial pressure, propane or propene, and stoichiometric coefficient.

When the DMV3 models were fitted to the data, a very low value of k_2, at or near zero emerged. As with the DMV1 models, k_2 was set as a fraction of the k_1 value to ensure that the model predicts an accurate propene selectivity under transient operation. The fraction was chosen so that the selectivity of the reactions from only the β-oxygen would be about 80%.

Table 9.4 shows the values of the least-squares parameters for each of the DMV3-type models. Correlation among parameters are low for all of the models. The residual sums of squares (SS) are 3.1×10^{-2}, 2.8×10^{-2} and 3.6×10^{-2} for the S1, P and S2 sub-models respectively. Based on the SS values, the DMV3-type models were at least as successful as the DMV1-type models at describing the experiments.

Table 9.4
Parameters of DMV3 models by least-squares regression*

Parameter	DMV3-S1	DMV3-P	DMV3-S2	Units
k_1	1.69×10^{-1}	1.39×10^{-1}	1.99×10^{-1}	ml STP min^{-1} (g cat)$^{-1}$ bar^{-1}
k_3	1.61×10^{-1}	1.57×10^{-1}	1.73×10^{-3}	ml STP min^{-1} (g cat)$^{-1}$ bar^{-1}
k_4	1.07×10^{3}	1.20×10^{2}	3.37	ml STP min^{-1} (g cat)$^{-1}$ bar^{-1}
k_5	2.14×10^{-1}	2.07×10^{-1}	1.69×10^{-1}	ml STP min^{-1} (g cat)$^{-1}$ bar^{-1}

* $k_2 = 0.25\ k_1$

Predictions of the DMV3-type models were similar to those of the DMV1-type models. Both models successfully described the increase in selectivity as the oxygen-to-propane feed

ratio decreased (not shown). Selectivity predictions between the different masses of catalyst showed less spread than the redox model with only one type of oxygen. The models also successfully predicted an almost constant propene concentration as the oxygen-to-propane feed ratio decreased. For the P and S1 models, the degree of reduction of the α-oxygen varied widely over the range of oxygen-to-propane feed ratios while the β-oxygen remained almost completely oxidized. The improvement in selectivity results from the decrease in the α-oxygen which only produces carbon oxides. The constant complete oxidation of the β-oxygen created problems in determining k_4. The rate constant, k_4, expresses the rate of reoxidation of the β-oxygen. Large values of k_4 maintained the complete oxidation of the β-oxygen and, as with the DMV1-type models, no optimal values for k_4 could be found. The confidence intervals for k_4 were very large. Other parameters were again determined with greater precision.

For the DMV3-S2 model, there were fewer problems with determining k_4 values. Also, with this model, the reduction of the α-oxygen varied widely with the feed ratio. However, the β-oxygen was somewhat reduced for some oxygen-to-propane feed ratios.

The DMV3-type models are better versions of the DMV2-type models. For both model types, the α-oxygen can be considered as 'overflow' oxygen produced when there is a large quantity of β-oxygen on the catalyst surface. The key to the success of the DMV3-type models is that the formation of α-oxygen depends on the gas phase partial pressure of oxygen. Since the α-oxygen produces only carbon oxides, the changing gas phase oxygen partial pressure has a greater influence on the propene selectivity.

DMV4 model

The rate equations for the DMV4-S model are

$$r_1 = k_1 P_{C_3H_8}(1-\beta) \tag{9.24}$$

$$r_2 = k_2 \theta_{C_3H_6}(1-\beta) \tag{9.25}$$

$$r_3 = k_3 P_{O_2} \theta_{C_3H_6} \tag{9.26}$$

$$r_4 = k_4 P_{O_2} \beta \tag{9.27}$$

The rate equations for the DMV4-P model are the same except equation 9.25 would depend on the propane partial pressure instead of the surface coverage of propene. The resulting expression for the degree of reduction of the catalyst for the DMV4-P model is

$$\beta = \frac{0.5k_1 P_{C_3H_8} + \frac{3(3x+2)}{2(x+1)} k_2 \theta_{C_3H_6}}{k_4 P_{O_2} + 0.5k_1 P_{C_3H_8} + \frac{3(3x+2)}{2(x+1)} k_2 \theta_{C_3H_6}} \tag{9.28}$$

and, for the DMV4-S model, it is

$$\beta = \frac{0.5k_1 P_{C_3H_6} + \frac{(10x+7)}{2(x+1)} k_2 P_{C_3H_6}}{k_4 P_{O_2} + 0.5k_1 P_{C_3H_6} + \frac{(10x+7)}{2(x+1)} k_2 P_{C_3H_6}} \tag{9.29}$$

The expression for the surface coverage of propene is

$$\theta_{C_3H_6} = \frac{K_{C_3H_6} P_{C_3H_6}}{1 + K_{C_3H_6} P_{C_3H_6}} \tag{9.30}$$

Table 9.5 shows the values of the least-squares parameters for both of the DMV4-type models. Correlations among parameters was low for both of the models. The residual sum of squares (SS) were 4.1×10^{-2} and 3.2×10^{-2} for the S and P sub-models respectively.

Table 9.5
Parameters of DMV4 models by least-squares regression

	DMV4-S		DMV4-P	
	Value	Units	Value	Units
k_1	2.54×10^{-1}	ml STP min^{-1} (g cat)$^{-1}$ bar^{-1}	1.85×10^{-1}	ml STP min^{-1} (g cat)$^{-1}$ bar^{-1}
k_2	2.12	ml STP min^{-1} (g cat)$^{-1}$	6.96×10^{-2}	ml STP min^{-1} (g cat)$^{-1}$ bar^{-1}
k_3	2.84×10^{-2}	ml STP min^{-1} (g cat)$^{-1}$ bar^{-1}	1.56×10^{-2}	ml STP min^{-1} (g cat)$^{-1}$ bar^{-1}
k_4	2.73	ml STP min^{-1} (g cat)$^{-1}$ bar^{-1}	3.23	ml STP min^{-1} (g cat)$^{-1}$ bar^{-1}
K_{C3H6}	1.36×10^{3}	bar^{-1}	7.47×10^{3}	bar^{-1}

Figure 9.8 compares the DMV4-P model predictions to the experimental data at 4% propane feed. The predictions of the DMV4-S model were similar. Propene selectivity increased as the oxygen-to-propane feed ratio decreased. Just as the data indicate, there was little difference in the selectivity for different masses of catalyst. Thus, the improved selectivity predicted by the model at lower oxygen partial pressure is not only caused by lower propane conversion. There were, however, somewhat larger differences in the selectivities at different masses of catalyst for the DMV4-S model due to reaction mechanism's partially consecutive structure.

Parameters for both models had small confidence intervals except the adsorption equilibrium constant for propene. Values of the adsorption equilibrium constants shown in Table 9.5 are large and this is reflected by the high propene surface coverage (θ) at all oxygen-to-propane feed ratios. An upper limit for the propene adsorption equilibrium constants could not be found resulting in their large confidence intervals. To describe the data best, it is apparent that the rate of production of carbon oxides, expressed by r_3 (equation 9.26), ought to depend only on the oxygen partial pressure which requires

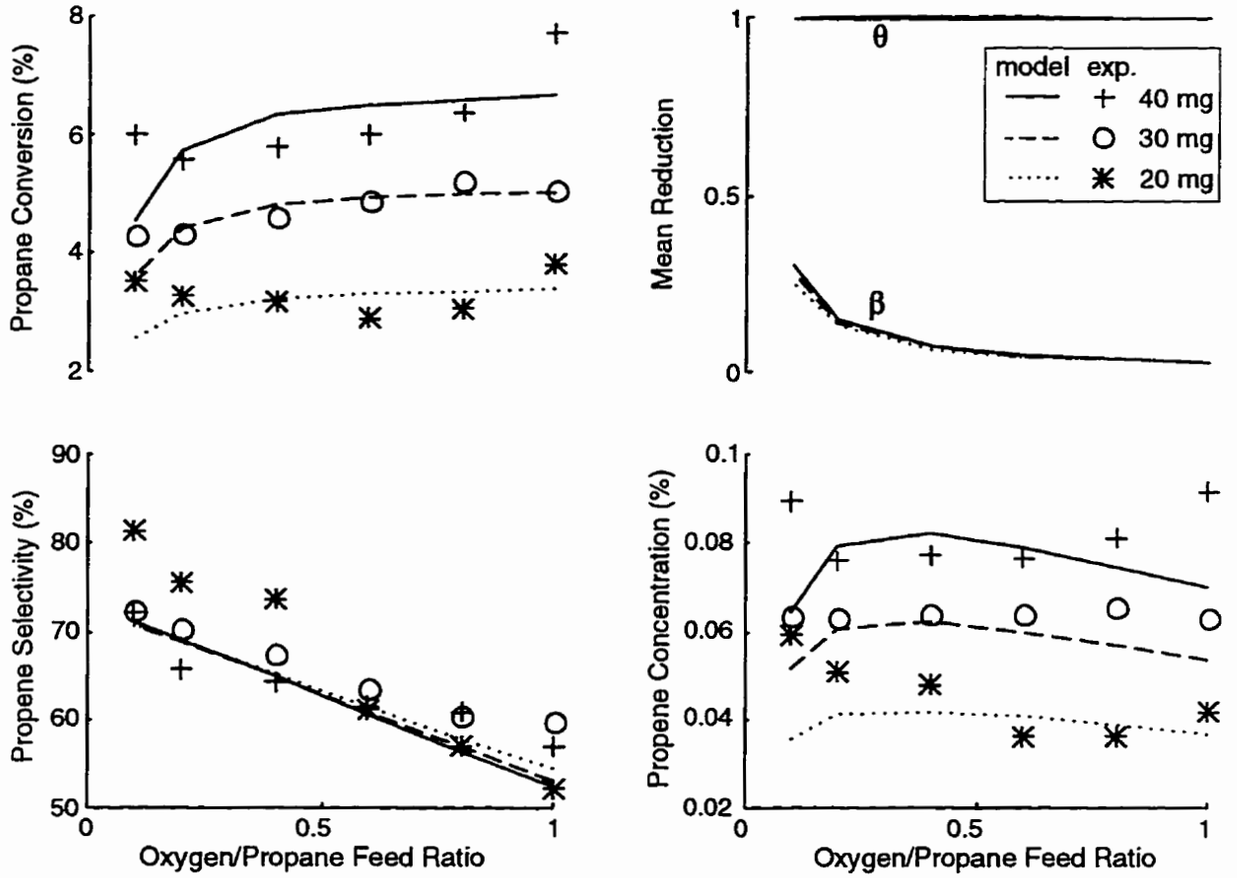

Figure 9.8 Comparison of experimental data at 4% propane and predictions of DMV4-P model

complete coverage of propene adsorption sites. When this rate depends only on the oxygen partial pressure, the propene selectivity increases as the oxygen partial pressure is lowered.

The propene concentration seems at first to increase and then to decrease as the oxygen partial pressure is lowered; however, there is no indication that the data reflect this trend. Initially, as the oxygen partial pressure is lowered, the propene concentration increases because the rate of further oxidation of propene (r_3) is lowered, while the degree of reduction of the catalyst (β) increases only slowly. With further decreases in the oxygen partial pressure, the degree of reduction of the catalyst changes more quickly, causing larger decreases in the rate of production of propene (r_1).

9.2.5 Comparison of models with dual carbon oxide production paths

The DMV1, DMV3 and DMV4-type models describe the experimental data with varying oxygen partial pressure better than the simpler redox model (MV). Table 9.6 compares the residual sum of squares for each of the models examined. The fact that the DMV2 models were no better than the basic MV model emphasizes the importance of a

dependence on the oxygen partial pressure. The DMV2 model did include an additional pathway for production of carbon oxides but its rates were not directly dependent on the oxygen partial pressure. The success of the DMV models reinforces our claim that improved propene selectivity is indeed obtainable at lower gas-phase partial pressures of oxygen and that this improvement need not be at the expense of lower propane conversion.

Table 9.6
Sum of squared residuals (SS) for redox models

Model	Reaction scheme type	Number of parameters	SS
MV		3	5.3×10^{-2}
DMV1	P	4	3.3×10^{-2}
	S1	4	3.7×10^{-2}
	S2	4	4.2×10^{-2}
DMV3	P	4	2.8×10^{-2}
	S1	4	3.1×10^{-2}
	S2	4	3.6×10^{-2}
DMV4	P	5	3.2×10^{-2}
	S	5	4.1×10^{-2}

It is less clear that any one of the DMV-type models stands out above the others. The DMV3-type models have only slightly lower SS values than the DMV1 and DMV4-type models. For the DMV4 models, it is questionable whether the reaction of the gas-phase oxygen is really with adsorbed propene since the adsorption equilibrium constant was so large that it forced complete coverage of propene at all conditions. It can also be argued that a gas-phase oxygen molecule is not sufficiently reactive. Perhaps provided the reaction temperature is sufficiently high, the reaction occurs between a desorbed hydrocarbon radical species and gas-phase oxygen to produce carbon oxides.

There are few differences in the characteristics of the DMV1 and DMV3 models at these steady-state conditions. First of all, if the reaction involves the production of carbon oxides from different surface oxygen species, it is unclear whether the non-selective surface oxygen is an intermediate species, as with the DMV1 model, or is formed separately, as with the DMV3 model. The DMV3-type models seemed to fit the data slightly better with lower SS values than the DMV1 models. This may be due to the flexibility of the model, since the α-type surface oxygen is formed independently of the β-type surface oxygen, whereas the DMV1 models are more awkward, since the α-oxygen is an intermediate species between the gas phase and β-oxygen.

For all of the DMV models, the P sub-models fit the data with lower SS values than the S sub-models. This indicates that at the reaction conditions used the reaction scheme is predominantly competitive with most of the reaction products produced directly from propane. Among the two partially consecutive reaction schemes examined, the S1 type seemed to fit the data better than the S2. Consequently, if carbon oxides are produced at all from propene, it is more likely to occur with the β-oxygen rather than the α-oxygen. It does seem reasonable that the more reactive and deeply oxidizing α-oxygen would produce carbon oxides directly from propane.

Certainly more complex models can be formulated and tested. Models which allowed for reversible exchange of oxygen between the types of surface oxygen were examined. The additional parameters in these models tended to be highly correlated and yielded little further improvements in the residual sums of squares. Also, partial pressures and surface concentrations could be raised to adjustable powers which may improve the fit of the models. The DMV models presented are the simplest with the fewest additional parameters over those of the MV redox model with only one path for the production of carbon oxides.

9.3 Transient kinetic modelling

The DMV models were applied to some periodic operation conditions to examine to what extent these models are applicable to transient systems.

9.3.1 Transient Reactor model

The transient reactor model used was similar to that in chapter 7. In order that ordinary differential equations could be used, the reactor was modelled as a series of ideal well-stirred tank reactors. As in chapter 7, ten identical tank reactors were adequate to model the concentration gradients of a single tubular reactor with reasonable accuracy. The experimental reactor was assumed isothermal and isobaric. The void fraction of the catalyst bed (ε) was assumed to be 0.4, the same value used in chapter 7. A PC-based program, MATLAB, was used to perform numerical integrations.

The system of equations 7.4 to 7.9 expressed the transients in the gas phase concentration of each component, with the inclusion of the reaction kinetics for the appropriate DMV model. Equations were also needed to express the rate of change of the surface concentrations of oxygen. The exact form of these equations varied with the type of DMV model, but for the case of the DMV3-P model they were

$$\frac{d\alpha}{dt} = \frac{\left(\left(\frac{10x+7}{x+1}\right)r_3 + 2r_5 - 2r_4\right)W}{Q_\alpha} \tag{9.31}$$

$$\frac{d\beta}{dt} = \frac{\left(r_1 + \left(\frac{10x+7}{x+1}\right)r_2 - 2r_5\right)W}{Q_\beta} \tag{9.32}$$

Unless otherwise stated, the DMV models as developed from the steady-state data were applied directly in the transient simulations. The only two adjustable parameters were the number of adsorption sites for β-type surface oxygen (Q_β) and, if applicable α -type surface oxygen (Q_α). In fitting the transient response data, Q_α and Q_β were estimated as fractions of the oxygen contained in the magnesium orthovanadate ($Mg_3V_2O_8$) phase, denoted by X_α and X_β respectively. Since X-ray diffraction analysis (section 3.1) indicated the catalyst consisted mainly of a mixture of magnesium oxide (MgO) and magnesium orthovanadate, it was assumed that the entire vanadium content of the catalyst was incorporated into the magnesium orthovanadate phase.

In the models, rate equations that allowed for the transport of bulk oxygen to the surface of the catalyst were included. The simple bulk oxygen diffusion model, as described in section 7.1.2 was used. This would add one additional adjustable parameter to the transient model, the lumped oxygen transport parameter (ω). The oxygen transported from the bulk of the catalyst was assumed only to form β-type surface oxygen.

9.3.2 Periodic Operation Simulation Results

Figure 9.9 compares the experimental data and the DMV model predictions for the product responses during periodic operation with a 400 s cycle period. The values of the adjustable parameters, used for all the models, are shown in Table 9.7. Only the P-types of the DMV models are shown in Figure 9.9. A simplified form of the DMV4 model was used. The predicted value of the propene adsorption constant ($K_{C_3H_8}$) from the steady-state data was very large; thus, the propene adsorption sites were filled at all conditions. It was assumed that for the transient form of the model, the propene adsorption sites would fill immediately after exposure to propane. This was also a necessary condition for the transient modelling in chapter 7, which included propene adsorption. There, a small number of propene adsorption sites was used in order that they would saturate quickly after the start-up of the reaction. The instantaneous saturation of the propene adsorption sites was necessary in order to obtain the observed fast increase in the propene concentration.

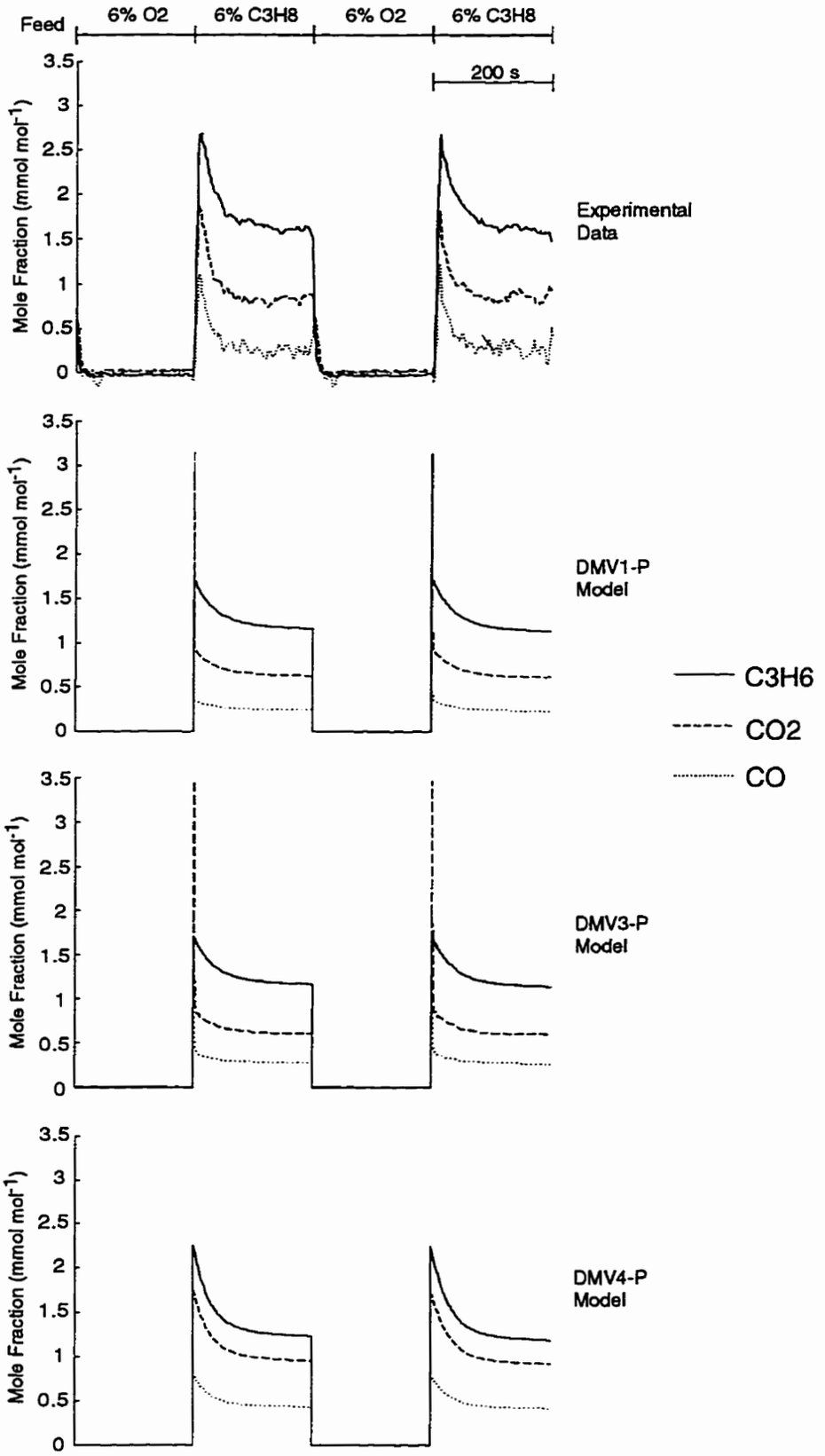

Figure 9.9 Comparison of experimental data and DMV models for periodic operation

Table 9.7
Transient model parameter values

Parameter	Value	Units
X_β	0.04	-
X_α*	0.001	-
ω	5×10^{-10}	$m^3\ min^{-1}$

* X_α not applicable to DMV4 model

The kinetic models were derived from only steady-state data and their predictions are extrapolated to transient conditions in this section. Thus, it is not surprising that large differences in concentrations between the models and experimental data result; what is of most interest are the dynamics of the models. The most striking difference between the experimental data and simulation results lies in the large peaks in carbon oxide concentrations for the DMV1 and DMV3 models immediately after the feed is switched to propane. These result because the sites for α-type oxygen are filled (completely oxidized) after the oxidation half of the cycle. Upon exposure of the catalyst to propane this oxygen produces carbon oxides and is completely consumed within a few seconds. Figure 9.10 shows the degree of reduction of the α and β-type surface oxygen for the DMV3 models. Responses of DMV1 models are almost identical. The value of X_α, the quantity of α-oxygen, controls only the width of these carbon oxide peaks but not their height. The value of X_α used is very small, so that the α-oxygen is quickly consumed and the carbon oxide peaks are narrow. The value of the rate constant for production of carbon oxides from the α oxygen controls the height of the peaks. The experimental propene selectivity does increase during the first 20 to 30 s after exposure to propane. Thus, consumption of the non-selective α oxygen may explain this increase in propene selectivity; however, the rate constants for the production of carbon oxides from the α oxygen are too large in the DMV1 and DMV3. It was found that by reducing these rate constants by about 60%, the DMV1 and DMV3 models could predict the small increase in propene selectivity observed in the experimental data after exposure to propane. The DMV1 and DMV3 models do not allow for any surface adsorption of reaction products or reaction intermediates. TPO experiments, discussed in section 8.4.1, indicated that carbon-containing species are adsorbed to the catalyst surface after exposure to propane in the absence of oxygen. Also, step-change mass balances (Figure 6.7) indicated that upon start-up of the reaction, without oxygen, most of this carbon deposits on the catalyst, within 20 s after exposure to propane. Also, during periodic operation of the reaction (Figure 8.1), it was found that carbon dioxide lagged behind the responses of other products when feed to the reaction was switched from propane to oxygen. This slow response of carbon dioxide suggested either the desorption of carbon dioxide itself or that carbon-containing species may have been oxidized from the catalyst surface. The agreement of the DMV1 and DMV3 models transient responses with the data could be improved if

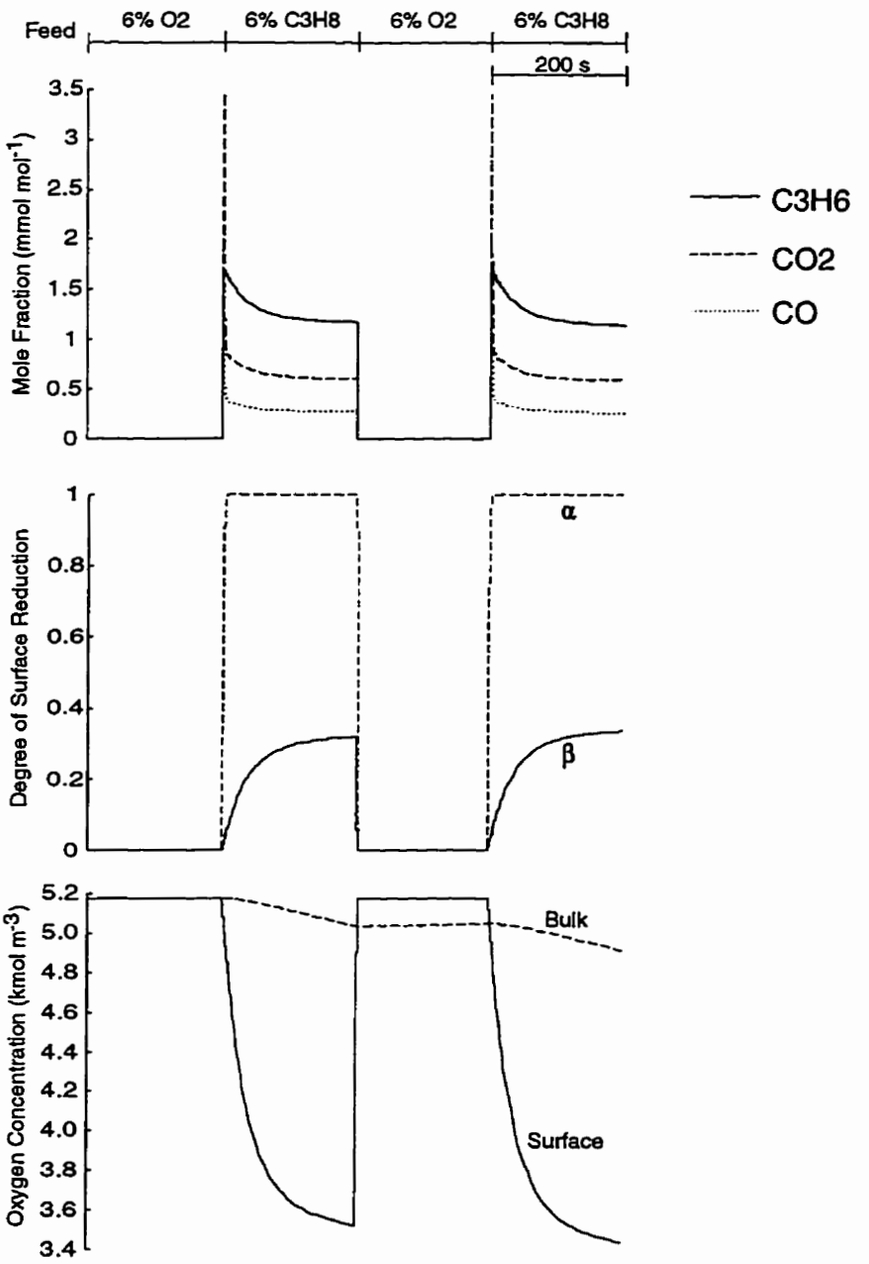

Figure 9.10 Reduction of surface oxygen and bulk oxygen concentration for DMV3 model

allowance is made for the adsorption of carbon oxides on the catalyst upon exposure to propane. Alternatively, carbon oxide precursors may adsorb to the catalyst surface such as propane or propene. Essentially the catalyst should trap carbon oxides or carbon oxide precursors upon exposure to propane and then release them as carbon dioxide upon exposure to oxygen.

The DMV4 model appears to be best for simulating the periodic operation. In this model, gas-phase oxygen directly produces carbon oxides from adsorbed propene. Thus,

when the feed of oxygen is interrupted the extra production of carbon oxides from the gas-phase oxygen is immediately stopped.

It can be seen in Figure 9.10 that after the feed was switched from propane to oxygen, both the α and β oxygen were completely reoxidized within seconds. This fast rate of reoxidation agrees with the periodic operation results (Figure 8.3). In those experiments, the cycle split was varied such that the oxygen feed half of the cycle was successively shortened. It was found that the catalyst was essentially fully reoxidized after only 10 s of oxygen exposure.

Periodic operation with the longest cycle period of 400 s is most difficult to model. This occurs because the activity of the catalyst, after exposure to propane, declined rapidly for about 50 s, but then became almost constant. With the use of the redox models without allowance for diffusion of bulk oxygen to the catalyst surface, the predicted activity of the catalyst declines at a more constant rate. The value of X_β used was rather small in order that the rates of production decrease quickly after propane exposure. However, after about 50 s, these rates stabilized because the β-oxygen was re-supplied by oxygen from the catalyst bulk. Figure 9.10 shows the concentrations of bulk (C_{Ob}) and surface oxygen (C_{Os}) for the DMV3 model. The difference between the bulk and surface oxygen concentrations determines the driving force for transport of oxygen from bulk to surface or from surface to bulk. It is apparent, for the two cycles of periodic operation simulated, that the bulk oxygen concentration is not stable. Experimentally, the periodic operation was run for ten cycles. The product responses appeared to be stable after only about three; however, with long-term periodic operation, it is possible that there may have been a slow depletion of the bulk oxygen resulting in a very slow deterioration in activity. Of course, the model for the bulk diffusion of oxygen may be inadequate. The fully oxidized bulk and surface concentrations of oxygen were assumed to be equal. If a larger surface oxygen concentration were used the predicted bulk concentration of oxygen could be made stable under periodic operation.

Propane pulsing experiments, the results of which are shown in Figure 8.9, indicated that diffusion of bulk oxygen may not have been an important process because an overshoot response was not observed for each propane pulse. An alternative explanation for the initially fast and then slower decline in activity observed is that the rate constants for production of propene and carbon oxides from the β-oxygen are a function of the degree of reduction of the catalyst

$$k = f(\beta) \tag{9.33}$$

It seem reasonable that the rate constants might depend on the quantity and binding strengths of the oxygen on the catalyst surface. Initially, after the switch to propane feed, weakly bound highly reactive surface oxygen is consumed and gradually the remaining oxygen is more strongly bound and less reactive.

Figure 9.11 compares the experimental data and the DMV model predictions for the product responses during periodic operation in which the feed of propane is split between the two halves of the cycle. The values of the adjustable parameters, shown in Table 9.7 are again used in the models. The results for the DMV1 model, although not shown in Figure 9.11, were very similar to those of the DMV3 model.

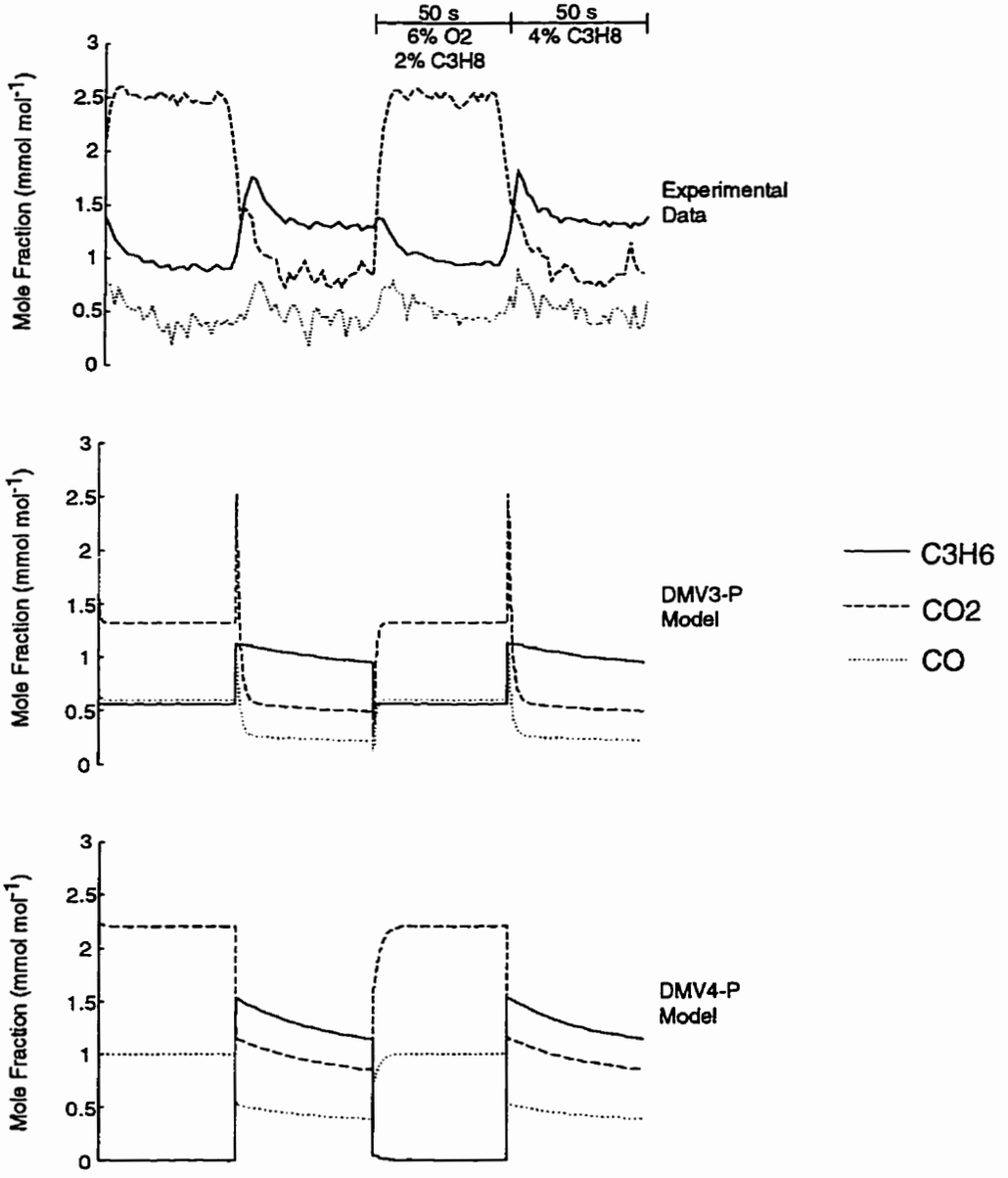

Figure 9.11 Comparison of experimental data to predictions of DMV models for periodic operation with constant feed of propane

Large peaks in the carbon oxide concentrations, upon increase in the feed concentration of propane from 2 to 4%, are evident for the DMV3 model. In this case the α-oxygen is partially reduced during the oxidation half of the feed cycle, because a low concentration of

propane is fed along with the oxygen. The peak in carbon oxide concentration results because of the sudden increase in propane feed concentration. Again the carbon oxide concentrations decline rapidly as a result of the small quantity of α-oxygen that is quickly consumed. As with the simulations shown in Figure 9.9, the DMV4 model more accurately predicts the carbon oxide responses after the switch to feed of only propane.

From the experimental data in Figure 9.11, large variations are observed in the ratio of carbon oxides as the ratio of oxygen-to-propane in the feed is alternated. This same relation between the carbon oxide ratio and oxygen-to-propane feed ratio was observed for the steady-state data, as illustrated in Figure 9.3. The variation in ratio of carbon oxides is not duplicated by the models because they use only a fixed ratio for the production of the carbon oxides. The propene selectivity predictions of the DMV4 model are also poor. During the feed of both propane and oxygen, no propene is produced. This is due to the large ratio in the feed of oxygen-to-propane at these conditions, i.e. 3:1. Figure 9.8 shows that the DMV4 model predicts a linear relation between selectivity and the oxygen-to-propane feed ratio; however, for the DMV3 and DMV1 models (Figure 9.6) the selectivity decreases very little beyond the oxygen-to-propane feed ratio of 1:1. The DMV4 models predict a constant variation in propene selectivity because a portion of the carbon oxide production in the model depends directly on the oxygen gas phase partial pressure. For the steady-state data shown in chapter 4, the oxygen-to-propane feed ratio was varied from 1:1 to 3:1. In that data, a strong dependence of the selectivity on the oxygen-to-propane feed ratio was not indicated. It does seem that in fact the propene selectivity is more stable with a large excess of feed oxygen, as the DMV1 and DMV3 models predict.

9.3.3 Conclusions from Periodic Operation Simulations

In general, the DMV4 model appears to simulate more accurately the product responses during periodic operation of the reaction than the DMV1 and DMV3 models. This suggests that the lower selectivity of the reaction with gas phase oxygen results from production of carbon oxides directly from gas-phase oxygen as opposed to from non-selective α-oxygen that is present only with gas-phase oxygen. However, at steady-state conditions with varying gas phase oxygen concentrations, the DMV1 and DMV3 models more accurately simulate the variation in propene selectivity than does the DMV4 model. According to the DMV4 model, the propene selectivity varies directly with the oxygen partial pressure; however, with the DMV1 and DMV3 models, the propene selectivity changes little at high partial pressures of oxygen because the α-oxygen sites become filled. However, if allowance is made in the DMV1 and DMV3 for the adsorption of carbon oxides or carbon oxide precursors, it is expected that the DMV1 and DMV3 models could simulate periodic operation equally well as the DMV4 model. TPO and step-change experiments support the adsorption of carbon-containing species on the catalyst during reaction in the absence of gas phase oxygen.

Overall, the inclusion of carbon oxide adsorption in the DMV1 and DMV3 models would make them the most suitable models for simulating both the steady-state and transient behaviour of the reaction.

An alternative that has not been tested in the models is that the α-oxygen is only surface-adsorbed oxygen in equilibrium with the gas-phase oxygen partial pressure. However, such a model for the α-oxygen would produce the same dynamics as the redox-supplied oxygen in the DMV1 and DMV3 models. After exposure of the catalyst to feed without gas phase oxygen, the α-oxygen would still have to be consumed, which would result in a peak of the carbon oxide concentrations. The surface adsorption of oxygen would allow for the desorption of some of the α-oxygen once oxygen is removed from the gas phase; however, the height of the carbon oxide peaks would be unaffected by the rate of desorption.

10. Conclusions

The examination of the oxidative dehydrogenation of propane, presented in this thesis, can be essentially divided into four parts. First, steady-state data collected at a range of reaction conditions were used to test various kinetic models by nonlinear regression analysis. In the second part, transient analysis techniques were used to further examine the reaction mechanism and investigate the catalytic behaviour under nonsteady-state conditions. Findings about the selectivity of the reaction under nonsteady-state conditions inspired part three; a brief investigation of the periodic operation of the reaction which provided even further information about the reaction mechanism. Finally, in the fourth part, additional steady-state data were collected at a wider range of oxygen partial pressures. The kinetic models developed in the first part were extended to describe an apparent relationship between the selectivity of the reaction and the oxygen gas-phase partial pressure.

Steady-state kinetic modelling

The initial steady-state kinetic data were collected based on a factorial design of experiments about a set of standard reaction conditions. Simple power law models indicated the reaction rates had a stronger dependence on the hydrocarbon partial pressures than on oxygen. This suggested the catalyst was almost saturated with surface oxygen. With mechanistic models, difficulties were encountered in modelling surface oxygen in equilibrium with gaseous oxygen. Oxygen equilibrium models predicted a higher surface concentration of oxygen at higher temperatures. Models in which oxygen reacted separately with its own kinetics to re-oxidize the catalyst by Mars-Van Krevelen type kinetics fit the data better. Finally, a general model was proposed based on a simple consecutive reaction scheme in which propane reacts with surface oxygen species to form adsorbed propene. The adsorbed propene can desorb or be further oxidized to carbon oxides.

It was found that the selectivity of the catalyst at any given set of reaction conditions may be sensitive to previous conditions to which the catalyst had been exposed. When the catalyst was initially exposed to reaction conditions with an excess of oxygen, the selectivity for propene was observed to deteriorate with time on stream. On the other hand, the propene selectivity was stable when the catalyst was initially exposed to equal concentrations of propane and oxygen. There was evidence that if the catalyst was exposed initially to excess oxygen, its propene selectivity continued to be low when exposed to other feed concentrations.

Transient kinetic analysis

Many of the transient response characteristics qualitatively supported the Mars-Van Krevelen or redox type reaction kinetics. During start-up of the reaction, it was observed that propane began to react first, reducing the catalyst. The reaction of oxygen to re-oxidize the catalyst was delayed by a few seconds. Also, the transient response of the products consisted of an overshoot type response, suggesting the reaction rate was initially high because of an excess of oxygen on the catalyst surface but then the reaction rate slowed as the catalyst was reduced and steady-state was approached. Mass balances appeared to confirm that the catalyst was partially reduced during start-up of the reaction. Redox kinetics were further supported by the observation that the catalyst was active without the presence of gas-phase oxygen, for at least 10 min at the reaction conditions examined. Oxygen on the surface and in the bulk of the catalyst was sufficient to drive the reaction. During operation of the reaction under these transient conditions without gas-phase oxygen, the propene selectivity was found to be higher than at steady-state. This was true even at comparable levels of conversion of the propane.

Carbon mass balances during start-up and interruption of the reaction were less clear, but seemed to indicate that little to no carbon was present on the catalyst surface during steady-state reaction with both propane and oxygen feed. However, temperature-programmed oxidation and desorption experiments indicated that a significant quantity of carbon, in some form, was present on the catalyst surface at steady-state reaction conditions. Because elevated reaction temperatures were required to oxidize these carbon species, they were apparently strongly bound to the catalyst surface. However, they did not seem to contribute to deactivation of the catalyst. These carbon-containing species, present at steady-state, were apparently slowly deposited on the catalyst surface during reaction. On the other hand, when the reaction was started without gaseous oxygen, a carbon mass balance indicated that carbon species were deposited on the catalyst surface for a short period immediately after start-up. Lags in the response of carbon dioxide during periodic operation of the reaction supported the presence of these carbon species. Temperature-programmed oxidation experiments indicated that the majority of the carbon species deposited on the catalyst during start-up of the reaction without gas-phase oxygen, were removed immediately upon exposure to oxygen, suggesting they were weakly bound to the catalyst surface.

The kinetic model proposed from the examination of steady-state data was used to construct a dynamic kinetic model. The dynamic model could successfully reproduce the observed transient responses during start-up of the reaction with catalyst previously exposed to reaction conditions and then re-oxidized. The observed rapid propene overshoot response required that the model include a small number of sites on the catalyst for propene adsorption. This result tended to agree with the experimental carbon mass balances for start-up of the reaction at steady-state conditions. Mass transport of oxygen may be an important

process during the transient responses; however, it seemed to be correlated with the surface oxygen content of the catalyst.

The dynamic model failed to predict the high propene selectivity observed immediately after start-up of the reaction without gas phase oxygen. The model predicted a higher propene selectivity only after partial reduction of the catalyst, an expected result because of the consecutive sequence of the model's reaction scheme. There were apparently additional reaction pathways that produce carbon oxides involving gas phase oxygen, not accounted for in the model.

Periodic operation

The high selectivity of the reaction without oxygen suggested than an obvious strategy for improvement of the performance of the reaction would be by periodic operation consisting of the alternate feeding of propane and oxygen. Under periodic operation at a 1:1 cycle split, a higher time-average propene yield could be obtained compared to steady-state operation over a range of cycle periods. Propene selectivities too were well above steady-state values. At periods longer than about 150 s, the time-average propane conversion for periodic operation was too low for the propene yield to exceed steady-state. However, due to the overshoot response at shorter periods the conversion could be increased so as to increase the yield over that at steady-state. At very short cycle periods of less than about 50 s, the time-average selectivity and even eventually yield for periodic operation decreased because the instantaneous selectivity of the reaction tended to be lower immediately after re-exposure to propane.

Variation of the periodic operation cycle split indicated that the rate of re-oxidation of the reaction was considerable faster than the rate of reduction. When the propane feed half-cycle was 50 s, the catalyst was fully re-oxidized within 10 s during the oxygen feed half-cycle. These results suggest that at steady-state the catalyst is nearly fully oxidized. This agrees with power-law kinetic findings that the steady reaction rates have only a weak dependence on oxygen partial pressure.

Periodic operation was carried out without catalyst re-oxidation, in which propane was alternated with pure helium feed. Under these conditions, the catalyst could be significantly reduced. The oxygen removal corresponded to the complete reduction of the magnesium orthovanadate phase. As the catalyst was reduced, the propene selectivity increased and, simultaneously, propane conversion decreased. However, comparison of the propene selectivity at about the same conversion of propane but different degrees of catalyst reduction indicated that the yield of the catalyst was greater in the more reduced state.

Oxygen effects on selectivity

Additional steady-state data were obtained in which the oxygen partial pressure was varied over a large range at constant propane partial pressures. In order to vary the propane conversion as well, experiments were repeated with different masses of catalyst. The propene selectivity increased as the partial pressure of oxygen was decreased; simultaneously, propane conversion decreased. At low propane partial pressures, the decrease in propane conversion was small enough that the propene yield increased. This suggested that an alternative to periodic operation for improving the propene selectivity could be simply to operate at steady-state with a low partial pressure of oxygen.

A simple redox model with a consecutive reaction scheme was inadequate for modelling the improved selectivity at reduced oxygen partial pressures. Models which included additional pathways for the production of carbon oxides dependent on the partial pressure of the oxygen were more successful. These models included either separate surface oxygen sites that produced only carbon oxides or allowed for gas-phase oxygen to react directly with surface adsorbed propene to produce carbon oxides. Dynamic forms of these extended redox models were also used for simulating periodic operation results. The model that included the direct reaction of gas-phase oxygen to produce carbon oxides simulated the high propene selectivity observed immediately after the catalyst is re-exposed to propane. Models with separate surface oxygen sites required the inclusion of adsorption of carbon oxides or carbon oxide precursors in order to accurately simulate dynamic responses. Overall, models with separate oxygen sites were considered best for describing both the steady-state and transient data.

What does it all really mean?

On the whole, results indicate that the concentration of oxygen both in the gas phase and on the surface of the catalyst is crucial for determining reaction conditions for selectively producing propene. Oxygen-starvation of the reaction appears to be the best strategy for minimizing the complete oxidation of propane to carbon oxides. The low propane conversion at these conditions can be compensated for by increasing quantities of catalyst. It is unclear whether the same mechanisms are at work, when the propene selectivity is improved at steady-state conditions with a lower gas-phase partial pressure of oxygen as opposed to at non-steady-state conditions with increasing reduction of the catalyst. The improved selectivity at non-steady-state conditions can probably be attributed to the increased binding strength of lattice oxygen at increased reduction of the catalyst. The oxygen sites that produce only carbon oxides in the extended-redox models could be considered weakly bound, perhaps surface adsorbed oxygen whose concentration is dependent on the oxygen partial pressure. These models did successfully describe the

steady-state data, and with the inclusion of carbon oxide adsorption, can be expected to successfully simulate transients under periodic operation.

11. Recommendations for future work

The low alkene selectivity of the oxidative dehydrogenation reaction remains a problem. If the thermal advantages of this reaction, discussed in the introduction, are ever to be exploited commercially, the selectivity of the reaction for combustion products must be as low as or lower than the selectivity of the direct thermal dehydrogenation reaction for producing carbonaceous deposits on the catalyst.

The aim of this research work has been to study the reaction kinetics and mechanism both under steady-state and transient conditions. The results have indicated that the performance of the reaction for selective production of propene is dependent on the partial pressure of oxygen in steady-state conditions and the catalyst surface concentration of oxygen in non-steady-state conditions without gas-phase oxygen. The complete oxidation of propane to carbon oxides is minimized by operating at non-steady-state without gas-phase oxygen and with the catalyst in a reduced state. This suggests that ideally the reaction ought to be carried out in a cyclic process with alternating feeds of propane and oxygen. Industrially this would be most conveniently realized in a fluidized bed type reactor in which the catalyst is transported between reduction and oxidation reactors. There is a concern though that in order for the selectivity of the reaction to be sufficiently high, the catalyst would have to be maintained in a severely reduced state. Thus, in order for such a process to have acceptable productivity, excessive quantities of catalyst would have to be transported, possibly making the process economically unattractive. An alternative to a fluidized bed reactor process would be a membrane type reactor, in which the reoxidation of the catalyst would be controlled by the rate of diffusion of oxygen through a membrane. But here again, achieving acceptable productivity per mass of catalyst could be problematic. In the work presented in this thesis, the reaction has been operated at low levels of conversion in order to ease the interpretation of the transient response experiments. More work needs to be done to investigate the achievable yields under various modes of periodic operation at higher levels of conversion that would be of industrial interest.

Another possible aim for future research is catalyst improvement which certainly is aided by an understanding of the reaction mechanism. There does seem to be room remaining for catalyst development and already recent investigations with alkaline additives, which presumably aid in the desorption of the alkene, have shown some success in this area [54-59]. Who knows, if the best possible catalyst is used in the best possible way: there could be hope yet!

An interesting alternative approach for future research would be the thermal coupling of oxidative dehydrogenation with the direct dehydrogenation reaction. This is an attractive direction for future research if development of a competitive process based solely on

oxidative dehydrogenation seems futile. The aim here would be to carry out just enough oxidative dehydrogenation to clean the catalyst of deactivating carbonaceous deposits and provide enough heat to be consumed by the direct thermal dehydrogenation. Prevention of catalyst deactivation and improved energy efficiency would be the advantages of such a process. An 'in situ' redox fluidized bed reactor, as discussed in chapter 8, could be used to carry out such a process. This research would probably have to be combined with catalyst development since a catalyst suitable for both oxidative and thermal dehydrogenation reaction routes would be required. In addition if the catalyst were to be used in an 'in situ' redox fluidized bed type reactor it would have to be resistant against erosion.

More work could be done to study the mechanisms of the catalytic reaction, carrying on the efforts of this thesis. There are many other modes of periodic operation at which the reaction could be operated. Of particular interest would be variation of the oxygen partial pressure during periodic operation. In the periodic operation work presented in this thesis the reactant partial pressures were held constant. Although, it was found that the oxygen partial pressure had a significant effect on the selectivity of the reaction during steady-state operation. During periodic operation of the reaction can the partial pressure of oxygen during the oxygen half of the feed cycle control presumably the types of oxygen generated on the catalyst and then affect the product responses during the subsequent propane half of the feed cycle? In addition, the use of oxygen isotopes could provide further clarification regarding the roles of gas-phase versus surface oxygen in the reaction and the extent of the diffusion of oxygen from the catalyst bulk during periodic operation. Oxygen isotopes could also perhaps provide information about the various types of active surface oxygen.

Nomenclature

A	= area (m^2)
C_O	= oxygen concentration (mol m^{-3})
E_{ai}	= activation energy of reaction i (J mol^{-1})
ΔH_i	= heat of adsorption for component i (J mol^{-1})
k_i	= rate constant for reaction i
k_{iO}	= Arrhenius pre-exponential factor for reaction i
k_D	= oxygen diffusivity in catalyst bulk (m^2 min^{-1})
K_i	= adsorption equilibrium constant for component i
L	= length of catalyst bed in reactor volume element (m)
P_i	= partial pressure of component i (bar)
Qi	= quantity of adsorption sites for component i (mol)
r_i	= reaction rate of reaction i (mol min^{-1} (g cat.)$^{-1}$)
R	= ideal gas constant (8.314 Pa m^3 mol^{-1} K^{-1})
ΔS_i	= change in entropy on adsorption (J mol^{-1} K^{-1})
T	= temperature (K)
t	= time (min)
u	= superficial gas velocity (m min^{-1})
V_b	= volume of catalyst bed in reactor volume element (m^3)
W	= mass of catalyst (g)
x	= ratio of production of CO_2 to CO
X_i	= fraction of total sites for adsorption of component i available at surface

Greek letters

α	= degree of reduction of catalyst α-oxygen surface sites
β	= degree of reduction of catalyst β-oxygen surface sites
δ	= equivalent thickness (m)
ε	= catalyst bed void fraction
θ_i	= degree of occupation of surface adsorption sites for component i
ρ	= catalyst bulk density (g m^3)
ω	= lumped bulk oxygen transport parameter (m^3 min^{-1})

Subscripts

ads	= adsorption
b	= bulk

des	= desorption
in	= inlet
m	= mean
O	= surface atomic oxygen
s	= surface
ss	= steady state

References

1. R.C. Reid, J.M. Prausnitz, B.E. Poling, The Properties of Gases and Liquids, 4th Ed., McGraw-Hill, New York, 1987.
2. J.M. Smith, H.C. Van Ness, Introduction to Chemical Engineering Thermodynamics, 4th Ed., McGraw-Hill, New York, 1987.
3. R.M. Stephenson, Introduction to the Chemical Process Industries, Reinhold, New York, 1966.
4. F. Cavani, F. Trifirò, Catal. Today, 24 (1995) 307.
5. I.M. Dahl, K. Grande, K.-J. Jens, E. Rytter, Å Slagtern, Appl. Catal., 77 (1991) 163.
6. S.B. Ushkov, Z.G. Osipova, V.D. Sokolovskii, S.V. Ketchik, Kinet. Katal., 29 (1988) 195.
7. Y. Takita, H. Yamashita, K. Moritaka, Chem. Lett., 10 (1989) 1773.
8. C. Mazzocchia, C. Aboumrad, C. Daigne, E. Tempesti, J.M. Herrmann, G. Thomas, Catal. Lett., 10 (1991) 181.
9. Y.S. Yoon, W. Ueda, Y. Moro-oka, Catal. Lett., 35 (1995) 57.
10. R.H.H. Smits, K. Seshan, J.R.H. Ross, J. Chem. Soc., Chem. Comm., 8 (1991) 558.
11. R.H.H. Smits, K. Seshan, J.R.H. Ross, Stud. Surf. Sci. Catal., 72 (1992) 221.
12. R.H.H. Smits, K. Seshan, J.R.H. Ross, ACS Symp. Ser. 523, Catalytic Selective Oxidation, S.T. Oyama, J.W. Hightower, Eds., (1993) 380.
13. R.H.H. Smits, K. Seshan, J.R.H. Ross, L.C.A. van den Oetelaar, J.H.J.M. Helwegen, M.R. Anantharaman, H.H. Brongersma, J. Catal., 157 (1995) 584.
14. E.E. Gonzo, L.C. Romero, React. Kinet. Catal. Lett., 41 (1990) 39.
15. L.C. Romero, E.E. Gonzo, Gottifredi, React. Kinet. Catal. Lett., 38 (1989) 375.
16. L.C. Romero, E.E. Gonzo, Gottifredi, React. Kinet. Catal. Lett., 43 (1991) 43.
17. S.C. Shenoy, M.S. Rao, J. Chem. Tech. Biotech., 36 (1986) 95.
18. S.C. Shenoy, M.S. Rao, J. Chem. Tech. Biotech., 36 (1986) 110.
19. D. Singh, J.K. Gehlwat, M.S. Rao, J. Chem. Tech. Biotech., 47 (1990) 127.
20. K. Fujimoto, I. Nakamura, K. Yotota, Zeolites, 9 (1989) 120.
21. P.M. Michalakos, M.C. Kung, I. Jahan, H.H. Kung, J. Catal., 140 (1993) 226.
22. E. Morales, J.H. Lunsford, J. Catal., 118 (1989) 255.
23. R. Burch, E.M. Crabb, Appl. Catal. A, 97 (1993) 49.
24. H.M. Swaan, A. Toebes, K. Seshan, J.G. van Ommen, J.R.H. Ross, Catal. Today, 13 (1992) 629.
25. S.J. Conway, J.H. Lunsford, J. Catal., 131 (1991) 513.
26. S. Albonetti, F. Cavani, F. Trifirò, Cat. Rev. Sci. Eng., 38(4) (1996) 413.

27. E.A. Mamedov, V. Cortés Corberán, Appl. Catal. A, 127 (1995) 1.
28. L. Owens, H.H. Kung, J. Catal., 144 (1993) 202.
29. G. Centi, F. Trifirò, Appl. Catal. A, 143 (1996) 3.
30. P. Concepción, A. Corma, J.M. López Nieto, J. Pérez-Pariente, Appl. Catal. A, 143 (1996) 17.
31. F. Cavani, C. Comuzzi, G. Dolcetti, E. Etienne, R.G. Finke, G. Selleri, F. Trifirò, A. Trovarelli, J. Catal., 160 (1996) 317.
32. F. Cavani, M. Koutyrev, F. Trifirò, Catal. Today, 24 (1995) 365.
33. J.B. Moffat, Appl. Catal. A, 146 (1996) 65.
34. M.A. Chaar, D. Patel, M.C. Kung, H.H. Kung, J. Catal., 105 (1987) 483.
35. M.A. Chaar, D. Patel, H.H. Kung, J. Catal., 109 (1988) 463.
36. D. Sam, V. Soenen, J.C. Volta, J. Catal., 123 (1990) 417.
37. D. Bhattacharyya, S.K. Bej, M.S. Rao, Appl. Catal. A, 87 (1992) 29.
38. Burch, R., Crabb, E.M., Appl. Catal. A, 100 (1993) 111.
39. A. Corma, J.M. López Nieto, N. Paredes, N. Perez, Y. Shen, H. Cao, S.L. Suib, Stud. Surf. Sci. Catal., 72 (1992) 213.
40. A. Corma, J.M. López Nieto, N. Paredes, Appl. Catal. A, 104 (1993) 161.
41. A. Corma, J.M. López Nieto, N. Paredes, J. Catal., 144 (1993) 425.
42. X. Gao, P. Ruiz, Q. Xin, X. Guo, B. Delmon, Catal. Lett., 23 (1994) 321.
43. X. Gao, P. Ruiz, Q. Xin, X. Guo, B. Delmon, J. Catal., 148 (1994) 56.
44. S.R.G. Carrazán, C. Peres, J.P. Bernard, M. Ruwet, P. Ruiz, B. Delmon, J. Catal., 158 (1996) 452.
45. X. Gao, Q. Xin, X. Guo, Appl. Catal. A, 114 (1994) 197.
46. K.T. Nguyen, H.H. Kung, Ind. Eng. Res., 30 (1991) 352.
47. K.T. Nguyen, H.H. Kung, Chem. Ind., 46 (1992) 285.
48. K.T. Nguyen, H.H. Kung, R.L. Burwell, Chemtracts: Inorg. Chem., 3 (1991) 22.
49. N. Krishnamachari, C. Calvo, Can. J. Chem., 49 (1971) 1629.
50. R. Gopal, C. Calvo, Acta Crystal. B., 30 (1974) 2491.
51. H.N. Ng, C. Calvo, Can. J. Chem., 50 (1972) 3619.
52. H.H. Kung, M.A. Chaar, U.S. Patent 4 777 319 (1988).
53. M.C. Kung, H.H. Kung, J. Catal., 134 (1992) 668.
54. R. Grabowski, B. Grzybowska, K. Samson, J. Sloczynski, J. Stoch, K. Wcislo, Appl. Catal. A, 125 (1995) 129.
55. R.M. Martin-Aranda, M.F. Portela, L.M. Madeira, F. Freire, M. Oliveira, Appl. Catal. A, 127 (1995) 201.
56. G.E. Vrieland, C.B. Murchison, Appl. Catal. A, 134 (1996) 101.
57. G.E. Vrieland, B. Khazai, C.B. Murchison, Appl. Catal. A, 134 (1996) 123.
58. A. Galli, J.M. López Nieto, A. Dejoz, M.I. Vazquez, Cat. Lett., 34 (1995) 51.

59. T. Blasco, J.M. López Nieto, A. Dejoz, M.I. Vazquez, J. Catal., 157 (1995) 271.
60. O.S. Owen, M.C. Kung, H.H. Kung, Catal. Lett., 12 (1992) 45.
61. D. Patel, P.J. Andersen, H.H. Kung, J. Catal., 125 (1990) 132.
62. P.J. Andersen, H.H. Kung, *in* New Frontiers in Catalysis, Proc. 10th Int. Congr. Catal., L. Guczi, F. Solymosi and P. Teteryi, Eds., (1992) 205.
63. V. Soenen, J.M. Herrmann, J.C. Volta, J. Catal., 159 (1996) 410.
64. D. Patel, M.C. Kung, H.H. Kung, Proc. 9th Int. Congr. Catal., 4 (1988) 1554.
65. H.H. Kung, P. Michalakos, L. Owens, M. Kung, P. Andersen, O. Owen, I. Jahan, ACS Symp. Ser. 523, Catalytic Selective Oxidation, S.T. Oyama and J.W. Hightower, Eds., (1993) 389.
66. H.H. Kung, Adv. Catal., 40 (1994) 1.
67. B. Zhaorigetu, R. Kieffer, J.P. Hindermann, Proc. 11th Int. Congr. Catal., *in* Stud. Surf. Sci. Catal., J.W. Hightower, W.N. Delgass, E. Iglesia, A.T. Bell, Eds., 101 (1996) 1049.
68. S.L.T. Andersson, Appl. Catal. A, 112 (1994) 209.
69. J. Le Bars, J.C. Vedrine, A. Auroux, Appl. Catal. A, 88 (1992) 179.
70. J. Sloczynski, Appl. Catal. A, 146 (1996) 401.
71. A. Pantazidis, C. Mirodatos, Proc. 11th Int. Congr. Catal., *in* Stud. Surf. Sci. Catal., J.W. Hightower, W.N. Delgass, E. Iglesia, A.T. Bell, Eds., 101 (1996) 1029.
72. J.M. Ruth, Anal. Chem., 40 (1968) 747.
73. D. Creaser, B. Andersson, Appl. Catal. A, 141 (1996) 131.
74. G.E.P. Box, W.G. Hunter, J.S. Hunter, Statistics for Experimenters, Wiley, New York, 1978, p. 312.
75. N.R. Draper, H. Smith, Applied Regression Analysis, 2nd ed., Wiley, New York, 1981, p. 257.
76. S.M. Senkan, in J. Wei, J.L. Anderson, K.B. Bischoff and J.H. Seinfeld (Editors), Detailed Chemical Kinetic Modeling: Chemical Reaction Engineering of the Future, Adv. Chem. Eng., Vol. 18, Academic Press, New York, 1992, p. 95.
77. G.H. Aylward, T.J.V. Findlay, SI Chemical Data, 2nd ed., Wiley, New York, 1974.
78. N.R. Draper, H. Smith, Applied Regression Analysis, 2nd ed., Wiley, New York, 1981, p. 484.
79. M. Huff, L.D. Schmidt, J. Catal., 155 (1995) 82.
80. E.A. Mamedov, Appl. Catal. A, 116 (1994) 49.
81. H. Kobayashi, M. Kobayashi, Cat. Rev. Sci. Eng., 10(2) (1974) 139.
82. C.O. Bennett, Cat. Rev. Sci. Eng., 13(2) (1976) 121.
83. M. Kobayashi, Chem. Eng. Sci., 37 (1982) 393.
84. A. Renken, in Yu. Sh. Matros (Editor), Unsteady State Processes in Catalysis, VSP, Utrecht, Tokyo, 1990, p. 183.

85. S.N. Wang, H. Hofmann, in Yu. Sh. Matros (Editor), Unsteady State Processes in Catalysis, VSP, Utrecht, Tokyo, 1990, p. 253.
86. G.F. Froment, K.B. Bischoff, Chemical Reactor Design and Analysis, 2nd ed., John Wiley & Sons, New York, 1990, p. 406.
87. J. Coronas, M. Menéndez, J. Santamaría, Ind. Eng. Chem. Res., 34 (1995) 4229.
88. A.L. Tonkovich, J.L. Zilka, D.M. Jimenez, G.L. Roberts, J.L. Cox, Chem. Eng. Sci., 51(5) (1996) 789.
89. A. Pantizidis, J.A. Dalmon, C. Mirodatos, Catal. Today, 25 (1995) 403.
90. C. Téllez, M. Menéndez, J. Santamaría, Proceedings 5th World Congress of Chemical Engineering, AICHE, 4 (1996) 610.
91. R. Wang, M. Xie, P. Li, C. Ng, Catal. Lett., 24 (1994) 67.
92. P.L. Silveston, Composition Modulation of Catalytic Reactors, *in press*, Gordon-Breach (U.K.), 1997, chap. 11 and 12.
93. A.D. Eastman, J.H. Kolts, US Patent 4,370,259 (1983).
94. C.A. Jones, J.J. Leonard, J.A. Sofranko, US Patent 4,737,595 (1988).
95. B. Khazai, E.G. Vrieland, G.B. Murchison, European Patent 0 409 355 B1 (1995).
96. L.P. Shapovalova, V.I. Voznyuk, T.V. Lysukho, V.P. Luk'yanenko, M.Yu. Kutnyaya, V.S. Solodkaya, L.P. Dolya, J. Appl. Chem. USSR, 60(2) (1987) 343.
97. V.A. Doroshenko, L.P. Shapovalova, L.P. Dolya, J. Appl. Chem. USSR, 59(5) (1986) 1176.
98. V.P. Luk'yanenko, L.P. Shapovalova, M.Yu. Kutnyaya, V.S. Solodkaya, J. Appl. Chem. USSR, 60(5) (1987) 1169.
99. R. Ramos, J. Herguido, M. Menéndez, J. Santamaría, J. Catal., 163 (1996) 218.

Appendix A
Gas Chromatography Analysis and Sample Calculations

Tables A1 and A2 show the integrated areas for the component peaks for a sample mixture and for the calibration gas mixtures respectively. For this sample data the reactor contained 30 mg of catalyst and the reaction temperature was 510°C. The inlet or feed gas composition was 6% C_3H_8 and 6% O_2 in helium with a total flow rate of 50 ml min^{-1} at STP. Two calibration gas mixtures were used. One was a specialty gas mixture supplied by AGA Gas, containing 0.99% CO, 1.02% CO_2 and 2.01% C_3H_6 in helium. The second was the actual feed gas mixture to the reactor containing 6% C_3H_8 and 6% O_2 in helium.

Table A1
Sample mixture component integrated areas

Component	Integrated Area (A_i^S)	Retention time (min)
CO	702	3.49
CO_2	1378	4.38
C_3H_6	2535	12.98
C_3H_8	106230	13.34

Table A2
Calibration mixtures component integrated areas

Trial	CO	CO_2	C_3H_6	C_3H_8
1	5344	5221	34943	111330
2	5362	5018	34074	110210
3	5216	5097	34501	110120
4	-	-	-	111710
5	-	-	-	107640
Average (A^C)	5307	5112	34506	110202

The sensitivity coefficient (S) for component i is calculated from the average calibration area (A^C) and the components concentration in the calibration mixture (C^C):

$$S_i = \frac{A_i^C}{C_i^C} \qquad \text{(A1)}$$

The resulting sensitivity coefficients for each component are shown in Table A3.

Table A3
Sensitivity coefficients

Component	S_i (area %$^{-1}$)
CO	1.865×10^{-4}
CO_2	1.995×10^{-4}
C_3H_6	5.825×10^{-5}
C_3H_8	5.445×10^{-5}

The concentrations of the carbon containing components (C) in the sample mixture are calculated from the sensitivity coefficients (S) and the integrated area for these components (A) in the sample mixture:

$$C_i = S_i * A_i \qquad \text{(A2)}$$

The resulting concentrations are shown in Table A4.

Table A4
Concentrations of carbon-containing components in sample mixture

Component	C_i (%)
CO	0.1309
CO_2	0.2750
C_3H_6	0.1477
C_3H_8	5.7837

The propene selectivity can be calculated directly from the concentrations of the carbon-containing products:

$$Selectivity = \frac{3C_{C_3H_6}}{3C_{C_3H_6} + C_{CO} + C_{CO_2}} * 100\% = 52.2\% \qquad \text{(A3)}$$

An iterative procedure is used to rigorously solve for the normalized outlet concentrations of each component. The inlet total flowrate to the reactor (F^{in}) is in all cases 50 ml min^{-1} at STP. For the first iteration it is assumed that the outlet total flowrate (F^{out}) is also 50 ml min^{-1} at STP. The overall reactions that produce each of the products are

$C_3H_8 + 0.5\ O_2 \rightarrow C_3H_6 + H_2O$

$C_3H_8 + 3.5\ O_2 \rightarrow 3\ CO + 4\ H_2O$

$C_3H_8 + 5\ O_2 \rightarrow 3\ CO_2 + 4\ H_2O$

Based on the stoichiometry of these overall reactions, the outlet concentrations of water and

oxygen can be calculated from the concentrations of carbon-containing products:

$$C_{H_2O} = \frac{4}{3}C_{CO} + \frac{4}{3}C_{CO_2} + C_{C_3H_6} = 0.6889\% \quad \text{(A4)}$$

$$C_{O_2} = \frac{C_{O_2}^{in}F^{in} - \left(\frac{C_{CO}}{2} + C_{CO_2} + \frac{C_{H_2O}}{2}\right)F^{out}}{F^{out}} = 5.3151\% \quad \text{(A5)}$$

In this case the feed oxygen concentration (C_{O2}^{in}) is 6%. The new outlet flow rate and the carbon balance are calculated:

$$F^{out} = \left(\frac{100 - C_{O_2}^{in} - C_{C_3H_8}^{in}}{100 - C_{CO} - C_{CO_2} - C_{C_3H_6} - C_{C_3H_8} - C_{O_2} - C_{H_2O}}\right)50\_ml \cdot \min^{-1} \quad \text{(A6)}$$

where the feed propane concentration in this case is 6%. The resulting outlet flow rate is 50.195 ml min^{-1} at STP. The carbon balance is calculated:

$$Carbon\_Balance = \left(\frac{\left(C_{CO} + C_{CO_2} + 3C_{C_3H_6} + 3C_{C_3H_8}\right)F^{out}}{3C_{C_3H_8}^{in}F^{in}}\right)100\% = 101.5\% \quad \text{(A7)}$$

The concentration of each component based on a normalized carbon distribution is calculated

$$C_i^N = \frac{C_i}{\left(C_{CO} + C_{CO_2} + 3C_{C_3H_6} + 3C_{C_3H_8}\right)F^{out}} \cdot 3C_{C_3H_8}^{in}F^{in} \quad \text{(A8)}$$

Table A5 shows the resulting normalized concentrations for the first iteration.

Table A5
Normalized Concentrations of carbon-containing components for first iteration

Component	C_i^N (%)
CO	0.1290
CO_2	0.2709
C_3H_6	0.1455
C_3H_8	5.6979

The normalized concentrations of each component are calculated repeatedly based on the new outlet flow rate values by equations A4 to A8 until they converge. Table A6 shows the normalized concentrations and total flow rate for each subsequent iteration.

Table A6
Normalized Concentrations for each iteration

	2nd iteration	3rd iteration	4th iteration
CO (%)	0.1292	0.1292	0.1292
CO_2 (%)	0.2713	0.2713	0.2713
C_3H_6 (%)	0.1457	0.1457	0.1457
C_3H_8 (%)	5.7055	5.7045	5.7045
H_2O (%)	0.6787	0.6797	0.6797
O_2 (%)	5.3019	5.3089	5.3079
F^{out} (ml min^{-1} at STP)	50.128	50.137	50.136

The propane and oxygen conversions are calculated:

$$C_3H_8\_conversion = \left(\frac{\left(C^{in}_{C_3H_8} F^{in}\right) - \left(C^{N}_{C_3H_8} F^{out}\right)}{\left(C^{in}_{C_3H_8} F^{in}\right)} \right) 100\% = 4.67\% \qquad \text{(A9)}$$

$$O_2\_conversion = \left(\frac{\left(C^{in}_{O_2} F^{in}\right) - \left(C^{N}_{O_2} F^{out}\right)}{\left(C^{in}_{O_2} F^{in}\right)} \right) 100\% = 11.29\% \qquad \text{(A10)}$$

Appendix B
Mathematical treatment of mass spectrometry data

Method of data analysis

The following continues in detail a description of the method of treatment of MS data started in Section 3.3.2. In the simplest method of qualitative analysis of mass spectrometry data the sensitivity coefficients, S_{ij}, must be known for each component, j, at each mass value, i. The number of mass peaks, n, must equal the number of components in the mixture. If the concentrations of the components of the mixture are partial pressures, p_j, the sensitivity coefficients express the mass peak intensity per unit pressure. Then a set of n simultaneous linear equations must be solved to determine the partial pressure of each component

$$\begin{aligned} &S_{11}p_1 + S_{12}p_1 + \ldots + S_{1n}p_n = I_1 \\ &S_{21}p_1 + S_{22}p_2 + \ldots + S_{2n}p_n = I_1 \\ &\ldots\ldots\ldots\ldots\ldots\ldots\ldots\ldots \\ &S_{n1}p_1 + S_{n2}p_2 + \ldots + S_{nn}p_n = I_n \end{aligned} \qquad \text{(B1)}$$

The above system of equations can be expressed in matrix notation as

$$\boldsymbol{Sp = I} \qquad \text{(B2)}$$

As discussed in section 3.3, the direct application of equation B2 is inadequate and the following describes the refinements used to overcome problems with slight total pressure differences between analysis of the calibration and sample gases. The partial pressures, p_j are replaced by $m_j p_c$, where m_j is the mole fraction of component j in the standard mixture and p_c is the unknown total pressure of the calibration mixture. Thus the general terms in equations B1 become

$$S_{ij}p_j = S_{ij}m_j p_c \qquad \text{(B3)}$$

The number of sensitivity coefficients can be reduced to the number of components by expressing the sensitivity coefficients at secondary mass peaks as equal to a fraction of the coefficients at the primary mass peak by use of the primary to secondary mass peak ratio defined by equation 3.3,

$$S_{ij} = r_{ij}S_{Pj} \qquad \text{(B4)}$$

Then the general term, $S_{ij}p_j$, can be further modified to

$$S_{ij}p_j = r_{ij}S_{Pj}m_j p_c \qquad \text{(B5)}$$

By defining

$$Q_j = S_{pj}p_c \qquad \text{(B6)}$$

and

$$a_{ij} = m_j r_{ij} \qquad \text{(B7)}$$

The general terms of equations B1 become

$$S_{ij}p_j = a_{ij}Q_j \quad \text{(B8)}$$

Then for each calibration mixture, the set of equations, in matrix form

$$\boldsymbol{aQ} = \boldsymbol{I_c} \quad \text{(B9)}$$

is obtained. By measuring the mass peak intensities, I_c, for each mass in each calibration mixture, the equations can be solved

$$\boldsymbol{Q} = \boldsymbol{a}^{-1}\boldsymbol{I_c} \quad \text{(B10)}$$

There are three unknown values of p_c, one for each calibration mixture. At this point it is necessary to adjust the Q values such that they are all based on the same pressure, by using helium as a tie component. Q values are calculated for helium in each calibration mixture. The ratio of the Q values for helium for the first and second calibration mixture are

$$Q_{He,1}/Q_{He,2} = p_{c,1}/p_{c,2} = R_{12} \quad \text{(B11)}$$

Since for all components in the second calibration mixture

$$Q_{j,2} = S_{pj}p_{c,2} \quad \text{(B12)}$$

then each can be expressed in terms of the pressure of the first calibration mixture by

$$Q_{j,2}R_{12} = S_{pj}p_{c,1} \quad \text{(B13)}$$

The same procedure can be used to express the Q values for the third calibration mixture in terms of the pressure of the first calibration mixture. From this point on, $p_{c,1}$ will be represented by p_c and each Q value can be expressed by equation B6.

Let p_x be the total pressure of the unknown mixture and x_j be the unknown mole fraction of component j in it. R will represent the ratio of the pressures of the unknown mixture and the first calibration mixture by

$$p_x = Rp_c \quad \text{(B14)}$$

Equations B1 can be applied to the unknown mixture and the general term $S_{ij}p_j$ may be rewritten as before

$$S_{ij}p_j = S_{ij}x_jp_x = r_{ij}S_{Pj}x_jRp_c = r_{ij}Q_jx_jR \quad \text{(B15)}$$

By defining

$$b_{ij} = r_{ij}Q_j \quad \text{(B16)}$$

and

$$y_j = x_jR \quad \text{(B17)}$$

Then

$$S_{ij}p_j = b_{ij}y_j \quad \text{(B18)}$$

giving the set of equations

$$\boldsymbol{by} = \boldsymbol{I_x} \quad \text{(B19)}$$

By measurement of the intensity of each mass peak, I_x, in the unknown mixture, the equations can be solved by

$$\boldsymbol{y} = \boldsymbol{b}^{-1}\boldsymbol{I_x} \quad \text{(B20)}$$

Finally to obtain the values x_j, it is known that for any mixture

$$\Sigma x_j = 1 \tag{B21}$$

Then from equation B17,

$$\Sigma y_j = \Sigma x_j R = R \tag{B22}$$

and by combining equations B17 and B22

$$x_j = y_j / \Sigma y_j \tag{B23}$$

In applying the procedure described above, first the calibration data must be used to calculate the matrix $\boldsymbol{b}$, by equations B7, B10 and B16. The mole fractions of the components in the unknown mixture, x_j, are then calculated by equations B20 and B23.

Sample data and calculations

Sample ion currents and cross-contributions

The matrix of ratios of primary and secondary mass peaks, as listed in Table 3.1, is

$$r = \begin{bmatrix} r_{4,He} & r_{4,H_2O} & r_{4,CO} & r_{4,C_3H_8} & r_{4,O_2} & r_{4,C_3H_6} & r_{4,CO_2} \\ r_{18,He} & r_{18,H_2O} & r_{18,CO} & r_{18,C_3H_8} & r_{18,O_2} & r_{18,C_3H_6} & r_{18,CO_2} \\ r_{28,He} & r_{28,H_2O} & r_{28,CO} & r_{28,C_3H_8} & r_{28,O_2} & r_{28,C_3H_6} & r_{28,CO_2} \\ r_{29,He} & r_{29,H_2O} & r_{29,CO} & r_{29,C_3H_8} & r_{29,O_2} & r_{29,C_3H_6} & r_{29,CO_2} \\ r_{32,He} & r_{32,H_2O} & r_{32,CO} & r_{32,C_3H_8} & r_{32,O_2} & r_{32,C_3H_6} & r_{32,CO_2} \\ r_{41,He} & r_{41,H_2O} & r_{41,CO} & r_{41,C_3H_8} & r_{41,O_2} & r_{41,C_3H_6} & r_{41,CO_2} \\ r_{44,Je} & r_{44,H_2O} & r_{44,CO} & r_{44,C_3H_8} & r_{44,O_2} & r_{44,C_3H_6} & r_{44,CO_2} \end{bmatrix}$$

$$= \begin{bmatrix} 1 & 0 & 0 & 0 & 0 & 0 & 0 \\ 0 & 1 & 0 & 0 & 0 & 0 & 0 \\ 0 & 0 & 1 & 0.676 & 0 & 0.0427 & 0.1393 \\ 0 & 0 & 0 & 1 & 0 & 0 & 0 \\ 0 & 0 & 0 & 0 & 1 & 0 & 0 \\ 0 & 0 & 0 & 0.231 & 0 & 1 & 0 \\ 0 & 0 & 0 & 0.220 & 0 & 0 & 1 \end{bmatrix} \tag{B24}$$

The sample data is for steady state reaction with feed of 3% propane and 6% oxygen with 21 mg of catalyst at a reaction temperature of 510°C. The measured ion currents with units mA at these conditions are

$$I = \begin{bmatrix} I_4 \\ I_{18} \\ I_{28} \\ I_{29} \\ I_{32} \\ I_{41} \\ I_{44} \end{bmatrix} = \begin{bmatrix} 1.930\times10^{-8} \\ 8.412\times10^{-10} \\ 1.340\times10^{-8} \\ 1.920\times10^{-8} \\ 1.680\times10^{-8} \\ 4.650\times10^{-9} \\ 4.950\times10^{-9} \end{bmatrix} \tag{B25}$$

Feed Gas Calibration mixture

The first calibration gas mixture is the feed gas. The mole fractions of the components in this mixture are

$$m^{fg} = \begin{bmatrix} m_{He} & m_{C_3H_6} & m_{O_2} \end{bmatrix} = \begin{bmatrix} 0.91 & 0.03 & 0.06 \end{bmatrix} \tag{B26}$$

The ion currents measured for this gas mixture, in mA, are

$$I^{fg} = \begin{bmatrix} I_4 \\ I_{29} \\ I_{32} \end{bmatrix} = \begin{bmatrix} 1.851\times10^{-8} \\ 1.885\times10^{-8} \\ 1.715\times10^{-8} \end{bmatrix} \tag{B27}$$

Since in this gas mixture none of the components produce secondary mass peaks which have the same mass as primary mass peaks of other components, The elements of the Q^{fg} matrix are simply the ratios of the elements of the m^{fg} and I^{fg} matrices

$$Q^{fg} = \begin{bmatrix} 2.034\times10^{-8} \\ 6.283\times10^{-7} \\ 2.858\times10^{-7} \end{bmatrix} \tag{B28}$$

Product Gas Calibration mixture

The second calibration gas mixture consists of the product components. The mole fractions of the components in this mixture are

$$m^{pg} = \begin{bmatrix} m_{He} & m_{CO} & m_{C_3H_6} & m_{CO_2} \end{bmatrix} = \begin{bmatrix} 0.9597 & 0.0099 & 0.0210 & 0.0103 \end{bmatrix} \tag{B29}$$

The ion currents measured for this gas mixture, in mA, are

$$I^{pg} = \begin{bmatrix} I_4 \\ I_{28} \\ I_{41} \\ I_{44} \end{bmatrix} = \begin{bmatrix} 2.522 \times 10^{-8} \\ 5.762 \times 10^{-9} \\ 1.175 \times 10^{-8} \\ 5.032 \times 10^{-9} \end{bmatrix} \tag{B30}$$

The a matrix is constructed according to equation B7

$$a = \begin{bmatrix} 0.9597 & 0 & 0 & 0 \\ 0 & 0.099 & 0.0009 & 0.0014 \\ 0 & 0 & 0.0201 & 0 \\ 0 & 0 & 0 & 0.0103 \end{bmatrix} \tag{B31}$$

The Q^{fg} matrix is calculated

$$Q^{fg} = a^{-1} I^{fg} = \begin{bmatrix} 0.263 \times 10^{-7} \\ 4.606 \times 10^{-7} \\ 5.844 \times 10^{-7} \\ 4.866 \times 10^{-7} \end{bmatrix} \tag{B32}$$

Water Calibration gas mixture

The final calibration gas mixture is produced by reacting propane and oxygen over a platinum mesh catalyst. The feed concentrations of propane and oxygen are 3% and 6% respectively, the reaction temperature is 550°C and about 0.4 g of platinum mesh catalyst is used. At these conditions, the limiting reactant is oxygen, and the products almost entirely consist of carbon dioxide, water and unreacted propane. GC analysis indicated that the concentrations of helium and water in the product gases are

$$m^{wg} = \begin{bmatrix} m_{He} & m_{H_2O} \end{bmatrix} = \begin{bmatrix} 0.8971 & 0.0494 \end{bmatrix} \tag{B33}$$

The ion currents measured for this gas mixture, in mA, are

$$I^{wg} = \begin{bmatrix} I_{He} \\ I_{H_2O} \end{bmatrix} = \begin{bmatrix} 1.952 \times 10^{-8} \\ 1.140 \times 10^{-8} \end{bmatrix} \tag{B34}$$

Since in this gas mixture none of the components produce secondary mass peaks which have the same mass as primary mass peaks of other components, The elements of the Q^{wg} matrix are simply the ratios of the elements of the m^{wg} and I^{wg} matrices

$$Q^{wg} = \begin{bmatrix} 0.218 \times 10^{-7} \\ 2.307 \times 10^{-7} \end{bmatrix} \tag{B35}$$

Expression of Q values on same total pressure basis

The ratio of the Q values for helium for the product gas and feed gas calibration mixtures is

$$r^{pf} = \frac{Q_{He}^{pg}}{Q_{He}^{fg}} = 1.292 \tag{B36}$$

The ratio of the Q values for helium for the product gas and water calibration mixtures is

$$r^{pw} = \frac{Q_{He}^{pg}}{Q_{He}^{wg}} = 1.208 \tag{B37}$$

The Q values of the feed and water calibration mixtures can be expressed in terms of the total pressure of the product calibration mixture by multiplying by these ratios. Finally the Q values of all of the calibration mixtures can be combined to into one Q matrix based on the total pressure of the product calibration mixture

$$Q = \begin{bmatrix} Q_{He} \\ Q_{H_2O} \\ Q_{CO} \\ Q_{C_3H_8} \\ Q_{O_2} \\ Q_{C_3H_6} \\ Q_{CO_2} \end{bmatrix} = \begin{bmatrix} 0.263 \times 10^{-7} \\ 2.787 \times 10^{-7} \\ 4.606 \times 10^{-7} \\ 8.115 \times 10^{-7} \\ 3.692 \times 10^{-7} \\ 5.884 \times 10^{-7} \\ 4.886 \times 10^{-7} \end{bmatrix} \tag{B38}$$

Final Calculations

The b matrix is constructed from the elements of the r and Q matrices, according to equation B16

$$b = \begin{bmatrix} 0.0263 & 0 & 0 & 0 & 0 & 0 & 0 \\ 0 & 0.2787 & 0 & 0 & 0 & 0 & 0 \\ 0 & 0 & 0.4606 & 0.5486 & 0 & 0.0250 & 0.0681 \\ 0 & 0 & 0 & 0.8115 & 0 & 0 & 0 \\ 0 & 0 & 0 & 0 & 0.3692 & 0 & 0 \\ 0 & 0 & 0 & 0.1875 & 0 & 0.5844 & 0 \\ 0 & 0 & 0 & 0.1785 & 0 & 0 & 0.4886 \end{bmatrix} \quad \text{(B39)}$$

According to equation B20

$$y = b^{-1}I = \begin{bmatrix} 0.7345 \\ 0.0030 \\ 0.0007 \\ 0.0237 \\ 0.0455 \\ 0.0004 \\ 0.0015 \end{bmatrix} \quad \text{(B40)}$$

The sum of the elements of y, according to equation B22, and represented by R, are equal to 0.8092. Finally, the mole fraction of each component in the outlet gas from the reactor is obtained by normalizing y, each element of y is divided by R

$$x = \begin{bmatrix} x_{He} \\ x_{H_2O} \\ x_{CO} \\ x_{C_3H_8} \\ x_{O_2} \\ x_{C_3H_6} \\ x_{CO_2} \end{bmatrix} = \begin{bmatrix} 0.9077 \\ 0.0037 \\ 0.0008 \\ 0.0292 \\ 0.0562 \\ 0.0005 \\ 0.0018 \end{bmatrix} \quad \text{(B41)}$$

Mass spectrometry was the analytical technique used for operation of the reaction under transient or periodic operation conditions. For calculations of the propane and oxygen conversions and carbon and oxygen balances under these conditions, the rigorous method shown in Appendix A was not used. It was assumed that the total inlet and outlet flow rates were equal. Due to the low concentrations of reactants used at all of the reaction conditions and the low levels of conversion, the outlet total flow rate was typically less than 2% greater

than the inlet flow rate. Thus accounting for the change in total flow rate makes little difference in the results as can be seen for the sample calculations in Appendix A. Thus the propane and oxygen conversion based on the mass spectrometry analysis are

$$C_3H_8\_conversion = \left(\frac{x^{in}_{C_3H_8} - x^{out}_{C_3H_8}}{x^{in}_{C_3H_8}} \right) \cdot 100\% = 2.67\% \tag{B42}$$

$$O_2\_conversion = \left(\frac{x^{in}_{O_2} - x^{out}_{O_2}}{x^{in}_{O_2}} \right) \cdot 100\% = 6.33\% \tag{B43}$$

The carbon and oxygen balances are

$$Carbon\_Balance = \left(\frac{x_{CO} + x_{CO_2} + 3x_{C_3H_6} + 3x^{out}_{C_3H_8}}{3x^{in}_{C_3H_8}} \right) \cdot 100\% = 101.9\% \tag{B44}$$

$$Oxygen\_Balance = \left(\frac{x_{H_2O} + x_{CO} + 2x_{CO_2} + 2x^{out}_{O_2}}{2x^{in}_{O_2}} \right) \cdot 100\% = 100.4\% \tag{B45}$$

The propene selectivity is calculated

$$C_3H_6\_selectivity = \left(\frac{3x_{C_3H_6}}{x_{CO} + x_{CO_2} + 3x_{C_3H_6}} \right) \cdot 100\% = 36.6\% \tag{B46}$$

Appendix C
Estimation of adsorption entropy change

Reason for estimating the adsorption entropy change

The following thermodynamic relation applies between the adsorption equilibrium constant (K_{ads}) and the Gibbs free energy of adsorption (ΔG°_{ads}) at standard conditions 298 K and 1 atm:

$$\ln K_{ads} = -\frac{\Delta G^{\circ}_{ads}}{RT} \qquad \text{(C1)}$$

The Gibbs free energy of adsorption is related to the enthalpy (ΔH°_{ads}) and entropy (ΔS°_{ads}) of adsorption by

$$\Delta G^{\circ}_{ads} = \Delta H^{\circ}_{ads} - T\Delta S^{\circ}_{ads} \qquad \text{(C2)}$$

By combining equations C1 and C2, the following is obtained

$$K_{ads} = \exp\left(\frac{\Delta S^{\circ}_{ads}}{R} - \frac{\Delta H^{\circ}_{ads}}{RT}\right) \qquad \text{(C3)}$$

The entropy of adsorption could be expressed as the adsorption equilibrium constant (K°_{ads}) at standard conditions

$$K_{ads} = K^{\circ}_{ads} \exp\left(-\frac{\Delta H^{\circ}_{ads}}{RT}\right) \qquad \text{(C4)}$$

In fitting this equation to data two adjustable parameters are available, the adsorption equilibrium constant (K°_{ads}) and the enthalpy of adsorption (ΔH°_{ads}) at standard conditions. This is the approach taken for the LH2 model in chapter 4, except that K°_{ads} is at the standard temperature of 530°C. In order to reduce the number of parameters to be fitted in the regression analysis, an estimate of ΔS°_{ads} in equation C3 may be made. The following describes how estimates of the entropy of adsorption at standard conditions were made for oxygen, propene and carbon monoxide.

Method of estimating the adsorption entropy change

According to quantum mechanical theory [76] the translational contribution to the gas phase entropy of a molecule can be estimated by

$$S_{trans} = \left\{\ln\left(\frac{M^{1.5}T^{2.5}}{P}\right) - 1.165\right\}R \qquad \text{(C5)}$$

where M is the molecular weight of the molecule, T is the temperature, P is the total pressure and R is the ideal gas constant. The total gas phase entropy (S_g) is the sum of its translational (S_{trans}), rotational (S_{rot}) and vibrational (S_{vib}) components

$$S_g = S_{trans} + S_{rot} + S_{vib} \qquad \text{(C6)}$$

The vibrational contribution can be considered negligible for low molecular weight molecules. It is possible by quantum mechanical theory to estimate the rotational gas phase entropy, although detailed knowledge of the molecule's geometry and atomic coordinates relative to its center of gravity is required. To simplify the estimation, the rotational gas phase entropy was calculated from literature values of the total gas phase entropy [77] and assuming the vibrational gas phase entropy was negligibly small

$$S_{rot} = S_g - S_{trans} \qquad \text{(C7)}$$

Table C1 shows the calculated translational and rotational gas phase entropies and the total gas phase entropy for oxygen, propene and carbon monoxide at standard conditions.

Table C1
Calculated translational and rotational gas phase entropies*

Component	S_g (J mol^{-1} K^{-1})	M (amu)	S_{trans} (J mol^{-1} K^{-1})	S_{rot} (J mol^{-1} K^{-1})
oxygen	205	32.00	152.0	53.1
propene	267	42.08	155.4	111.6
carbon monoxide	198	28.01	150.3	47.7

* at standard conditions 298 K, 1 atm

It was assumed that upon adsorption, a molecule loses all of its translational entropy and two thirds of its rotational entropy. Thus, the adsorption entropy change at standard conditions was calculated

$$\Delta S^{\circ}_{ads} = -S_{trans} - \frac{2}{3} S_{rot} \qquad \text{(C8)}$$

Mixture effects on the gas phase entropy were considered negligible. It should be noted that such an estimate of the gas phase entropy change upon adsorption must be considered a maximum, since it is possible for a molecule to have some limited mobility on the catalyst surface and retain a portion of its translational entropy. Table C2 shows the calculated adsorption entropy change at standard conditions.

Table C2
Calculated adsorption entropy change*

Component	ΔS°_{ads} (J mol^{-1} K^{-1})
oxygen	-178.5
propene	-229.8
carbon monoxide	-174.1

* at standard conditions 298 K, 1 atm

Appendix D
Transient and periodic operation experimental data

The transient and periodic operation experimental data are contained on an accompanying 3.5" floppy diskette. All of the data are stored in an ASCII format. None of the files on the diskette contain documenting text, thus the following tables in this appendix explain exactly the kind of data and its configuration in each file.

Transient data

Table D1 lists the files that contain transient reaction data. This data was all first presented in chapter 6 and the table also lists the figures in which the data appear. Some data may appear in different formats in multiple figures and some figures contain data from multiple files. In order to avoid possible confusion, the reaction conditions for each set of data is also listed.

The data files consist of columns of numbers. Table D2 lists what each column contains. The data are transient responses after disturbances imposed on the reaction and all of the data is relative to the time at which the disturbance was imposed. Thus, the disturbance, resulting in the start-up or interruption of the reaction occur at time zero. Not all of the data files contain a 9^{th} and 10^{th} column. These columns contain estimates of the feed concentrations of propane and oxygen to the reactor, determined by repeating the experiments with the reactor not containing catalyst, i.e. blank experiments.

Table D1
Directory of files containing transient data

File name	Figure numbers	Reaction Conditions		
		Catalyst Mass (mg)	Feed C_3H_8 (%)	Feed O_2 (%)
d623.dat	6.2,6.3	21	3	6
d64a.dat	6.4a	30	6	6
d64b.dat	6.4b	21	3	6
d65a.dat	6.5a	17	6	0
d65b.dat	6.5b	17	6	6
d66a78.dat	6.6a,6.7,6.8	30	6	0
d66b.dat	6.6b	30	6	0
d68.dat	6.8	30	6	0

Table D2
Configuration of transient data files

Column number	Quantity	Units
1	time	s
2	helium	mole fraction
3	water	mole fraction
4	carbon monoxide	mole fraction
5	propane	mole fraction
6	oxygen	mole fraction
7	propene	mole fraction
8	carbon dioxide	mole fraction
9	propane (inlet estimation)	mole fraction
10	oxygen (inlet estimation)	mole fraction

Periodic operation data

Tables D3 to D6 list the files that contain periodic operation data. This data was all first presented in chapter 8 and the tables also list the figures in which the data appear. The tables also list the strategy of periodic operation used for each set of data. For complete details one should refer to the discussion in chapter 8 regarding each figure.

Table D7 lists what each column contains. The data files contain the product transient responses during up to 10 cycles of periodic operation. In the case of the propane pulsing experiments the data is for 30 cycles of operation. For most of the data, at time zero feed to the reactor is switched from that at steady state conditions to the oxygen-containing half of the periodic operation feed cycle. In the case of the propane pulsing experiments, at time zero feed to the reactor is switched from helium to the propane-containing half of the feed cycle.

Table D3
Directory of files containing periodic operation data at varying cycle periods

File name	Figure numbers	cycle period (s)
per10.dat	8.2	10
per20.dat	8.2	20
per40.dat	8.1,8.2	40
per60.dat	8.2	60
per80.dat	8.1,8.2	80
per100.dat	8.2	100
per130.dat	8.1,8.2	130
per160.dat	8.2	160
per200.dat	8.2	200
per300.dat	8.2	300
per400.dat	8.1,8.2	400

Table D4
Directory of files containing periodic operation data at varying cycle splits

File name	Figure numbers	cycle splits (C_3H_8:O_2)
sp11.dat	8.3,8.4	1:1
sp21.dat	8.4	1:1.2
sp18.dat	8.4	1:0.8
sp16.dat	8.3,8.4	1:0.6
sp14.dat	8.4	1:0.4
sp12.dat	8.3,8.4	1:0.2
sp15.dat	8.3,8.4	1:0.1

Table D5
Directory of files containing periodic operation data with varying propane feed schemes

File name	Figure numbers	Propane conc. in oxidation half of feed cycle (%)	cycle period (s)
fs650.dat	8.8,8.6	6	100
fs550.dat	8.8,8.6	5	100
fs450.dat	8.8,8.6	4	100
fs350.dat	8.8,8.6	3	100
fs630.dat	8.8,8.7	6	60
fs530.dat	8.8,8.7	5	60
fs430.dat	8.8,8.7	4	60
fs330.dat	8.8,8.7	3	60

Table D6
Directory of files containing propane pulsing data

File name	Figure numbers	Catalyst mass (mg)
pul20.dat	8.9,8.11	20
pul30.dat	8.9,8.11	30
pu140.dat	8.9,8.10,8.11	40

Table D7
Configuration of periodic operation data files

Column number	Quantity	Units
1	time	s
2	carbon monoxide	mole fraction
3	propene	mole fraction
4	carbon dioxide	mole fraction

Temperature-programmed oxidation/desorption data

Table D8 lists the files that contain temperature-programmed oxidation and desorption data. This data was presented in chapter 8 and the tables also list the figures in which the data appear. The tables also list some of the experimental conditions for each set of data. For complete details one should refer to the discussion in chapter 8 regarding each figure. Separate files listed in Table D8 contain the measured reactor temperature during the temperature-programmed experiments.

Tables D9 and D10 list what each column contains in the data files. At time zero, for each data file, feed to the reactor is switched from the pretreatment conditions to the conditions for the temperature-programmed experiment.

Table D8
Directory of files containing temperature-programmed oxidation/desorption data

File name	Figure numbers	Conditions	pretreatment	Temperature data file name
tpopl.dat	8.12a	oxidation	propane pulsing	tpopl_t.dat
tposs.dat	8.12b	oxidation	steady state	tposs_t.dat
tpxpl.dat	8.13a	desorption	propane pulsing	tpxpl_t.dat
tpxss.dat	8.13b	desorption	steady state	tpxss_t.dat

Table D9
Configuration of temperature-programmed oxidation/desorption data files

Column number	Quantity	Units
1	time	s
2	carbon monoxide	mole fraction
3	carbon dioxide	mole fraction

Table D10
Configuration of temperature data files

Column number	Quantity	Units
1	time	s
2	temperature	°C

Appendix E
Oxygen partial pressure effects steady-state data and modelling details

Table E1 contains the steady-state data used for modelling in chapter 9.

Table E1
Oxygen partial pressure effects steady-state data

Inlet Conc. (%)		Cat.	Outlet Concentration (%)[a]					C_3H_8	O_2	C_3H_6
C_3H_8	O_2	Mass (mg)	CO	CO_2	C_3H_6	C_3H_8	O_2[b]	conv. (%)	conv.[b] (%)	yield (%)
4	4	20	0.072	0.157	0.083	3.841	3.613	3.82	9.52	1.99
4	3.2	20	0.039	0.124	0.072	3.873	2.912	3.05	8.90	1.74
4	2.4	20	0.041	0.097	0.073	3.881	2.153	2.86	10.17	1.75
4	1.6	20	0.032	0.073	0.096	3.869	1.393	3.18	12.86	2.34
4	0.8	20	0.033	0.065	0.101	3.791	0.602	3.25	24.63	2.45
4	0.4	20	0.029	0.052	0.118	3.855	0.220	3.52	44.90	2.86
6	6	20	0.100	0.368	0.109	5.735	5.215	4.13	12.82	1.70
6	4.8	20	0.068	0.333	0.098	5.768	4.116	3.64	14.05	1.54
6	3.6	20	0.059	0.225	0.098	5.807	3.107	3.03	13.53	1.54
6	2.4	20	0.063	0.185	0.101	5.817	1.968	2.88	17.87	1.58
6	1.2	20	0.040	0.107	0.107	5.844	0.921	2.47	23.13	1.69
6	0.6	20	0.045	0.108	0.104	5.845	0.317	2.45	47.15	1.64
4	4	30	0.086	0.167	0.125	3.791	3.559	5.03	10.84	3.01
4	3.2	30	0.083	0.173	0.130	3.785	2.750	5.19	13.88	3.13
4	2.4	30	0.065	0.156	0.127	3.799	2.000	4.86	16.52	3.07
4	1.6	30	0.058	0.127	0.127	3.811	1.257	4.57	21.29	3.08
4	0.8	30	0.068	0.092	0.125	3.821	0.504	4.32	36.84	3.03
4	0.4	30	0.053	0.094	0.126	3.825	0.118	4.25	70.49	3.06
6	6	30	0.115	0.299	0.181	5.681	5.276	5.01	11.77	2.85
6	4.8	30	0.093	0.230	0.167	5.726	4.224	4.32	11.76	2.62
6	3.6	30	0.122	0.220	0.160	5.726	3.010	4.30	16.14	2.51
6	2.4	30	0.081	0.181	0.161	5.752	1.923	3.92	19.68	2.54
6	1.2	30	0.081	0.121	0.159	5.773	0.824	3.58	31.16	2.52
6	0.6	30	0.085	0.114	0.161	5.773	0.231	3.59	61.44	2.55
4	4	40	0.121	0.292	0.182	3.680	3.281	7.71	17.71	4.39
4	3.2	40	0.111	0.198	0.161	3.736	2.660	6.36	16.67	3.88
4	2.4	40	0.087	0.200	0.153	3.751	1.889	6.00	21.11	3.70
4	1.6	40	0.077	0.180	0.153	3.761	1.134	5.77	28.97	3.70
4	0.8	40	0.090	0.148	0.152	3.769	0.373	5.58	53.30	3.66
4	0.4	40	0.074	0.133	0.179	3.752	0.003	6.00	99.38	4.33
6	6	40	0.228	0.437	0.248	5.530	4.881	7.34	18.22	3.88
6	4.8	40	0.182	0.380	0.229	5.584	3.839	6.52	19.66	3.59
6	3.6	40	0.149	0.356	0.230	5.602	2.719	6.26	24.18	3.61
6	2.4	40	0.169	0.304	0.220	5.522	1.586	5.93	33.67	3.46
6	1.2	40	0.126	0.201	0.213	5.678	0.612	5.08	48.85	3.36
6	0.6	40	0.082	0.147	0.203	5.721	0.158	4.43	73.61	3.22

[a]Normalized carbon distribution.
[b]Calculated from normalized carbon distribution in products and assuming the only additional product is water.

The following tables list confidence intervals for all of the models discussed in chapter 9.

Table E2
Parameter 95% confidence intervals for redox model based on MV2

Parameter	Confidence interval	Units
k_1	$\pm 1.37\times10^{-2}$	ml STP min^{-1} $(g\ cat)^{-1}$ bar^{-1}
k_2	$\pm 9.53\times10^{-5}$	ml STP min^{-1} $(g\ cat)^{-1}$ bar^{-1}
k_3	$\pm 5.41\times10^{-1}$	ml STP min^{-1} $(g\ cat)^{-1}$ bar^{-1}

Table E3
Parameter 95% confidence intervals for DMV1 models

Parameter	DMV1-S1	DMV1-P	DMV1-S2	Units
k_1	$\pm 9.64\times10^{-3}$	$\pm 5.73\times10^{-3}$	$\pm 1.42\times10^{-2}$	ml STP min^{-1} $(g\ cat)^{-1}$ bar^{-1}
k_3	$\pm 6.88\times10^{-3}$	$\pm 7.94\times10^{-3}$	$\pm 1.02\times10^{-4}$	ml STP min^{-1} $(g\ cat)^{-1}$ bar^{-1}
k_4	$\pm 1.43\times10^{-1}$	$\pm 1.62\times10^{-1}$	$\pm 1.93\times10^{-1}$	ml STP min^{-1} $(g\ cat)^{-1}$ bar^{-1}
k_5	$\pm 5.39\times10^{12}$	$\pm 2.87\times10^{9}$	$\pm 1.93\times10^{1}$	ml STP min^{-1} $(g\ cat)^{-1}$

Table E4
Parameter 95% confidence intervals for DMV3 models

Parameter	DMV3-S1	DMV3-P	DMV3-S2	Units
k_1	$\pm 9.08\times10^{-3}$	$\pm 5.99\times10^{-3}$	$\pm 1.07\times10^{-2}$	ml STP min^{-1} $(g\ cat)^{-1}$ bar^{-1}
k_3	$\pm 4.69\times10^{-2}$	$\pm 4.34\times10^{-2}$	$\pm 2.92\times10^{-4}$	ml STP min^{-1} $(g\ cat)^{-1}$ bar^{-1}
k_4	$\pm 7.67\times10^{5}$	$\pm 2.76\times10^{3}$	± 8.90	ml STP min^{-1} $(g\ cat)^{-1}$ bar^{-1}
k_5	$\pm 5.94\times10^{-2}$	$\pm 5.15\times10^{-2}$	$\pm 9.70\times10^{-3}$	ml STP min^{-1} $(g\ cat)^{-1}$ bar^{-1}

Table E5
Parameter 95% confidence intervals for DMV4 models

	DMV4-S		DMV4-P	
	Value	Units	Value	Units
k_1	$\pm 1.03\times10^{-2}$	ml STP min^{-1} $(g\ cat)^{-1}$ bar^{-1}	$\pm 9.01\times10^{-3}$	ml STP min^{-1} $(g\ cat)^{-1}$ bar^{-1}
k_2	$\pm 7.57\times10^{-1}$	ml STP min^{-1} $(g\ cat)^{-1}$	$\pm 6.89\times10^{-3}$	ml STP min^{-1} $(g\ cat)^{-1}$ bar^{-1}
k_3	$\pm 9.54\times10^{-3}$	ml STP min^{-1} $(g\ cat)^{-1}$ bar^{-1}	$\pm 8.76\times10^{-3}$	ml STP min^{-1} $(g\ cat)^{-1}$ bar^{-1}
k_4	$\pm 8.96\times10^{-1}$	ml STP min^{-1} $(g\ cat)^{-1}$ bar^{-1}	± 1.02	ml STP min^{-1} $(g\ cat)^{-1}$ bar^{-1}
$K_{C_3H_6}$	$\pm 9.77\times10^{2}$	bar^{-1}	$\pm 1.83\times10^{4}$	bar^{-1}